Universidad del País Vasco Euskal Herriko Unibertsitatea

université de BORDEAUX

The energy cost of primary metabolism and vacuole expansion: Central to shape tomato leaf development under ammonium nutrition

Théo Poucet

2020

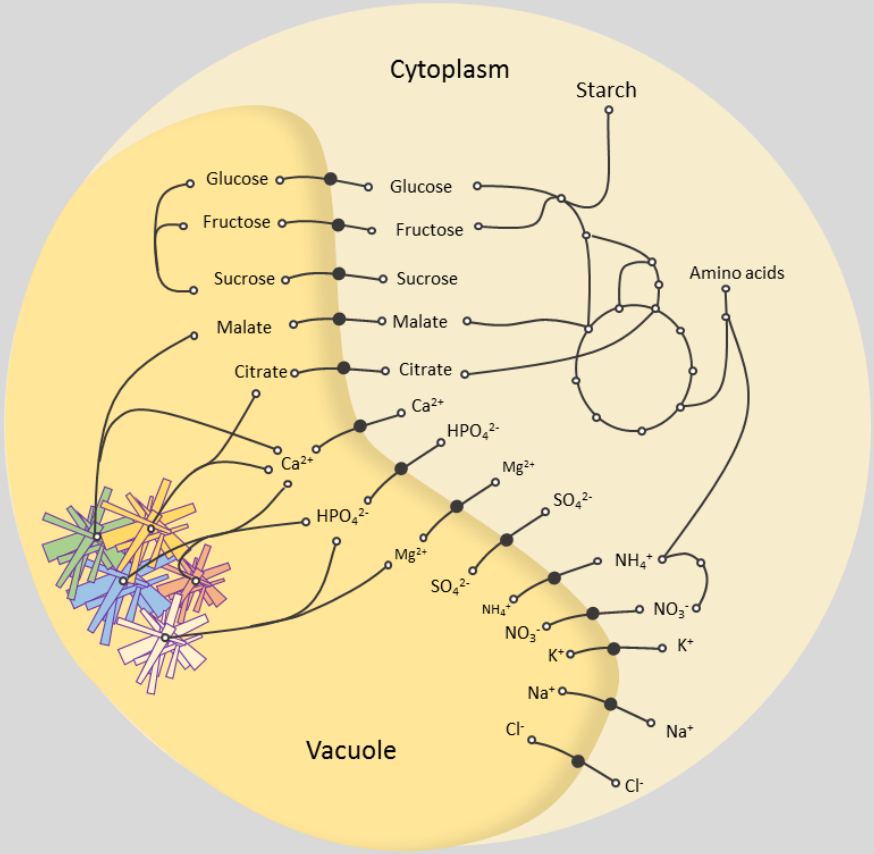

A thesis submitted to

The doctoral school of Agrobiología Ambiental from the University of the Basque Country (UPV/EHU)

and

The doctoral school of Science de la Vie et de la Santé (speciality: Plant biology) from the University of Bordeaux

Under the supervision of **Dr. Martine Dieuaide-Noubhani** and **Dr. Daniel Marino Bilbao**

Jury members:

Pr. Dominique Rolin	Professor in the University of Bordeaux
Dr. Nadine Paris	Research Associate INRAE Montpellier
Dr. Céline Masclaux-Daubresse	Research Director of INRAE Versailles
Pr. Cesar Arrese-Igor	Professor in the Public University of Navarre
Pr. Usue Pérez	Lecturer in the University of the Basque Country

Acknowledgements

For giving me opportunity to work in their laboratory, I would like to thank **Dr. Carmen González-Murua**, leader of NUMAPS group from the Department of Plant Biology and Ecology of the University of the Basque Country (UPV/EHU, Spain), and **Dr. Yves Gibon** director of the laboratory of Biologie du Fruit et Pathologie from the INRAE institute (France).

For the opportunity of carrying out this thesis and their continuous support, I would especially thanks my thesis supervisors **Dr. Martine Dieuaide-Noubhani** and **Dr. Daniel Marino Bilbao**.

Likewise, I would like to thank:

Dr. Ricardo Andrade from the unit of analytical microscopy of SGIKER for technical and human support during the set-up of the confocal microscopy experiments.

Dr. Stephane Bernillon, **Amelie Flandin** and **Dr. Pierre Petriacq** for technical and human support for the analysis of amino acids by UHPLC and secondary metabolites by LC-MS.

Dr. Nadine Paris for providing valuable advice concerning the intracellular pH measurement using BCECF-AM probe.

Dr. Yves Gibon, **Cedric Cassan** from the Biologie du fruit et pathologie laboratory for the technical and human support during metabolite and enzyme activity measurements.

Dr. Bertrand Beauvoit from the university of Bordeaux and INRA institute for great support and valuable discussions during the construction of the mathematical model.

I am greatly indebted to the university of **Basque country (UPV/EHU)** for providing the post-graduate scholarship in the context of cotutelle, which has been a wonderful experience. I also received an additional grant mobility from the University of Basque Country when I changed of working laboratory from Leioa to Bordeaux.

I would like to acknowledge the **ERASMUS program** for international exchanges. It creates and supports a nice and dynamic Europe. I owe it for giving me various personal and professional opportunities that led me to this thesis.

Gracias **Merci** **Thank You** **Eskerrik Asko**

To my thesis supervisor, Daniel and Martine. Thanks to you, I enjoyed great freedom of mind and action during this thesis, which I think, allowed us to explore new scientific horizons. I had a lot of pleasure in being the center of your collaboration marked by your scientific complementarities.

A **Daniel**, has confiado en mí desde el principio y te has comprometido conmigo varias veces. Tu dedicación para hacer bien las cosas, tu minuciosidad y tu saber ser son semillas que me llevo conmigo. Espero que sepa desarrollar estas cualidades en el futuro. Tras estos tres años, puedo decir sin equivocarme que hice la buena elección en hacer mi tesis contigo. Gané una gran experiencia y un amigo.

Martine tu m'as toujours soutenu et ta patience lors des moments difficiles ainsi que ta bonne humeur générale ont confirmé la belle vision que j'ai de la recherche. De plus, comme une guide, tu as très bien su me canaliser tout en me laissant exprimer mes idées.

A **Carmen** por tus sabias parabras, tu energía.

A **Yves** pour tes excellentes idées.

A **Bertrand**, cela a été un immense plaisir de travailler avec toi. Ta bonne humeur, ta camaraderie et tes compétences scientifiques ont fait de toi un véritable catalyseur de créativité.

A **Begoña**, ha sido un encanto tenerte a mi lado durante esta tesis, al nivel de ciencia tal como el nivel humano. Echaré de menos a tus bromas.

A **Cécile**, merci pour ton humanité et tes conseils avisés (super bonne idée de mesurer l'osmolarité !).

A **Simon**, super compagnon de bureau tu m'as manqué pendant l'écriture en Espagne. Je ne doute pas que nous nous reverrons bientôt sur un cours de tennis.

A **Sylvain** c'est toujours un plaisir de tomber d'accord avec toi sur une infinité de sujets. A quand le prochain concert des sales majestés ?

A **Zoé**, jolie rencontre de BAP 2018, reste toujours aussi motivé dans ta vie que tu ne l'es maintenant.

Les doctorants de l'équipe métabolisme qui savent se serrer les coudes tout en s'amusant. Ça a été un plaisir de vous rencontrer **JiaoJiao, Guillaume, Alice et Thomas**. Bonne chance pour la suite !

A **Amélie, Cédric** et **Pierre** pour votre aide et votre bonne humeur c'était un plaisir de vous avoir à mes côtés.

Aux 5 stagiaires qui en plus de m'avoir permis de développer mes capacités d'enseignement, m'ont été aussi d'une grande aide, il s'agit de **Ana Renovales**, **Mandy Bordas**, **Léa Gintowt**, **Alexandre Lebrere**, **Hamza Badrari**.

Asier, siendo tu alumno, fuiste tú que me enseñó a medir el contenido de amonio. Llevabas siempre buen ambiente y me alegro haberte conocido.

Los doctorantes y post-doc de fisiología vegetal, a tope, pero encontrando siempre un rato para una buena conversación. Un placer haberos conocido, **Marlon, Adrian, Mario, Ander, Agustin, Inma, Marina**.

To all people who went through the metabolism platform, it has been a pleasure to meet you. You have all spiced up our routine. I named **Leslie, Emilia, Francesca and Marlon**.

A l'équipe de ma thèse en 180 seconde vous avez été une bouffée d'oxygène pour moi, on s'ancre dans le sol et voici: **Katixa, Delphine, Manon, Pierre, María, Sophie**.

A mon Fidèle amis de toujours, **Arthur**, déclencheur de grandes aventures.

A mes nouveaux amis de toujours, **Floris, Mathias et Lelia.**

Gracias a **hostelería** por la divina comida que nos servían.

A **Aitor** por haber convivido conmigo mientras escribía.

Merci à **Paul, Ursule, Pierre, valentin, Lucas, Mathieu** (lequel ? Devine**), Anthony, Juliette, Charles, Nico, Eva, Elias, Coralie, Ricardo et Adeline**, pour m'avoir permis de m'échapper d'une manière ou d'autre avec vous.

Gracias a ti, mi querida **Blanca** por haber vivido la tesis conmigo. Tu solo sabes el día a día que ha sido, y te prometo que no volveré a hacer una tesis. Espero poder seguir tus pasos para mucho tiempo y vivir muchas aventuras contigo.

Merci à ma famille, **Robin, Eloi, Papa et Maman**. Vous avez toujours été là pour me soutenir dans les bons et les mauvais moments. Vous avez grandement contribué à ce travaille dans la joie et la bonne humeur #COVID-19.

Content

Summaries

Illustration of tomato plant (source: New York, NY: Syndicate Publishing Company, 1912)

RÉSUMÉ

Version courte du résumé

L'ammonium (NH_4^+) est une source d'azote d'un grand intérêt dans le cadre d'une agriculture durable. Son application en champs avec des inhibiteurs de nitrification s'est montré efficace pour limiter les pertes de N par rapport à l'utilisation de nitrate (NO_3^-). NH_4^+ est un intermédiaire commun impliqué dans de nombreuses voies métaboliques. Cependant, des concentrations élevées peuvent conduire à une situation de stress chez la plante provoquant un « syndrome ammoniacal », caractérisé par une croissance réduite. Ces symptômes sont causés par la combinaison, entre autres, d'une reprogrammation métabolique, d'une perturbation de la photosynthèse, d'une dérégulation du pH et d'un déséquilibre ionique. De nombreuses études ont décrit la façon dont la plante s'adapte à la nutrition ammoniacale. Cependant, le stade de développement des organes a été souvent négligé.

Pour combler cette lacune, dans le premier chapitre nous étudions comment le métabolisme s'adapte en fonction de la position des feuilles sur l'axe vertical de plants de tomates (*Solanum lycopersicum*) cultivées en présence de NH_4^+, NO_3^- ou NH_4NO_3. Nous avons disséqué la composition de la biomasse foliaire et le métabolisme grâce à une analyse complète des métabolites, ions et activités enzymatiques. Nos résultats montrent que l'ajustement métabolique du C et du N en fonction de la source d'azote était plus intense chez les feuilles âgées par rapport au plus jeunes. Surtout, nous révélons un compromis entre l'accumulation de NH_4^+ et l'assimilation afin de préserver les jeunes feuilles du stress ammoniacal. Par ailleurs, les plantes alimentées en NH_4^+ présentaient un réarrangement des squelettes carbonés impliquant un coût énergétique élevé. Nous expliquons une telle réallocation par l'action du pH-stat biochimique, pour compenser la production différentielle de protons dépendante de la forme azotée fournie.

La nutrition ammoniacale peut limiter l'expansion cellulaire. Entre autres, la croissance cellulaire dépend largement de la pression interne exercée par la vacuole sur la paroi cellulaire. Cependant, l'impact du stress ammoniacal sur la vacuole a été rarement abordé. Dans le second chapitre, nous évaluons l'effet de la nutrition ammoniacale sur le développement des feuilles en se focalisant sur l'expansion et le métabolisme vacuolaire.

Pour cela, nous avons suivi le développement d'une feuille depuis son apparition jusqu'à son expansion complète avec du NH_4^+ ou NO_3^- comme seule source d'azote. Nous avons d'abord mis en évidence que la réduction de l'expansion cellulaire en nutrition ammoniacal était associée à des vacuole plus petite et aussi plus acide que celles recevant du NO_3^-. De plus, un modèle a été construit pour prédire l'équilibre thermodynamique de différentes espèces solubles de part et d'autre du tonoplaste. Le modèle intègre les volumes subcellulaires, les gradients électrochimiques et la formation de complexe ionique dans la vacuole afin de prédire les concentrations subcellulaires des ions, acides organiques et sucres mesurée dans la feuille. De plus, ces prédictions ont été validées avec des données obtenus par fractionnement non aqueux. Finalement, l'estimation des flux de soluté dans la vacuole nous a permis de démontrer que la déficience en malate dans les cellules des feuilles nourries avec NH_4^+ est central dans la limitation de l'expansion vacuolaire. De plus, nous concluons que le coût énergétique du transport de soluté dans la vacuole est plus élevé sous nutrition ammoniacale en raison du gradient électrochimique plus élevé généré de part et d'autre du tonoplaste.

Ce travail souligne l'importance de considérer l'état phénologique des feuilles lors de l'étude du métabolisme de l'azote. De plus, notre approche place le contrôle du pH cytosolique et l'expansion des vacuoles au centre de l'adaptation des feuilles de tomate à ce stress et ouvre la voie à de futures études dans le domaine de la nutrition ammoniacal.

Version longue du résumé

Les sols agricoles sont souvent déficients en azote et un apport supplémentaire est souvent nécessaire pour une production optimale. En effet, l'azote est un élément indispensable au développement des plantes, étant un constituant essentiel des protéines, des acides nucléiques et de la chlorophylle. Absorbé sous forme minérale (NH_4^+ ou NO_3^-), il provient soit de la minéralisation de la matière organique, soit des engrais. Cependant, l'utilisation intensive d'engrais peut causer des problèmes environnementaux majeurs. En effet, la pollution de l'eau par le nitrate (NO_3^-) et la pollution de l'air par le N_2O fait l'objet du préoccupation croissante (Foley *et al*., 2011). En ce sens, les engrais à base d'ammonium (NH_4^+) et appliqués avec des inhibiteurs de nitrification sont considérés comme une bonne alternative pour réduire l'impact environnemental de l'approvisionnement en azote dans les systèmes agricoles. Ils maintiennent le NH_4^+ disponible dans le sol pendant de plus longues périodes tout en atténuant certains des effets néfastes associés à la fertilisation azotée (GIEC-Groupe d'experts intergouvernemental sur l'évolution du climat 2007; Huerfano *et al*. 2015). Cependant, bien que le NH_4^+ soit un substrat fondamental pour la synthèse des biomolécules, sa présence en excès dans le sol peut conduire à une situation de stress, provoquant un ensemble de symptômes appelés communément « le syndrome ammoniacale » (Britto et Kronzucker, 2002). Chez les plantes, ce syndrome peut changer l'apparence de la plante avec l'apparition de chlorose foliaire, des changements du ratio de la partie radicale par rapport à la partie aérienne et une retardation de la croissance. Au niveau d'un organe ou cellulaire, cela peut être associé, parmi d'autres causes, à une perturbation de l'absorption de certains ions, une perturbation de la régulation du pH, une dérégulation hormonale ou une réorganisation importante du métabolisme carboné et azoté ; Ces symptômes conduisant finalement à une réduction de la biomasse (Britto et Kronzucker, 2002). Actuellement, aucun mécanisme unique ne peut fournir une explication adéquate de la toxicité de l'ammonium. De plus, Il n'y a pas de consensus sur les caractéristiques qui pourrait conférer une tolérance au NH_4^+ à une plante car cette tolérance semble provenir de processus multifactoriels et physiologiquement complexes.

Il est donc essentiel de comprendre les mécanismes physiologiques et métaboliques perturbés par la nutrition ammoniacale afin de pouvoir développer des variétés d'intérêt plus adaptées à ce type de nutrition azotée. Sur cette base, l'objectif général de cette thèse de

doctorat est de mieux comprendre la réponse des plantes à la nutrition ammoniacale en y associant la composante du développement.

Dans une première partie de ce travail, nous avons cherché à étudier comment le métabolisme est adapté en fonction de la position de la feuille sur l'axe vertical d'une plante de tomate (*Solanum lycopersicum* cv. M82) cultivée en présence de NH_4^+, NO_3^- ou NH_4NO_3. Pour ce faire, nous avons disséqué la composition et le métabolisme de la biomasse foliaire grâce à une analyse complète des métabolites, des ions et des activités enzymatiques. Les résultats ont montré que l'ajustement métabolique du C et du N en fonction de la source d'azote était plus intense chez les feuilles âgées par rapport aux plus jeunes. Surtout, nous mettons à jour un compromis entre l'accumulation de NH_4^+ et l'assimilation pour préserver les jeunes feuilles du stress ammoniacal. Par ailleurs, les plantes nourries au NH_4^+ ont présenté un réarrangement des squelettes carbonés, accumulant des sucres et de l'amidon au détriment des acides organiques, et ce, avec un coût énergétique plus élevé par rapport aux plantes alimentées avec du nitrate. Nous expliquons une telle réallocation par l'action du pH-stat biochimique, qui est un mécanisme couplant l'activité enzymatique de certaines enzymes cytosolique afin de réguler le pH du cytosol et serait différentiellement régulé selon la source d'azote fournies. En effet, il est classiquement admis que le besoin de NH_3 comme substrat du cycle GS/GOGAT induit la production de OH^- quand NO_3^- est l'unique source d'azote. Alors que l'apport direct de NH_4^+ conduit à la production de H^+. De cette manière, la production différentielle de protons, qui est dépendante de la forme azotée fournie, serait centrale dans la réorganisation de la composition de la biomasse de la plante.

La deuxième partie de ce travail se concentre sur l'importance de la compartimentation subcellulaire pendant le développement et l'adaptation des plantes en présence de concentrations élevé en NH_4^+. En effet, la toxicité de NH_4^+ est généralement associée à son accumulation dans le cytosol et une stratégie qui a été suggérée pour la tolérance à l'ammonium est sa compartimentation dans la vacuole. Cette hypothèse découle de plusieurs travaux, tels que la quantification de concentrations millimolaires de NH_4^+ à l'intérieur de la vacuole de cellules de *Chara corallina* (Wells et Miller, 2000). De plus, il a été démontré que des levures transformées avec deux aquaporines provenant d'*Arabidopsis thaliana* et localisant dans le tonoplaste (TIP2; 1 et TIP2; 3), augmentent leurs tolérances à l'ammonium grâce à la facilitation du transport de NH_3 dans la vacuole (Loqué *et al*., 2005). En outre, il a

également été observé que la kinase de type récepteur de tonoplaste CAP1 est importante dans le contrôle du stress de l'ammonium en contrôlant l'homéostasie de l'ion NH_4^+ entre le cytosol et la vacuole via un mécanisme qui doit encore être trouvé (Bai *et al*., 2014). Comme il a été montré dans le chapitre I, un autre aspect important qui influence grandement les performances des cellules par rapport à la source d'azote disponible semble être le contrôle du pH. En effet, il est connu que le pH est un facteur primordial impliqué dans la tolérance des plantes au stress ammoniacal (Sarasketa *et al*., 2016.). De fait, les mécanismes de transport vacuolaires peuvent être cruciaux pour le contrôle du pH cytosolique et de l'homéostasie de certains ions. Ce transport est en partie régulé par des pompes vacuolaires H^+, comprenant les pyrophosphatases et les ATPases qui établissent le gradient electrochimique de part et d'autre du tonoplaste (Bassil et Blumwald, 2014). Par ailleurs, dans la plupart des tissus matures, la vacuole occupe un grand volume, jusqu'à 90% de la cellule, et l'élargissement osmotique de la vacuole est souvent impliqué dans le contrôle de l'expansion cellulaire. Chez les tomates, il a été récemment démontré que des accumulations élevées de sucres solubles et d'acides organiques étaient responsables de l'expansion des vacuoles au début de la division cellulaire (Beauvoit et al., 2014), bien que d'autres métabolites tels que les acides aminés et les sels minéraux (y compris le nitrate et l'ammonium dans les feuilles) pourraient également être impliqués. De fait la réorganisation du métabolisme et la déplétion de certains cations en nutrition ammoniacale pourraient affecter le remplissage de la vacuole en osmolyte et donc son expansion. Il a en effet été prouvé que la source d'azote influence l'expansion et la division des cellules dans le tabac (Walch-Liu et al., 2000 ; Podgórska et al., 2013). Finalement, l'expansion des vacuoles implique un transport actif, qui est un processus à forte consommation d'énergie et pourrait être impliqué dans la réduction du rendement dans des conditions de limitation d'énergie. En ce sens, l'étude du rôle de la vacuole dans l'adaptation métabolique des cellules végétales devient essentielle pour mieux comprendre les performances des plantes lors de leurs développements sous différents régimes nutritionnels azotés.

Dans ce deuxième chapitre, nous évaluons l'effet du stress ammoniacal sur le développement des feuilles en nous focalisant particulièrement sur l'expansion et le métabolisme de la vacuole. Pour atteindre cet objectif, nous avons suivi le développement d'une feuille depuis son apparition jusqu'à son expansion complète avec des plantes de tomate cultivées en

présence exclusive de NH_4^+ ou NO_3^- comme source d'azote. Premièrement, une analyse cytologique a démontré que l'expansion cellulaire était effectivement réduite en nutrition ammoniacal et était aussi associée à des vacuoles de plus petite taille. Ensuite, l'utilisation de la sonde BCECF-AM sensible au pH intracellulaire nous a permis de démontrer une acidification de la vacuole des plantes nourries avec de l'ammonium par rapport à la nutrition à base de nitrate. Pour approfondir l'étude de l'implication des vacuoles dans le stress ammoniacale, nous avons combiné dans un modèle mathématique, les données de cytologie, la détermination *in vivo* du pH cellulaire et l'analyse biochimique de la composition des feuilles au niveau tissulaire et subcellulaire via le fractionnement non aqueux. Ce modèle a été construit en s'appuyant sur une révision bibliographique approfondie des transporteurs vacuolaires existant afin de prédire l'équilibre thermodynamique des solutés les plus abondants à travers le tonoplaste. Cela nous a permis d'estimer les flux vacuolaires dans la vacuole tout au long du développement foliaire. Dans l'ensemble, nos résultats montrent que l'entrée des solutés dans les vacuoles était plus faible dans les feuilles nourries au NH_4^+, ce qui pouvait potentiellement affecter l'expansion des vacuoles et des cellules. Cela était dû en partie à la réorganisation métabolique des cellules entraînant une déplétion du malate en nutrition ammoniacale. De plus, l'augmentation de l'acidité vacuolaire dans les cellules alimentées en ammonium induit un coût énergétique plus élevé pour transporter les solutés à travers le tonoplaste par rapport aux cellules alimentées en nitrate. Dans l'ensemble, nous soulignons un compromis énergétique entre le maintien du pH cytosolique, et l'expansion cellulaire, la vacuole y jouant un rôle central.

Dans sa globalité, ce travail souligne l'importance de considérer l'état phénologique des feuilles lors de l'étude du métabolisme de l'azote. De plus, notre approche place le contrôle du pH cytosolique et l'expansion des vacuoles au centre de l'adaptation des feuilles de tomate à ce stress et ouvre la voie à des études futures dans le domaine de la nutrition ammoniacale.

Mots clés: Vacuole ; métabolisme de l'azote ; métabolisme du carbone ; pH ; développement foliaire ; ammonium ; nitrate ; modélisation; nutrition minérale.

Cette thèse a été préparé dans **deux instituts de recherche:**

- Dans l'équipe « Métabolisme » de l'UMR 1332 BFP (Biologie du Fruit et Pathologie) de l'institut INRAE (Institut national de recherche pour l'agriculture, l'alimentation et l'environnement) à Bordeaux, France.
- Dans l'équipe de recherche NUMAPS (Nutrition MAnagment in Plant and Soil) du département de Biologie des Plantes et Écologie de la faculté de science et technique de l'université du pays basque UPV/EHU à Leioa, Espagne.

ABSTRACT

Ammonium (NH_4^+) is a nitrogen source of great interest in the context of sustainable agriculture. Its application in the field together with nitrification inhibitors has been extensively proven efficient to limit detrimental N losses compared to the use of nitrate (NO_3^-). NH_4^+ is a common intermediate involved in numerous metabolic routes. However, high NH_4^+ concentrations may lead to a stress situation provoking a set of symptoms collectively known as “ammonium syndrome” mainly characterized by growth retardation. Those symptoms are caused by a combination of, among others, a profound metabolic reprogramming, disruption of photosynthesis, pH deregulation and ion imbalance. Numerous studies have described the way plant copes to ammonium nutrition. However, the organ developmental stage has been generally neglected.

To fill in this gap, in the first chapter we first aimed studying how the metabolism is adapted in function of the leaf position in the vertical axis of the tomato plants (*Solanum lycopersicum*) grown with NH_4^+, NO_3^- or NH_4NO_3 supply. To do so, we dissected leaf biomass composition and metabolism through a complete analysis of metabolites, ions and enzyme activities. The results showed that C and N metabolic adjustment in function of the nitrogen source was more intense in older leaves compared to younger ones. Importantly, we propose a trade-off between NH_4^+ accumulation and assimilation to preserve young leaves from ammonium stress. Besides, NH_4^+-fed plants exhibited a rearrangement of carbon skeletons with a higher energy cost respect to plants supplied with NO_3^-. We explain such reallocation by the action of the biochemical pH-stat, to compensate the differential proton production that depends on the nitrogen form provided.

Ammonium nutrition may limit cell expansion, suggesting that the cellular processes involved would be altered. Among others, cell growth is largely dependent of the internal pressure exerted on the cell wall by the vacuole. However, the role of the vacuole in ammonium stress has been rarely addressed. In the second chapter, we evaluated the effect of ammonium stress on leaf development with a special focus on vacuole expansion and metabolism. To carry out this aim, we monitored the leaf development from its appearance until its complete expansion in plants grown under NH_4^+ or NO_3^- as unique nitrogen source. Cytological analysis

evidenced that the reduced cell expansion under ammonium nutrition was associated with smaller vacuole size. Besides, we reported an acidification of the vacuole of NH_4^+-fed plants compared to nitrate nutrition. Moreover, a model was built to predict the thermodynamic equilibrium of different soluble species across the tonoplast. The model was set up through an extensive reviewing of vacuolar transporters and integrated subcellular volumes, vacuolar electrochemical gradients and the formation of ionic complex in the vacuole to fit the subcellular concentration of ions, organic acids and sugars measured in the leaf. Further, predictions obtained with the model were cross validated with data from non-aqueous fractionation. Firstly, the entrance of solutes was higher in vacuoles of NO_3^--fed leaves but was not associated with higher vacuolar osmolarity likely because of the adjustment of the vacuolar volume. In this sense, we proposed that the lack of malate in cells of ammonium-fed leaves was central in the limitation of vacuolar expansion. Secondly, we conclude that the energy cost of solute transport into the vacuole is higher under NH_4^+ based nutrition because of the higher electrochemical gradient generated by the proton pumps across tonoplast.

This work highlights the importance of considering leaf phenological state when studying nitrogen metabolism. In addition, our integrated approach place cytosolic pH control and vacuole expansion in the center of tomato leaf adaptation to ammonium stress and pave the way for future studies in the field of ammonium nutrition.

Key words: Vacuole ; nitrogen metabolism; carbon metabolism ; pH ; leaf development ; ammonium ; nitrate ; modelling ; mineral nutrition

This work was carried out in **two research center:**

- In the “metabolism” team of the UMR 1332 BFP (Biology of Fruit and Pathology) laboratory in the INRAE institute (National Institute of Agricultural Research) center in Bordeaux, France.
- In the research team of NUMAPS (NUtrition MAnagment in Plant and Soil) from the department of Plant Biology and Ecology in the Faculty of Science and Technology of the University of the Basque Country UPV/EHU in Leioa, Spain.

RESUMEN

El amonio (NH_4^+) es una fuente de nitrógeno de gran interés en el contexto de la agricultura sostenible. Su aplicación en campo en combinación con inhibidores de la nitrificación ha demostrado ser efectiva para limitar las pérdidas de N en comparación con el uso de nitrato (NO_3^-). El NH_4^+ es un intermediario común de muchas vías metabólicas. Sin embargo, altas concentraciones pueden conducir a una situación estresante en la planta denominada "síndrome amoniacal", caracterizada por un crecimiento reducido. Estos síntomas son causados por la combinación de, entre otras cosas, la reprogramación metabólica, la alteración de la fotosíntesis, la desregulación del pH y el desequilibrio iónico. Muchos estudios han descrito cómo la planta se adapta a la nutrición amoniacal. Sin embargo, en éstos estudios el estadio de desarrollo de los órganos es un factor muy a menudo pasado por alto.

Así, en el primer capítulo de esta tesis estudiamos la adaptación metabólica de las hojas de plantas de tomate (*Solanum lycopersicum*) cultivadas en presencia de NH_4^+, NO_3^- o NH_4NO_3 de acuerdo con su posición/estadio de desarrollo en el eje vertical de la planta. El estudio de la composición y el metabolismo de la biomasa foliar a través de un análisis exhaustivo de los metabolitos, iones y actividades enzimáticas mostró que el ajuste del metabolismo de C y N a la fuente de nitrógeno proporcionada fue más intenso en las hojas más viejas en comparación con las más jóvenes. En particular, revelamos una solución de compromiso (*trade-off*) entre la acumulación de NH_4^+ libre y su asimilación para preservar las hojas jóvenes del estrés amoniacal. Además, las plantas crecidas con NH_4^+ presentaron una reorganización de los esqueletos de carbono con mayor costo energético respecto de las plantas crecidas con nitrato. Explicamos Este cambio en el metabolismo de carbono por la acción del sistema de pH-stat bioquímico, para compensar la producción diferencial de protones que es dependiente de la forma de nitrógeno proporcionada.

Se ha descrito que la nutrición amoniacal también puede limitar la expansión celular. Entre otros, el crecimiento celular depende en gran medida de la presión interna ejercida por la vacuola sobre la pared celular. Sin embargo, el impacto del estrés por amonio sobre la vacuola rara vez ha sido abordado. Así, en el segundo capítulo, evaluamos el efecto de la nutrición amoniacal en el desarrollo de las hojas centrándonos en la expansión y el metabolismo

vacuolar. Para ello, monitorizamos el desarrollo de una hoja desde su aparición hasta su completa expansión en plantas crecidas con NH_4^+ o NO_3^- como única fuente de N. En primer lugar, destacamos una menor expansión celular en hojas bajo nutrición amoniacal asociada con el menor tamaño de la vacuola así como con la mayor acidez vacuolar en comparación con la nutrición nítrica. Además, construimos un modelo matemático para predecir el equilibrio termodinámico de diferentes metabolitos a cada lado del tonoplasto. El modelo integra los volúmenes subcelulares, gradientes electroquímicos y la formación de complejos iónicos en la vacuola para predecir las concentraciones subcelulares de iones, ácidos orgánicos y azúcares medidos en la hoja. Además, estas predicciones se validaron bioquímicamente con datos obtenidos por fraccionamiento no acuoso. Finalmente, la estimación de los flujos de los metabolitos nos permitió observar que la deficiencia de malato en las células de las hojas de plantas crecidas con NH_4^+ es central en la limitación de la expansión vacuolar. Además, concluimos que el coste energético del transporte de solutos en la vacuola es mayor bajo la nutrición amoniacal debido al mayor gradiente electroquímico generado en ambos lados del tonoplasto.

Este trabajo destaca la importancia de considerar el estado fenológico de las hojas al estudiar el metabolismo del nitrógeno. Además, nuestros resultados colocan el control del pH citosólico y la expansión vacuolar en el centro de la adaptación de las hojas de tomate a este estrés y abre el camino a futuros estudios en el campo de la nutrición amoniacal.

Palabras claves: Vacuola ; metabolismo del nitrógeno ; metabolismo del carbono ; pH desarrollo foliar ; amonio ; nitrato; modelización; nutrición mineral

La tesis se desarrolló en **dos institutos de investigación diferentes:**

- En el grupo de investigación “Metabolismo” del Laboratorio de Biología de Frutas y Patología del centro INRAE en Burdeos, Francia.
- En el grupo de investigación NUMAPS (NUtrition Management in Plant and Soil) del Departamento Biología Vegetal y Ecología en la Facultad de Ciencia y Tecnología de la Universidad del País Vasco UPV/EHU en Leioa, España.

Abbreviations

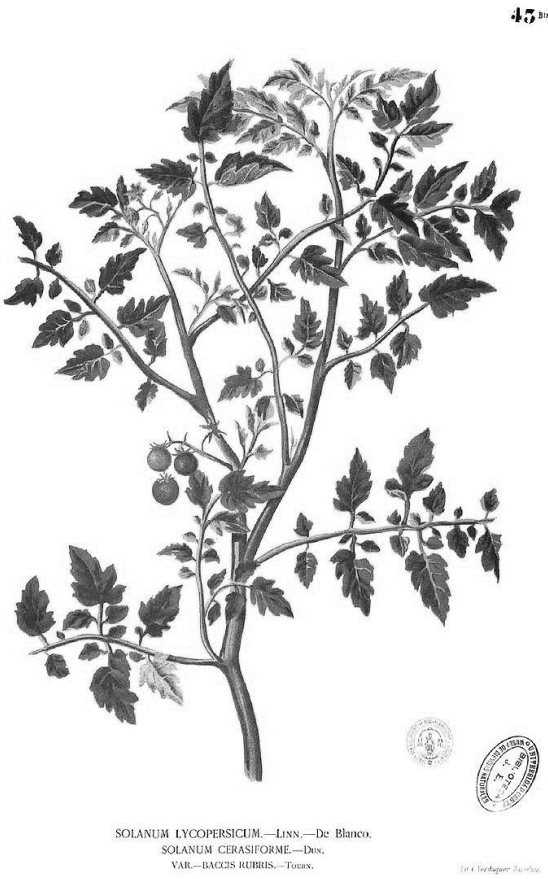

SOLANUM LYCOPERSICUM.—Linn.—De Blanco.
SOLANUM CERASIFORME.—Dun.
VAR.—BACCIS RUBRIS.—Tourn.

ABBREVIATIONS

AI: Acid invertase

AGR: Absolute growth rate

AOX. Alternative oxidase

As: Asparagine synthetase

BCECF: 2,7-bis-(2-carboxyethyl)-5-(and-6)-carboxyfluorescein

CLC: Chloride channel

DW: Dry weight

FW: Fresh weight

GABA: γ-aminobutyric acid

GABA-T: γ-aminobutyric acid transaminase

GAD: Glutamate decarboxylase

GDH: Glutamate dehydrogenase

GOGAT: Glutamate synthase

GS: Glutamine synthetase

HATS: High affinity transport system

H-experiment: Horizontal experiment

LATS: Low affinity transport system

LV: Lytic vacuole

ME: Malic enzyme

MDH: Malate dehydrogenase

NAF: Non-aqueous fractionation

NiR: Nitrite reductase

NR: Nitrate reductase

NRT: Nitrate transporter

NUE: Nitrogen use efficiency

PC: Pyruvate carboxylase

PCA: Principal component analysis

PEPC: Phosphoenol pyruvate carboxylase

PSM: Plant specific metabolite

PSV: Protein storage vacuole

RVR: Relative vacuole volume expansion

SLA: Specific leaf area

SP: Soluble product

TCA: Tricarboxylic acid

TIP: Tonoplast intrinsic proteins

V-ATPase: Vacuolar proton ATPase

V-experiment: Vertical experiment

V-PPase: Vacuolar proton pyrophosphatase

General introduction

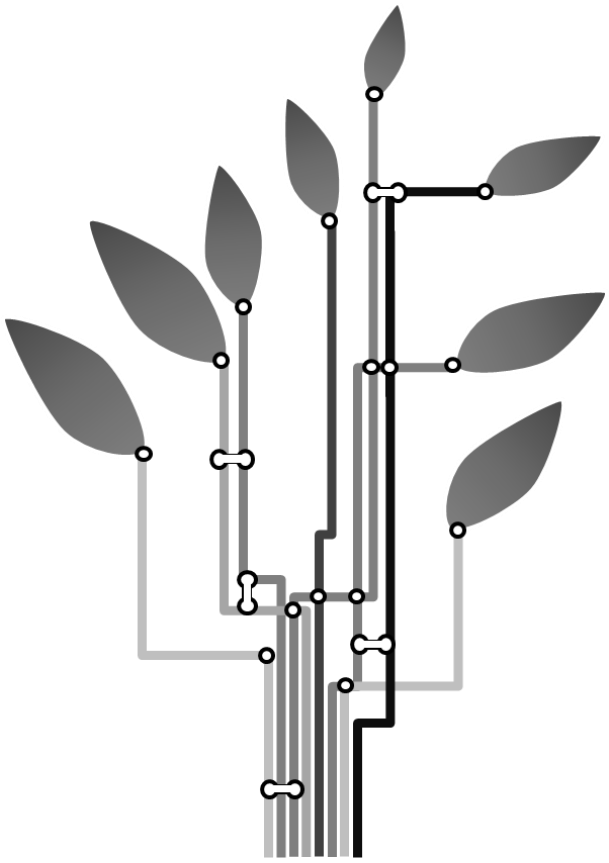

GENERAL INTRODUCTION

1 Nitrogen in agriculture

Plants produce organic matter from inorganic elements obtained from the soil and the atmosphere using the energy obtained from the light through photosynthesis. Apart from light, for optimal plant growth, adequate external factors consisting in water and 17 essential nutrients have to be gathered. C, O and H are absorbed from the air whereas the rest of the elements are obtained from the soil. The macronutrients, comprising N, P, K, Ca, S, Mg, Cl, are consumed in larger quantities than micronutrients composed of Fe, B, Cl, Mn, Zn, Cu, Mo and Ni. The deprivation of any of those essential elements will have deleterious effects on plant morphology and can even cause its death (Maillard *et al.*, 2016).

After C, O and H, N is the most important element since it forms part of a considerable variety of compounds as proteins, nucleic acids, coenzymes, chlorophyll (pyrolle rings) and secondary metabolites. N_2 is the main component of the atmosphere (78%). However, the triple covalent bound of N_2 makes it a very stable molecule and not directly available in this form. Indeed, most of plants have only access to soil inorganic (ammonium and nitrate) or organic N (amino acids, peptides and proteins) which range from 0.1% to 0.6% of soil mass in the top 15 cm of no fertilized soils (Cameron *et al.*, 2013). This makes N a scarce resource often limiting plant productivity in many natural ecosystems and in agriculture. Thus, farmers need to supplement the natural soil N reserve to match the plant needs for an optimum yield. That is why N, together with P and K, is a major component of fertilizers. Organic fertilizers can be synthetically manufactured as urea, derived from vegetable matter such as compost and crop residues, or obtained from animal residues such as manure. In inorganic fertilizers, N is commonly present in the form ammonium (NH_4^+) and nitrate (NO_3^-). They can be extracted from rocks but are mainly chemically synthetized (Holloway and Dahlgren, 2002). In fact, industrial N fixation comes from the Haber-Bosch process, consisting in the synthesis of ammonia (NH_3) from H_2 and N_2 under high pressure, with a high energy cost (Kandemir *et al.*, 2013). Then NH_3 can be oxidized to form NO_3^- through the Oswald process (Offermans *et al.*, 2006). Haber-Bosch process led to a global exponential increase in the amount of synthetic nitrogenous fertilizer applied to agriculture since 1950 to reach 93 millions of tons per year in

2017 (UN Food and Agricultural Organization, FAO). Consequently, it is estimated that more than 3.5 billion of people are fed using synthetic nitrogen fertilizers.

1.1 Nitrogen cycle

N is an incredible multifaceted element with diverse accessible forms. Indeed, it is present in many oxidation states (from +5 in NO_3^- to +3 in NH_4^+ or organic compounds) as well as in different organic and inorganic forms that are obtained from specific (bio)chemical reactions in atmosphere, terrestrial and marine ecosystems. The movement of N in different forms between the different reservoirs is called the N cycle (Figure 1).

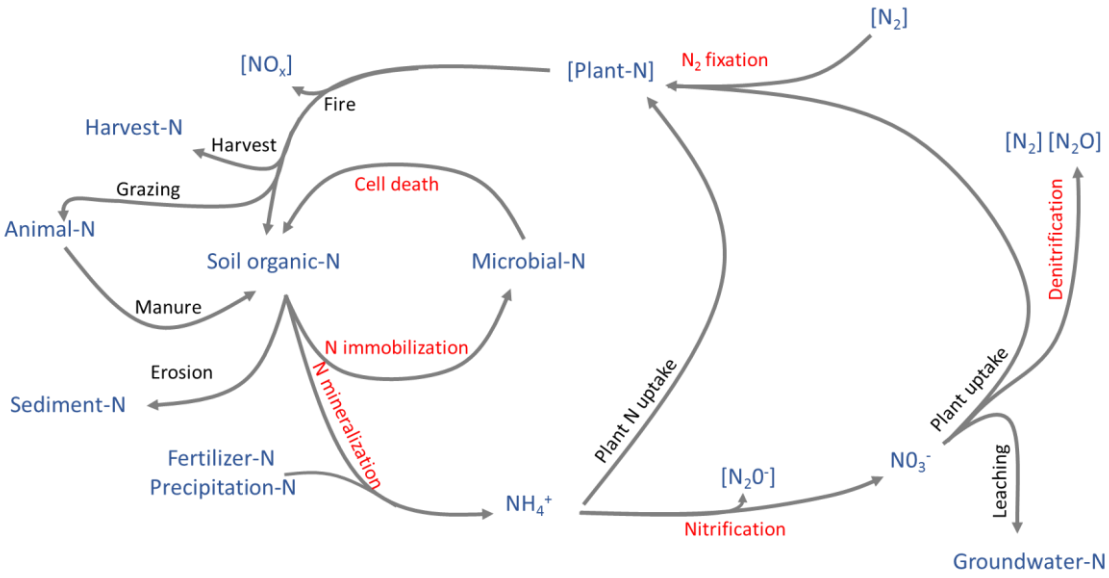

Figure 1: Schematic representation of the major processes of the terrestrial nitrogen cycle. Those processes mediated by soil microbes appear in red. Gases appear in brackets (modified diagram from Robertson and Groffman, (2015).

N cycle starts with the process known as "nitrogen fixation", which consists in the conversion of atmospheric N_2 to NH_3: artificially by chemical synthesis of fertilizer and naturally, during electric shocks (lightning) or mainly through the activity of nitrogen-fixing microorganisms. In fact, some bacteria from a subgroup of diazotroph are able to establish a symbiotic interaction with mainly legume plants (Fabaceae), and fix N_2 thanks to an enzyme complex called nitrogenase (Vessey *et al.*, 2005). Once fixed, NH_4^+ is transferred to microbial or plant biomass (immobilization and uptake, respectively), eventually finishing in the soil organic

matter pool after senescence, littering and decomposition. Also, microorganisms are involved in the reverse process called mineralization, which represents the breakdown of complex organic matter molecules into monomeric organic nitrogen compounds and inorganic NH_4^+ or NO_3^- available for plants (P. Schimel and Bennett, 2004). Further, in a process called nitrification, chemo-lithotrophic or heterotrophic microbes will use NH_4^+ to gain energy or structural monomers. This consists in a first anaerobic oxidation of NH_4^+ to hydroxylamine and nitrite (NO_2^-) by the action of ammonia-oxidizing bacteria and archaea. NO_2^- is then oxidized to nitrate (NO_3^-) by nitrite-oxidizing bacteria (NOB). Another notable process is the anaerobic ammonia oxidation (ANAMMOX), carried out by bacteria belonging to the Planctomycetes phylum, in which NH_4^+ is oxidized to N_2, using NO_2^- as acceptor of electrons (Kartal *et al.*, 2012).

Besides, a diverse group of prokaryotes can use NO_3^- as an alternative electron acceptor instead of O_2 and convert it to several gaseous nitrogen compounds (N_2, NO and N_2O) during stepwise reductions (Robertson and Groffman, 2015). This reduction process is called denitrification. Finally, there is assimilatory and dissimilatory NO_3^- reductions, both conducted by plant and bacteria, which consist in the conversion of NO_3^- or NO_2^- to NH_4^+ (Rutting *et al.*, 2011).

1.2 Nitrogen fertilization and its derived environmental problems

Human modification of the N cycle is profound: anthropogenic activity is more productive in N_2 fixation than all of the terrestrial natural processes combined. In fact, although most of this N has as primarily purpose to increase food production, an important part ends up in the environment. Gaseous losses and leaching are the main reasons why more than half of the N applied to agricultural land does not go towards its intended use; feeding plants. In this sense, N pollution has exceeded safe levels outlined in the planetary boundaries literature (Rockström *et al.*, 2009).

Firstly, the industrial synthesis of N-fertilizers, in form of NH_4^+, urea or NO_3^-, are based on a high energy-consuming process (around 1–2% of the world's energy supply) that contributes to greenhouse gases emission. Furthermore, with a pK_a = 9.25, NH_4^+ is the predominant N form in neutral and acidic soils. NH_4^+ is soluble and well retained in the soil. However, in

alkaline conditions NH_4^+ is deprotonated to NH_3, which is highly diffusible (Figure. 2). In fact, NH_3 is a colorless gas, which penetrates the biological membranes by diffusion or can be volatilized to the atmosphere (MacDonald et al. 1994; Sumner 1999; Schjoerring et al. 2002). In this line, in agriculture when N-fertilizers are applied in form of urea ($(NH_2)_2CO$), it can be rapidly hydrolyzed in the soil by urease enzyme to form NH_3 and be lost by volatilization. The NH_3 lost by volatilization, can subsequently return to the earth's surface through wet deposition (dissolved in rainwater) or dry deposition (attached to particulate matter) causing acidification. Also, the environmental impact of N_2O emission coming from denitrification and nitrifiers denitrification is drastic due to its global warming potential, 265 times higher than CO_2 (IPCC, 2014). In addition, N_2O has negative impact on ozone layer being one of the most important O_3 destroyer through NO formation (Stocker *et al.*, 2013). In fact, it is expected that N_2O emissions from agriculture will account for the 59% of total anthropogenic N_2O emissions in 2030 (Hu et al., 2015).

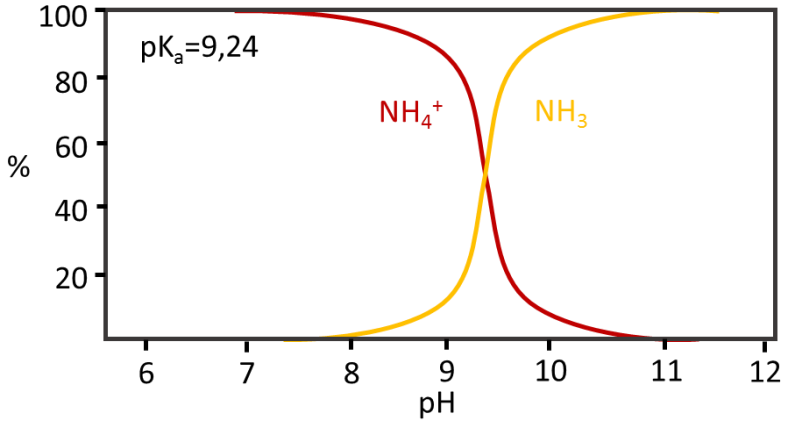

Figure 2: Schematic model of ammonium ion (NH_4^+) and neutral ammonia (NH_3) proportions in function of the pH. At acidic and neutral pHs, NH_4^+ is the most abundant species. However, NH_3 is dominant in highly alkaline solutions.

In addition, because of the application of N fertilizers in form of NO_3^- or because its formation during transformations during the N cycle, N can be lost through leaching, because of the NO_3^- high solubility and lack of adhesion to soil clays. NO_3^- leaching is more intense in function of the soil properties or seasonal rainfall affecting water flow.

NO_3^- leaching together with atmospheric N deposition can provoke an enrichment of minerals and nutrient of nutrients in aquatic ecosystems that is called eutrophication. A primary effect

of eutrophication is the excessive growth of algae that promulgates hypoxic conditions and restricts the development of other organisms that require oxygen (Bricker *et al.*, 2008). Moreover, it is worth stressing that climate change–induced precipitation changes would exacerbate the N contamination by eutrophication (Sinha *et al.*, 2017). Beside, from a more anthropocentric point of view, high NO_3^- content of drinking water or plant tissue can lead to sanitary issues. After ingestion, NO_3^- is converted to NO_2^- by gastrointestinal microflora leading to methemoglobinemia provoking an increment of free oxide radicals that predispose cells to irreversible damages. For this reason, NO_3^- content is rigorously regulated in human foodstuff and drinkable water (Gupta *et al.*, 2017).

To sum up, amount of mineral-N in the soil at any time can be described by the following N balance equation based on the N cycle:

$$N = Np + Nb + Nf + Nu + Nm - Npl - Ng - Ni - Nl - Ne$$

where *p* is precipitation deposition, *b* is biological fixation, *f* is fertilizer, *u* is urine and manure returns to the soil, *m* is mineralization and nitrification, *pl* is plant uptake (assimilation), *g* is gaseous losses (volatilization, denitrification and annamox oxidation), *i* is immobilization, *l* is leaching loss and *e* is erosion and surface runoff (adapted from Cameron *et al.* 2013).

1.3 Strategies to reduce Nitrogen losses from agriculture

By 2050, global population will reach to 9.2 billion of people. Estimation showed it would require an increase in food production of 50-100% and a concomitant increment of global N supply. Taking into account the high amount of energy needed for industrial production of N, as well as the deleterious effect of N losses on ecosystem and human health, improving nitrogen use efficiency (NUE) is considered as a key for building a more sustainable agriculture.(Kanter and Searchinger, 2018). NUE is understood as the fraction of applied N that is absorbed and used by the plant in terms of biomass or grain yield (Xu *et al.*, 2012).

Decisive practical methods exist to reduce N losses (gazes emissions and leaching). For instance, the laying of N fertilizers 3–5cm below the soil surface reduces the risk of NH_3 volatilization because it reduces the NH_3/NH_4^+ concentration at the soil surface. The timing of application is also important, by applying the correct amount in function of the crop needs.

The use of crop rotation and of the use of genotypes selected for their high NUE could also improve the use of the available nitrogen (Cameron *et al.*, 2013; Robertson and Groffman, 2015).

NUE is also improved by the use of polymer-coated fertilizers, which release nutrients by diffusion through a semi-permeable polymer membrane. Then, release rate is controlled by varying the composition and thickness of the coating. Furthermore, the application of N fertilizers together with urease and/or nitrification inhibitors can maintain N available in the soil for longer periods while decreasing the environmental impact of N losses. Urease inhibitors constrain the urease enzyme to limit NH_3 volatilization whereas nitrification inhibitors delay the conversion of NH_4^+ to NO_3^- to limit nitrogenous gas emissions and NO_3^- leaching. According to a meta-analysis of field studies, adding nitrification inhibitors to fertilizers or using polymer-coated fertilizers reduced N_2O emissions by an average of 38 and 35%, respectively, compared with conventional application of nitrogen (Hiroko *et al.*, 2010). Importantly, the efficiency of different type of nitrification inhibitor was consistent in diverse environmental conditions whereas polymer-coated fertilizers showed less systematic effectiveness. Hence, to mitigate N losses and concomitant N pollution, the use of nitrification inhibitors together with NH_4^+ based-fertilizers constitutes a good strategy.

2 Nitrogen metabolism

2.1 Nitrogen uptake

Most plant species are able to take up and assimilate NH_4^+, NO_3^-, urea, amino acids, peptides or even proteins as source of N. The preferred form in which N is taken up mostly depends on the genetic background inherited during plant adaptation to soil conditions (Sarasketa *et al.*, 2014). Plants adapted to low pH and reducing soils, such as found in mature forests or arctic tundra, tend to take up NH_4^+ or amino acids (Kronzucker *et al.*, 1997), whereas plants adapted to higher pH and more aerobic soils appear to prefer NO_3^- (reviewed in Maathuis 2009). To maximize N uptake efficiency and translocation within the plant under a wide range of extracellular nitrogen concentrations (NH_4^+ or NO_3^-), roots own transporters with different properties. There are two types of nitrate transport systems known as Low Affinity Transport Systems (LATS) and High Affinity Transport Systems (HATS). The non-saturable system LATS

allows transport in high external NO_3^- concentrations (> 0.5 mM) whereas the saturable system HATS provides a capacity for NO_3^- absorption at low external concentrations (< 0.5 mM) (reviewed in Masclaux-Daubresse et al. 2010). Importantly, most nitrate transporters (NRT) from NRT1 (previously named Nitrate transporter1/peptide transporter family (NPF); Neran et al., 2014) and NRT2 families, of low and high affinity respectively, are proton-coupled transporters, favoring the entrance of protons into the cytosol (Parker and Newstead, 2014). Conversely, entrance of NH_4^+ is mediated by AMT (Ammonium transporter) family transporters (Masclaux-Daubresse *et al.*, 2010). The nature of substrate translocation (NH_3 or NH_4^+) by the distinct members of this family is still a matter of controversy but it appears that NH_4^+ is deprotonated during its passage through the AMT transporters (Ariz *et al.*, 2018). In addition, several other distinct mechanisms are probably involved in the NH_3/ NH_4^+ transport process. In fact, they may be also transported via aquaporins, nonselective cation channels, potassium channels or simple osmotic diffusion (reviewed in Bittsánszky et al. 2015).

2.2 Nitrogen assimilation

The N assimilation process consists in reactions leading to the integration of N atoms in organic molecules of plants. When NO_3^- is use as N-source, its previous reduction to NH_4^+ is required before assimilation. Two catalytic NO_3^- reductions, taking place in both root and shoot, are carried out by the nitrate reductase (NR) and the nitrite reductase (N_iR). The NR is a molybdoprotein protein localized in the cytosol, that catalyzes the electron transfer from NADH/NAD(P)H until NO_3^- to obtain nitrite (NO_2^-). Then, NO_2^- is translocated by NO_2^- transporters into the plastid where it is reduced to NH_4^+ by N_iR. In this case, the electron donor is ferredoxin (reviewed in Britto and Kronzucker 2005; Masclaux-Daubresse *et al.* 2010). Thus, NH_4^+ originated either from direct absorption, NO_3^- reduction, or its release during photorespiration or amino acids catabolism is mainly assimilated into amino acids by the so-called GS/GOGAT cycle (Keys, 2006). Glutamine synthetase (GS) carries out the fixation of NH_4^+ to a molecule of glutamate to produce glutamine. This reaction consumes ATP. Afterwards, the amine group of the glutamine is transferred to 2-oxoglutarate by glutamine 2-oxoglutarate amino transferase (GOGAT) to produce two molecules of glutamate. Two major isoforms of GS exist: GS1, localized in the cytosol, is thought to be mainly involved in NH_4^+ recycling during particular developmental stages such as leaf senescence or grain filling,

and in glutamine synthesis for transport into the phloem sap (Martin *et al.*, 2006). GS2 localizes in the chloroplast and is involved in the primary assimilation of NH_4^+ coming from NO_3^- reduction and in the re-assimilation of NH_4^+ produced during photorespiration (Bernard and Dimah, 2009). Two GOGAT isoforms exist in plants. The ferredoxin-dependent GOGAT is present in the chloroplast of photosynthetic tissues and NADH-dependent GOGAT is located in plastids of non-photosynthetic tissues (reviewed in Masclaux-Daubresse et al. 2010).

Besides the GS/GOGAT cycle, asparagine synthetase (AS) and NADH–glutamate dehydrogenase (GDH) also cooperated in N assimilation. AS is a cytosolic enzyme that catalyzes the formation of asparagine (Asn) from aspartate by transferring the amide group of Gln with ATP consumption (Xu *et al.*, 2012). In addition, using azaserine inhibitor, ASN in tobacco has been suggested to be able to directly assimilate NH_4^+ in the dark (Masclaux-Daubresse et al., 2006). However, other authors have not observed such reaction, among others, in tomato (Vega-Mas et al., 2019) and wheat (Vega-Mas et al., 2019). Although controversial, GDH, which is located in the mitochondria, is a reversible enzyme that appears to be able of incorporating NH_4^+ into 2-oxoglutarate to form glutamate in response to high levels of NH_4^+ under stress conditions (Vega-Mas *et al.*, 2019). However, its low affinity for NH_4^+ (Km of 5.8 mM) suggests that GDH primarily acts in its deaminating sense in physiological conditions. In this manner, the main function of GDH would be to support plant metabolism under C-limitation providing 2-oxoglutarate (Dubois *et al.*, 2003; Xu *et al.*, 2012). For instance, GDH activity was shown to be involved in the process of leaf senescence, which consists in the coordinated recycling of nitrogen and carbon, to be rapidly remobilized to sustain the growth of young developing tissues (Masclaux *et al.*, 2000).

N assimilation is an energetically costly process, requiring a continuous and adequate amount of NAD(P)H to drive the previous reductions of NO_3^- to NH_4^+, as well as ATP, which is essential in the integration of NH_4^+ and produce amino acids. On the other hand, it is well established that a significant amount of fixed C is required to provide the C skeletons needed for NH_4^+assimilation (Nunes-nesi *et al.*, 2010). Hence, the activity of N-assimilation machinery means that products from photosynthesis must be partitioned between the respiration pathway and the synthesis of amino acids. In this sense, TCA cycle is central for providing 2-oxoglutarate, a carbon skeleton used by the GS/GOGAT cycle for glutamate synthesis. The TCA cycle comprises a set of eight enzymes in the mitochondrial matrix that couple the

product of oxidation of pyruvate and oxaloacetate (generated in the cytosol) to CO_2 with the generation of NADH during oxidations by the respiratory chain. Then, this reductive power is converted to ATP, yielding 15 ATP equivalents per pyruvate molecule (Fernie *et al.*, 2004). However, pyruvate dehydrogenase introduces two molecules of C to the TCA cycle, which in return releases two molecules of CO_2. In this manner, the N assimilation drainage of carbon from the TCA cycle must be compensated via the so-called anaplerotic reactions, which allow net introduction of C (Nunes-nesi *et al.*, 2010; Setién *et al.*, 2014; Vega-Mas *et al.*, 2015). Phosphoenol pyruvate carboxylase (PEPC) replenishes the cycle with the transformation of phosphoenol pyruvate to oxaloacetate consuming HCO_3^- (Leary *et al.*, 2011). Further, NAD(H)-dependent malate dehydrogenase (MDH) catalyses the reversible reduction of oxaloacetate to malate consuming NADH (Fernie *et al.*, 2004). In another way, the pyruvate carboxylase (PC) re-supplies the TCA cycle with oxaloacetate from pyruvate. Finally the malic enzyme (ME) makes possible the return of malate to pyruvate with the emission of HCO_3^- and production of reducing power in form of NADPH for NADP-dependent ME (plastidic and cytosolic) or NADH for NAD-dependent ME (mitochondria)(Sun *et al.*, 2019). The trade-off existing between N-assimilation and energy metabolism for the use of carbon-skeletons is obviously highly regulated. In this sense, the availability of substrate and products of those different reactions are involved in regulation of gene expression and regulation of enzyme activities to coordinate N and C metabolism. For instance, PEPC activity is regulated by the Gln/Glu ratio, which is dependent of GS activity. In this manner, PEPC orchestrates the synchronization of C entrance in the TCA cycle and assimilation (Britto and Kronzucker 2005).

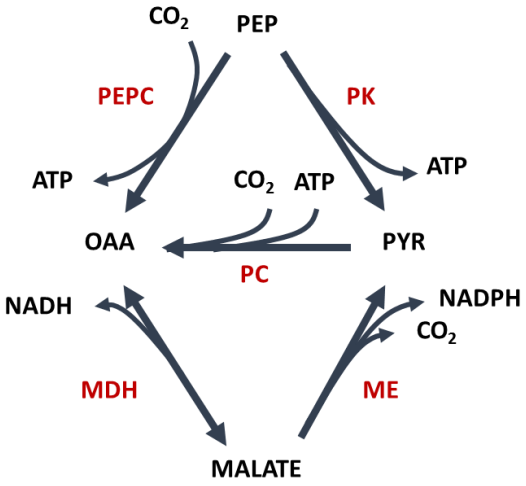

Figure 3: Anaplerotic reactions that replenish TCA cycle with oxaloacetate and malate from phosphoenol pyruvate and pyruvate. Enzymes are indicated in red. Abbreviations: PEPC, phosphoenol pyruvate carboxylase; PK, pyruvate kinase; ME, malic enzyme; MDH, malate dehydrogenase; PC, pyruvate carboxylase.

2.3 Ammonium paradox

The use of NH_4^+-based fertilizers combined with nitrification inhibitors, instead of NO_3^-based ones, is a relevant strategy to mitigate the negative environmental impact of N fertilization. In addition, in theory, the use of NH_4^+ would have a lower energetic cost for the plant since there is no need of previous reduction steps before its assimilation. Indeed, NO_3^- reduction mediated by NR and NiR consumes one NADPH and the transfer of 6 electrons (six reduced ferredoxins) which was estimated at the level of the plant to represent 12-26% of the reductant generated during photosynthesis (Noctor and Foyer, 1998; Patterson *et al.*, 2010). Paradoxically, although NH_4^+ is a fundamental substrate for biomolecule synthesis, when present in high concentrations, notably when applied as sole source of N, most plant species develop stress symptoms (Britto and Kronzucker, 2002). In general, sensitivity to NH_4^+ is observed in many biological systems, including human for which excessive ammonia levels could be involved in neurological disorders such as Alzheimer disease (Adlimoghaddam *et al.*, 2016).

In plants, the degree of tolerance/sensitivity towards ammonium stress is highly variable, mainly depending of the species as well as the environmental conditions of growth. Nevertheless, ammonium nutrition-related stress in plants is usually accompanied by a cortege of indicators characteristic of the so-called “ammonium syndrome”. Among others, these symptoms include leaf chlorosis, decreasing of root : shoot ratio, inhibition of lateral roots production, and more generally, growth retardation (Walch-Liu *et al.*, 2000; Britto and Kronzucker, 2002). The understanding of ammonium stress has revealed that a single mechanism that could fully explain its deleterious effects in plants does not exist. For this reason, ammonium syndrome is considered as a multifactorial stress.

Even if NH_4^+ can originate from photorespiration or amino acids catabolism (Keys, 2006), when external concentration of NH_4^+ is high, passive or active diffusion as well as active transporter favor its massive translocation into the cell. Because of the potential cytotoxicity of NH_4^+ (Choudhary et al., 2016) or provoking damages to the photosynthetic apparatus (Zhu *et al.*, 2000), it was often assumed that NH_4^+ concentration in the cytosol is maintained at very low level. This is despite the relatively high cytosolic concentrations, in the millimolar range, reported for rice and barley by using a positron tracing technique (Britto *et al.*, 2001), or by NMR in maize (Lee & Ratcliff, 1991). To prevent its over-accumulation, NH_4^+ can be

transformed to organic molecules through the stimulation of N assimilation which happens mainly in the root and to a lesser extent in the shoot (Setién *et al*., 2014 ,Sarasketa *et al*., 2016). Notably, favoring the synthesis of amino acids of lower C/N ratio as well as increasing protein content. Nevertheless, this enhancement of N-assimilation has a high carbon demand since, as stated, the integration of NH_4^+ via the GS/GOGAT cycle needs the input of 2-oxoglutarate (Ariz *et al.*, 2012). Interestingly, a recent study with Arabidopsis mutants for GS2 showed that the reduction of assimilation of NH_4^+ in the chloroplast could alleviate ammonium stress symptoms regardless the extremely high accumulation of free NH_4^+ (Hachiya *et al.*, 2019).

Another consequence of ammonium nutrition is ionic disequilibrium mainly resulting from the decreased uptake of essential cations such as K^+, Ca^{2+} and Mg^{2+} (Lang and Kaiser, 1994; Hachiya *et al.,* 2012). For instance, it has been shown in *A.thaliana* and barley that NH_4^+ is in competition with K^+ entrance into the cell via K^+ transporters and non-selective cation channels of the plasma membrane (Spalding *et al.*, 1999; Szczerba *et al.*, 2008; Hoopen *et al.*, 2010). Consequently to the decline of tissue level of cations, there is an increase of inorganic anions mainly phosphate, chloride and sulfate (Kirkby and Mengel, 1967; Van Beusichem *et al.*, 1988).

At the same time, NH_4^+ uptake into the cell is coupled with proton extrusion, which leads to the acidification of the external medium such as the rhizosphere or the apoplast (Mengel *et al.*, 1994; Escobar *et al.*, 2006). Conversely, the uptake of NO_3^- promotes the alkalinization of the external medium (Van Beusichem *et al.*, 1988). The resulting decrease of external pH under ammonium nutrition is often considered as one of the fundamental causes of ammonium stress. Indeed, acidic-tolerant plants are often better adapted to ammonium stress and the deleterious effects of ammonium nutrition are often alleviated when growth solutions are pH-buffered (Li *et al.*, 2014).

The disruption of the hormonal balance under NH_4^+ supply has been also proposed as a cause underlying ammonium stress. Plant hormones, also known as phytohormones, are signal molecules produced within the plant that regulate growth and development. In this sense, consistent findings showed that ammonium stress is associated with perturbations of hormone levels, including ethylene, abscisic acid, auxin, and cytokinins (Barker and Corey, 1991; Cao *et al.*, 1993; Walch-Liu *et al.*, 2000; Li *et al.*, 2014). In accordance, cytokinins, which

are involved in proliferation and differentiation of plant cells, have been sometimes reported at lower level when NH_4^+ is the sole source of N such as in tobacco (Walch-Liu *et al.*, 2000). In this line of evidence, NO_3^- is a positive regulator of cytokinin synthesis (Sakakibara *et al.*, 2006) and thus, its near absence in plants fed with NH_4^+ would be critical for maintaining sufficient levels of cytokinins to mediate normal tissue morphogenesis. This positive effect that have NO_3^- on cytokinin signaling has been put forward as a reason underlying the observed beneficial role of small amounts of NO_3^- in the alleviation of ammonium stress symptoms (Hachiya *et al.*, 2012).

Furthermore, another cause of ammonium stress would be a red-ox imbalance in plant cells likely because the electron-consuming reaction catalyzed by NR and NiR do not take place when only NH_4^+ is supplied. In fact, a reductive stress was reported by Podgorska et al, (2013), associated to high NADH/NAD^+ and NADPH/$NADP^+$ ratios in leaves of Arabidopsis fed with NH_4^+. The authors associated this response to an excessive mitochondrial reactive oxygen species (ROS) production. In this sense, NO_3^- and NH_4^+ have strong and opposing effects on the expression and activity of several respiratory family proteins such as type II NAD(P)H dehydrogenases or the alternative oxidases (AOXs), involved in the regulation of the respiratory ATP production (Escobar *et al.*, 2006). Hence, red-ox imbalance and AOX deregulation caused by the high concentration of NH_4^+ may result in oxidative stress.

Finally, the control of several environmental factors can also alleviate ammonium stress. As stated above, it is known that controlling external pH medium is a key factor for mitigating ammonium toxicity (Sarasketa *et al.*, 2016*a*). In addition, the carbon starvation symptom relative to the enhancement of assimilation during NH_4^+ nutrition can be partially relieved with the supply of extra C such as with increasing atmospheric CO_2 concentration (Vega-Mas *et al.*, 2015), with higher light intensity (Ariz *et al.*, 2012) or with the external addition of organic (Magalhaes *et al.*, 1992) and inorganic carbon (Roosta and Schjoerring, 2007). Increasing cation concentration in the root medium (Spalding *et al.*, 1999) to inhibit the acquisition of NH_4^+ by low affinity transporters (Szczerba *et al.*, 2008) is also relevant to alleviate ammonium stress. Moreover, the use of signaling molecules such as ABA, auxins (Li *et al.*, 2014) or little concentration of NO_3^- (Hachiya *et al.*, 2012) have also been linked to the alleviation of ammonium nutrition toxicity. However, most of these strategies remain complicated to be applied in the field.

3 pH and nitrogen

Most plant species are adapted to moderately low-pH in the external medium and the sharp NH_4^+-related acidification of the extracellular medium by proton extrusion (Van Beusichem *et al.*, 1988) may provoke acidic stress and thus, have an enormous impact on cell structure and function. In fact, when NH_4^+ is exclusively provided, decreases of half pH unit in apoplast (Mengel *et al.*, 1994) and several pH units in rhizosphere (Escobar *et al.*, 2006; Hu *et al.*, 2019) have been reported. For instance, such acidic stress in roots leads to disorders in the plasma membrane, reduction of cell elongation and appearance of fissures between cells (Koyama *et al.*, 1995). On the contrary, NO_3^- promotes the alkalinization of the external medium. The form of N taken up by the plant is also of special importance for intracellular pH homeostasis since N assimilation is producer or consumer of H^+ (Raven and Smith, 1976). Indeed, the need of NH_3 as substrate of GS/GOGAT cycle promotes the production of OH^- when NO_3^- is the unique source of nitrogen:

$$NO_3^- + 8H^+ + 8e^- \rightarrow NH_3 + 2H_2O + OH^-$$

Whereas direct NH_4^+ uptake leads to H^+ production:

$$NH_4^+ \rightarrow NH_3 + H^+$$

Nevertheless, this extreme difference in behavior between NO_3^- and NH_4^+ assimilation for OH^- or H^+ production is qualitative, specifically because this model does not account for the H^+ transport accompanying inorganic N transport. In this sense, the uptake of NO_3^- is a cytosol-acidifying process and conversely, NH_4^+ uptake is a cytosol-alkalinizing process (Britto and Kronzucker 2005). Then, whole processes of uptake and assimilation of different forms of inorganic nitrogen would be neutral for cytosolic pH. However, it is worth stressing that the uptake of inorganic N is not immediately followed by its assimilation since $NH_4^+$and NO_3^- can accumulate in plant cell. In between, cytosol acidification or alkalization relative to transport, would be compensated and neutralized. Altogether, various studies show that ammonium nutrition produces more H^+s inside cells in comparison to nitrate nutrition (Van Beusichem *et al.*, 1988; Carroll *et al.*, 1994; Mengel *et al.*, 1994; Hachiya *et al.*, 2019; Hu *et al.*, 2019).

Importantly, despite cytosolic pH is sensitive to those fluctuations, the complex interaction between passive and active mechanisms of pH regulation makes cytosolic pH to be extremely stable. Three major processes contribute to cytosolic pH control: 1. Physico-chemical buffering, 2. Transmembrane fluxes of H^+s or biophysical pH-stat and, 3. Biochemical pH-stat.

3.1 Physico-chemical buffering

Physico-chemical buffering is based on the dissociation and association of H^+ or OH^- with compounds already present in the cell. Since it is a passive process which is not directly modulated, the input of energy by the plant is not necessary (Smith and Raven, 1979). The main examples are the dissociation of $H_2PO_4^-$ to HPO_4^- and H^+ (pK_a = 7.2) and that of H_2CO_3 to HCO_3^- and H^+ (pK_a =6.4). Those fast reactions are destined to compensate moderate and sudden variations of pH. Nevertheless, this neutralization manner is limited to the buffer capacity of the cytoplasm varying between 20 and 100 mM per unit of pH in function of plant species (Raven and Smith, 1976; Kurkdjian and Guern, 1989) and would not be effective for countering long term production of protons. As a reminder, buffer capacity is defined as the number of moles of an acid or base necessary to change the pH of a solution by 1.

3.2 Transmembrane fluxes of H^+s

The biophysical pH-stat is constituted by the membrane transport systems that are involved in the regulation of cytosolic pH. pH translocation of weak acids and bases in the cytosol, as well as H^+-co-transporters such as NHX-type Na^+/H^+ antiporters (Bassil *et al.*, 2011) play critical role in maintaining cellular pH homeostasis. However, biophysical pH-stat regulation is mainly controlled by the active transport of proton through pumping proteins. Three type of proton pumps exist in plants: 1. The H^+-ATPase localized to the plasma membrane that drives H^+ efflux from cytosol to acidify the apoplast/extracellular space whereas; 2. The vacuolar ATPase (V-ATPase) and; 3. vacuolar pyrophosphorylase (V-PPase) localized in the tonoplast to acidify the vacuole space (reviewed in Martinoia, Maeshima, and Neuhaus, 2007 and Schubert, 1997). Pumping H^+s, is an energy consuming process that maintain an electro-chemical gradient across membranes (ΔpH and ΔΨ, pH and electric potential difference across the tonoplast, respectively), which also energizes the passive transport and H^+-

cotransport of various molecules across the membranes. These pump activities are strongly dependent of changes in ΔpH as well as ΔΨ to maintain the cytosolic pH in a physiological range. Indeed, the acidification of the cytosol activates H^+-ATPases since their optimum cytosolic pH is around 6.3 (Schubert, 1997). Similarly, a patch clamp study revealed that imposed acidity in the cytosol enhanced by 100 fold the V-ATPase activity, whereas vacuole acidification had relative little effect (Dreyer *et al.*, 2012). To conclude, the buffering capacity of the biophysical pH-stat is an efficient mechanism for long term regulations of cytosolic pH, but finds its limit in the volume of both apoplast and vacuole and their capacity to be acidified without causing deleterious effects for the cell.

Overall, since NH_4^+ and NO_3^- nutrition lead to pH alterations in cell´s cytosol,it is not surprising that the biophysical pH-stat is differentially regulated by the N-form. For instance, it is known that NO_3^- supply decreases the activity of H^+-ATPases of the plasma membrane (Schubert, 1997) and indeed, it is sometimes used in electrophysiology methods to inhibit the electro-chemical gradient across the tonoplast (Oleski *et al.*, 1987). Similarly, Alvarez-pizarro, Miranda, and Mesquita (2018) showed a fine gene expression regulation of proton pumps in sorghum roots when varying N-sources. They particularly suggested a possible transcriptional control of the sorghum *SbVHA2* V-ATPase by NH_4^+.

3.3 Biochemical pH-stat

The biochemical pH-stat is also a mechanism for controlling the pH homeostasis in plant cells. It consists in a diverse set of carboxylating and decarboxylating enzymes with different optimum pH, which work in coordination without depending on the hydrolysis of ATP. A popular model is the one of Davies, developed in the 70's, where the pH-dependent enzymes PEPC and ME orchestrate the consumption and production of cytosolic malate (Figure 4): when cytosolic pH changes to acidic values, ME, with its optimum in the acidic range, decarboxylates more malate and then consumes H^+s to shift towards the physiological pH. Conversely, when cytosol turns alkaline, the H^+ consuming activity of ME decreases whereas the PEPC, with its optimum of activity in the alkaline range, produces more oxaloacetate, which is then rapidly transformed in malate by the MDH. Those reactions produce H^+s and contribute to the readjustment of the cytosolic pH (Davies *et al.* 1974). Despite the model of

Davies suffered some revisions, mainly by being integrated with alternative pathways of glycolysis and respiration (also consumer and producer of protons), the biochemical pH-stat is not under debate (Sakano, 1998, 2001). Moreover, another pH-stat pathway involved in pH regulation is the GABA shunt. It is constituted of glutamate decarboxylase (GAD), and γ-aminobutyric acid transaminase (GABA-T) enzyme, which lead to the production of GABA through H^+ consuming reactions (Carroll *et al.*, 1994; Sawaki *et al.*, 2009).

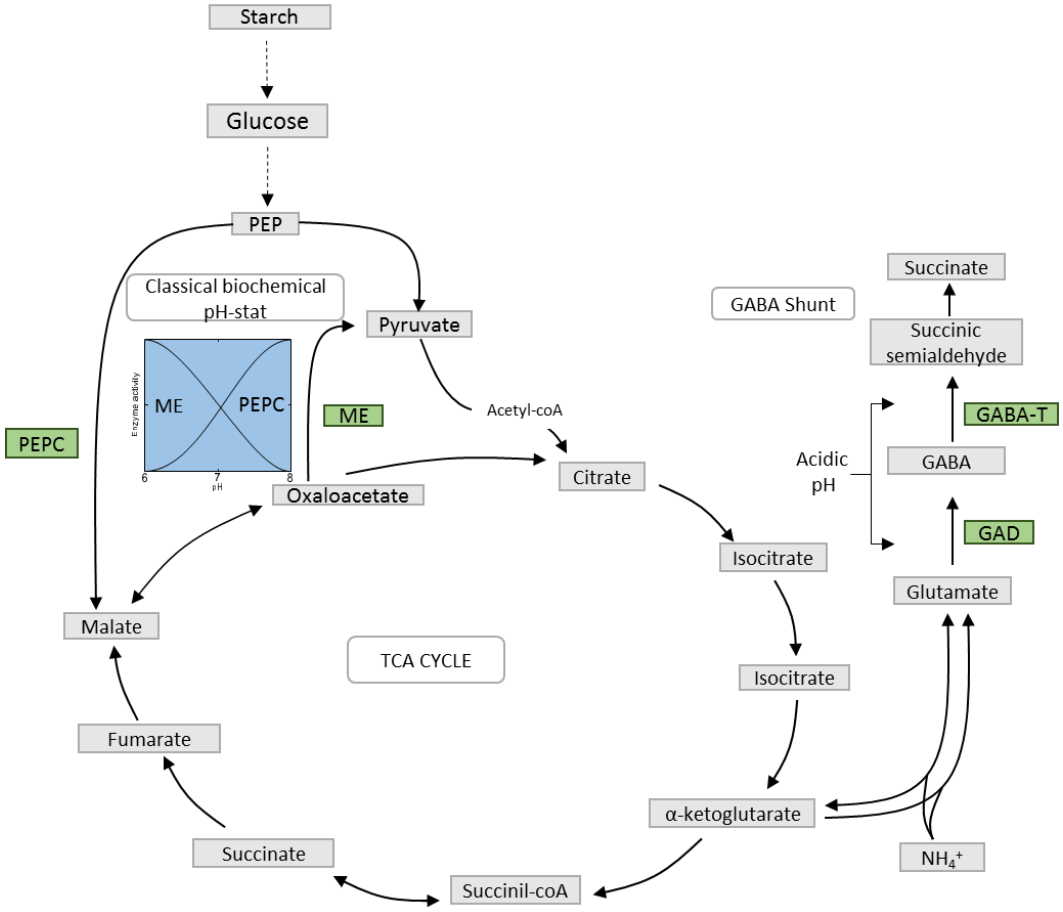

Figure 4: The structure and function of the different components of the biochemical pH-stat in plant cell. Grey boxes refer to metabolites and green boxes refer to enzymes involved in the regulation of the biochemical pH-stat. The classical biochemical pH-stat is based on the regulation of the activity of PEPC and ME in function of the cytosolic pH (blue figure).The GABA shunt, also involved in the pH-stat is based on the activity of GABA-T and GAD enzymes (part at the right). ME is proton producer whereas PEPC, GABA-T and GAD are proton consumers.

Given organic acid metabolism is central to regulate pH, it is worth stressing that the vacuole could carry a role in pH homeostasis since most of malate, a major organic acid in

concentration, is localized to the vacuole space (reviewed in Martinoia et *al.* 2007). In the same way, previous works proposed that the strong accumulation of organic acids when NO_3^- instead of NH_4^+ is provided, could be associated to the pH regulation of enzymes of the biochemical pH-stat (Van Beusichem *et al.*, 1988; Pasqualini *et al.*, 2001; Coleto *et al.*, 2019). Finally, an obvious interaction between N metabolism and pH control would be the synthesis of GABA promoted by the GABA shunt in order to prevent cytosolic acidification (Carroll *et al.*, 1994).

4 Plant vacuole

The term “vacuole” was first introduced by the French biologist Felix Dujardin (1841) when he described blank intracellular spaces of protozoan contractile vesicles. Similar empty structures had long been observed in vegetal tissues and rapidly, plant scientist used this term for the large and central vacuole of plants. Since then, in part through the appearance of new technologies, the vacuoles have not ceased to surprise and now it is known that they carry out a great number of essential functions for the cell. Microscopy, together with the use of neutral red staining, allowed concluding at the end of 19th century that vacuoles are acidic compartments surrounded by a membrane called “tonoplast”. However, the detail composition and functions were hampered by the lack of methods to isolate this extremely fragile organelle. In fact, in the middle 70’s, Wagner and Siegelman (1975) set up a gentle osmotic rupture of the protoplasts to release intact vacuoles ready for study. This allowed the analysis of most lytic enzymes and vacuolar constituents present in almost all plant species. In addition, it was further showed that vacuoles also ensure the role of short and long-term store compartment for toxic and physiological compounds. One last important boost for vacuole research occurred with the possibility to isolate membranes into vesicles to study the transport mechanisms through the tonoplast (Blumwald and Poole, 1985).

Obviously, vacuoles are no longer considered as the empty space described by Felix Dujardin. Indeed, through highly regulated active transport systems, vacuoles carry, among others, roles in the maintenance of cell homeostasis, in the storage and biosynthesis of metabolites, and are fundamental in plant cell expansion. The scope of this part is to give a short overview

of the different knowledge accumulated on vacuole formation and its roles with a special interest on the mechanisms monitoring its enlargement.

4.1 Vacuole genesis in plant and their classification

Despite some genesis theories try to explain the formation of the vacuole, the mechanisms are still not completely elucidated. Biosynthetic pathways leading to genesis of vacuole involve: 1. The fusion of vesicles derived from theGolgi apparatus or the endoplasmic-reticulum that merge to form a small vacuole (Matile and Moor, 1968); 2. Endocytosis of substances from plasma membrane to form a prevacuolar compartment (Cui *et al.*, 2016) or; 3. Autophagy, a process where parts of the cytoplasm that are intended to be degraded are enclosed into membranes from the Golgi apparatus or the endoplasmic reticulum. The degradation occurs later, after transportation to lysosomes or vacuoles (Yano *et al.*, 2016).

Two types of vacuoles exist in plants and they are classified by the presence/lack of specific enzymes. The best characterized, because most plant cells contain one or more, is the large lytic vacuole (LV) which exhibits an acidic pH together with a cortege of degradation enzymes. LVs carry mainly the function of turgor generation since they stored most of the inorganic and organic (ions) compounds including toxic ones. Less studied, the protein storage vacuole (PSV) is much smaller than LV and is heterogeneously present in different plant tissues of different species. Although PSVs also have a lytic activity they mainly accumulate large amounts of defense and storage proteins (reviewed in Isayenkov, Isner, and Maathuis 2010). In this study we will further focus on the large and central LV.

4.2 A compartment for storage with multifaceted roles

4.2.1 Cell detoxification

Vacuole was long considered has a “rubbish dump” for the cell as it accumulates numerous compounds at concentrations that would impair cytosol metabolism and enzyme functionalities. Indeed, vacuolar sequestration is one of the main mechanism by which plants control toxic material abundance as it is the case with cadmium and arsenic (Zhang *et al.*, 2018). Similarly, in *Salicornia bigelovii* the ability to remove sodium from the cytosol to the vacuole was associated to salt-tolerance adaptations (Parks *et al.*, 2002). Another example is

illustrated by the lipophilic xenobiotics, which are exogenous toxins such as herbicides. After entrance into the cell, a process of degradation starts in the cytosol by making the products more polar through enzymatic reactions and finishes with their compartmentalization inside the vacuole to be hydrolyzed (Coleman and Randall, 1997).

4.2.2 Regulation of cytosol homeostasis

In plant cells, vacuoles are the major reservoir for most organic and inorganic soluble compounds excluding proteins, and together with tonoplast transporters, they constitute a central buffering system for maintaining cytosol homeostasis. As already seen above, vacuoles are involved in pH homeostasis through the biophysical pH-stat, but also have an influence on the biochemical pH-stat since most of organic acids are stored inside the vacuole. Heavy metal elements such as zinc or iron are essential micronutrients for plant metabolic reactions, but their presence in the cytosol is regulated by sequestration with specific transporters since they become toxic at high cytosolic concentration (reviewed in Martinoia *et al*. 2007). Similarly, macro-elements such as K^+, Ca^{2+}, Cl^-, Mg^{2+} or PO_4^{2-} are crucial for molecule synthesis, osmotic regulation, pH regulation and are also involved in intracellular signaling and enzyme regulation. In this sense, the maintenance of their cytosolic concentration is finely regulated. Given that a large proportion of cellular ions localize into the vacuole, it constitutes an indispensable organelle for their maintenance and/or signaling events by their release in the cytosol (reviewed in Shitan and Yazaki, 2013).

4.2.3 Metabolism

Vacuole also takes part in carbon metabolism not only by sequestering most sugars and organic acids but also through the synthesis or degradation of sugar polymers. For example, fructans are water soluble carbohydrates with polymerization grades of 3 to 50 fructose molecules, and their synthesis takes place in the vacuole (Darwen and John, 1989). In parallel, sucrose, a pivotal metabolite in plant cells, can be metabolized in the cytosol or transported to the vacuole, where it is stored, integrated into fructans or hydrolyzed by vacuolar invertase (Beauvoit *et al.*, 2014).

4.2.4 Cell expansion

Plant growth and development depends on anisotropic cell expansion. Biophysically, plant cell expansion requires three main factors: 1) a continuous deposition of cell wall polymers, to prevent thinning during elongation; 2) the uptake of water into the cells to increase volume and maintain turgor; and 3) the accumulation of solutes inside the cell and further into the vacuole, to drive the entrance of water through osmosis.

a. Vacuole water uptake

Vacuole expansion, mainly driven by water uptake, typically results in a 10-20 fold increase of the cell volume. If an equivalent quantity of water would be accumulated in the cytosol, such dilution would disrupt numerous reactions catalyzed by the cytosolic enzymes and would be harmful for the plant. Accordingly, most of water and solutes entering in the cell are destined to the large central vacuole. As consequence, the vacuole : cytosol volume ratio increases during cell expansion. Whereas cytosol volume is almost stable, vacuolar volume increase many folds, concomitantly pushing against the cell wall to promote cell elongation.

Entrance of water follows rapidly the transport of osmotically active molecules across the tonoplast. Even if passive diffusion occurs, rapid adjustment of water status can only be explained by water channels facilitator called aquaporins, presents in the plasma membrane (PIPs) and the tonoplast (TIPs). Interestingly, studies conducted on isolated vacuoles (Morillon and Lassalles, 1999) and plasma membrane vesicles (Maurel *et al.*, 1997) showed a very high water permeability of the tonoplast (>200 µm s^{-1}) contrasting with a much lower permeability of the plasma membrane (<30 µm s^{-1}). First, this difference raises the plasma membrane as the limiting factor for entrance of water into the cell. Secondly, the fact that the vacuole is able to take up or release water more rapidly than the cytosol makes vacuolar water readily available to regulate cell water homeostasis (Tyerman *et al.*, 2002).

b. Transport of solute

Mediated by transporters

Once inside the cell, solutes can cross the tonoplast. Most of the driving force for solute transport comes from the electrochemical gradient (ΔpH and ΔΨ) between the two

compartments. Those gradients are generated by the activity of H^+-pumps (V-ATPase and V-PPase) that consume ATP as already seen in the previous "biophysical pH-stat" section. Typically a more acidic pH is established in the vacuole but the ΔΨ of tonoplast remains lower (0-30mV) (Oleski *et al.*, 1987; Cuin *et al.*, 2003) when comparing with that of the plasma membrane (100-200mV) (Carden *et al.*, 2003; Cuin *et al.*, 2003). Hence, the transport and accumulation of solutes involves primary and secondary transport energized directly by ATP or indirectly by ΔpH and ΔΨ, respectively. Here, I will briefly summarize the transport pathways of the main solutes accumulated into the vacuole, namely organic acids, inorganic ions and different sugars as well as plant specialized metabolites (PSMs).

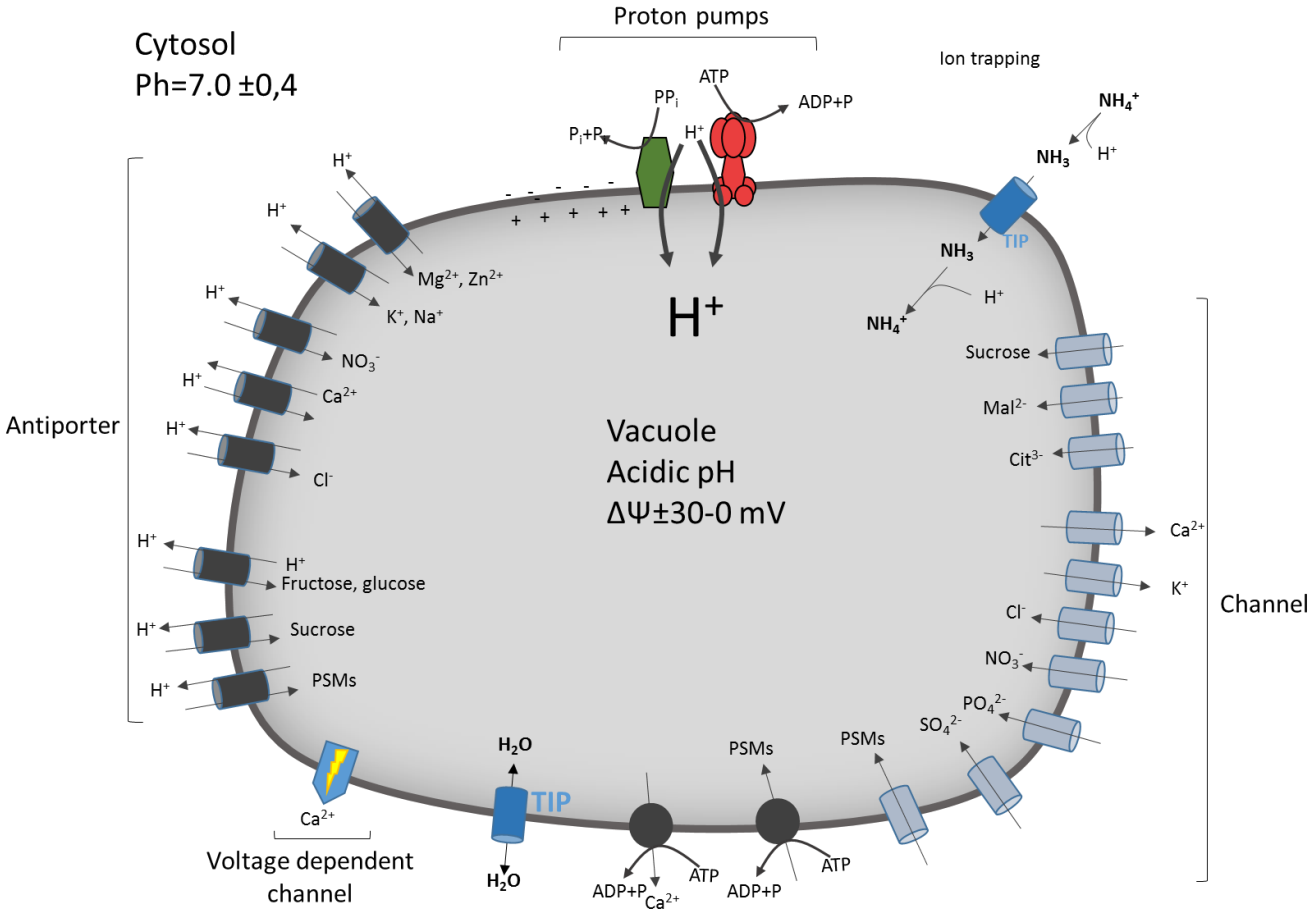

Figure 5: Schematic representation of the various vacuolar transport systems documented for plant cells. Passive transport of water is mediated by water channels called tonoplast intrinsic proteins (TIP). Primary active transporters use the hydrolysis of ATP to transport molecules across the tonoplast such as calcium, PSMs or protons. Secondary active transporters are energized through the establishment of an electro-chemical gradient across the tonoplast by proton pumps. Antiporters use the proton gradient whereas channels use the membrane potential to transport molecules. Voltage dependent channels are activated by voltage signal. Finally, weak base compounds can be trapped into the vacuole without any transporter by diffusion of the non protonated form across the tonoplast followed by its protonation in the acidic compartment. Notably, the passage of NH_3^+ can be facilitated by water channels, (Kirscht *et al.*, 2016).

In *A. thaliana* , transporters of the Tonoplast dicarboxylate transporter (TDT) (Emmerlich *et al.*, 2003) as well as the aluminum-activated malate transporter (ALMT) families function as vacuolar malate channels (Kovermann *et al.*, 2007). Similarly, a study with tonoplast vesicles from tomato fruits revealed that citrate uptake in the vacuole was dependent of the membrane potential and suggested its transport is mediated by low-specific anion channels (Oleski *et al.*, 1987).

Regarding inorganic anions. The chloride channel (CLC) family has been reported as Cl^- channels and Cl^-/H^+ antiporters, depending on the member (De Angeli *et al*., 2009). NO_3^- accumulation in the vacuole is mediated by two types of transporters belonging to 1) CLCa and CLCb families, which function also as antiporters transporting two NO_3^- versus one H^+ (De Angeli *et al*., 2009) and 2) nitrate transporter 2 (NRT2.) family which are anionic uniporter (Chopin *et al.*, 2007). A vacuolar phosphate transporters essential for phosphate homeostasis has been recently characterized and was in agreement with a study on *Catharanthus roseus* showed that phosphate transport at the tonoplast was dependent on the positive membrane potential inside the vacuole (Massonneau *et al.*, 2000). Beside, specific protein for vacuolar transport of SO_4^{2-} has not been identified yet. However, Kaiser, Schroppel-meier and Heber (1989) showed in barley seedlings that SO_4^{2-} uptake was dependent on the positive membrane potential.

Regarding inorganic cations, K^+ accumulation in the vacuole is mainly mediated by tonoplast-type Na^+/H^+ exchangers (NHXs) that function as an antiport with protons (Venema *et al.*, 2002). Importantly, NHX transporters are involved in the control of vacuolar pH together with K^+ homeostasis (Bassil *et al.*, 2011). Cellular levels of K^+ would also be strictly maintained through its release in the cytosol by, among others, voltage-independent two-pore K^+ channels (TPK) (Dreyer and Uozumi, 2011). The AtMHX1 (Mg^{2+}/H^+ exchanger) has been identified as a proton antiporter for Mg^{2+} and Zn^{2+}(Berezin *et al.*, 2008). Since Ca^{2+} is an important intracellular signaling molecule, many different transporters regulate Ca^{2+} transport in and out of the vacuole. P-type Ca^{2+}-ATPases transport Ca^{2+} into the vacuole requiring ATP hydrolysis (Bonza and Michelis, 2011), whereas cation/H^+ exchangers (CAXs) transport Ca^{2+} by using the proton gradient (Manohar *et al.*, 2011). So far, Ca^{2+} efflux would be monitored by a voltage-dependent slow-activating vacuolar channel called tandem-pore calcium (TPC1) (Hedrich and Marten, 2011).

Sugars are also accumulated inside vacuoles and released to the cytosol when required. Sucrose uptake can be catalyzed by a proton antiporter (Jung *et al.*, 2015) as well as by facilitated diffusion (Kaiser and Heber, 1984). Tonoplast monosaccharide transporter (TMT) (Aluri and Büttner, 2007) and vacuolar glucose transporter (VGT) (Aluri and Buttner, 2007) belong to the major facilitator super family (MFS) and both transport glucose into the vacuole using the proton gradient. Importantly, it was evidenced that SWEET17 acts to export fructose from the vacuole to the cytosol and was determinant to control the fructose cell content (Chardon *et al.*, 2013).

Recently, significant progress was made in the identification and functioning of plant specific metabolite (PSM) vacuolar transport mechanisms (reviewed in Francisco and Martinoia, 2018). Despite the huge diversity of molecules to transport, the vacuolar PSM transporters can be divided into three families, the ATP- binding cassette (ABC) transporters, the multidrug and toxic compound extrusion (MATE) transporters and the nitrate/peptide family transporters (NPFs).

Transport by passive diffusion

Weak base compounds of small size such as NH_4^+ or acetate are presumed to be trapped into the vacuole in a transporter independent pathway, by the so-called “ion trapping” mechanism. In fact, compounds that lose their charge at the neutral pH of cytosol (pKa of ammonium is 9.4) can cross the tonoplast by diffusion which can be facilitated by specific proteins. For instance, aquaporins of the TIP subfamily would accelerate the permeation of NH_3 through the vacuole membrane (Kirscht *et al.*, 2016). Once inside the acidic vacuole, a high proportion of molecules are protonated and thus, become hydrophilic ions unable to cross the tonoplast. Resulting in the over-accumulation of weak bases in the vacuole.

Transport mediated by vesicles

Vesicle mediated transport appears to play an important role for vacuolar accumulation. For instance, it has been suggested that under high salt treatment, sodium ions accumulate in small vesicles in the cytosol, which are then transported into the vacuole (Hamaji *et al.*, 2009).

Vesicle-mediated transport system was also proposed for some PSMs, for instance anthocyanins (Chanoca *et al.,* 2015; Grotewold, 2004).

4.3 Vacuoles and nitrogen nutrition

Leaf expansion is a major feature in plant performance and its achievement integrates various factors. For instance, Pantin *et al.* (2011) claimed that water and carbon emerge as main limiting factors of leaf expansion. Nevertheless, N supply is also of a great importance since expanding leaves require an adequate amount of stored N for growth (Liu *et al.*, 2018). Most of stored N is under the form of protein into the chloroplast in leaves since the rubisco enzyme, which is the most abundant in plants, localizes in the stroma of thylakoids (Gruber and Leiz, 2018). Importantly, a relevant fraction that comprises inorganic forms of nitrogen, free amino acids and PSMs localize potentially in the vacuole and therefore does not participate in any metabolic processes and structural constituent. From this manner, vacuoles constitute a nitrogen pool of great importance to co-ordinate cell expansion.

Plant growth is optimal when NO_3^- is supplied as N-source, whereas with NH_4^+ it is greatly reduced in many plant species (see section *2.3. the ammonium paradox*). Despite ammonium syndrome is an old paradigm, a growing number of cell biology studies recently made the link of this growth retardation with a reduction of cell expansion (Walch-Liu *et al.*, 2000; Liu *et al.*, 2013; Podgórska *et al.*, 2013). This suggests that factors controlling cell expansion have to be studied in relation with ammonium stress. Recently, Podgórska *et al.* (2013) followed by Głazowska *et al.* (2019) evidenced that alterations of the cell wall under NH_4^+ nutrition could impair cell elongation. However, few studies have focused on N-source effect on factors promoting vacuole enlargement to drive cell wall expansion.

Ammonium stress is generally associated with NH_4^+ accumulation in the cytosol and one strategy that has been suggested for ammonium tolerance is its compartmentalization into vacuoles. This hypothesis arises from several evidences including the quantification of millimolar NH_4^+ concentrations inside the vacuole of *Chara corallina* cells (Wells and Miller, 2000) and that yeast transformed with two Arabidopsis aquaporins of the tonoplast (TIP2;1 and TIP2;3) increased their tolerance to NH_4^+ through the facilitation of NH_3 transport into the vacuole (Loqué *et al.*, 2005). Moreover, it has also been observed that CAP1 tonoplast

receptor-like kinase is important in ammonium stress controlling cytosol vs. vacuole NH_4^+ transport by a mechanism that still needs to be found (Bai *et al*., 2014). Another important aspect that greatly influences cell performance in relation with the available N-source is the control of cell pH. Indeed, it is known that pH is an important factor involved in plants tolerance towards ammonium stress (Sarasketa *et al*., 2016). Thus, vacuolar transport mechanisms can be crucial for the control of cytosol pH and ions homeostasis among others by vacuolar H^+ pumps including V-PPase and V-ATPases (Martinoia, Maeshima, and Neuhaus., 2007).

5 *Tomato plants* as a model of study

Cultivated tomato (*Solanum lycopersium*) belongs to the family Solanaceae and is closely related to many commercially important plants such as potato, eggplant, peppers, tobacco, and petunias. Tomato is a dicotyledonous plant (*Lycopersicon lycopersicum Mill*., 2n =2X=24) and is the second most important vegetable crop following potato. The world tomato production in 2018 was about 244 million metric tonnes of fresh fruit from an estimated 5.8 million hectares (FAO)

It is a perennial plant, but is often grown outdoors in temperate climates as an annual plant. Typically reaching to a height of 1 to 3 m, it has a weak, woody stem that often vines over other plants. The leaves are 10 to 25 cm long, odd pinnate, with 5 to 9 leaflets on petioles. Each leaflet grows up to 8 cm long, with a serrated margin and both the stem and leaves are densely glandular-hairy. Tomato plant can have a fibrous root system or a taproot system depending on how the plant was grown. The edible tomato fruits are berries with different morphology depending of the variety. The fruit consists of the external layer called the pericarp, the pulpy part formed by cells with thin round walls called the mesocarp and the thicker tissue that divides and limit the pulp sections called the endocarp (Peralta *et al.*, 2008).

Tomato has been widely used not only as food, but also as research material. The tomato plant has many interesting features agronomically important such as fleshy fruit, a sympodial shoot, and compound leaves, which other model plants (e.g., rice and Arabidopsis) do not have. The tomato genome was released in 2012 (Tomato Consortium, 2012) culminating years of work by the Tomato Genome Consortium, a multi-national team of scientists from

14 countries. There are more than 5000 different cultivars of tomato. Seeds of many of these cultivars can be purchased from commercial companies, but most of them are hybrid stocks. In research, the most cultivars studied are *Microtom*, *Money maker*, and *M82*. *M82* tomato variety, used in the present study, is characterized by a "determinate" phenotype where sympodial segments develop progressively fewer nodes until the shoot is terminated by two consecutive inflorescence (Pnueli *et al.*, 1998). *M82* genome is fully sequenced and is available from the European Nucleotide Archive (ENA) under accessions HG975439–HG975452 (Bolger *et al.*, 2014).

General objectives

Tomato leaves photography (South Africa Gardening, Garden update archives)

GENERAL OBJECTIVES

Nitrogen fertilization in agriculture affects negatively the environment mainly because of NO_3^- leaching and the emission of nitrogenous gazes with high contribution to global warming, notably N_2O. The use of ammonium-based fertilizers combined with nitrification inhibitors is greatly efficient in the mitigation of these N losses to the environment. However, plants under ammonium nutrition often display reduced biomass. Therefore, it is essential to understand the physiological and metabolic mechanisms that are perturbed by ammonium nutrition in order to be able to develop crop varieties more adapted to this type of N-nutrition.

Based on this, the **general objective** of this PhD thesis is **to gain further insight into plant response upon ammonium nutrition focusing on the role of the vacuole and the metabolic adaptation in the context of leaf development**

This general objective is supported in two specific objectives:

1) To get an integrative picture of the metabolic modulation linked to leaf growth in the context of ammonium nutrition.

2) To determine the impact of vacuolar expansion and metabolism on leaf development in function of the nitrogen source provided.

Chapter I

Leaf metabolic analysis on a whole-plant scale: The importance of energy partitioning to manage with ammonium supply

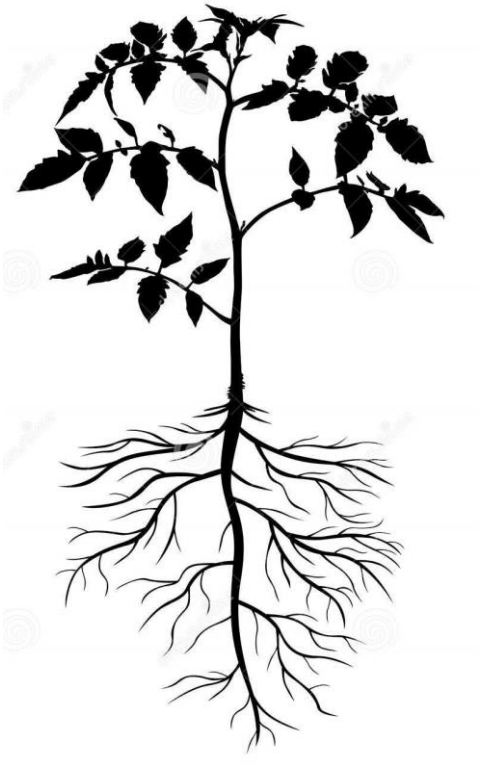

ABSTRACT

Nitrate (NO_3^-) and ammonium (NH_4^+) are the main inorganic nitrogen sources available for plants. However, exclusive ammonium nutrition may lead to a stress situation characterized by growth inhibition, generally associated with a profound metabolic reprogramming. In this chapter, we aimed studying how the metabolism is adapted in function of the leaf position in the vertical axis of a tomato (*Solanum lycopersicum* cv. M82) plant grown with NH_4^+, NO_3^- or NH_4NO_3 supply. To do so, we dissected leaf biomass composition and metabolism through a complete analysis of metabolites, ions and enzyme activities. The results showed that C and N metabolic adjustment in function of the nitrogen source was more intense in older leaves compared to younger ones. Importantly, we propose a trade-off between NH_4^+ accumulation and assimilation to preserve young leaves from ammonium stress. Besides, NH_4^+-fed plants exhibited a rearrangement of carbon skeletons, accumulating sugars and starch at the expense of organic acids, with a higher energy cost respect to plants supplied with NO_3^-. We explain such reallocation by the action of the biochemical pH-stat, to compensate the differential proton production that depends on the nitrogen form provided. This work underlines the importance of considering leaf phenological state when studying nitrogen metabolism.

INTRODUCTION

Inorganic nitrogen is essential for plants as building element for the synthesis of a wide range of compounds such as amino acids, proteins or nucleic acids. The main inorganic N forms that plants take up from the soil are nitrate (NO_3^-) and ammonium (NH_4^+). In agricultural and natural environments, their relative abundance mostly depends on the physicochemical, biochemical and microbiological properties of the soil. Nitrogen source predilection depends on the plant species or genetic background but also on environmental variables that include, among others, soil pH and temperature. Indeed, the availability of NO_3^- and NH_4^+ in the soil may determine plant diversity and species distribution in nature (Britto and Kronzucker 2013; van den Berg *et al*., 2005).

Although organic N is initially derived from NH_4^+ assimilation, when plants are exposed to high concentration of NH_4^+ in the external medium most species suffer from the so-called "ammonium syndrome". This syndrome is typically associated with a decrease in net photosynthesis, oxidative stress, metabolic imbalance, cation uptake inhibition, hormonal deregulation, etc., which are commonly evidenced by alterations in root : shoot ratio, leaf chlorosis and growth retardation (Britto & Kronzucker, 2002; Esteban *et al.,* 2016). In parallel, NH_4^+-mediated repression of growth has also been linked with the reduction of cell elongation in *Arabidopsis thaliana* (Podgórska *et al.*, 2017).

The differences in electrochemical properties of NO_3^- and NH_4^+, which are respectively an anion (oxidation state of N, +5) and a cation (oxidation state of N, −3) have important consequences on their uptake and metabolism. NO_3^- is cotransported with one proton whereas NH_4^+ is mainly transported via electrogenic transport through AMT channels or cation transporters (Mayer *et al.*, 2006). This uptake difference in terms of charge balance together with a direct competition between NH_4^+ and other cations during transport through plasma membrane, has important consequences on the cell ion homeostasis that, for instance, may lead to deficiency in essential mineral nutrients such as K^+, Ca^{2+} or Mg^{2+} (Hoopen *et al*., 2010; Rayar & Hai, 1977; Van Beusichem, Kirkby, & Baas, 1988)

Once inside the cell, and in order to prevent NH_4^+ over-accumulation in the cytosol that may provoke cytotoxicity (Choudhary *et al*., 2016) ,NH_4^+ can be 1) effluxed out of the cell, 2) stored

into the vacuole or 3) assimilated via the glutamine synthetase/glutamate synthase (GS/GOGAT) cycle. In this line of evidence, Arabidopsis GS1 mutants displayed enhanced sensitivity towards ammonium stress (Guan *et al.*, 2016). The functioning of GS/GOGAT cycle needs the fuel of 5-C skeletons and indeed, when plants deal with ammonium stress, the activity of tricarboxylic acid (TCA) cycle together with its associated anaplerotic routes have been shown to match GS/GOGAT carbon demand in different species, including wheat and tomato (Setién *et al.* 2014; Vega-Mas *et al.* 2019). Overall, these energy-demanding processes may impose a limitation for plant growth.

Deregulation of pH also plays a primary role in the stress generated by NH_4^+ excess (Hachiya *et al.*, 2019). Indeed, even though the nature of substrate translocation (NH_3/NH_4^+) is still a matter of controversy, the entrance of NH_4^+ mediated by AMT transporters favors the acidification of the extracellular medium (Ariz *et al.*, 2018). Besides, for the synthesis of one glutamate molecule, NO_3^- assimilation produces OH^- whereas NH_4^+ assimilation produces two H^+s (Raven and Smith, 1976; Andrews *et al.*, 2013). Among other mechanisms, cells are thought to compensate this pH deregulation by using the biochemical pH-stat, which consists in pH-sensitive carboxylation and decarboxylation reactions in organic acid metabolism that produce and consume protons (Davies, 1973; Sakano, 2001). Importantly, anaplerotic enzymes, as phosphoenolpyruvate carboxylase (PEPC), malate dehydrogenase (MDH) and NAD(P)-dependent malic enzyme (ME), would be involved in the biochemical pH-stat in addition to their important role in nitrogen assimilation.

In most studies conducted on nitrogen metabolism, the organ phenological status is rarely attempted. Among previous works, the evolution of carbon and nitrogen metabolism as related to the leaf position and/or developmental stage was described in tobacco (Masclaux *et al*., 2000; Terce-Laforgue, Mack, and Hirel, 2004), *Arabidopsis thaliana* (Diaz *et al*., 2008) or barley (Wiedemuth *et al*. 2005), to study leaf source/sink transition. Regarding N-source effect, there is scarce knowledge concerning how the different leaves of the plant manage the assimilation of NH_4^+ and/or its storage, and which is the trade-off between plant development and N-assimilation. In this work, we used an integrated approach to understand the metabolic management of different nitrogen sources from upper leaves to lower leaves. To do so, we grew tomato plants under three N-sources: exclusive ammonium or nitrate provision and equivalent ammonium:nitrate (50:50) supply. According to growth parameters,

we focused on five leaf positions to examine ionic contents, enzyme activities and the main metabolite pools from nitrogen and carbon metabolism. The whole dataset generated, among others, allowed estimating the potential role of the osmotic concentration, as well as the energy cost of leaf biomass construction when different nitrogen sources are supplied. Our results also indicate that excessive assimilation of NH_4^+, more than its accumulation in leaves, is associated with the apparition of ammonium symptoms.

GROWTH CONDITIONS AND EXPERIMENTAL DESIGN

Tomato (*Solanum lycopersicum*, cv. M82) seeds were sown in trays filled with perlite:vermiculite (1:2, v:v) inert substrate mixture and watered with deionised water. Trays were kept during 14 days in a growth chamber under a 14/10 h photoperiod with a light intensity of 350 µmol m^{-2} s^{-1} and 60/70% relative humidity and 23/18 °C day/night conditions, respectively.

Homogeneous seedlings were transferred into 500 mL pots (1 seedling per pot) filled with perlite:vermiculite (1:2, v:v) and set up for 30 days in a greenhouse (Greenhouse Service, SGIker, UPV/EHU). Afterwards plants were transferred to 2.8 L pots until the end of the experiment. The greenhouse conditions were 14/12 h day/night period with the support of additional light sources ensuring a minimum of 200 µmol $m^{-2}s^{-1}$ of radiation. Temperature and relative humidity were 25/18 °C and 50/60%, respectively (day/night). The whole experiment was conducted between May and July 2017.

Plants were irrigated three times per week with a nutrient solution adjusted at pH 6 that contained macronutrients (1.15 mM K_2HPO_4, 0.85 mM $MgSO_4$, 0.7 mM $CaSO_4$, 2.68 mM KCl, 0.5 mM $CaCO_3$, 0.07 mM NaFeEDTA) and micronutrients (16.5 µM Na_2MoO_4, 3.5 µM $ZnSO_4$, 3.7 µM $FeCl_3$, 0.47 µM $MnSO_4$, 0.12 µM $CuSO_4$, 16.2 µM H_3BO_3, 0.21 µM $AlCl_3$, 0.126 µM $NiCl_2$ and 0.06 µM KI). Nitrogen was applied at a final concentration of 15 mM in three different forms that corresponded to the three studied conditions, 100% ammonium applied as 7.5 mM $(NH_4)_2SO_4$, 100% nitrate applied as 7.5 mM $Ca(NO_3)_2$, and 50% : 50% ammonium : nitrate applied as 7.5 mM NH_4NO_3. To appropriately compare the three nutrient regimes, nitrate and ammonium nitrate nutritions were supplemented with 7.5 mM $CaSO_4$ to equilibrate the sulphate supplied in A treatment.

Thirty plants were grown per treatment. After 70 days in the greenhouse the 24 plants with the most homogenous appearance were kept. Out of them, 4 were randomly selected to determine plant growth parameters and the resting 20 were used for metabolic analyses. Plant growth performance was evaluated determining whole plant biomass. Accordingly to the aim, each leaf was numbered from the top to the bottom (basipetally), in function of its

position in the vertical plant axis (stem), thus giving number 1 to the youngest leaf. Fresh weight (FW), dry weight (DW) and area were determined for each leaf. Dry weight was determined after incubating the plant material in an oven at 80 °C for 72 h. Relative water content was calculated as: 100*(FW – DW)/FW.

RESULTS

Leaf growth and biomass distribution are affected by the nitrogen source

Tomato plants were grown during the whole experiment under three nitrogen nutritional regimes supplying 7.5 mM $Ca(NO_3)_2$, 7.5 mM $(NH_4)_2SO_4$ or 7.5 mM NH_4NO_3. Provision of nitrogen as 50% NO_3^-/50% NH_4^+ did not modify plant growth compared to NO_3^- as the sole N-source, whereas plants grown on NH_4^+ presented a biomass reduction of 30% (Figure 1A).

To study the interaction between leaf phenological status and nitrogen nutrition, leaves were numbered sequentially from top (the youngest leaf) to bottom, until the 12th leaf, and harvested in function of their position in the plant. Leaf area, FW and DW were measured (Figures 1B and Figure S1). In nitrate and ammonium nitrate plants, almost indistinguishable growth profiles were observed: leaf area and biomass increased from leaf 1 to 8, remained almost constant from leaf 8 to 10 and then decreased in older leaves (Figure 1B). This decrease in leaf size in the older leaves, which was described in the tomato leaf plastochron index (Coleman and Greyson, 1976), is explained by the appearance of the older leaves on a more juvenile plant. From leaf 1 to 6, no growth differences were observed among the three nitrogen nutritions. However, unlike nitrate and ammonium nitrate, a decrease of leaf growth (FW, DW and leaf area) was already registered in leaf 8 under ammonium nutrition. The effect of nutrition regime (ammonium compared with nitrate and ammonium nitrate conditions) became significant from leaf 9, with a reduction of 35% of the biomass (Figure 1B and Figure S1B). Specific leaf area and (SLA) water content remained stable along the leaf stages in nitrate and ammonium nitrate regimes and similar between both treatments. Interestingly, water content was lower in leaf 1 to 6 (Figure 1D) in ammonium condition and accordingly SLA slightly increased (Figure 1C). Based on these first results, leaf stages for further analyses were defined: leaves 1, 2, 3 corresponding to growing leaves, leaf 6 corresponding to the youngest fully expanded leaf, and leaf 9 whose growth was severely impaired in NH_4^+-fed plants. In those leaf positions, chlorophyll content was quantified as a physiological marker (Figure 1E). Regardless leaf ageing and nutrition type, for these phenological stages no leaf yellowing was evident. However, in nitrate and ammonium nitrate treatments, chlorophyll

amount decreased progressively from leaf 3 to 9, whereas it remained constant in NH_4^+-fed leaves (Figure 1E).

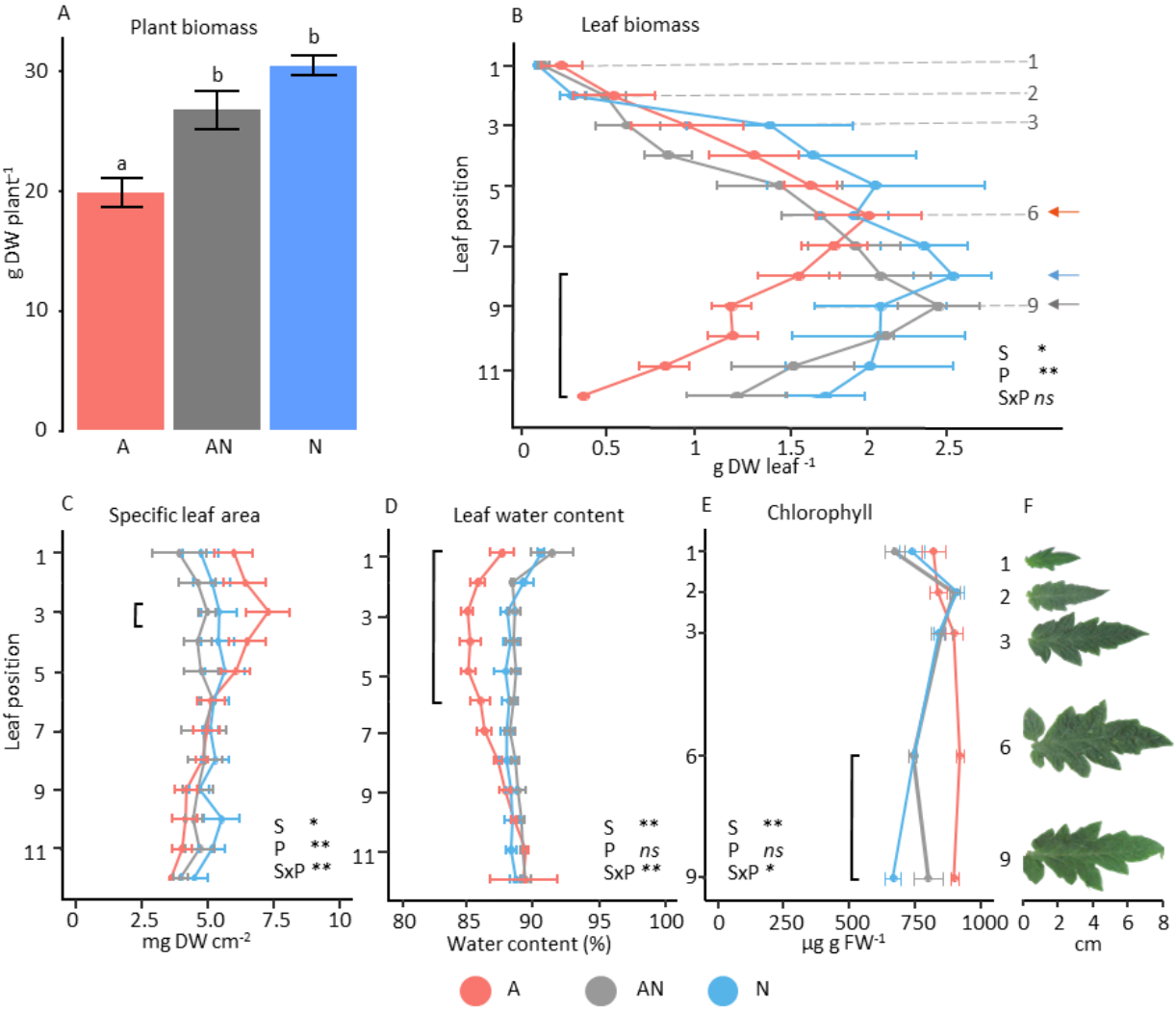

Figure 1: Whole-plant biomass and leaf physiology of tomato plants grown with ammonium (A: red), ammonium nitrate (AN: grey), and nitrate (N: blue) as nitrogen source, considering leaf vertical position in the plant. Whole plant biomass (A), leaf biomass (B), specific leaf area (C), leaf water content (D), chlorophyll content of selected leaves (E) and representative photograph of the apical leaflet of selected leaves (F). In panel B, broken horizontal lines indicate the selected leaf positions for metabolic studies and colored arrows indicate maximum growth for each nutrition type. Values represent mean ± se (n = 4). In panel A different letters indicate significant differences according to one-way ANOVA followed by Duncan´s test ($p<0.05$). For panels B-E, significant differences are shown according to two-way ANOVA (**: $p<0.01$; *: $p<0.05$; *ns*: not significant) where S indicates nitrogen source effect; P indicates leaf position effect and S×P indicates interaction effect. For each leaf position, significant differences between A and N treatments are highlighted with a square bracket (t-test $p<0.05$).

Nitrogen source effect is enhanced in basal leaves

In order to gain insight into the impact of the nitrogen source on leaf metabolism according to the position on the plant, 21 metabolites and 9 ions were measured in leaves harvested at the 5 different stages previously defined (leaves 1, 2, 3, 6 and 9). Moreover, the activity of 6 enzymes involved in TCA cycle replenishment and nitrogen assimilation was also evaluated. An unsupervised PCA was performed to evaluate overall differences in the metabolic profiles of leaves.

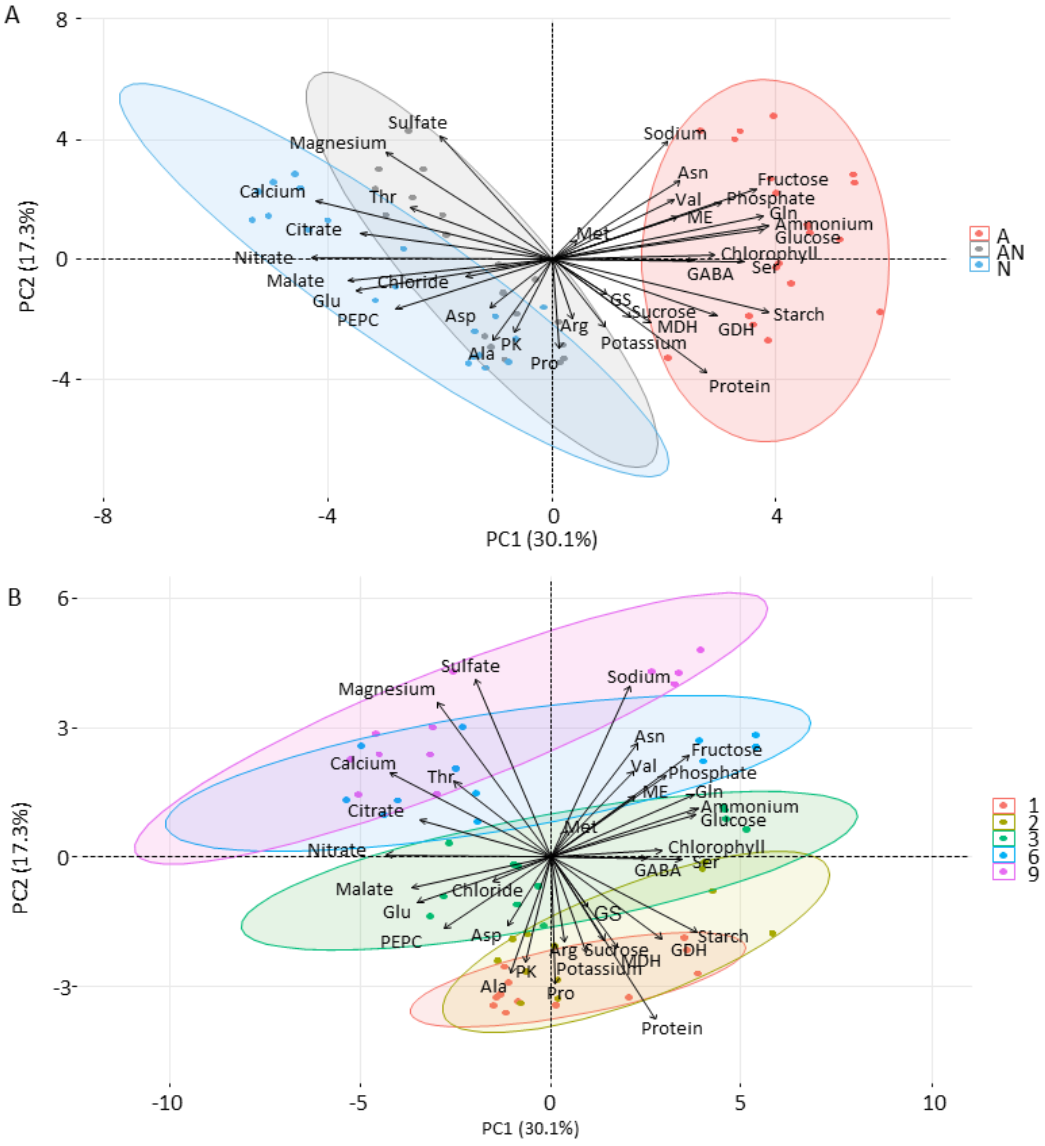

Figure 2: Principal component analysis (PCA) of metabolites, ions and enzymatic activities determined in leaves (positions 1,2,3,6 and 9) of tomato plants grown with different nitrogen sources (A: ammonium; AN: ammonium nitrate; and N: nitrate). PCA was performed from the correlation matrix generated with a total of 29 variables, with 4 replicates per treatment and leaf position. PC1 and PC2 explained respectively 30.1% and 1.3% of the total variance. Biplot A shows observations discrimination by nutrition conditions. Biplot B shows observations discrimination by leaf position on the plant.

The first two principal components (PC1 and PC2) explained 47.4% of total variance and revealed differences in metabolism according to the N-source but also to the leaf stage. The first PC accounting for 30.1% of the variance thus underlined the impact of the N-source. Leaf metabolic adaptation to nitrogen condition segregated clearly leaves under ammonium condition from those of nitrate and ammonium nitrate nutrition, both being closer each other and overlapped (Figure 2A). Examination of the PC1 loadings suggests that the separation of plants grown on different nitrogen nutrition regimes was mainly explained by variation in NH_4^+, hexoses, starch, on the positive extreme of PC1 and NO_3^-, citrate, malate and glutamate on the negative extreme. The second PC, accounting for 17.3% of the variance, mostly separated leaf positions, with an important positive contribution of SO_4^{2-}, Na^+, Mg^{2+} and a negative contribution of protein content (Figure 2). When data were analyzed separately for each nutrition type (Figure S2) leaves were again clearly separated by their growth position in the plant, in this case mainly along PC1, with an important contribution of ions (Mg^{2+}, Na^+, Ca^{2+} and SO_4^{2-}), protein and starch content, regardless the nutrition type.

The effect of the nitrogen source on primary metabolism depends on the leaf position

In general, the content of primary metabolites was similar between leaves grown under nitrate or ammonium nitrate conditions. Conversely, under exclusive ammonium nutrition the content of the majority of metabolites was different from what observed in NO_3^- and NH_4NO_3-fed leaves.

Regarding sugars (Figure 3), in NO_3^- and NH_4NO_3-fed leaves, sucrose content varied, from a maximum of arround 10 µmol glucose eq g FW^{-1} in leaf 2 to ca. 5 µmol glucose eq in leaf 9. Under NH_4^+ nutrition, sucrose content was substantially higher with arround 18 µmol glucose eq g FW^{-1} in leaf 1 to 6-8 µmol glucose eq g FW^{-1} from leaf 3 to those above. Glucose and fructose contents were overall higher in ammonium respect to nitrate and ammonium nitrate conditions by a factor ranging to 2.5-3.5. Starch content was higher in younger leaves compared to the older ones regardless the nutrition type. For instance, under nitrate and ammonium nitrate conditions, starch content was close to 50-60 µmol glucose eq g FW^{-1} in growing leaves (leaves 1 to 3), and then decreased around 10 µmol glucose eq g FW^{-1} in mature leaves. Importantly, ammonium nutrition induced an increase in starch accumulation by a factor 3 regardless of the position in the plant. Regarding the two major organic acids

related to the TCA cycle, in NO_3^--fed plants, the content of citrate in young leaves was 2-3 µmol g^{-1} FW in young leaves (positions 1 and 2), and then it progressively increased reaching 12-16 µmol g FW^{-1} in leaf 6 and above (Figure 3). Malate was the most abundant of the two organic acids measured, and especially in nitrate plants. Its concentration, already high in young leaves (ca 90 µmol g FW^{-1}) growing under nitrate condition, increased gradually with the position of the leaf to reach 160 µmol g FW^{-1} (Figure 3). Importantly, both organic acids were strongly decreased when NO_3^- was partially replaced by NH_4^+ in ammonium nitrate treatment and almost totally with only ammonium: citrate becoming almost undetectable, and malate dropping to about 10 µmol g FW^{-1}. Interestingly, feeding tomato plants with NH_4^+/NO_3^- led to intermediate concentrations, notably for malate that ranged 45-60 µmol g FW^{-1} regardless leaf position (Figure 3).

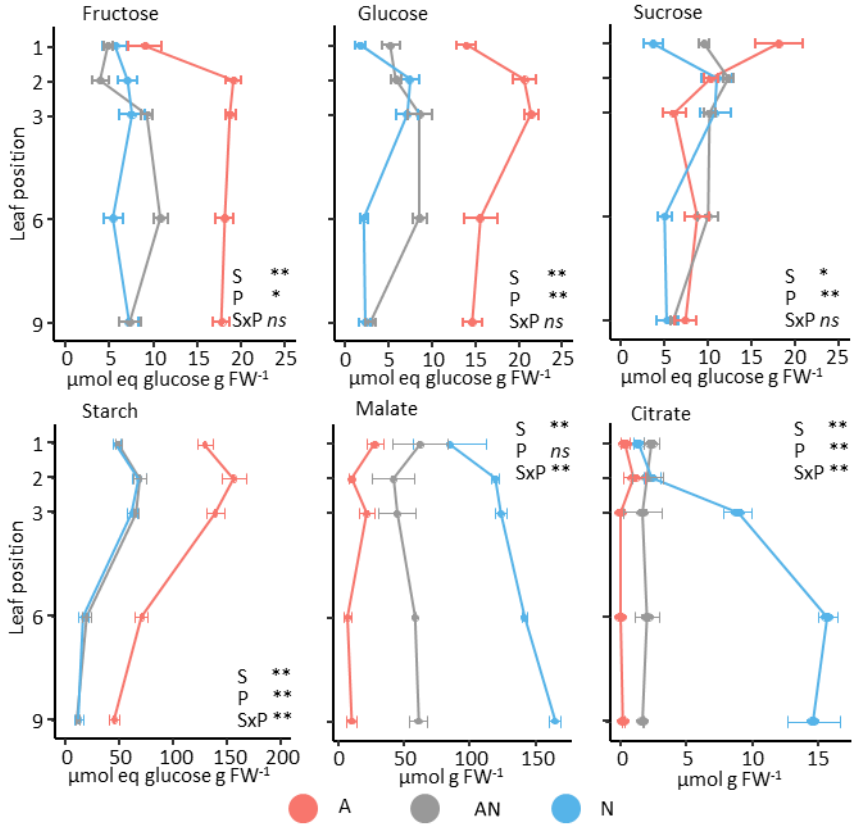

Figure 3: Carbon-related metabolites (sugars, starch and organic acids) in leaves of tomato plants, grown with ammonium (A; red), ammonium nitrate (AN; grey) and nitrate (N; blue) as nitrogen source, considering their position in the plant. Values represent the mean ± se (n = 4). Significant differences are shown according to two-way ANOVA (**: p<0.01; *: p<0.05; *ns*: not significant) where S indicates nitrogen source effect; P indicates leaf position effect and S×P indicates interaction effect.

Regarding nitrogen-containing molecules (Figure 4 and Figure S5), the content of total amino acids was only affected by the nitrogen source from leaf 6 to 9, at which ammonium plants presented the highest content in total free amino acids. However, when looking at changes in individual major amino acids, in plants grown on ammonium we found a dramatic decrease in glutamate and aspartate mirrored by a strong increase in glutamine and asparagine. Consequently, the ratio (Gln + Asn)/Glu + Asp), which is often considered as a criteria for nitrogen assimilation in the leaf (Watanabe *et al.*, 1997; Foyer *et al.*, 2003), was strongly increased in plants grown on ammonium. Protein content, which as mentioned above made a major contribution to the leaf position in the PCA (Figure 2), decreased differentially in function of N-source, from 26-30 in leaves 1-2 until leaf 9, reaching around 12 mg g FW^{-1} for nitrate and ammonium nitrate plants and 20 mg g FW^{-1} for ammonium plants. Interestingly, whereas the nutrition regime had no effect on the protein content of young leaves (leaves 1-3), mature leaves (leaves 6 and 9) grown under ammonium condition had significantly higher protein levels.

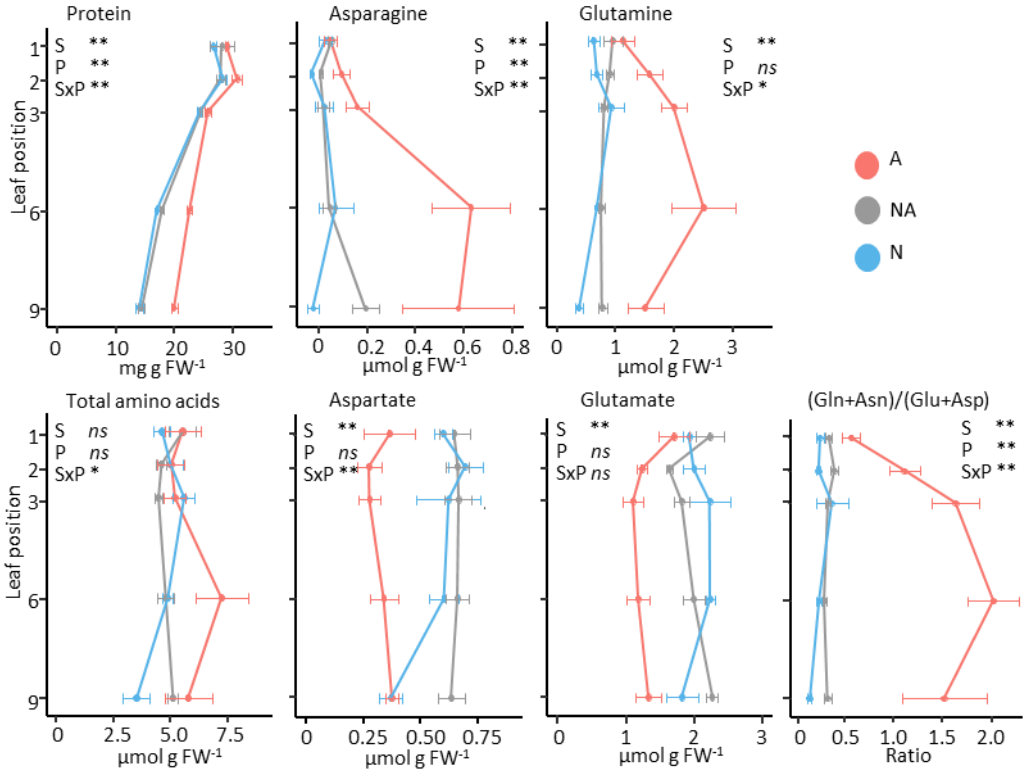

Figure 4: Metabolites related to nitrogen metabolism in leaves of tomato plants, grown with ammonium (A; red), ammonium nitrate (AN; grey) and nitrate (N; blue) as nitrogen source, considering their position in the plant. Values represents the mean ± se (n=4). Significant differences are shown according to two-way ANOVA (**: p<0,01; *: p<0,05; *ns*: not significant) where S indicates nitrogen source effect; P indicates leaf position effect and S×P indicates interaction effect.

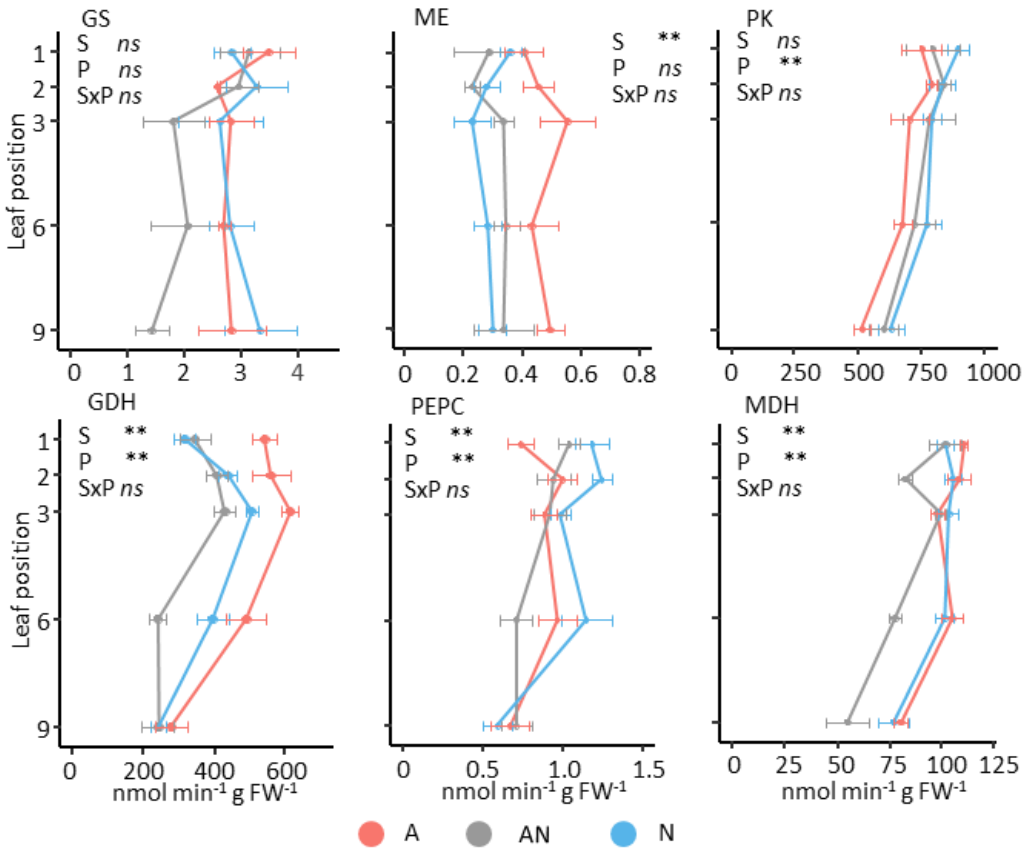

Figure 5: Enzyme activities in leaves of tomato plants, grown with ammonium (A; red), ammonium nitrate (AN; grey) and nitrate (N; blue) as nitrogen source, considering their position in the plant. ME stands for NADP-malic enzyme; PEPC for phosphoenolpyruvate carboxylase; GDH for glutamate dehydrogenase; MDH for NADH malate dehydrogenase; GS for glutamine synthetase and PK for pyruvate kinase. Values represent the mean ± se (n=4). Significant differences are shown according to two-way ANOVA (**: p<0.01; *: p<0.05; *ns*: not significant) where S indicates nitrogen source effect; P indicates leaf position effect and S×P indicates interaction effect.

The activity of PK, PEPC, MDH, NADP-ME, GS and GDH enzymes was measured (Figure 5). In general, the leaf position x nitrogen source interaction (SxP) had little impact on the measured enzymatic activities. PK, PEPC, MDH and GDH activities were affected by the position of the leaf according to the ANOVA test (Figure 4). Only GDH and PK had a clear pattern decreasing their activity by 50% and 30%, respectively, between growing leaves (leaf 1 to 3) and mature leaves (leaf 6 and 9). With regard to the nitrogen source, the cultivation of plants on NH_4^+ doubled significantly the activity of ME independently of the leaf position. GDH was also higher in ammonium respect to ammonium nitrate conditions, with NO_3^--fed plants showing an intermediate behavior, except for leaf 9 where no differences were found. Furthermore, ammonium nitrate nutrition led to a decrease of MDH activity from leaf 3 to leaf 9, whereas in ammonium and nitrate regimes the decrease of the enzyme is triggered in leaf 6. No clear significant differences between treatments were observed for PEPC activity in every leaf

positions, but ANOVA test showed a relevant effect of the nitrogen source. Excluding the leaf 9, PEPC activity was always lower of around 20% in NH_4^+ compared to NO_3^--fed plants. GS and PK were little affected by the nitrogen source.

Ammonium nutrition increases biomass construction costs

To estimate biomass construction cost, the potential energy contained in metabolite pools, expressed as moles of ATP equivalents per g DW, was calculated (Figure 6).

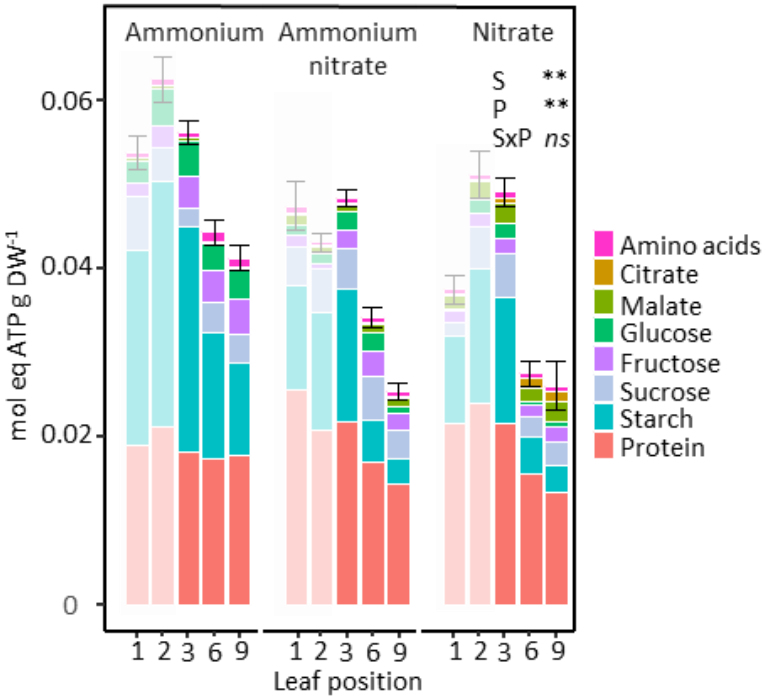

Figure 6: Potential energy contained in different metabolites in leaf tissue of tomato plants, grown with ammonium, ammonium nitrate, and nitrate as nitrogen source, considering their position in the plant. The potential energy corresponds to the ATP equivalent released after total oxidation for each metabolite. The energy estimation fort young leaves (1 and 2) is not precise since they mostly acquire carbon skeletons from import rather than from de novo synthesis; thus, colors for these leaves are shown faded. Data represent the mean ± se (n=4). Significant differences are shown according to two-way ANOVA *(**: p<0.01; *: p<0.05; ns*: not significant) where S indicates nitrogen source effect; P indicates leaf position effect and S×P indicates interaction effect.

For young leaves (positions 1-3), the potential energy of leaf biomass was 25% higher under ammonium nutrition than under nitrate and ammonium nitrate treatment. However, for young leaves (faded colors in Figure 6) this estimation is not precise since they mostly acquire carbon skeletons from import rather than from de novo synthesis. For fully expanded leaves, the leaf potential energy value remained lower under nitrate and ammonium nitrate

conditions compared to ammonium conditions, with values reaching 0.25 mol ATP per g FW for NO_3^- and NH_4NO_3-fed leaves and 0.45 mol ATP per g FW when NH_4^+ is provided. This difference was mainly explained by the abundance of high energy-costing compounds such as sugars, proteins or starch under NH_4^+ nutrition. Conversely, in NO_3^- and NH_4NO_3-fed leaves, a larger part of leaf biomass was explained by organic acids, which possess a lower potential energy (Figure 6).

Ion balance adaptation to the nitrogen source is modulated by the leaf position

The concentration of the main soluble inorganic anions and cations was measured to evaluate the effect of the nutrition type and leaf position on ionic balance (Figure 7). NH_4^+ was 5 to 20 times more concentrated under ammonium nutrition than under nitrate and ammonium nitrate nutrition. Besides, NH_4^+ content varied considerably with the leaf position; it increased in growing leaves (from 7 µmol g FW^{-1} in leaf 1 to 17 µmol g FW^{-1} in leaf 3) and then decreased in mature leaves (leaves 6 and 9). On the other hand, as expected, NO_3^- was almost undetectable under ammonium conditions, but showed intermediate levels under ammonium nitrate and high levels under nitrate supplies. Nitrate was also increasing between growing and mature leaves, i.e. by 42 and 128% in NO_3^- and NH_4NO_3-fed leaves respectively. The levels of Na^+, Mg^{2+}, Ca^{2+} and SO_4^{2-} increased progressively with the leaf position regardless the nutrition type. Notably, Mg^{2+} and Ca^{2+} concentrations were much higher in plants grown with nitrate or ammonium nitrate. For SO_4^{2-} both nitrate and ammonium nitrate treatment presented higher values compared to ammonium, especially at leaf 6. K^+ concentration was quite similar among nutrition regimes as it decreased between leaves 1 and 3. However, in leaves 6 and 9, K^+ was increased under ammonium treatment while under nitrate and ammonium nitrate treatment it wents on decreasing or remained stable, respectively (Figure 7). For Cl^-, a relatively high content was found in leaf 1 under ammonium nutrition (about 40 µmol g FW^{-1}), but in older leaves it was halved and actually was lower than under nutrition regimes with nitrate and ammonium nitrate. Conversely, PO_4^{2-} increased 2-to-3-folds between leaves 3 and 9 grown under ammonium whereas it remained stable and lower under nitrate and ammonium nitrate conditions (Figure 7).

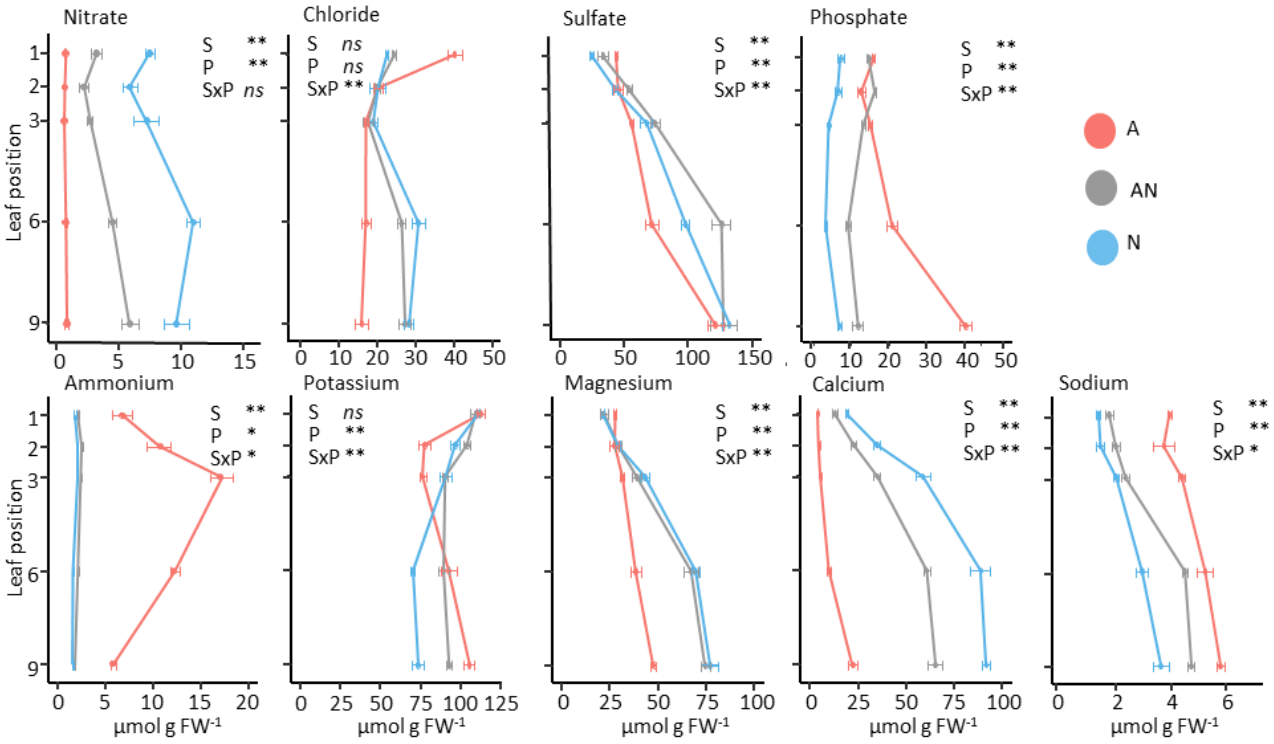

Figure 7: Inorganic soluble ions content in leaves of tomato plants, grown with ammonium (A; red), ammonium nitrate (AN; grey) and nitrate (N; blue) as nitrogen source, considering their vertical position in the plant. Values represent the mean ± se (n=4). Significant differences are shown according to two-way ANOVA (**: p<0,01; *: p<0,05; *ns*: not significant) where S indicates nitrogen source effect; P indicates leaf position effect and S × P indicates interaction effect.

The contribution of ions to cell osmolarity is greater than that of organic molecules

The osmotic concentration, determined using an osmometer (Figure 8 black line), increased with the leaf position in every condition, (around 33% from leaf 1 to 9) but no significant differences were observed between nutrition regimes, except in leaf 1 for which NH_4^+-fed plants presented higher levels than in NO_3^- and NH_4NO_3 fed-plants (Figure 7).

As next, the respective contributions to cell osmolarity of the measured soluble organic (sugars, amino acids and organic acids) and mineral compounds was estimated and summed up (Figure 7). Differences between measured and calculated cell osmolarities were found to be around 25%, suggesting a good coverage of the main contributors to osmolarity. The global trend found between leaves (measured or calculated) was very similar between nutrition regimes, indicating that the N-source did not affect cell osmolarity. Regardless of the nitrogen source, we observed that inorganic osmolytes played a major role in cell osmolarity (accounting for at least 65% of the osmotic concentration), and that their relative importance

increased with the leaf position, at the expense of sugars, organic acids and amino acids (Figures 5 and Figure S3). Interestingly, the contribution of ions was higher under ammonium compared to ammonium nitrate and more notably with only nitrate, mainly because of the lower content in organic acids observed under ammonium nutrition. Interestingly, potassium was the major non-organic osmolyte in young leaves (about 30%), but decreased in mature leaves, notably in nitrate conditions, while the contribution of other ions, mainly SO_4^{2-}, Ca^{2+} and Mg^{2+} increased (Figure S3).

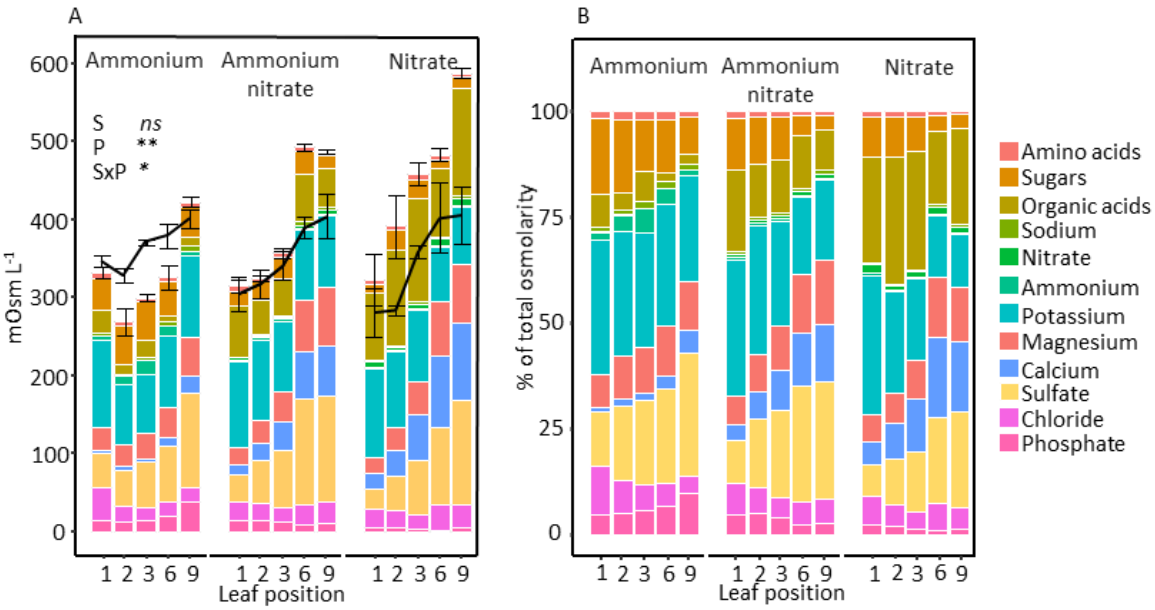

Figure 8: Solutes contribution to osmolarity in leaves of tomato plants, grown with ammonium, ammonium nitrate and nitrate as nitrogen source, considering the leaf position in the plant. (A) Black lines correspond to leaf osmolarity measured with an osmometer and colored bars show the theoretical contribution of the measured solutes that contribute to osmolarity. Values represent mean ± se (n=4). Significant differences are shown according to two-way ANOVA (**: p<0,01; *: p<0,05; *ns*: not significant) where S indicates nitrogen source effect; P indicates leaf position effect and S×P indicates interaction effect. (B) Contribution of the determined metabolites and ions to the theoretical osmolarity. Values represents the mean ± se (n=4).

DISCUSSION

In this work, the impact of the nitrogen-source was analyzed along the vertical axis of the plant by describing the changes in organic and inorganic compounds within leaves. At the time of harvest, although differences were observed in protein or chlorophyll content along the leaf positions (Figures 1E and Figure 4), leaves did not still enter in senescence programmes associated with nutrients remobilization. For instance, in Arabidopsis and barley a dramatic drop in nitrogen assimilation was associated with leaf senescence (Wiedemuth *et al.*, 2005; Diaz *et al.*, 2008), accompanied by the increase of metabolic markers of senescence such as GDH activity (Masclaux *et al.*, 2000). In contrast, in our work, regardless of the nutrition type, the drop in nitrogen assimilation was not still evident in lower leaves, since among others, C and N content (Figure S4) were relatively stable, the ratio (Gln + Asn) / (Glu + Asp) (Figure 4) increased while no increase in GDH activity was observed (Figure 5). Therefore, we can exclude a strong remobilization of the nitrogen reserves and thus a process of senescence in basal leaves.

Exclusive ammonium nutrition is often considered a stressful situation for the plant and may provoke a set of symptoms such as decreased biomass production, ionic imbalance and leaf chlorosis (Britto and Kronzucker, 2002). The sequential apparition of new leaves was similar between treatments, showing that leaf phenology was not affected by ammonium nutrition at 15 mM. However and as expected, feeding plants with NH_4^+ resulted in the reduction of plant biomass (Figure 1A), in association with important metabolic and ionic changes; but the occurrence of chlorosis was not observed. Furthermore, mature leaves (leaves 6 and 9) grown under ammonium nutrition had more chlorophyll than under nitrate and ammonium nitrate conditions (Fig 1). Notably, high chlorophyll content has been associated with mild ammonium stress (Sanchez-Zabala, González-Murua, & Marino, 2015). Altogether, these observations suggest that in tomato plants the supply of 15 mM NH_4^+ induced moderate stress, rather than ammonium toxicity.

Coping with ammonium stress: A trade-off between nitrogen assimilation and growth

The overall data allowed distinguishing 3 sections vertically in the tomato plants in response to nitrogen treatment, notably in view of NH_4^+ accumulation in the leaves. The first section corresponding to leaves 1 and 2 on the top of the plant, for which growth was not influenced by N-source (Figures 1B and Figure S1), despite they showed metabolic differences. Thus, these young leaves had low levels of NH_4^+, which suggests that ammonium supply to young growing leaves was low or that these leaves rapidly metabolizes it. In fact, these leaves were quite similar to those grown under nitrate or ammonium nitrate treatment, especially regarding total amino acids and protein content, the main sink for nitrogen (Figure 4). One hypothesis is that carbon and nitrogen requirements of young sink leaves were fulfilled by the import of sugars and amino acids produced by mature leaves (Tegeder and Masclaux-Daubresse, 2018). Such import entails saving the energy of the costly assimilation of inorganic N, thus allowing an optimum growth regardless of the nitrogen source.

The second section corresponds to the next constantly growing leaf (leaf 3) (Figures 1B and Figure S1). In this leaf, NH_4^+ accumulation in the tissue reached the highest value among the leaves studied, but still had no impact on growth (Figure 4). It appears that this leaf (leaf 3) corresponds to a transition, in which NH_4^+ was probably massively stored in the vacuole; thus, its assimilation being relatively low. In contrast, in the lower vertical section, which corresponds to mature leaves (leaf positions superior to 6), NH_4^+ content decreased (Figure 4). Mature leaves were also smaller in response to ammonium nutrition compared to nitrate and ammonium nitrate treatments, especially as they were closer to the plant base (Figures 1B and Figure S1). Indeed, these leaves showed the typical characteristics of ammonium nutrition, namely a great accumulation of free amino acids and proteins compared to nitrate treatment (Setién *et al.*, 2014; Vega-Mas *et al.*, 2017). Surprisingly, there was no evident link between overall NH_4^+ accumulation and assimilation. Indeed, those leaves that were more affected by ammonium stress regarding their biomass (leaves 6 and 9) were the ones with the highest N-assimilation rate, in view of metabolites content and the increase in the (Gln + Asn) / (Glu + Asp) ratio compared to younger leaves (Figure 4). Therefore, suggesting that in mature leaves a larger part of the NH_4^+ is assimilated and stored as nitrogen-rich compounds. This could be a consequence of higher availability and usage of carbon skeletons for assimilation in source leaves compared to actively-growing leaves. In agreement, a number

of studies have shown that increased carbon availability promoted the assimilation of NH_4^+, such as in tomato grown under elevated CO_2 conditions or in wheat grown under high irradiance by improving the photosynthesis process (Setién *et al.*, 2013; Vega-Mas *et al.*, 2015).

Altogether, our results suggest that tomato plants manage the ammonium stress by avoiding the accumulation of NH_4^+ in young growing leaves. Instead, it appears that the energy devoid for NH_4^+ assimilation in the older leaves in order to prevent cytosolic NH_4^+ accumulation, would suppose a trade-off for leaf growth. Furthermore, the estimations of the potential energy contained in the metabolite pools in Figure 6 suggest that leaf biomass construction is more expensive under ammonium nutrition. Accordingly, a recent work with GS2 deficient mutant plants suggested that excessive NH_4^+ assimilation by plastidic GS was a major cause of ammonium toxicity in *Arabidopsis thaliana* (Hachiya *et al.,* 2019). Apart from the energetic cost of NH_4^+ assimilation, the authors suggested that the excessive production of H^+ by GS would be a cause of ammonium stress. Finally, it is interesting to note that our results suggest that NH_4^+ content cannot be considered as a systematic quantitative metabolic marker of ammonium stress (Cruz *et al.*, 2006; Lasa, Frechilla, & Lamsfus, 2001).

Inorganic ions adjust their levels in function of the nitrogen source to ensure the osmolarity

In mature leaves, excessive NH_4^+ assimilation appears detrimental for their growth. Besides, the negative impact of ammonium nutrition on growth has also been associated with changes in cell ionic balance (Hoopen *et al.*, 2010; Hachiya *et al.*, 2012). In order to maintain the ionic balance, the absorption of NO_3^-, which is negatively charged, must be accompanied by the import of positive charges (H^+ or cations), while the accumulation of NH_4^+ must be compensated by a reduction of the positive charges or by an increase of the negative ones. For instance, NH_4^+ uptake has been shown to compete with the uptake of cations, notably K^+, Ca^{2+} and Mg^{2+} (Lang and Werner, 1994; Hoopen *et al.*, 2010; Hachiya *et al.*, 2012). In our study, the impact of ammonium nutrition on cations levels appears evident in view of Mg^{2+} and Ca^{2+} contents (Figure 7). In contrast, an increase in anions concentration has been reported for instance in tomato (Kirkby and Mengel, 1967) and *Ricinus communis (*van Beusichem *et al*. 1988). In agreement, we observed an increase in Cl^- content that was specific to the youngest leaves (leaf 1) and that of HPO_4^{2-} in mature leaves. This ionic compensation was responsible

for the adjustment in cell osmolarity when NO_3^- was replaced by NH_4^+ in the nutrient solution (Figure 8) as already observed in tobacco leaves (Walch-Liu *et al.*, 2000). Nevertheless, the impact of the nitrogen source in cell osmolarity might be species-dependent since previous studies, among others, in sunflower (Ashraf, 1999) and maize (Hessini *et al.*, 2019), reported an increase of osmolarity under ammonium nutrition. Independently to the nitrogen source, our results clearly show that inorganic ions played a major role in the maintenance of leaf cell osmolarity (Figure 8), with a minor contribution of NO_3^- and NH_4^+. Moreover, under nitrate conditions, organic acids had greater contribution to the osmolarity than in ammonium conditions. Notably, in mature leaves of NO_3^--fed plants they accounted for 25-18% of the osmolarity, with a great contribution of malate (90%). In contrast, when NO_3^- was progressively replaced by NH_4^+ as nitrogen source, malate decrease was compensated by inorganic ions (Figure S3), thus avoiding the depression of the osmolarity (Figure 8).

Biochemical pH-stat regulation would explain impaired C management on NH_4^+-fed plants

Plant cells are very efficient in maintaining the pH of the cytosol and this is achieved independently of the apoplastic and vacuolar pH variations (Britto and Kronzucker, 2005; Hachiya *et al.*, 2012). For example, several studies have shown that ammonium nutrition exerted little impact on the cytosolic pH (Kosegarten *et al.*, 1997; Aarnes *et al.*, 2007; Hachiya *et al.*, 2012). Likely thanks to biochemical buffering and by proton exchange with the apoplast and vacuole (Sakano, 2001).

Regarding N metabolism, the assimilation of NO_3^- produces OH^- that may alkalinize the cytosol (Raven and Smith, 1976). The pH-stat theory developed by Davies proposes that the increase in pH, activates PEPC and inhibits ME. Consequently, malate accumulates and in turn, OH^- ions generated in shoot assimilation are neutralized. Conversely, NH_4^+ assimilation by GS generates H^+, thus leading to acidification (Hachiya *et al.*, 2019) that is adjusted by the inhibition of PEPC whereas ME is activated, which would favor the conversion of malate to pyruvate (Davies, 1973; Sakano, 2001). Although controversial (Britto and Kronzucker, 2005), the biochemical pH-stat has been commonly proposed to justify low levels of malate in NH_4^+-fed plants (Van Beusichem *et al.*, 1988; Pasqualini *et al.*, 2001; Coleto *et al.*, 2019).

In our work, we clearly observed a positive correlation between the contents of intracellular NO_3^- and malate (Figure S6). When comparing the nitrogen source, since protein and amino

acid levels were similar between nitrate and ammonium nitrate conditions (Figure 4), it becomes clear that the differential accumulation of malate between these two treatments (Figure 3) cannot be justified because of its use by TCA cycle to generate carbon skeletons for amino acid synthesis. Ben-zioni, Vaadia, & Lips (1970) also showed a link between NO_3^- content and malate accumulation in leaves of different species. Overall, they suggested that NO_3^- metabolic reduction is functionally coupled to malate synthesis. Then, it seems that, in tomato, the availability and nitrate reduction process, which are dependent on leaf position and nitrogen nutrition, determine malate accumulation (Figure 3, Figure 7 and Figure S6). Therefore, when NO_3^- is replaced by NH_4^+ in the nutrient solution, the low levels of malate would be explained by the biochemical pH-stat to control cytosolic pH (Davies, 1973) and probably also by the fact that under ammonium nutrition the consumption of carbon skeletons is prioritized towards amino acids synthesis (Vega-Mas *et al*., 2019).

Consistent findings demonstrated that the regulation of plant glycolysis is in part controlled by the levels of PEP (reviewed in Park, and Plaxton, 2011). Then PEPC and PK play a central role in the overall regulation of plant respiration dictating the rate of mobilization of sucrose or starch. Accordingly, and in agreement with the potential role of PEPC in the context of pH-stat under ammonium nutrition (Pasqualini *et al.*, 2001), we observed an increase in the levels of soluble sugars and starch together with carbon content (Figure 3 and Figure S4). On one hand this suggests that in ammonium condition, photosynthesis is not affected and on the other hand that there is a deregulation of carbon use, which indeed is known to be key for NH_4^+ detoxification through its assimilation (Vega-Mas *et al.*, 2019). Other works also showed starch and sugar accumulation in response to ammonium, for example in tomato (Vega-Mas *et al.*, 2017), barley (Lang and Werner, 1994*a*) or *A. thaliana* (Hachiya *et al.*, 2012). In the same way, Scheible *et al.* (1997) showed the importance of NO_3^- as a signal for starch degradation and organic acid synthesis in tobacco. Conversely, they also evidenced the increase of ADP-glucose pyrophosphorylase (AGPase) gene expression by NH_4^+, which encodes a key enzyme for starch biosynthesis. Overall malate levels and the accumulation of carbon in the form of sugars and starch support the idea of the regulation of PEPC and ME by the cytosolic pH under ammonium nutrition. Therefore, the measured lower PEPC activity together with the induction of ME activity would be relevant in the context of the biochemical pH-stat in order to maintain the cytosolic pH.

Finally, the regulation of anaplerotic routes associated to TCA cycle, including ME and PEPC, is commonly observed upon ammonium nutrition to supply the cycle with the needed intermediary carbon skeletons to sustain the high NH_4^+ assimilation rates typical of NH_4^+-fed plants (Sarasketa *et al.,* 2016; Vega-Mas *et al.,* 2019).

CONCLUSION

Through an integrative approach at plant scale, the present work reveals a differential adaptation of tomato leaves to the nitrogen source in function of their vertical position in the plant. In mature leaves, the most likely hypothesis for the growth reduction observed is that excessive assimilation of NH_4^+ would suppose an energy trade-off for growth. Besides, ammonium nutrition triggers a reallocation of carbon into sugar and starch at the expanse of organic acid with an energy cost for the plant. The most likely hypothesis for such deregulation is the need to maintain the cytosolic pH through the biochemical pH-stat. In contrast, although carbon metabolism is also adjusted in very young leaves, it must be noted that these leaves act as sink organs receiving organic matter already assimilated to produce their structural compounds (Tegeder and Masclaux-Daubresse, 2018). Moreover, in these leaves NH_4^+ assimilation is probably low. Altogether young leaves spend lower energy for their metabolic adaptation respect to mature ones, which makes their growth is not still affected by the nutrition type. Finally, this works underlines the importance of taking into account the leaf phenological state when studying nitrogen metabolism.

Supplementary information

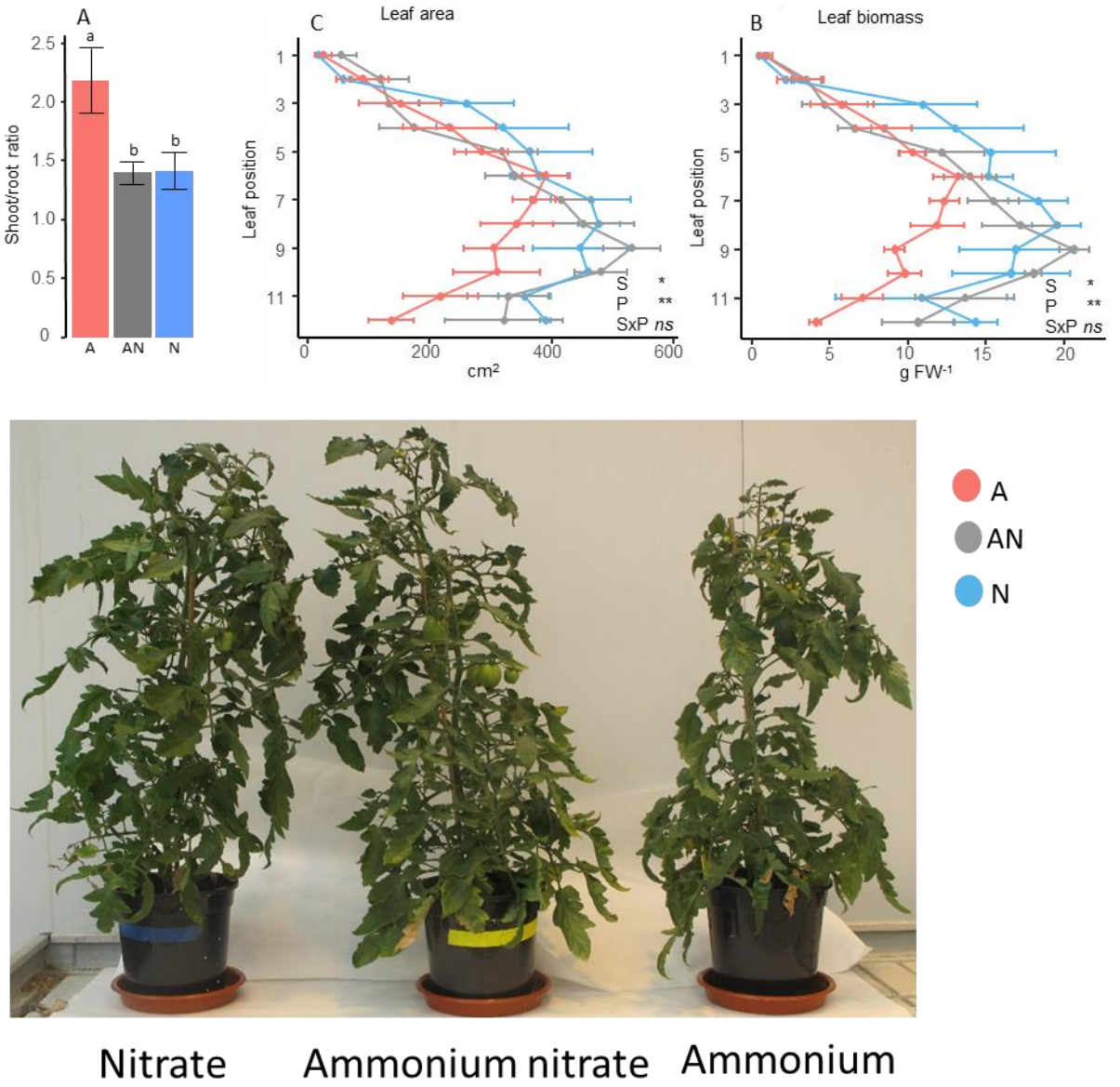

Figure S1: Root to shoot ratio (A), leaf fresh weight (B), leaf area (C) an representative picture of tomato plants grown with ammonium (A: red), ammonium nitrate (AN: grey), and nitrate (N: blue) as nitrogen source, considering their vertical position in the plant. Values represent the mean ± se (n=4). In panel A different letters indicate significant differences according to one-way ANOVA followed by Duncan´s test ($p<0.05$). Significant differences in panels B and C are shown according to two-way ANOVA (**: $p<0.01$; *: $p<0.05$; *ns*: not significant) where S indicates nitrogen source effect; P indicates leaf position effect and S×P indicates interaction effect.

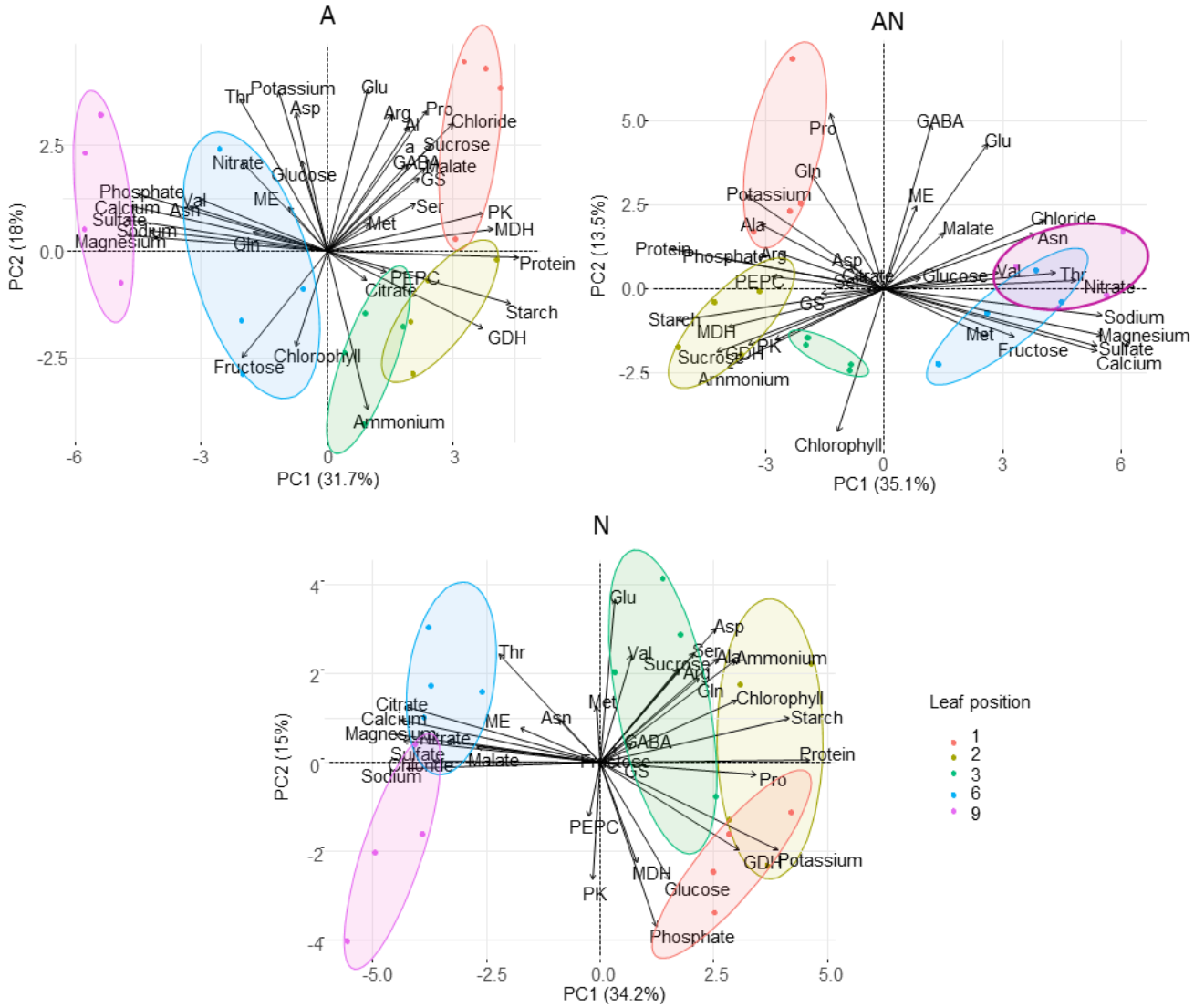

Figure S2: Principal component analysis (PCA) of metabolites, ions and enzymatic activities determined in leaves (positions 1,2,3,6 and 9) of tomato plants grown with ammonium, ammonium nitrate and nitrate as nitrogen sources analysing each nutrition type separately. PCA was performed from the correlation matrix generated with 29 variables, with 4 replicates per treatment and leaf position.

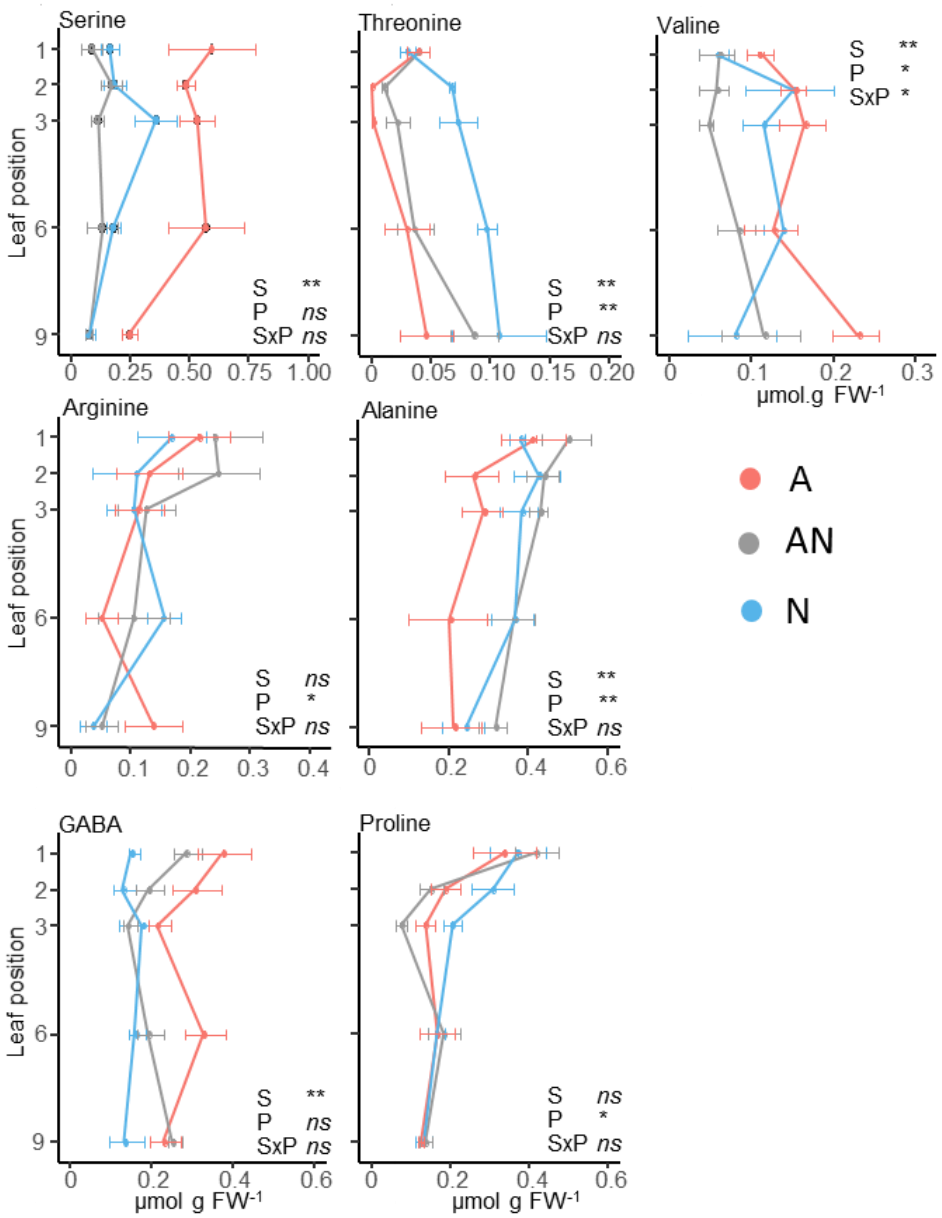

Figure S3: Serine, threonine, valine, arginine, alanine, GABA and proline content in leaves of tomato plants, grown with ammonium (A; red), ammonium nitrate (AN; grey) and nitrate (N; blue) as nitrogen source, considering their position in the plant. Values represent mean the ± se (n = 4). Significant differences are shown according to two-way ANOVA (**: p<.01; *: p<0.05; *ns*: not significant) where S indicates nitrogen source effect; P indicates leaf position effect and S×P indicates interaction effect.

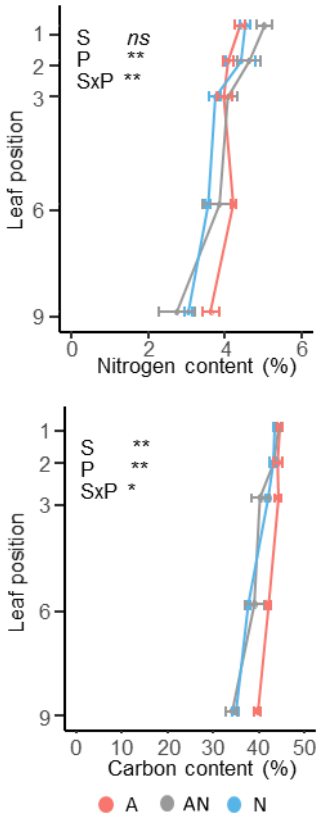

Figure S4 : Carbon and nitrogen content in leaves of tomato plants, grown with ammonium (A; red), ammonium nitrate (AN; grey) and nitrate (N; blue) as nitrogen source, considering their position in the plant. Values represent the mean ± se (n=4). Significant differences are shown according to two-way ANOVA (**: p<0.01; *: p<0.05; *ns*: not significant) where S indicates nitrogen source effect; P indicates leaf position effect and S×P indicates interaction effect.

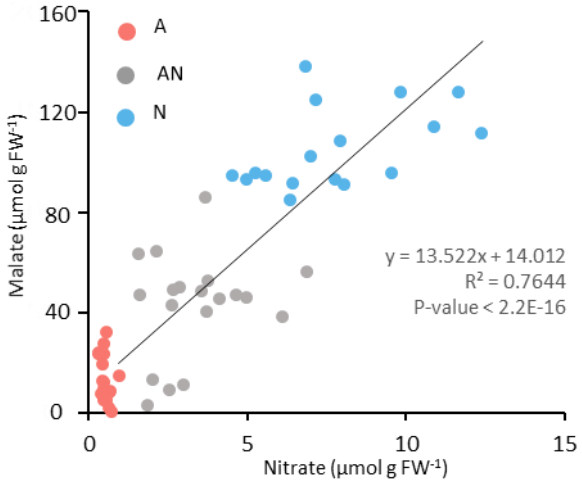

Figure S5: Correlation between malate content and nitrate content in leaves of tomato plants grown with ammonium (A; red), ammonium nitrate (AN; grey) and nitrate (N; blue) as nitrogen source. Significance is given according to Pearson correlation.

Table S1: ATP equivalents released during the complete oxidation for different plant metabolites according to the literature.

Metabolite	Potential energy (equivalent of ATPs)	Reference
Alanine	18.5	Craig & Weber, (1991)
Arginine	10	
Asparagine	4	
Aspartate	1	
Glutamate	8.5	
Glutamine	9.5	
Glycine	4	
Phenylananine	63	
Proline	12.5	
Serine	15	
Threonine	6	
Valine	25	
Glucose	36	Rich & Rich, (2003)
Fructose	36	
Sucrose	37	
Starch	37	
Malate	2.5	
Citrate	10	
Protein	(8.5+5)/115	Piques *et al.*, (2009)

Chapter II

Building a vacuole under ammonium nutrition:

A costly trade-off between pH adaptation and expansion

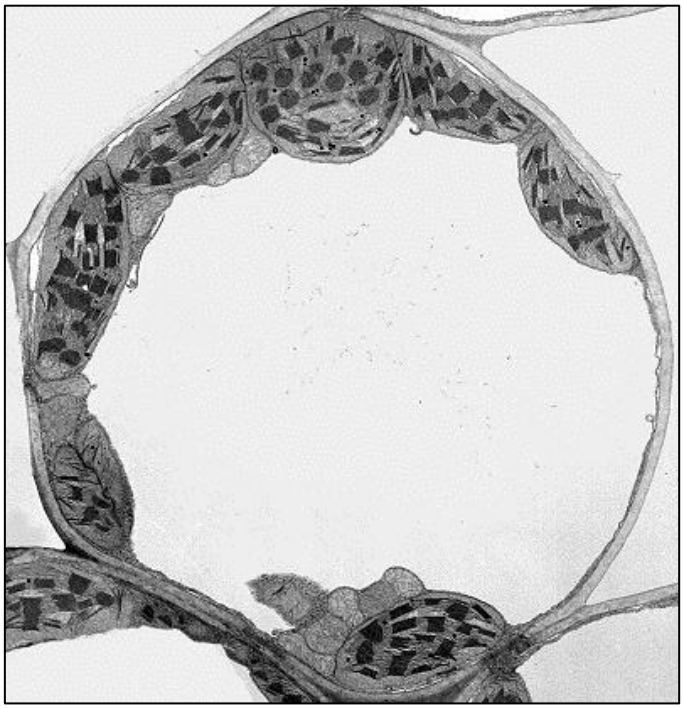

Whole view of parenchyma cell with a large central vacuole. Transmission electron micrograph from the University of Wisconsin Digital Collections (United States)

ABSTRACT

Ammonium (NH_4^+) and nitrate (NO_3^-) are the main source of inorganic nitrogen available for the plant. However, a plant fed with nitrate usually reaches an optimum growth higher respect of plants fed with NH_4^+. Indeed, ammonium nutrition is known to represent a stress for the plant. Among others, impaired growth in NH_4^+-fed plants has been associated with a repression of cell elongation. In this context, we aimed to study the effect of the N-source on the vacuole, an essential component of cell expansion, by monitoring leaf development in tomato plants grown with NH_4^+ or NO_3^- as unique N-source. First, a microscopy morphometric analysis evidenced that the reduced cell expansion under ammonium nutrition was associated with smaller vacuole size. To further study of vacuole involvement in ammonium stress we combined biochemical analysis, including non-aqueous fractionation*, in vi*vo determination of cell pH and mathematical modeling. The model was built to predict the thermodynamic equilibrium of solutes across the tonoplast and estimate vacuolar fluxes into the vacuole all along the leaf development. Overall, we show that the entrance of solutes in vacuoles was lower of NH_4^+-fed leaves thus, potentially affecting vacuole and cell expansion. In part, this was due the metabolic reorganization of the cells leading to malate depletion under ammonium nutrition. Moreover, increased vacuolar acidity in ammonium-fed plants provoked that a higher energy cost for the transport across the tonoplast respect to nitrate-fed plants. Altogether, we underline an energy trade-off between the control of cytosolic pH and growth with the vacuole playing a central role.

INTRODUCTION

Nitrogen is a fundamental building element for most organic molecules such as amino acids, proteins or nucleic acids. Excluding the few species, mostly legumes, able to use N_2 as source of nitrogen (N), plants take up N from the soil mainly in the form nitrate (NO_3^-) and ammonium (NH_4^+). Because of its redox state, the utilization of NH_4^+ is energetically more efficient than NO_3^-. In fact, the two reductive steps necessary to reduce NO_3^- to NH_4^+ consume one NADH and six ferredoxines, equivalent to 6 electrons (Hase *et al.*, 2006). Nevertheless, paradoxically, ammonium nutrition can entail a stressful situation that induces a set of symptoms typically called "Ammonium syndrome". The threshold of the NH_4^+ concentration needed to provoke this syndrome is highly variable and mostly dependent on the plant species/genotype (Cruz *et al.*, 2011; Sarasketa *et al.*, 2014). The symptoms associated to ammonium syndrome are mainly growth retardation, alterations in root:shoot ratio, leaf chlorosis ending up in yield reduction (Britto and Kronzucker, 2002; Esteban *et al.*, 2016). The mechanisms responsible for ammonium syndrome have still not been fully elucidated. Several factors have been described in the last decades associated to ammonium syndrome, among others, the decrease in net photosynthesis caused by the uncoupling of photophosphorylation process by NH_4^+ in the chloroplast (Britto and Kronzucker, 2002), the acidification of the external medium (Hachiya *et al.*, 2019) and the depletion in inorganic cations uptake because of the direct competition with NH_4^+ uptake (Kirkby and Mengel, 1967; Hachiya *et al.*, 2012). Besides, disruption in hormone balance, including ethylene, abscisic acid, auxin, and cytokinins has also been related to ammonium syndrome (Barker and Corey, 1991; Cao *et al.*, 1993; Walch-Liu *et al.*, 2000; Li *et al.*, 2014). Importantly, ammonium-fed plants also suffer of energy impairment; indeed, the control of cytosolic NH_4^+ levels, notably with a high rate of NH_4^+ assimilation, involves a high carbon/energy demand that would not be used for growth (Vega-mas *et al.,* 2019). In parallel, under severe ammonium stress, the occurrence of oxidative stress has also been reported associated to the lower reductive power needed for NH_4^+ assimilation (Podgórska *et al.*, 2013). Today, it appears clear that no single mechanism is responsible for the observed ammonium syndrome but responds to a combination of the above mentioned factors.

The interest on studying ammonium nutrition relies on the fact that ammonium-based fertilization is known to limit the N losses associated with N fertilization in agriculture. Notably, through reducing NO_3^- leaching and nitrogenous gases emissions, specially N_2O due to its global warming potential, 265 times higher than CO_2 (IPCC, 2014). Overall, increasing crops nitrogen use efficiency (NUE) is essential to develop a sustainable agriculture. In addition, ammonium-based nutrition may also provoke beneficial alterations in plant physiology such as the induction of cross-tolerance to other stresses (Marino and Moran, 2019).

A number of cell biology studies have made a link between the growth retardation related to ammonium nutrition and the reduction of cell expansion (Walch-Liu *et al.*, 2000; Liu *et al.*, 2013; Podgórska *et al.*, 2013). This suggests that mechanisms controlling cell expansion might be affected when plants are grown with NH_4^+. For instance, Podgórska *et al.* (2013) followed by Głazowska *et al.* (2019) showed alterations of the cell wall under NH_4^+ nutrition that could potentially reduce cell elongation. However, cell growth is also largely dependent of the internal pressure exerted on the cell wall by the vacuole, a large compartment carrying numerous functions such as cell detoxification (Coleman and Randall, 1997), regulation of cytosol homeostasis (Shitan and Yazaki, 2013) and metabolites compartmentation (Beauvoit *et al.*, 2014). Indeed, the continuous transport of solutes into the vacuole leads to the uptake of water that maintains cell turgor.

The role of the vacuole in ammonium stress responses has been poorly studied. Accordingly, the question of the subcellular distribution and dynamics of metabolites concentrations has been rarely addressed when changing N-source. As ammonium stress is generally associated with NH_4^+ accumulation in the cytosol, it is often proposed that its compartmentalization into the vacuole is among the strategies that plants may deploy to deal with this stress. Several evidences support this hypothesis including the quantification of millimolar NH_4^+ concentrations inside the vacuole of *Chara corallina* cells using ion-selective microelectrodes (Wells and Miller, 2000*b*). Also, yeast transformed with the Arabidopsis TIP2;1 and TIP2;3 aquaporins of the tonoplast increased their tolerance to NH_4^+ by facilitating NH_3 transport to the vacuole (Loque *et al.*, 2005). Moreover, it has been observed that the tonoplast receptor-like kinase CAP1 is important for ammonium stress tolerance by the control of cytosol vs.

vacuole NH_4^+ levels by a mechanism that still needs to be identified (Bai *et al.*, 2014). Another important aspect that greatly influences cell performance in relation with the N-source provided is the control of cell pH. Indeed, it is known that external pH is an important factor involved in plants tolerance towards ammonium stress (Sarasketa *et al.*, 2016; Hachiya *et al.*, 2019). In fact, it is commonly assumed that the glutamine synthesis from NH_4^+ acidifies cytosol whereas its synthesis from NO_3^- would alkalinize the cytosol (Raven and Smith, 1976). For this reason, the regulation of cytosolic pH by different mechanisms (Davies *et al.,* 1974), including the vacuolar accumulation of H^+s would be crucial to maintain the pH homeostasis.

In this context, the objective of this chapter was to evaluate the importance of vacuole expansion and metabolism in plant responses to ammonium stress. To carry out this aim, we monitored the development of a leaf from its appearance until its complete expansion in tomato plants grown under the exclusive supply of NH_4^+ or NO_3^- as source of N. Overall, the combination of plant physiology, cell biology, metabolic analysis and mathematical modeling allowed us linking vacuole expansion with solute fluxes to unravel in which manner the N-source affects leaf cell growth.

GROWTH CONDITIONS AND EXPERIMENTAL DESIGN

Tomato (*Solanum lycopersicum*, cv. M82) seeds were sown in trays filled with perlite:vermiculite 1:2 (v:v) inert substrate mixture and watered with deionised water. Trays were kept during 14 days in a growth chamber under a 14/10 h photoperiod with a light intensity of 350 µmol m^{-2} s^{-1} and 60/70% relative humidity and 23/18 °C day/night conditions, respectively.

Six hundred homogeneous seedlings were transferred to pots (1 seedling per pot) filled with perlite:vermiculite 1:2 (v:v) and set up in a greenhouse (Greenhouse Service, SGIker, UPV/EHU). The greenhouse conditions were 14/12 h day/night period with the support of additional light sources ensuring a minimum of 200 µmol $m^{-2}s^{-1}$ of intensity. Temperature and relative humidity were 25/18 °C and 50/60% relative humidity, respectively (day/night). The whole experiment was conducted between May and July 2017.

Plants were irrigated three times per week with a nutrient solution adjusted at pH 6 that contained macronutrients (1.15 mM K_2HPO_4, 0.85 mM $MgSO_4$, 0.7 mM $CaSO_4$, 2.68 mM KCl, 0.5 mM $CaCO_3$, 0.07 mM NaFeEDTA) and micronutrients (16.5 µM Na_2MoO_4, 3.5 µM $ZnSO_4$, 3.7 µM $FeCl_3$, 0.47 µM $MnSO_4$, 0.12 µM $CuSO_4$, 16.2 µM H_3BO_3, 0.21 µM $AlCl_3$, 0.126 µM $NiCl_2$ and 0.06 µM KI). Nitrogen was applied at a final concentration of 15 mM in two different forms that corresponded to 100% ammonium applied as 7.5 mM $(NH_4)_2SO_4$ and 100% nitrate applied as 7.5 mM $Ca(NO_3)_2$. To appropriately compare both nutrient regimes, in the main experiment nitrate nutrition was supplemented with 7.5 mM $CaSO_4$ to equilibrate the sulphate supplied in ammonium treatment. Overall, 300 plants were grown per treatment. In addition, a control with 4 plants per condition was also performed by equilibrating Ca^{2+}, meaning that in this case ammonium-fed plants were supplemented with 7.5 mM $CaSO_4$ to equilibrate the calcium supplied nitrate treatment.

Plants were daily monitored to register and tag the appearance of the fourth leaf on every plant. Overall, we estimated that when the terminal leaflet of the leaf was of 3 cm length it corresponded to a 7 day-old leaf, which in turn corresponded to 30-35 day-old plants. With this criterion and to follow leaf development in function of the N-source provided, we

harvested the fourth leaf at seven time points corresponding to 7, 10, 13, 16, 21, 31 and 41 day-old leaves. Three plants per treatment and time point were harvested to determine biomass parameters (fresh weight (FW) and leaf area) and conduct the cytological analysis. Dry weight was determined after incubating the plant material in an oven at 80 °C for 72 h. For metabolic analyses three biological replicates were established per time point, each one consisting in a pool of the fourth leaf of ten plants. To do so, the central vein of the leaves was rapidly removed with a scalpel and the remaining lamina immediately frozen in liquid nitrogen and stored at -80 °C for further analysis.

RESULTS

Leaf physiological traits and growth

To evaluate the overall plant performance in function of their growth with nitrate or ammonium as N-source we determined total plant biomass in every time point (Figure 1A) by weighing the root and the aerial part separately (Figure S1). Between day 7 and 16 the total biomass of the plant was similar regardless the source of N. Thereafter, growth on ammonium was affected, with an effect that increased with plant age. At the end of the experiment, when the 4th leaf was 41-day-old, total plant biomass was reduced by 33% in ammonium-fed plants.

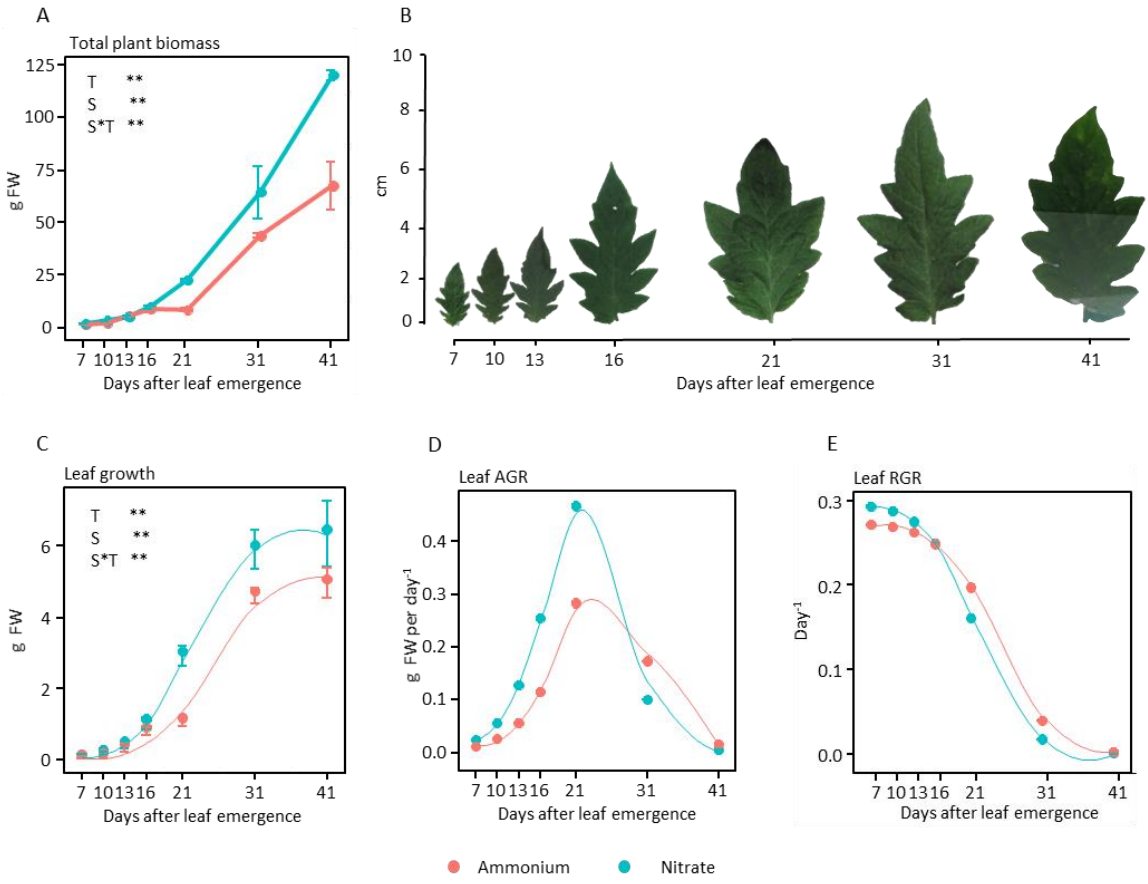

Figure 1: Time course evolution of whole-plant biomass and fourth leaf development of tomato plants grown with ammonium (red), and nitrate (blue) as nitrogen source. (A) Whole plant biomass during fourth leaf aging. (B) Representative images of the terminal leaflet of the fourth leaf. (C) Fourth leaf biomass. Continuous line represents regression analysis using a three-parameter logistic function. (D) Absolute growth rate (AGR) obtained by derivation of the logistic function and (E) relative growth rate (RGR) obtained by dividing the absolute growth rate by logistic function values. Values represent mean ± se (n = 3). For panels B and C, significant differences are shown according to two-way ANOVA (**: p<0.01; *: p<0.05; *ns*: not significant) where S indicates nitrogen source effect; T indicates days effect and S×T indicates interaction effect.

The growth of the 4th leaf followed a sigmoidal curve which is classically divided into the initial exponential phase, followed by a linear phase where growth rate is maximum, and finally the asymptotic phase where growth rate decreases until the maturation phase when growth ceases (Figure 1B to 1E). N-source did not affect leaf growth pattern (Figures 1C and 1D) and for both treatments, the maximum leaf growth rate was attained close to 21 days (Figure 1D). Importantly, the maximum growth rate of ammonium-fed leaves was lower compared to nitrate-fed leaf. Nitrate growth rate dropped from its maximum 0.46 g day^{-1} at day 21 to 0.1 g day^{-1} at day 31, whereas growth deceleration in NH_4^+-fed-leaf was more moderate and lasted until day 41. At the end of the experiment, fourth leaf biomass was 20% lower in NH_4^+-fed plants (Figure 1C).

Chlorophyll content was quantified as a physiological marker (Figure S2). The 4th leaf did not show chlorosis under any nutrition type; therefore, indicating that NH_4^+-fed plants were not subjected to a severe stress and also showing that, at this developmental stage, the leaves did not still enter a senescence process (Figure 1B). In general, chlorophyll content varied in a similar way under both nutritions, namely increasing between 7 and 13-16 days after emergence followed by a slow decrease thereafter (Figure S2).

Ammonium nutrition induced a reduction of cell and vacuole size

There is evidence suggesting that ammonium nutrition may affect cell expansion (Walch-Liu *et al.*, 2000; Liu *et al.*, 2013; Podgórska *et al.*, 2017). Since cell expansion is driven by vacuole expansion, we engaged a fine monitoring of the volume of leaf parenchymal cells, and their main subcellular compartments (vacuole, cytoplasm and cell wall), by a morphometric analysis (Figure 2). Leaf growth was closely related to individual cell expansion and this is highlighted by the similar shape of leaf and cell absolute growth rate (AGR) curves between both treatments (Figure 1D and 2B). Parenchyma cell volume increased by a factor of 11 during the expansion phase with a maximum AGR at 21 days after leaf emergence (Figure 2B). At the end of the expansion the mean cell volume was 0.013 nL under ammonium nutrition and 0.020 nL under nitrate nutrition. By contrast, cytoplasmic and cell wall volumes increased slowly mainly between 7 and 16-21 days (Figure 2B). Interestingly, the vacuolar volume

correlates perfectly with the total cell volume irrespective of the N-source (Figure 2C), thus suggesting that ammonium nutrition may be affecting cell growth through vacuole expansion.

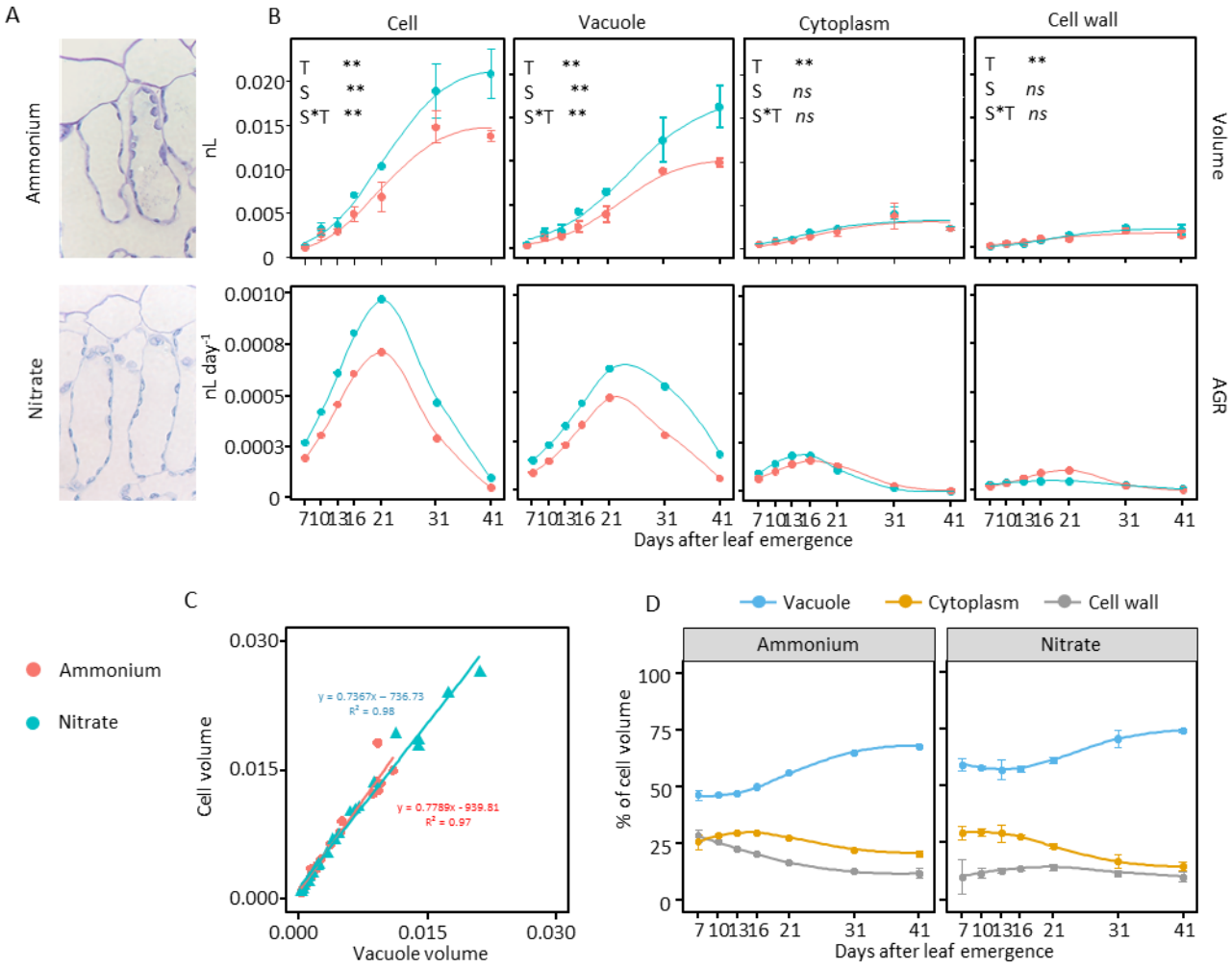

Figure 2: Time course evolution of cellular and subcellular volumes throughout the development of tomato leaf grown with ammonium (red) and nitrate (blue) as nitrogen source. (A) Representative images of a 21 days aged leaf cytology under different nutritional regimes. (B) Cell, vacuole, cytoplasm and cell wall volume. Continuous line represents regression analysis using a three-parameter logistic function. AGR, curves calculated by derivation of the corresponding logistic function are represented below. (C) Pearson correlations between cell volume and vacuole volume. (D) Time course of relative volumes (% cell) of vacuole (blue), cytoplasm (yellow), and cell wall (grey) obtained from fitted data shown in panel B. Values represent mean ± se (n = 3). Significant differences in panel B are shown according to two-way ANOVA (**: p<0.01; *: p<0.05; *ns*: not significant) where T indicates time effect; S indicates nitrogen source effect and T*S indicates interaction effect.

The proportion of vacuolar and cytoplasmic volume occupied in cells changed with time following a mirror-shaped pattern (Figure 2C): between 13 and 41 days after leaf emergence, the vacuole expanded from 47% to 67% under ammonium nutrition, and from 57% to 74% under nitrate nutrition. On the other side, the cytoplasm shrank from 29% to 20% of the cell

volume for ammonium treatment and from 30 to 15% for nitrate treatment (Figure 2D). Relative growth rate of the vacuole, cytoplasm, vacuole and cell wall are shown in Figure S3.

Changing N-source involved a profound change in cell metabolites and ions content

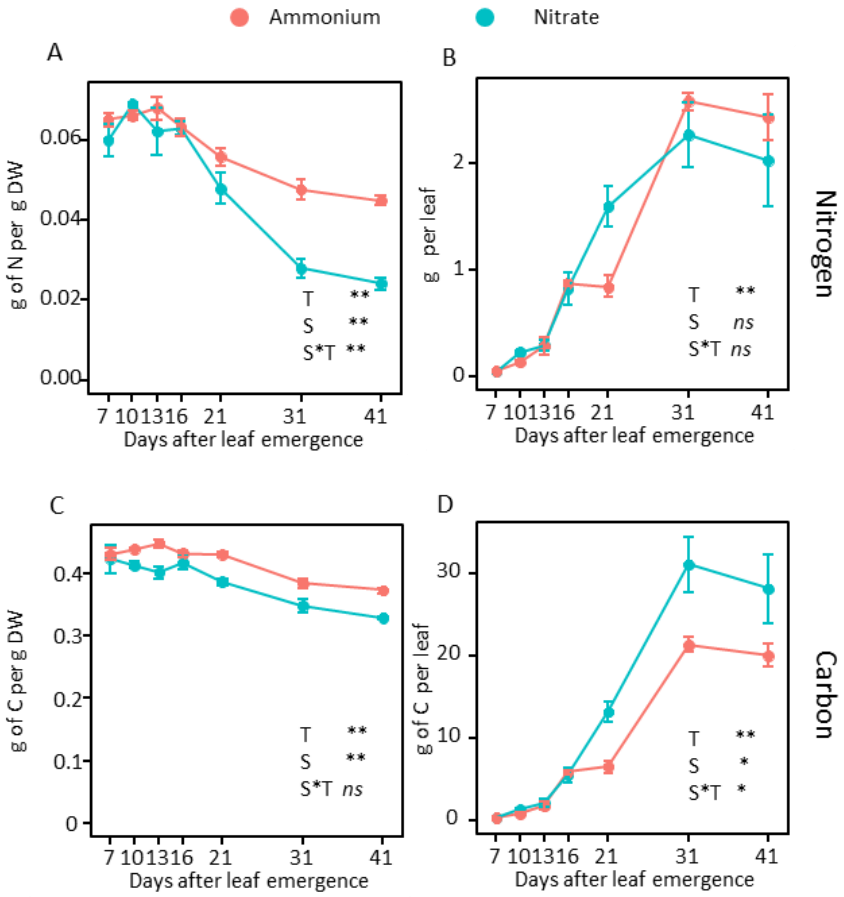

Figure 3: Time course evolution of nitrogen and carbon content throughout the development of tomato leaf grown with ammonium (red) and nitrate (blue) as nitrogen source. Nitrogen and carbon content per g of dry leaf (A, C) and per leaf (B, D). Values represent mean ± se (n = 3). Significant differences are shown according to two-way ANOVA (**: p<0.01; *: p<0.05; *ns*: not significant) where S indicates nitrogen source effect; D indicates days effect and S×D indicates interaction effect.

In young leaves (7 to 16 day-old), total N content was constant, close to 0.065 g DW^{-1} independently of the N-source. Then, it progressively decreased in both conditions, but twice faster in nitrate fed-leaves (Figure 3). Because leaf growth was affected by the N-source, N content was also calculated as g per leaf. In this case, N content increased over time similarly in both conditions, except for day 21 in which N content was higher under nitrate nutrition

(Figure 3B and 3D). This suggests that the root supply of N to individual leaves was similar when changing of N-source. Under ammonium nutrition, C content was higher along leaf development reaching a 30% decrease late time points (31 and 61 days). Interestingly, C and N content were correlated with RGR and protein content (Figure S5) in both nutritions (Figure S4). In fact, It is worth stressing that proteins, which are the main N storage pool in plant cells, seem associated with tissue expansion. However, it is known that proteins do not have a relevant contribution to the osmotic concentration of the cell (Liu *et al.*, 2018). Besides, starch content, as relevant pool of carbon, was higher from 7 to 21 days under ammonium nutrition relative to nitrate and then decreased to lower level than nitrate from 31 to 41 days (Figure S4).

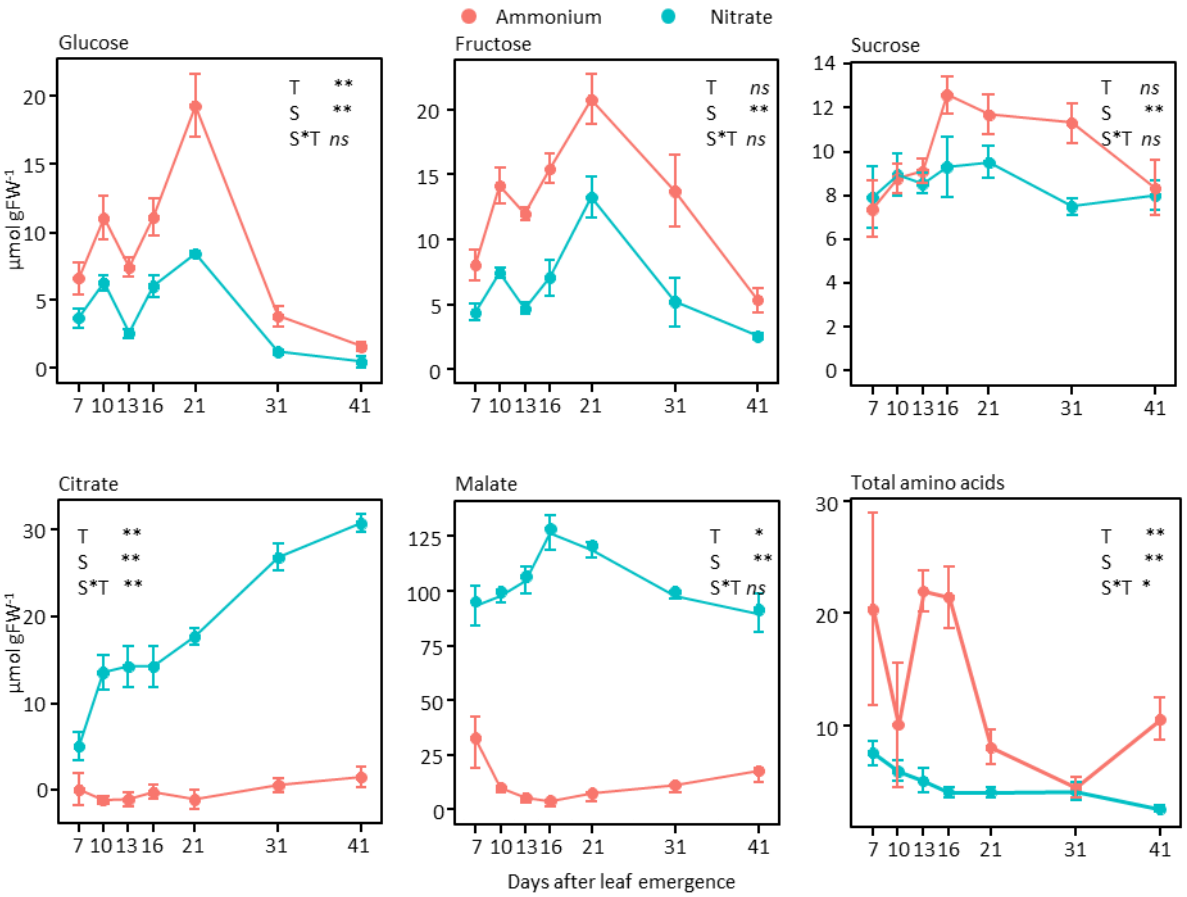

Figure 4: Time course evolution of sugars, organic acids and total amino acids throughout the development of tomato leaf grown with ammonium (red) and nitrate (blue) as nitrogen source. Values represent the mean ± se (n = 3). Significant differences are shown according to two-way ANOVA (**: p<0.01; *: p<0.05; *ns*: not significant) where S indicates nitrogen source effect; D indicates days effect and S×D indicates interaction effect.

Plant cell expands through the continuous deposition of solutes in the vacuole in order to maintain the osmotic force, resulting in the absorption of water (Fricke and Chaumont, 2006).The main soluble metabolites contributing to the total osmolarity were analyzed during leaf expansion (Figure 4). Namely, individual amino acids, main organic acids (malate, citrate), sugars (glucose, fructose, sucrose) and inorganic ions. Levels of glucose and fructose under ammonium nutrition were approximately twice of those observed under nitrate nutrition along whole leaf development. Under nitrate nutrition, sucrose content remained stable (7.5-9.5 µmol g FW^{-1}) during whole leaf development. Similar values were observed in ammonium conditions at the beginning and the end of development, with a transient increase to 12 µg FW^{-1} between 16 to 31 days. Ammonium nutrition is widely known to induce N assimilation (Setién *et al.*, 2014; Vega-Mas *et al.,* 2019); accordingly in our study amino acids were accumulated under ammonium nutrition (Fig 4 and S6) mainly because of a the higher content of Asn, Ser, Gln, Arg, GABA and Pro (Figure S6). By contrast, Asp was less abundant in ammonium compared to nitrate nutrition (Figure S6). The most abundant organic acid in tomato leaf is malate (Kirkby & Mengel, 1967). Under nitrate treatment, it increased between 7 days to 16 days from 89 µmol g FW^{-1} up to 126 µmol g FW^{-1} and then decreased gradually. By contrast, under ammonium treatment malate content was always extremely low (Figure 4). As also previously reported (Setién *et al.*, 2014), citrate was almost undetectable in NH_4^+-fed plants. In NO_3^--fed plants, citrate content gradually increased during leaf development from 5 µmol g FW^{-1} at day 7 to 30 at day 41.

Free inorganic ions play a major role in leaf cell osmolarity and growth (Quéro *et al.*, 2014). The influence of N-source on their accumulation is shown in Figure 5. Under nitrate treatment, Cl^- content remained low and almost stable whereas Na^+, Ca^{2+}, Mg^{2+} and SO_4^{2-} progressively increased with leaf growth. On the contrary, HPO_4^{2-} and K^+ decreased rapidly between day 7 and day 16. Then, HPO_4^{2-} remained stable (around 5 µmol g FW^{-1}) and also K^+ except between 31 and 41 where it importantly decreased. Under ammonium treatment, Na^+, Ca^{2+}, Mg^{2+} and SO_4^{2-} showed similar profiles, increasing along with leaf growth althoug their contents were always lower respect to NO_3^--fed plants. By contrast, HPO_4^{2-} accumulated at a constant rate along all leaf development, up to 33.3 µmol g FW^{-1}. On the other side, Cl^- and K^+ presented a very particular behavior, first decreasing between 7 days and 21 days and then increasing until day 41. Interestingly, K^+ And Cl^- were negatively correlated with AGR (R^2 equal

to 0.7 and 0.4 respectively, Figure S5): high levels of K^+ and Cl^- being associated with low growth rates time points. As expected, the major inorganic N forms in ammonium and nitrate treatments were NH_4^+ and NO_3^- respectively, but they exhibited different trends of accumulation over leaf development. NH_4^+ was highly correlated (R^2 equal to 0.8) to AGR curve under ammonium nutrition (Figure S5) presenting its maximum value at 21 days (Figure 5) while NO_3^- under nitrate treatment was mainly accumulated in the older leaves (at 41 days).

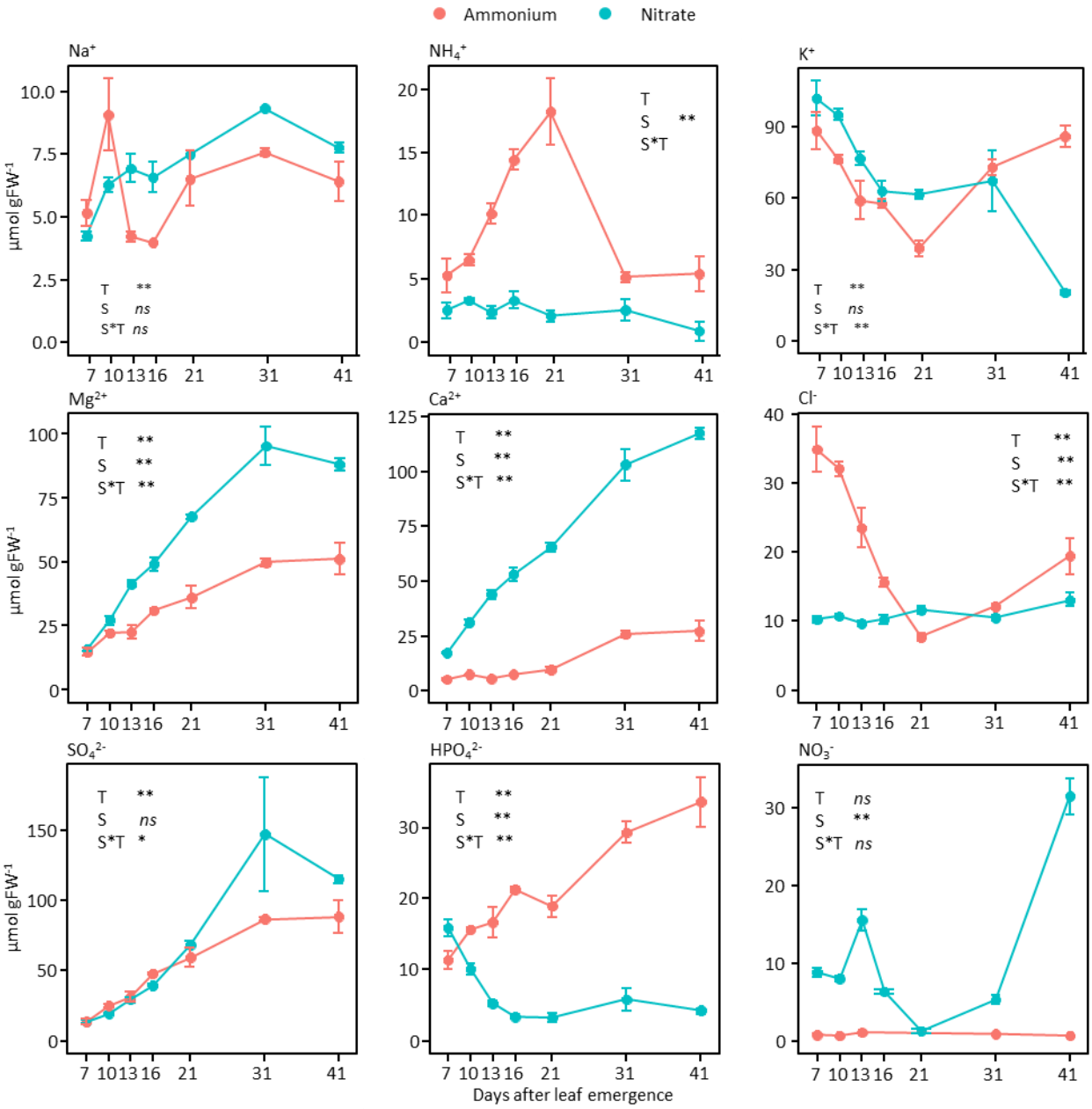

Figure 5: Time course evolution of the main soluble inorganic ions throughout the development of tomato leaf grown with ammonium (red) and nitrate (blue) as nitrogen source. Values represent the mean ± se (n = 3). Significant differences are shown according to two-way ANOVA (**: p<0.01; *: p<0.05; *ns*: not significant) where S indicates nitrogen source effect; D indicates days effect and S×D indicates interaction effect.

Vacuoles are more acidic under ammonium nutrition

To determine how the N-source affects the pH of different cellular compartments, we carried out an imaging approach using the membrane-permeable ratiometric fluorescent pH sensitive dye 2',7'-bis-(2-carboxyethyl)-5-(and-6)-carboxyfluorescein (BCECF).

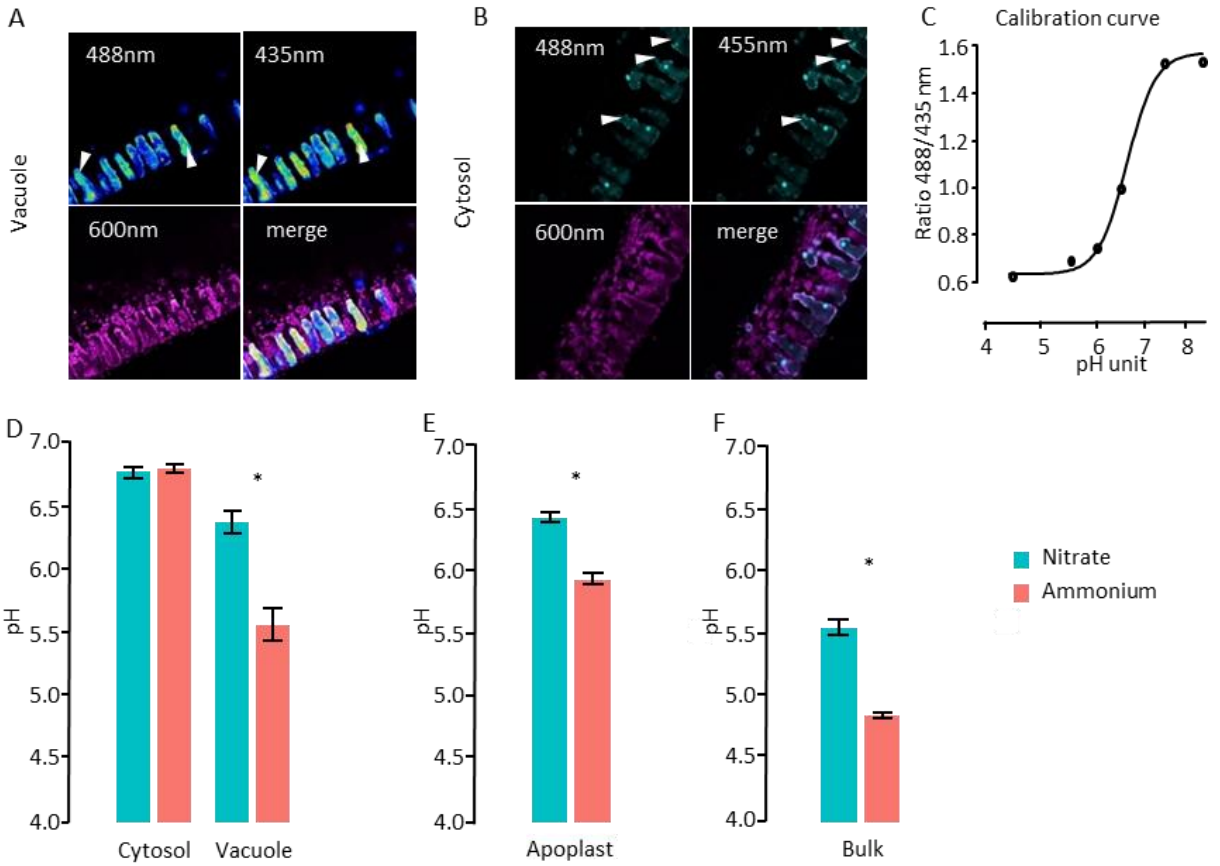

Figure 6: Apoplast and *in vivo* Intracellular pH measurement in tomato leaf grown with ammonium and nitrate as nitrogen source. Representative pattern of (A) vacuolar and (B) cytoplasmic BCECF signal. (C) Calibration curve of BCECF fluorescence ratio (488/435nm) in tomato leaf. (D) Vacuolar and cytosolic pH measurement based on BCECF signal in tomato leaf grown with ammonium and nitrate as nitrogen source. Values represent the mean ± se (n = 12 leaves/sections, each replicate corresponding to an average of 10 measurements per leaf/section). (E) Apoplast pH (Values represent the mean ± se (n = 4). (F) Bulk pH measurement of tomato leaf. Values represent the mean ± se (n = 4). Significant differences between ammonium and nitrate treatments are highlighted with an asterisk in panel D, E and F (t-test $p<0.05$).

In our conditions and as expected, the probe was loaded mainly in the vacuole (Figure 6A), because of its membrane-permeant acetoxymethyl (AM), ester but it is also detectable in the cytosol (Figure 6B). As seen in Figure 5, the ionic composition or reducing environment of leaves fed with NH_4^+ or NO_3^- varies greatly. First, to examine the possible influence of the nutrition type on the *in vivo* pH measurement, we performed a calibration curve in both leaf

sections coming from plants grown under ammonium or nitrate conditions (Figure S7). We observed identical curve profiles. Then, images of parenchyma leaves sections (as shown in figure 1, Material and methods) grown on ammonium and nitrate conditions were analyzed with the BCECF dye and the obtained 488/435 ratios were converted to pH values (Figure 6D). Ammonium nutrition led to a significant acidification of the vacuole with a pH of 5.6 ± 0.1 compared to nitrate nutrition with a pH of 6.4 ± 0.1 (Figure 6E). By contrast, the cytosolic pH was maintained around 6.8 ± 0.05 under both conditions. In addition, to discard the influence of the imbalance in Ca^{2+} supply ammong both nutrition on the pH measurements (Pittman, 2012), we also quantified vacuolar pH in an independent experiment performed in plants grown with balanced Ca^{2+} levels. Therefore supplying extra 7.5 mM $CaSO_4$ to ammonium-fed plants. Overall, we observed a similar vacuolar acidification as reported for the main experiment where SO_4^{2-} was balanced between treatments (Figure S8).

In addition to vacuolar and cytosolic pH, apoplastic fluids were extracted from leaves by infiltration–centrifugation technique and its pH measured with an electrode (Figure 6F). Under nitrate nutrition apoplastic pH was around 6 and under ammonium nutrition was significantly more acidic (pH 5.5). Taken together, more acidic pH vacuole and apoplastic fluid were in line with the pH determined from a bulk leaf extract that showed global leaf acidification under ammonium nutrition (Figure 6G).

Resolving cell metabolism under different N-source with subcellular resolution

In view that vacuole growth is affected under ammonium nutrition, in association with changes in vacuolar pH together with a differential accumulation of metabolites known to be accumulated in the vacuole, we decided to gain further insight into the metabolic compartmentation and subcellular localization of major solute pools. To do so, tomato leaf composition was analyzed combining the non-aqueous fractionation (NAF) methodology with enzymatic assays and metabolite quantification in a robotized platform combined with HPLC-MS and ion chromatography analyses. For both nutrition conditions, only time points after 21 days of the developmental series were suitable for fractionation. Indeed, before 21 days size of the cells was too small for proper fractionation. On day 31, two distribution patterns of

vacuolar and cytoplasmic markers were clearly observed in the gradient: one fraction enriched in vacuole (fraction 1) and one fraction enriched in cytosol (fraction 3). On the other hand, on day 16, the markers were distributed identically in the gradient, indicating that these two compartments were not separated (Figure S9). In order to obtain the relative distribution of each metabolite in the compartments studied, the proportion of the metabolites content was determined in the five fractions obtained from every sample and correlated with the distribution of the metabolic markers selected for each compartment (for more details see materials and methods section). In addition, the combination of subcellular metabolite repartition together with cell and compartments volumes, calculated by microscopy imaging (Figure 2), made possible to estimate the concentration of metabolites in each subcellular compartment. Table 1 shows the proportion and concentrations of different metabolites in vacuole and the cytoplasm. In our study the cytoplasm consists in the cytosol and chloroplast that have been merged to be compared with predicted data of cytoplasmic concentrations with the model described below. Data of relative distribution and absolute concentrations of chloroplast and cytosol are shown in table S1.

NO_3^- and NH_4^+ were found mainly in the vacuole with a concentration reaching a maximum of 42 mM for NO_3^- and 32 mM for NH_4^+. Interestingly, cytosolic NH_4^+, often considered as cytotoxic (Choudhary et al., 2016), reached a cytoplasmic concentrations of up to 13.9 mM in day 21 under ammonium nutrition (Table 1). Independently to the N-source, Ca^{2+}, Na^+, Mg^{2+}, K^+, PO_4^- and SO_4^- were mainly vacuolar with concentrations ranging from 7.11 to 208 mM depending of the ion, whereas the cytoplasmic concentration ranged from 46 to 0 mM. Conversely, independently of N-source, Cl^- concentration in the cytoplasm was similar to that of the vacuole and even higher (Table 1). Finally, malate proportion between cytosol and vacuole was unaffected by the nutritional regime. However, the higher content of malate in NO_3^--fed plants led to much higher vacuolar concentration of malate compared to NH_4^+-fed plants.

Regarding sugars, the cytosolic concentration of sucrose was higher than that of the vacuole regardless of the nitrogen N-source. However, the Cyt / Vac concentration ratio was in the order of 2 to 3 under ammonium nutrition, whereas in the NO_3^--fed leaves it reached a value that varied between 20 and 60. Although the vacuolar percentages of hexoses were lower under ammonium nutrition, their cytosolic and vacuolar concentrations have always

remained higher than under nitrate nutrition. Notably, elevated carbohydrate concentrations were associated with an enhancement of the glycolytic activities of fructokinase (FK) and glucokinase (GK) in the cytosol as well as with the acid invertase (IA) in the vacuole (Figure S10). In addition, malate dehydrogenase (MDH) and malic enzyme (ME) were stimulated with ammonium treatment whereas phosphoenolpyruvate carboxylase (PEPC) and pyruvate kynase (PK) enzyme activities decreased.

Table 1: Summary of non-aqueous fractionation results showing the vacuolar and cytoplasmic proportions and concentrations of metabolites and inorganic ions of 21, 31 and 41 aged tomato leaf supplied with nitrate or ammonium as unique source of nitrogen. Values represent mean ± se (n = 3). Cytoplasm results correspond to the sum of cytosol and chloroplasts results. Subcellular concentrations of NO_3^- ion is not given under ammonium nutrition since it was undetectable (*nd* means not detected). NAF data for NH_4^+-fed leaves at 41 days is missing because of technical problems during compartment markers determination.

		Nitrate								Ammonium							
		Vacuole				Cytoplasm				Vacuole				Cytoplasm			
	Days after emergence	Proportion (%)		Concentration (mM)		Proportion (%)		Concentration (mM)		Proportion (%)		Concentration (mM)		Proportion (%)		Concentration (mM)	
		mean	se	mean	se	mean	se	mean	se	mean	se	mean	se	mean	se	mean	se
Glucose	21	88	± 8	12	± 1	12	± 8	4	± 3	84	± 16	29	± 5	16	± 16	11	± 1
	31	93	± 2	2	± 0	8	± 2	1	± 0	76	± 9	4	± 1	24	± 9	4	± 2
	41	63	± 18	0	± 0	38	± 18	1	± 1								
Fuctose	21	93	± 6	20	± 1	7	± 6	4	± 3	82	± 18	31	± 7	18	± 18	14	± 14
	31	100	± 0	7	± 0	0	± 0	0	± 0	79	± 11	17	± 2	21	± 8	13	± 5
	41	100	± 0	3	± 0	0	± 0	0	± 0								
Sucrose	21	12	± 5	2	± 1	88	± 5	35	± 2	53	± 28	11	± 6	47	± 28	20	± 12
	31	78	± 3	8	± 0	22	± 3	10	± 1	41	± 24	7	± 3	59	± 18	30	± 9
	41	8	± 5	1	± 0	93	± 5	49	± 2								
Malate	21	88	± 6	171	± 11	12	± 6	58	± 30	94	± 3	9	± 0	6	± 3	1	± 1
	31	89	± 8	122	± 11	12	± 8	66	± 46	89	± 2	13	± 0	11	± 2	5	± 1
	41	100	± 0	121	± 0	0	± 0	0	± 0								
NH_4^+	21	33	± 30	1	± 1	67	± 33	6	± 2	97	± 3	32	± 1	3	± 3	2	± 2
	31	35	± 25	1	± 1	65	± 25	10	± 4	94	± 5	7	± 0	6	± 5	1	± 1
	41	53	± 33	1	± 0	47	± 33	3	± 2								
K^+	21	82	± 14	82	± 14	18	± 14	46	± 35	90	± 3	63	± 2	10	± 3	14	± 4
	31	100	± 0	95	± 0	0	± 0	0	± 0	100	± 0	112	± 0	0	± 0	0	± 0
	41	100	± 0	27	± 0	0	± 0	0	± 0								
Na^+	21	100	± 0	12	± 0	0	± 0	0	± 0	100	± 0	12	± 0	0	± 0	0	± 0
	31	90	± 7	12	± 1	10	± 7	5	± 4	98	± 1	11	± 0	2	± 1	1	± 0
	41	100	± 0	10	± 0	1	± 0	0	± 0								
Ca^{2+}	21	100	± 0	106	± 0	0	± 0	0	± 0	89	± 6	15	± 1	11	± 6	4	± 2
	31	100	± 0	146	± 0	0	± 0	0	± 0	100	± 0	39	± 0	0	± 0	0	± 0
	41	100	± 0	158	± 0	0	± 0	0	± 0								
Mg^{2+}	21	94	± 5	103	± 5	6	± 5	17	± 13	100	± 0	65	± 0	0	± 0	0	± 0
	31	100	± 0	135	± 0	0	± 0	0	± 0	100	± 0	76	± 0	0	± 0	0	± 0
	41	100	± 0	118	± 0	0	± 0	0	± 0								
SO_4^{2-}	21	100	± 0	111	± 0	0	± 0	0	± 0	100	± 0	106	± 0	0	± 0	0	± 0
	31	100	± 0	208	± 0	0	± 0	0	± 0	100	± 0	134	± 0	0	± 0	0	± 0
	41	100	± 0	155	± 0	0	± 0	0	± 0								
NO_3^-	21	68	± 14	1	± 0	32	± 14	2	± 1								
	31	77	± 16	6	± 1	23	± 16	7	± 5	*nd*		*nd*		*nd*		*nd*	
	41	100	± 0	42	± 0	0	± 0	0	± 0								
Cl^-	21	50	± 17	9	± 3	50	± 17	24	± 8	62	± 9	9	± 1	38	± 9	11	± 2
	31	86	± 10	13	± 2	15	± 10	9	± 6	59	± 7	10	± 1	41	± 7	22	± 4
	41	67	± 1	12	± 0	33	± 1	29	± 1								
PO_4^{2-}	21	62	± 12	3	± 1	38	± 12	5	± 2	100	± 0	34	± 0	0	± 0	0	± 0
	31	98	± 1	8	± 0	2	± 1	1	± 0	94	± 4	42	± 2	6	± 4	8	± 5
	41	100	± 0	6	± 0	0	± 0	0	± 0								

Construction and parameterization of a solute partitioning mathematical model between vacuole and cytoplasm

Vacuole expansion is of great importance for cell growth and plant development. Given the strong impact of the N-source on the cell composition of sugars, organic acids and ions, that are mainly stored in the vacuole, it is of high interest to study the mechanisms and energy dedicated to their accumulation, in order to assess whether it maybe a trade-off for cell growth. Answering this question means being able to track changes in the cytosolic and vacuolar concentrations of these compounds throughout development.

NAF made possible to characterize the subcellular composition of the leaves at the end of their development but not in the early stages when RGR is maximum. For this reason, we aim developing a mathematical model to estimate the equilibrated concentrations of solutes in both side of the tonoplast. This two-compartment model comprised a vacuole and homogeneous cytoplasm, considering together cytosol, mitochondria and chloroplasts. Thus, ignoring the potential exchanges between organelles within the cytoplasm.

Table 2: Summary of transport mechanisms used for model parameterization

Substrate	Driving force	References	Type of vacuolar transport	Stoichiometry
Glucose	ΔpH & ΔΨ	Aluri and Bu (2007)	Antiport	H^+: Glucose (1:1)
Fructose	ΔpH & ΔΨ	Aluri and Bu (2007)	Antiport	H^+: Fructose (1:1)
Sucrose	ΔpH & ΔΨ	Jung *et al* (2015)	Antiport	H^+: Sucrose (1:1)
Malate	ΔΨ	Kovermann *et al* (2007)	Channel	Malate
NH_4^+	ΔpH	Wood *et al* (2006)	Diffusion	H^+: NH_3 (1:1)
K^+	ΔpH	Venema *et al* (2002)	Antiport	H^+: K^+ (1:1)
Na^+	ΔpH & ΔΨ	Venema *et al* (2002)	Antiport	H^+: Ca^{2+} (1:1)
Ca^{2+}	ΔpH & ΔΨ	Manohar *et al* (2011)	Antiport	H^+: K^+ (1:1)
Mg^{2+}	ΔpH & ΔΨ	Berezin *et al* (2008)	Antiport	H^+: Mg^{2+} (1:1)
SO_4^{2-}	ΔΨ	Kaiser *et al* (1989)	Channel	SO_4^{2-}
NO_3^-	ΔpH & ΔΨ	Chopin *et al* (2007)	Antiport/Channel	H^+: NO_3^- (1:2)
Cl^-	ΔΨ	Angeli *et al* (2009)	Channel	Cl^-
PO_4^{2-}	ΔΨ	Liu *et al* (2015)	Channel	PO_4^{2-}

To define the subcellular concentrations of the 14 molecules investigated, the model consists of 28 equations: 14 describing the concentrations inside the vacuole and 14 describing the

concentrations in the cytoplasm (Table S2 to S5). For each compound, the equations have been parameterized making choices, in the basis of the literature, for the driving forces and stoichiometry of the transport involved in the distribution of each metabolite between both compartments (Table 2). Besides, in view that NAF results pointed out a global tendency of the different chemical species studied to accumulate in the vacuole (Table 1), we prioritized those transport mechanisms that promote the vacuolar accumulation (Table 2).

Equations, and parameter settings, are listed in supplemental Tables S2 to S5. The core-skeleton of every equation is based on the Nernst equation at the equilibrium, when diffusion (Δμ) is null as follows.

For an H^+ antiport system: *Equation 1*

$$\Delta_\mu = \ 0 \ = \Delta_\mu \mathrm{ion}_{\ v-c} + \ \Delta_\mu {H^+}_{c-v}$$

$$= \ \mathrm{R} * \mathrm{T} * \ln\left(\frac{[Ion_{Vacuole}]^n}{[Ion_{Cytosol}]^n}\right) + \mathrm{Z}_{ion} * \mathrm{F} * \Delta\Psi_{V-C} + \mathrm{R} * \mathrm{T} * \ln\left(\frac{[{H^+}_{cytosol}]}{[{H^+}_{vacuole}]}\right) + \mathrm{Z}_H * \mathrm{F} \ * \Delta\Psi_{C-V}$$

Or, for a channel (facilitated diffusion) system: *Equation 2*

$$\Delta_\mu = 0 = \mathrm{R} * \mathrm{T} * \ln\left(\frac{[Ion_{Vacuole}]}{[Ion_{Cytosol}]}\right) + \mathrm{Z}_{ion} * \mathrm{F} * \Delta\Psi_{V-C}$$

Where R is the universal gas constant (J mol K^{-1}), T the temperature (Kelvin), Z is the valence or charge number of the ion, F the Faraday constant (C mol^{-1}), $\Delta\Psi_{v\text{-}c}$ is the tonoplast potential or the voltage difference between inside and outside the vacuole (volt). Importantly, for PO_4^{2-}, citrate and malate the formation of different conjugated forms were considered in their equations listed in Table S3. For instance, malate is transported under the form of $malate^{2-}$, which is at the equilibrium across the tonoplast. Once into the acidic vacuole, the $malate^-$/$malate^{2-}$ ratio increases, which enhances the vacuolar accumulation (Lobit *et al.*, 2006).

Then, with the mass conservation law the measured tissue content of the given ion or solute (Figure 4-5) is linked with its concentration within vacuole and cytoplasm and their respective subcellular volumes: *Equation 3*

$$[Ion]_{tissue} = \frac{V_{vacuole}}{V_{cell}} * [Ion]_{vacuole} + \frac{V_{cytoplasm}}{V_{cell}} * [Ion]_{cytoplasm}$$

Because the tissue density was considered as 1 g FW mL^{-1}, the $[Ion]_{tissue}$ measured in µmol g FW^{-1} was equivalent to mM. $V_{vacuole}$, $V_{cytoplasm}$ and V_{cell} were the respective volumes of the vacuole, cytoplasm and the whole cell determined by microscopy (Figure 2). Final equations for cytoplasm or vacuolar concentrations were solved by replacing respectively $[Ion]_{vacuole}$ or $[Ion]_{cytoplasm}$ with solutions provided by Equations 1 and 2 based in Nernst equation.

Constraint-based optimization and validation

As seen in Equations 1 and 2, the thermodynamic equilibrium of the different chemical species studied depends on the electrochemical gradient established across the tonoplast. For antiporter systems depends on H^+ gradient. Accordingly, the pH difference between cytoplasm and vacuole has been measured *in vivo* by confocal microscopy: it represents 1.3 pH units in NH_4^+-fed plants and 0.4 pH units in NO_3^--fed plants (Figure 6). Thus, these ΔpH values from respective N-source were introduced as a constant in Equations 1.

Consequently, there was only one unknown parameter for the initial parameterization: the membrane electrical potential across the tonoplast (ΔΨ). Values of this parameter were estimated for each time point of both treatments (nitrate and ammonium) to reach the electroneutrality in both the cytosol and vacuole compartments. To estimate ΔΨ, the more optimal value was randomly searched by least square minimization in an iterative process calculating for each putative ΔΨ value its error (deviation from the electroneutrality). The error being defined by the sum of the squared positive and negative charges in cytoplasm and vacuole relative to the total quantity of charges in the respective compartments ($score_{initial\ parameters}$, Table S6). In this way, we calculated the error giving equal importance of cytoplasm and vacuolar errors (deviation from electroneutrality), regardless of its sign. With this iterative process, the best 200 ΔΨs values with the least error (score) were selected for each time point and nutritional regime and the median of these values kept for further analysis. Overall, the obtained medians of ΔΨ values were rather stable over the developmental series and situated in a physiological range for both treatments. Under ammonium nutrition ΔΨ ranged from 33 to 27 mV whereas under nitrate nutrition it ranged from 15 to 9 mV (Figure 7). With those respective optimized ΔΨ values, the model could predict the distributions and

concentrations of the different chemical species between the cytoplasm and the vacuole (Figure S9).

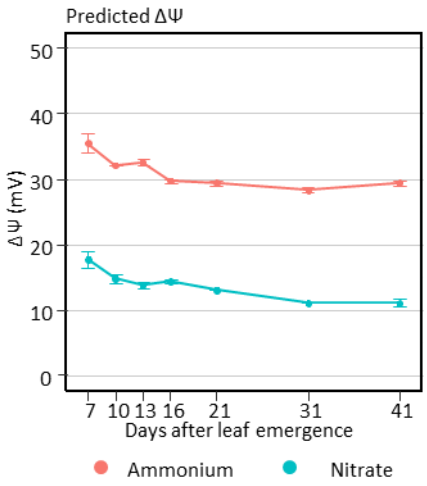

Figure 7: Predicted ΔΨ obtained by constraint-based optimization with the initial parameterization (without formation of ionic complex) throughout the development of tomato leaf grown with ammonium (red) and nitrate (blue) as nitrogen source. ΔΨ value was randomly searched by least square minimization of the cytoplasmic and vacuolar electroneutrality at each time point and treatment. ($Score_{initial\ parameter}$, Table S5). Median and standard error of the 200 best scoring of ΔΨ parameter obtained by randomized initial conditions.

As a means of cross-validation, the subcellular concentrations of 21, 31 and 41 days generated by the model were compared to the respective values empirically determined with NAF technique (Table 1). The simulated concentrations of cytoplasmic and vacuolar malate, HPO_4^{2}, Na^+, K^+, NO_3^- and NH_4^+ (Figures S11) were fairly close from the corresponding concentration estimated with the NAF (Table 1). Nevertheless, the model gave higher Cl^- concentrations in the vacuole and lower in the cytosol with respect to NAF data. We also found an important discrepancy for Ca^{2+}, Mg^{2+} and SO_4^{2-}, particularly in the cytosol of NO_3^- fed-plant. For those ions, the model predicted too high concentrations in the cytoplasm compared with the NAF technique. On one hand, this was evident for Ca^{2+}. Indeed, as a key second messenger, Ca^{2+} concentration in the cytosol is fine tuned and needs be extremely low because of its involvement in numerous signaling processes (Mertz and Higinbotham, 1976). On a second hand, at high concentrations, most of these ions tend to form complexes instead of being under free diffusible and osmotically active forms. This phenomenon of complexation could strongly influence their distribution across the tonoplast. Hence, in a given compartment, the reduction of the concentration of their soluble free form because of complex formation tends

to be compensated by further diffusion of ions from the neighboring compartment. To test this hypothesis, we extensively reviewed the constant of solubility product (K_{sp}) of various ion associations that most likely occur in the cell. Altogether, we considered the formation of seven different complexes whose K_{sp} is listed in Table S2. Thus, we performed a new parametrization of the model considering the formation of these seven complexes. To do so, ΔΨ need to be calculated again. Briefly, ΔΨ and ionic complex abundance were randomly searched by least square minimization of the error/score calculated (deviation from the electroneutrality) for each compartment following the equation $Score_{ionic\ complex}$ described in Table S6. In the equations, the solubility product (SP) of the different free ions is the result of the multiplication of the free ion concentrations according to their stoichiometry in the complex. The free molecule concentrations were calculated by the equations of Table S3 to S5 considering the decrease of free ions involved in complexes. Finally, for a good score, SP of a given compound must be smaller or equal to its K_{SP} (Table S2). As before, the whole iterative process was repeated using randomized initial conditions, and the 200 best scoring combinations of parameters were kept for each time point and nutritional regime to calculate the median of the parameters.

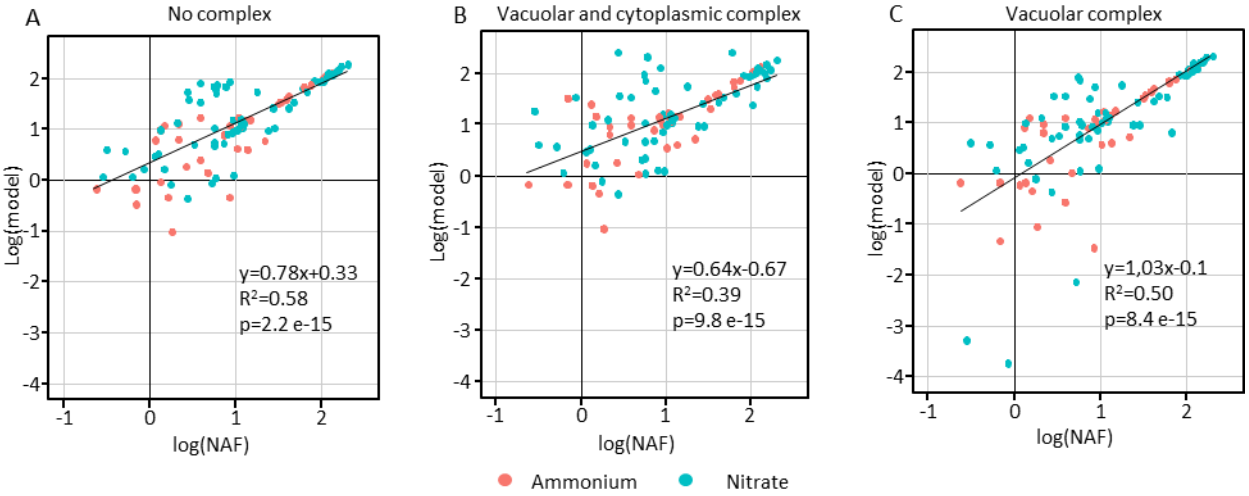

Figure 8: Comparative analysis of non-aqueous fractionation (NAF) measurements with data predicted by different parameterizations of the model. (A) NAF data and data from the initial parametrization without formation of complexes. (B) NAF data and data from the parameterization with the formation of vacuolar and cytoplasmic complexes. (C) NAF data from the parametrization with the formation of vacuolar and cytoplasmic complexes. Statistical analysis corresponds to Pearson correlation. Only data from 21, 31 and 41 days were used since NAF procedure was only working efficiently at these time points.

Figure 8 shows the correlations between the subcellular concentrations empirically determined by NAF and the concentrations calculated by the model without considering ion complexes (Figure 8A) and allowing complexes formation in both compartments (Figure 8B). In general, when the model considers the formation of complexes in both vacuole and cytoplasm, the comparison with NAF gets drastically degenerated (i.e. both the slope and the R squared) (Figure 8B) respect to modeling in the absence of complexes (Figure 8A). This worse comparison is because this parameterization entails an excessive formation of cytoplasmic ionic complexes (Figure S12) that leads to the accumulation of malate, Ca^{2+}, Mg^{2+} and HPO_4^- in the cytoplasm instead of the vacuole as observed with the NAF (Table1). For this reason, we repeated the same optimization by exclusively allowing the formation of ionic complexes in the vacuole. With this parameterization, the simulated values fitted better to NAF data compared again to the absence of complexes (Figure 8A), showing correlative slope close to 1 (Figure 8C). This was mainly due because of greater Ca^{2+}, SO_4^{2-} and PO_4^{2-} accumulation into the vacuole, notably in the form of ionic complexes (Figure S13).

For each metabolite and inorganic ion, the detailed comparison of their total subcellular concentrations predicted by the final selected model parameterization (with vacuolar complexes) against NAF data is shown in Figure S14. In agreement with the NAF, most of the predicted concentrations were relatively low in the cytosol compared to vacuole. For instance, we obtained good predictions for malate that remained mainly vacuolar and partially cytoplasmic. Overall, vacuolar malate levels reached around 30 mmol in the cytosol and ranged from 100 to 200 mmol in N plants. By contrast to other compounds, Mg^{2+} and SO_4^{2-} were surprisingly high in cytosol of N plants compared with NAF results.

Hexoses and sucrose, being non-charged molecules, did not participate to any ionic complex and consequently did not affect the constraint-based optimization. Hence, following the equation in Table S5 their subcellular concentration was also calculated, using the $\Delta\Psi$ optimized and the ΔpH measured. Simulated subcellular concentration of glucose and fructose fitted perfectly to NAF results for NO_3^--plants but they were slightly over-estimated in the vacuole of NH_4^+-fed plants (Figure S14). However, predicted concentrations of sucrose differed importantly from NAF measurements where they remained mainly cytoplasmic in both treatments. Therefore, we assume that subcellular concentrations of sucrose cannot be correctly estimated with our model.

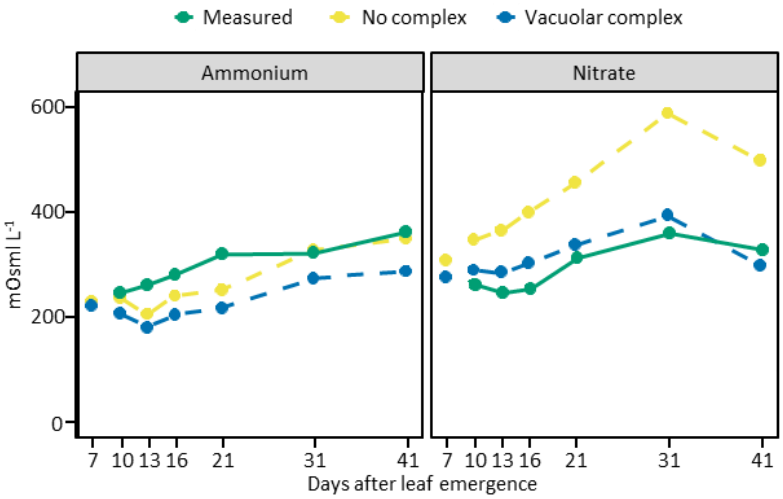

Figure 9: Comparison between simulated and experimentally measured osmolarity of tomato leaf grown with ammonium and nitrate as nitrogen source. Continuous green line represents experimental osmolarity measured with an osmometer. Yellow dashed line represents the osmolarity predicted by the model without formation of ionic complexes. Blue dashed line represents the osmolarity predicted by the model with formation of vacuolar ionic complexes. Predicted values are the sum of inorganic ions and organic metabolite accumulated in the vacuole and cytoplasm under soluble form.

Ionic complexes favored the accumulation of certain ionic species in the vacuole, but they also involve ions that will no longer be osmotically active. As a way to verify that the amount of ionic complexation predicted in our model is realistic, in Figure 9 we compared the tissue osmolarity predicted by the model with the bulk leaf osmolarity measured with an osmometer (model equations are shown Table S7 and results in Figure S15). For NO_3^--fed plants, the predicted osmolarity values obtained when allowing vacuolar complexes were clearly closer to the osmolarity measured with the osmometer compared to the ones predicted without complexes (Figure 9). In fact, soluble concentration of Ca^{2+} and PO_4^{2-} to a lesser extent, shrunk strongly in both compartments due the formation complex (Figure S13 and S15). Overall, showing the appropriateness of considering vacuolar complexes for the model. Under ammonium nutrition, the higher sugar, Cl^-, and HPO_4^{2-} content predicted in the vacuole together with higher concentration of SO_4^{2-} and K^+ compensated the huge depletion of malate when compared to nitrate nutrition (Figure 10). Notably, in NO_3^--fed plant at early time points most malate was soluble and contributed significantly to the osmolarity. However, at 31 and 41 days, free malate concentration was strongly reduced, and therefore its contribution to osmolarity, as it was complexed with Ca^{2+} up to 60% in the vacuole (Figure S15).

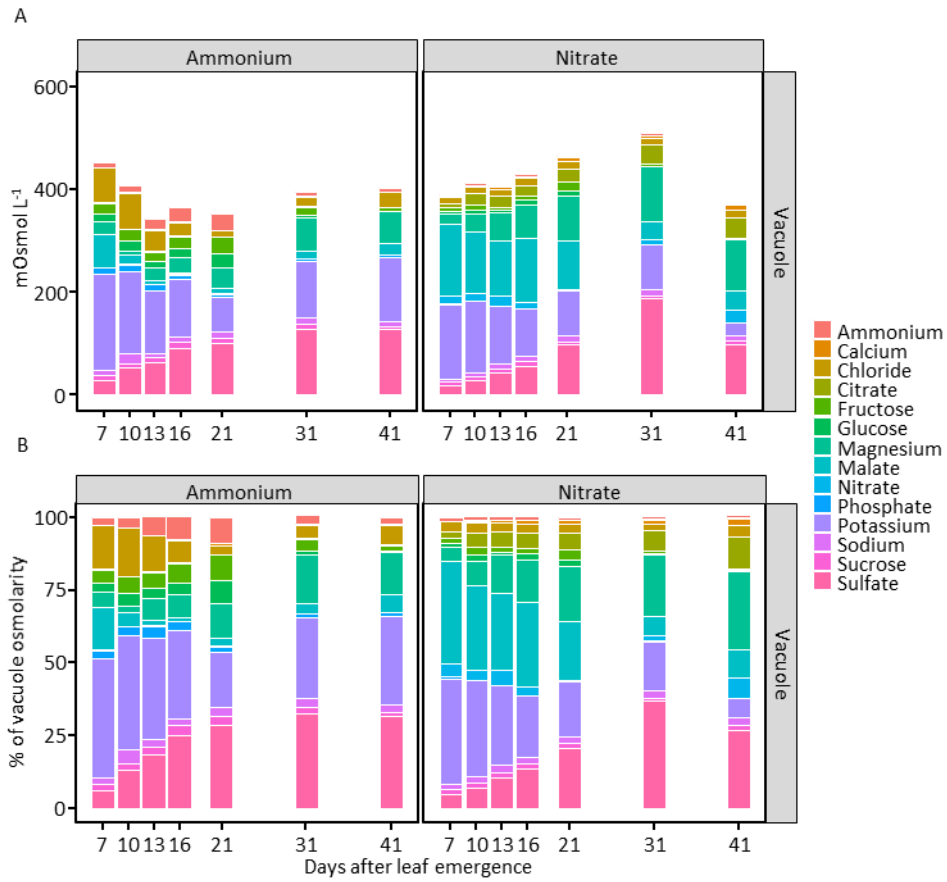

Figure 10: Model prediction of the vacuolar osmolarity concentration of tomato leaf grown with ammonium and nitrate as nitrogen source. (A) Additive role of the different predicted solutes in concentration. (B) Relative contribution of predicted solutes concentrations to the vacuole osmolarity. The predicted concentration values are the median of the 200 best scoring combinations of parameters kept for each stage and treatment.

The flux of solutes into the vacuole in NH_4^+-fed leaves is smaller with a higher energy cost.

Overall, the model predicted a predominant localization in the vacuole for most of organic and inorganic molecules (Figure S13 and S15), confirming the result obtained with the NAF (Table 1). However, given that vacuole expands during leaf development (see Figure 2), maintaining such high solute concentrations within the vacuole implies a constant high influx of solutes through the tonoplast during cell growth. Influx into the vacuole may have a differential impact on the energy cost of leaf growth depending on the source of N supplied. To estimate this energy cost, we first calculated the net flux of ions into the vacuole for each molecule using the following equation: *Equation 4*

$$Flux_{Vacuole} = (RVR * [solute]_{Vacuole} + \frac{d[solute]_{Vacuole}}{dt}) * \frac{V_{Vacuole}}{d * V_{Cytosol}}$$

Expressed in µmol of a given solute (g FW)$^{-1}$ days^{-1}, where RVR is the relative vacuole volume expansion rate in day^{-1} fitted from the microscopic data (Figure S1), [solute]$_{Vacuole}$, the vacuolar concentration of any solute in mM and d, the tissue density expressed in g FW mL^{-1}. Assuming that transports are carried out at an infinitely slow rate so that it is at all times infinitesimally *close* to a steady *state* of thermodynamic equilibrium *(see above)*, *d[solute]$_{vacuole}$/dt* was taken to be equal to zero, i.e. the net influx into the vacuole exactly compensates the dilution effect of vacuole expansion.

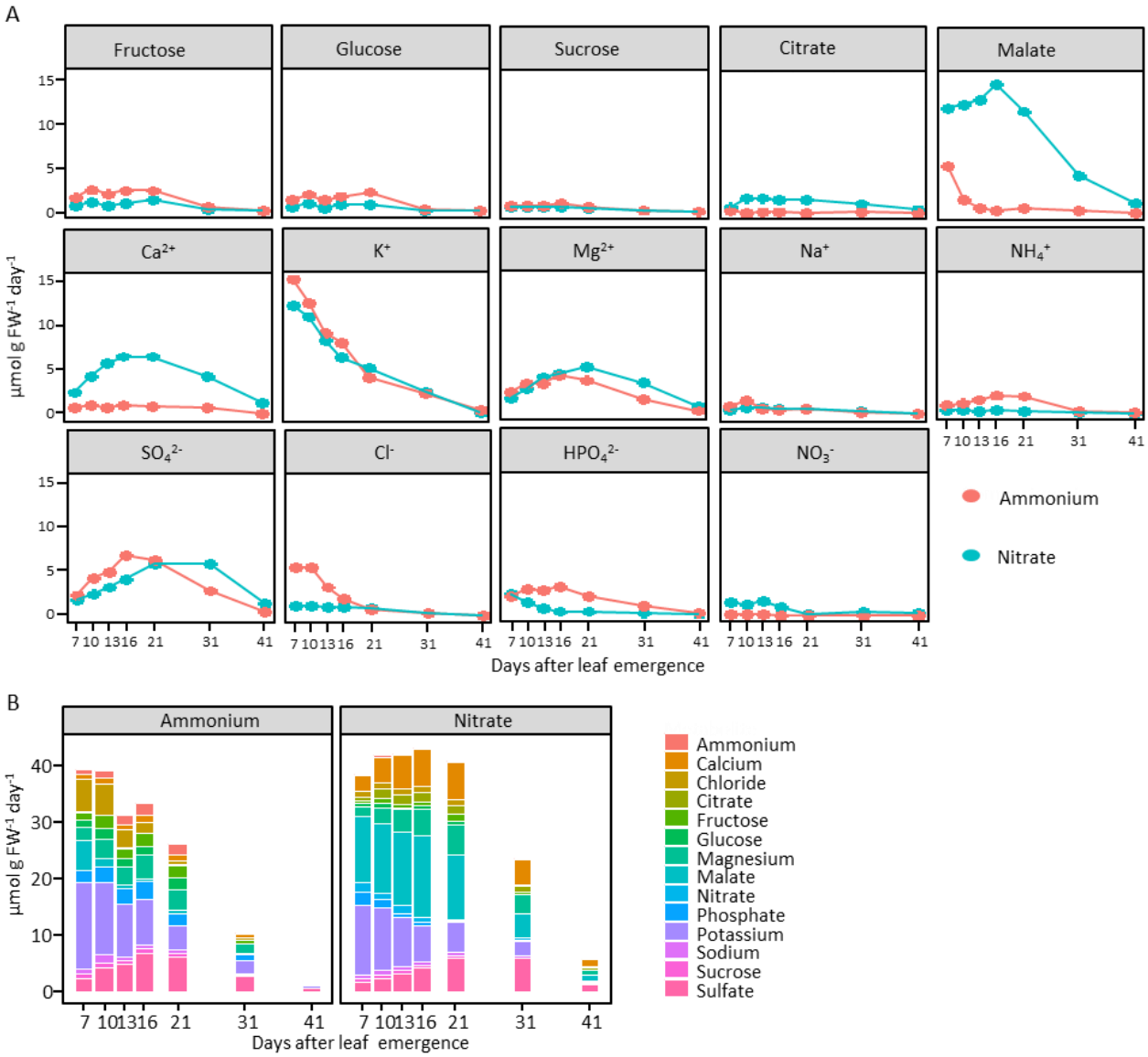

Figure 11: Net vacuolar flux of solutes throughout the development of tomato leaf grown with ammonium and nitrate as nitrogen source. Calculation was done using the concentrations predicted in the vacuole and considering the vacuole expansion (RVR). (A) Vacuolar influx or individual solutes (B) Net vacuolar influx of solutes.

As seen in Figure 11A, regardless of the nitrogen source, most fluxes were maximal between 7 and 21 days after leaf emergence, i.e., when growth was maximal (Figure 2). Then, fluxes sharply decreased until the end of leaf development. The most important differences between treatments were the higher fluxes of Ca^{2+} and malate under nitrate nutrition. Altogether, global tonoplast flux into the vacuole was higher in nitrate compared to ammonium conditions and that difference was particularly more pronounced for 21 to 41 day-old leaves (Figure 11B).

Next, we quantified the energy cost of the above calculated fluxes, using the following equation: *Equation 5*

$$Energy\ cost = Flux_{Vacuole} * \frac{n_{Charge} * F * \Delta\Psi + n_{Proton} * R * T * 2.3 * \Delta pH}{\Delta G_{ATP}}$$

Where the energy cost is expressed in µmol of ATP equivalent g FW^{-1} day^{-1}, n_{charge} and n_{proton} are the number of net quantity of charge or of proton exchanged between vacuole and cytosol during the transport process, ΔΨ is the transmembrane electrical potential difference, in Volt, ΔpH is the transmembrane pH difference, ΔG_{ATP} is the *in vivo* Gibbs energy of ATP synthesis, assumed to be 55000 J mol ATP^{-1} (Lobit *et al.*, 2006), F is equal to 96500 J mol^{-1} ,T to 298 Kelvin and R to 8.314 J mol^{-1} K^{-1}.

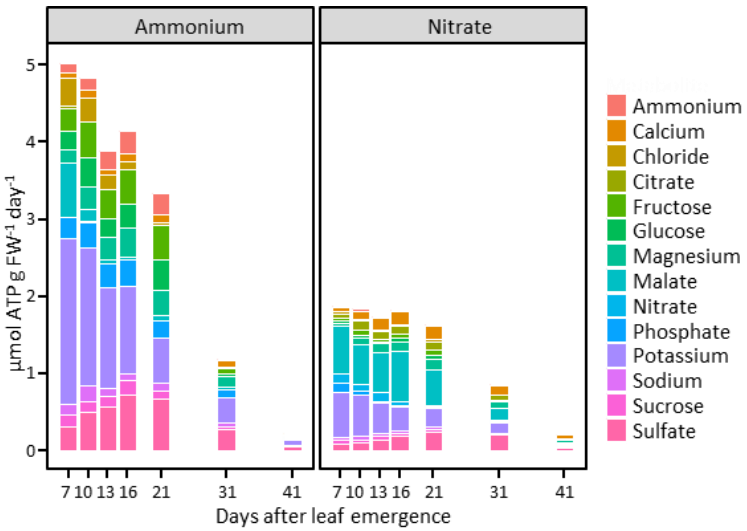

Figure 12: Energy cost of net vacuolar flux throughout the development of tomato leaf grown with ammonium and nitrate as nitrogen source. Flux energy cost of different solutes was calculated using net solute fluxes predicted by the model in the vacuole and considering the volumes calculated from the microscopy data and the electrochemical gradients established in different treatments and developmental stages. Energy cost is expressed as the mole of ATP needed to ensure the net vacuolar flux in one g of leaf FW.

Note that in the above Equation 5, the transport-linked energy cost depends both on the flux magnitude and on the transport mechanism (i.e. electrogenicity and protonicity). As seen in Figure 12, general higher flux was observed with nitrate nutrition. However, the higher ΔpH and ΔΨ under ammonium nutrition implied that transport through the tonoplast was energetically more expensive than in NO_3^--fed plant cells. Indeed, ATP needed to sustain the vacuolar fluxes under ammonium treatment was approximately twice higher between 7 and 21 days, compared to nitrate treatment. Afterwards, and in relation with the reduced growth rate, the energy cost was rather similar for both nutritions (Figure 13).

DISCUSSION

Compared to nitrate, ammonium nutrition is known to limit plant growth. This growth limitation appears among others related with an energetic trade-off where a bigger amount of the energy coming from photosynthesis would be used to control free NH_4^+ homeostasis in the cytosol, for instance by an excessive NH_4^+ assimilation (Hachiya *et al.*, 2019). Besides, a growing number of evidence suggests that ammonium nutrition may directly affect cell growth, for instance in tobacco (Walch-Liu *et al.*, 2000) and Arabidopsis (Liu *et al.,* 2013), by a mechanisms that remains to be identified. In the present work, cytological analysis of tomato leaf cross sections also evidence that the negative effect of ammonium nutrition on leaf development was associated with a reduction of the cell size (Figure 1). Among others, Walch-Liu *et al.,* (2000) suggested that cell growth could be associated by an imbalance in cytokinins, hormones known to be involved in cell division and elongation. More recently Podgórska *et al* (2017) reported stiffer cell walls in NH_4^+-treated plants, probably due to more intense interlinking of load-bearing wall polymers. Since, NO_3^- and NH_4^+ are known to be stored in the vacuole and vacuole expansion is the driving force of cell growth, we aimed to tackle the overlooked role of the vacuole in NH_4^+-induced alterations in cell and plant growth.

In our work, vacuole size was also affected by N-source and was highly associated to cell size regardless the nutrition type (Figure 2C). In this sense, the reduction of the vacuole expansion under ammonium nutrition could be limiting cell growth and therefore, leaf development.

Long-term ammonium nutrition induces vacuole acidification

Ammonium nutrition is widely known to produce the acidification of the external medium because of H^+s extrusion coupled to NH_3/NH_4^+ uptake (Lang and Werner, 1994*b*; Hachiya *et al.*, 2012). In agreement, we also show the acidification of the leaf apoplast in tomato plants fed with NH_4^+respect to those fed with NO_3^-. Inside the cell, it is globally assumed that NH_4^+ assimilation produces H^+s in the cytosol (Hachiya *et al.*, 2019) whereas NO_3^- assimilation is H^+s consumer (Raven and Smith, 1976). However, cytosolic pH appears to be highly regulated and little or no variations in cytosolic pH have been reported, among others, in Arabidopsis, Norway spruce or maize supplied with ammonium (Kosegarten *et al.*, 1997; Aarnes *et al.*,

2007; Hachiya *et al.*, 2012). Similarly, in our work, with the use of BCECF-AM probe, we observed almost identical cytosolic pH in NO_3^- and NH_4^+-fed plants (Figure 6). Regarding vacuolar pH, we here show that the vacuole compartment was more acidic under ammonium treatment (Figure 6D). This result contrasts with most of available studies that reported an increase of the vacuolar pH when cells were exposed to high external NH_4^+. Importantly, it must be noted that these studies reporting vacuolar alkalization, for instance with using in vivo NMR methods, are short-term studies where root tips are suddenly exposed from a few minutes to a few hours under high NH_4^+ concentration (Roberts *et al.*, 1982; Roberts and Pang, 1992; Gerendás and Ratcliffe, 2000). This rapid alkalization is in agreement with the generally accepted vacuolar transport process of ammonium, based on "ion trapping". This process is caused by the fact that biological membranes have higher permeability for NH_3 than NH_4^+. Then, NH_3 crosses the tonoplast by diffusion and is protonated once inside the more acidic compartment, in this case the vacuole. Consequently, NH_3 diffusion generates an acidification of the cytosol and an alkalization of the vacuole (Kosegarten *et al.*, 1997). Therefore, in short-term experiments pH variations are mainly a consequence of NH_3/NH_4^+ transport. In contrast in long term experiment, such as in our work where the leaves are exposed, and adapted, to ammonium nutrition for weeks, pH variations rather reflect the integrative cell metabolic response to cope with acidity during long periods. To our knowledge, the effect of long term nutrition on vacuolar pH has been only investigated in Norway spruce by an *in vivo* NMR approach (Aarnes *et al.*, 2007) and no significant differences were found between plants growing with NH_4^+ or NO_3^- as N-source. It is worth stressing that conifers are well adapted to acidic soils and can tolerate high concentration of NH_4^+ (Kronzucker *et al.*, 1997). By contrast, vegetable crops, such as tomato, display important sensitivity toward ammonium nutrition and would therefore differently manage the ammonium-induced acidic stress (Kirkby and Mengel, 1967; von Uexküll and Mutert, 1995).

Importantly, the pH value of bulk tissue was in line with the acidification of vacuole and apoplast under ammonium treatment (Figure 6F). The maintenance of the pH homeostasis in the cytosol (Figure 6D) suggests the enhancement of pH regulating mechanisms such as the biochemical pH-stat proposed by Davies (1986). This system is based on the pH-dependent activity of cytosolic enzymes such as the PEPC and ME couple, that orchestrates the formation or the release of carboxyl groups, which are proton-producer and proton-consumer

respectively. In agreement with the biochemical pH-stat function to control cytosolic pH, we found lower PEPC activity together with higher activity of MDH and ME under ammonium nutrition (Figure S10), which was consistent with the extremely low levels of malate (Figure 4). Besides, the biophysical pH-stat mechanism, which consists in the regulated net translocation of H^+s out of the cytosol is also key to maintain cytosolic pH. As a reminder, biophysical pH-stat is mainly controlled by the active transport of proton through plasma membrane H^+-ATPase and the tonoplaste H^+-ATPase and H^+-PPase (reviewed in Martinoia *et al.*, 2007). In our work, besides the widely known apoplastic acidification, we report the contribution of the vacuole compartment to keep cytosolic pH under control via the net uptake of H^+s likely through the regulation of proton pumps. This hypothesis is in line with the well-known inhibitory effect of NO_3^- on the V-ATPase and V-PPase, a property that is classically used to inhibit the electro-chemical gradient across the tonoplast in electrophysiological studies (Oleski *et al.*, 1987). Together, these results highlight vacuolar acidification as a new response mechanism to ammonium nutrition to preserve cytosol integrity.

Combining NAF technique and mathematical modeling enables to predict subcellular solutes distribution to understand the impact of N-source on vacuole expansion

Providing NH_4^+ instead of NO_3^- for plant growth induces, among others, important metabolic adaptations (Britto and Kronzucker, 2002; Marino and Moran, 2019) together with changes in inorganic ions uptake such as the widely reported inhibition of K^+ uptake (Britto and Kronzucker, 2002, Hachiya *et al.*, 2012). To decipher the consequences of such changes at the subcellular level, NAF technique combined with cytological study, allowed us to calculate the concentration of metabolites in the vacuole, cytosol and chloroplasts (Table 1 and S1).

NH_4^+ mainly localized into the vacuole reaching concentrations up to 32 mM (Table 1) when the higher levels in leaf tissue were reported (Figure 5). This is highly consistent with previous measurements of subcellular NH_4^+ concentrations in the giant alga *Chara coralline* that reached 30.8 mM in the vacuole and 7.3 mM in the cytosol after two days of incubation with 1 mM of NH_4^+ (Wells and Miller, 2000).

With this approach, we also found higher concentrations of sucrose in the cytoplasm whereas hexoses and organic acids rather accumulated into the vacuole, in agreement with other studies using the same procedure in potato and barley leaves (Winter *et al.*, 1993; Leidreiter *et al.*, 1995). Importantly, the same studies also reported that amino acids are almost exclusively localized in the cytoplasm. Therefore, the contribution of free amino acids to the osmotic strength of the vacuole is likely to be weak throughout leaf development. Quantitative data about ions concentration in the vacuole are scarce in the literature. However, it is overall accepted that they mostly accumulate in the vacuole and indeed many inorganic ions tonoplast transporters have been characterized in plants (Shitan and Yazaki, 2013). For instance, HPO_4^{2-} and inorganic cations were recently reported abundant in the vacuole of apple fruit (Beshir *et al.*, 2019).

NAF technique finds some of its limits when studying tissue expansion. Indeed, the first step of the NAF procedure, that consists in grinding frozen tissue to break the cell into several particles differentially enriched in vacuole, cytosol or chloroplasts, is crucial and dependent on cell size. Thus, this step was probably the reason why NAF failed for young leaves as shown in Figure S9. To overcome this difficulty, we developed a mathematical model that allowed the interpretation of metabolic data at the subcellular level throughout the entire leaf development. The model was built by integrating the information available in the literature on the vacuolar transporters for main soluble species (Table 2) into a set of equations (Table S3 to S5) and yielded the prediction of subcellular accumulation of metabolites during the whole time series. (Figure 13).

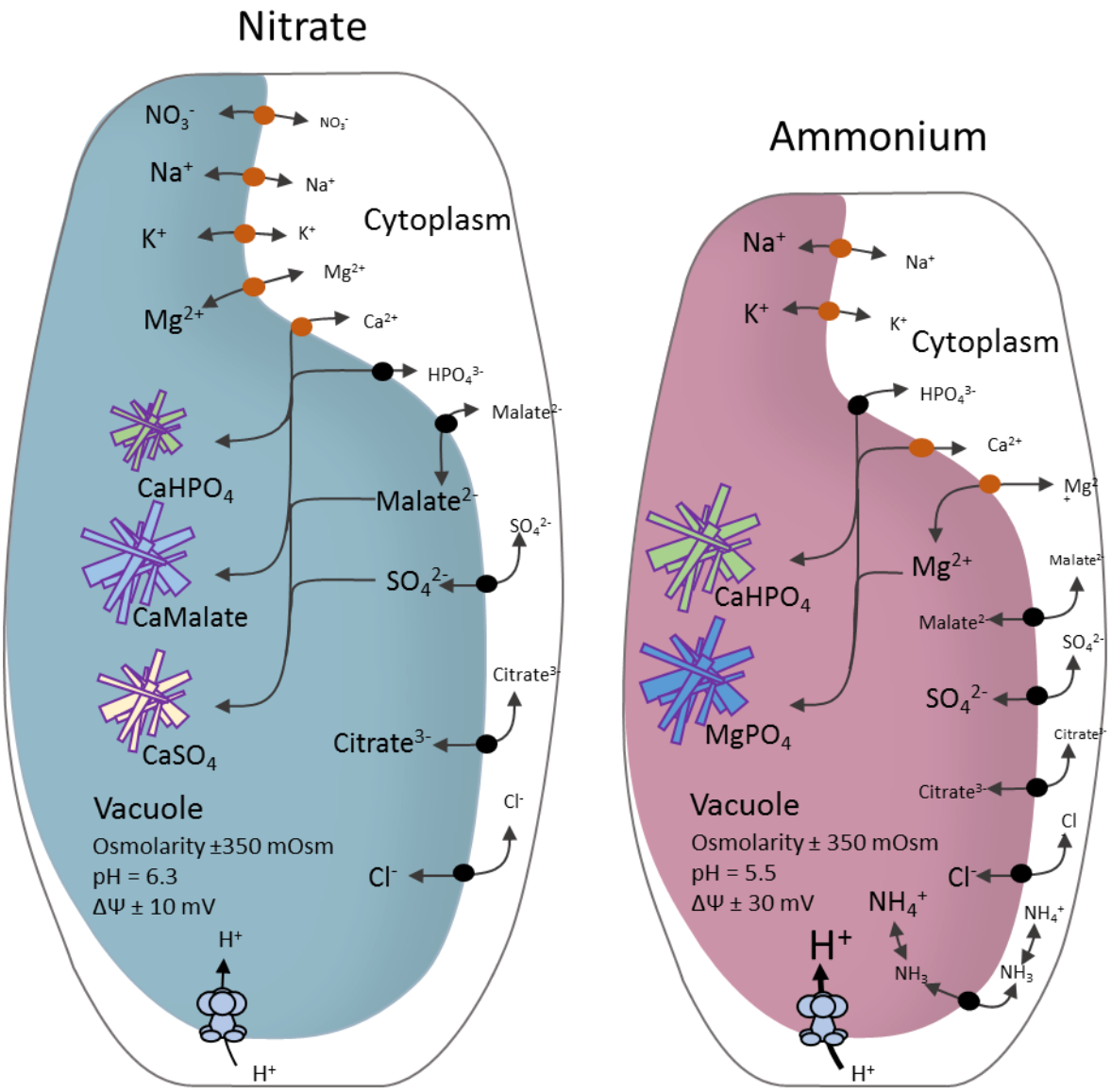

Figure 13: Summary illustration of the vacuolar accumulation of organic and inorganic species in leaves of tomato plant fed with nitrate (left panel, blue) and ammonium (right panel, red) as nitrogen source. Channel transporters (black circles) are energized by ΔΨ whereas H^+-antiport transporters (orange circles) are energized by the pH gradient across the tonoplast. Proton pumps establish both ΔΨ and ΔpH. Police size represents molecule concentration in the compartment. Left-right arrows indicate the thermodynamic equilibrium for each chemical species across the tonoplast. Calcium in NO_3^--fed plants and phosphate in NH_4^+-fed plants led to their association with other chemical compounds to form osmotically inactive ionic complexes, symbolized by crystal structures.

To run the equations, the proton gradient (ΔpH) across the tonoplast was measured *in vivo* by confocal microscopy (Figure 6), whereas the ΔΨ value together with the abundance of different ionic complexes in the vacuole were optimized for each leaf stage. Overall, the cross-validation with NAF data revealed that the model developed was able to provide realistic predictions of metabolites subcellular concentrations; the proton electrochemical gradient

making most of the compounds to accumulate inside the vacuole (Figure S11). This accumulating effect was in part due because of the formation of ion complexes into the vacuole (Figure S12), which is commonly associated to the regulation of ion homeostasis in plants (Volk *et al.*, 2002). For instance, a specific crystal matrix protein has been shown to be associated to calcium oxalate precipitates in the vacuole of specialized cells in *Pistia stratiotes* (Li *et al.*, 2003). In this sense, the formation of vacuolar complexes may be a mechanism to minimize the cytosolic accumulation of given ions without requiring any increase in the proton electrochemical gradient. For Mg^{2+} and SO_4^{2-}, in view of NAF data, the model did not always provide a realistic prediction, particularly because of the high concentrations predicted by the model in the cytoplasm of N fed-plants. This disagreement suggests the existence of additional transport mechanisms that enhance the vacuolar accumulation of these ions, such as the ATP-driven pumps identified for Ca^{2+} (Bonza and Michelis, 2011), vesicle transport as shown for Na^+ (Hamaji *et al.*, 2009) or the formation of other unexpected ionic complexes not considered in our model.

Similarly, the prediction for subcellular Cl^- and sucrose concentrations did not fit NAF measurements and showed higher concentrations in cytoplasm compared to vacuole in the older leaves (Figure S14). In mature leaves the low Cl^- content compared to other ions, makes Cl^- to bear a low contribution to global cytosolic negative charge pool and thus, has very little impact in the thermodynamic equilibrium of the cell (electroneutrality and $\Delta\Psi$). However, in the younger leaves under ammonium nutrition, the important Cl^- flux into the vacuole suggests it has an important contribution to vacuole osmolarity and osmotic strength. For sucrose, vacuolar accumulation appears dependent of additional transport mechanism as developed by Beauvoit *et al.*, (2014) and thus, could not be integrated to our model. However, its contribution and therefore the error committed on the vacuolar osmotic strength is minor when compared with other solutes such as malate, K^+ or SO_4^{2-} (Figure 10B).

Vacuole acidification appears an essential strategy to maintain cytosol homeostasis under ammonium nutrition but with a high energy cost for growth

The electrochemical gradient across the tonoplast is the driving force for most of vacuolar transporters that promote solute accumulation in the vacuole. This parameter is hardly measurable in cells of intact parenchymal tissue but is essential for our model parameterization. This was solved through the constraint-based optimization of the ΔΨ parameter, which suggested higher membrane potential across the tonoplast in NH_4^+-fed plants compared with plant fed with NO_3^- (Figure 7). ΔΨ adaptation in function of the external medium composition has for instance been observed by Mertz and Higinbotham (1976) in barley root cells upon the addition of 1 mM KCl that led to an increase of the tonoplastic ΔΨ from +9 to +35 mV. In our model, the increase of the membrane potential under ammonium nutrition was associated with the higher ΔpH across the tonoplast with respect to nitrate (Figure 6). Indeed, ΔpH energized the H^+-antiport transporters, which mainly translocate positively charged compounds such as K^+ or Ca^{2+} and thus, a higher ΔΨ was necessary to improve the transport of counterions across the tonoplast. This is in agreement with the calculations described by Lobit *et al* (2006) showing that membrane potential gradient declined when vacuolar pH diminished. Taken together, our results suggest the activation of the vacuolar proton pumps to maintain such electrochemical gradient under ammonium nutrition.

The higher electrochemical gradient in ammonium-fed plants entails consequences for vacuole performance. First, by increasing the sequestration capacity of the vacuole for different solutes. Second, by increasing the energy cost of the solute-driven vacuole expansion. In the same line, a study performed in propoplasts of bean mesophyll used a similar calculation to demonstrate the increase of the energetic cost of H^+ influx when ΔpH across the plasma membrane was more elevated (Wegner and Shabala, 2019). Therefore, decreasing the vacuolar pH is a good way to preserve the cytoplasm integrity under ammonium treatment but it incremented significantly the energy cost of solute fluxes needed for vacuole expansion (Figure 12). Hence, having a negative impact for cell growth and finally for leaf biomass accumulation. Accordingly, a more acidic vacuole would constitute a relevant metabolic energy trade-off that could impact cell energy budget and finally plant development.

The absence of vacuolar accumulation of malate affects cell expansion in NH_4^+-fed plants

Given the elevated flux intensity across the vacuole at the early development of the leaf (Figure 11), most osmolytes were accumulated during the exponential growth of the vacuole when RVR is maximal (Figure S3). This is in line with a constant deposition of osmoticum to ensure the entrance of water and thus, cell expansion. Interestingly, total solute flux across the tonoplast was greatly enhanced under nitrate nutrition mainly because of the important contribution of malate and Ca^{2+}. However, osmotically active concentration of free Ca^{2+} in the vacuole was very low, contrasting with the concentration of free malate, still maintained at high level under nitrate nutrition (Figure S13).

Special attention should be paid to the importance to couple subcellular metabolic study with cytology. In fact, It should first be noted that the cytological analyzes confirmed that cell growth was greater in plants under nitrate nutrition. This was not associated with a higher osmolarity but with the difference in the fluxes of solutes Thus, in NO_3^--fed leaves, the high flow of malate into the vacuole triggers an influx of water into the expanding vacuole, promoting vacuole and therefore cell growth. Concurrently with this increase in volume, the solute concentration, and therefore the osmolarity, decreased. In the end, the average osmolarities measured on ammonium and nitrate are of the same order of magnitude (Figure 9 and Figure 10).

Depletion of organic acid content under exclusive ammonium nutrition has been highlighted in various species including Arabidopsis, cereals or tomato (Kirkby and Mengel, 1967; Hachiya *et al.*, 2012; de la Peña *et al.*, 201; Vega-mas *et al.*, 2019) and was often associated with the metabolic adaptation to ammonium stress. Indeed, NH_4^+ assimilation into amino acids via the GS/GOGAT cycle requires an adequate supply of carbon skeletons, especially under ammonium nutrition where NH_4^+ assimilation is generally enhanced in order to control free NH_4^+ levels (Vega-mas *et al*., 2019). In this sense, the decrease of organic acids content illustrates the higher carbon consumed for NH_4^+ assimilation and has been put forward as a trade-off for the energy/carbon needed for growth.

In chapter 1, and as observed in the present chapter, we also integrated the depletion of organic acids by the action of the biochemical pH-stat, which compensates the differential H^+

production depending on the N form provided. However, when observing the contribution of free concentration of malate and citrate to the vacuolar osmolarity under nitrate treatment (Figure 10), it is clear that such depletion under ammonium treatment would affect the osmotic strength of the vacuole, and therefore the cell expansion.

Limitations of the model

Our model is based on the hypothesis that different molecules are permanently at a state of thermodynamic equilibrium. From this manner, and when comparing with NAF data, we obtained good predictions of the concentration of different solutes in the cytoplasm and vacuole that allowed us to calculate the net accumulation of compounds in the vacuole over the leaf development. Nevertheless, equilibrated system theory assumes that transporters are not involved in a dynamic system of flux, which is incorrect.

Considering NAF measurements, sucrose and hexoses to a lesser extend were overestimated in the vacuole by the model predictions (Figure S12), and particularly when NH_4^+ was the unique source of N. As extensively studied in Beauvoit *et al.,* (2014), vacuolar sequestration of hexoses depends of two transport mechanisms which would be in conflict in a model parameterized at the equilibrium. Those transport systems are 1) H^+-coupled antiporters, which transport directly sugars including sucrose into the vacuole, and 2) the sucrolytic activity of the vacuolar acid invertase which enables the production of glucose and fructose into the vacuole. The flux of sucrose through the H^+-coupled antiporter depends in part of the gradient established across the tonoplast. This gradient is determined by sucrose synthesis and degradation, mediated mainly by sucrose synthase (Stein and Granot, 2019) but also sucrose-phosphate synthase (Dali *et al.*, 1992) and the neutral invertase (Qin *et al.*, 2016) in the cytosol. Therefore, the higher activity of some glycolytic and TCA cycle enzymes under ammonium nutrition (Figure S3) should be considered since they influence the availability of hexoses in the cytosol. From this manner, the occurrence of a higher vacuolar sucrolytic activity under ammonium treatment also observed in *Beta vulgaris* (Raab and Terry, 1995), together with a relevant sucrose content in the cytosol (Table 1), would suggest a hexose efflux to the cytsol coupled to a sucrose influx into the vacuole that could induce a net

entrance of H^+s in the vacuole. These are relevant aspects that merit to be explored in depth in future works.

Discrepancies were also found between measurements and predictions of some inorganic ions. For instance, Cl^- content followed a very different trend respect to other ions regardless the N-source with similar concentrations of the ion found in both sides of the tonoplast. In our model, Cl- transport was driven by a specific anion channel energized by ΔΨ that favored its accumulation in the vacuole. However, different transport systems for inorganic ions can coexist on the tonoplast. For instance, Cl^- or NO_3^- are transported by channels that ensure simple diffusion, as well as by H^+-coupled antiporter (De Angeli *et al.*, 2006). In fact, these transport systems will tend to reach different thermodynamic equilibrium and would generate a futile cycle that could not be considered in a model at the equilibrium: entrance of the ion in the vacuole by a transporter and its release in the cytosol by the other. In this line, and as seen when comparing with NAF data, the prediction of Cl^- and NO_3^- concentrations could be more complicated than thermodynamic equilibrium state.

In another line, the tonoplast permeability for cations such as K^+ , Na^+ , and NH_4^+ is not null (Bonales-Alatorre *et al.*, 2013). Therefore, the presence of constant passive leaks of positively charged species from the vacuole to the cytoplasm can be considered as a transport working in the inverse direction respect to vacuolar transporter. That would generate a cycle with a potential energy cost. Under ammonium nutrition, this diffusion would be probably more intense since the tonoplast potential is higher but the smaller surface of the vacuoles in cells of ammonium–fed leaves would also moderate it.

All these cycles are generated by the coexistence of antagonist transporters or transports with different thermodynamic equilibrium that could not be managed in our model. As every mathematic model, ours also is not perfect but remained highly useful to provide good subcellular concentrations predictions and fluxes prediction to better understand the importance of the vacuole in tomato leaf cells adaptation to ammonium nutrition (Figure 13).

CONCLUSION

It is well accepted that cell expansion is affected by the N-source. Among others, cell growth is largely dependent of the internal pressure exerted on the cell wall by the vacuole. In this line of evidence, our study provides the first extensive characterization of how vacuole expansion is affected by the change of N-source and the impact it has on growth at the cellular and organ scale. To do so, the cell expansion related to ammonium and nitrate nutrition was monitored through a cytological analysis during tomato leaf development and associated to metabolic analysis at the organ and subcellular scale. Besides, the ΔpH across the tonoplast was determined. These data were integrated into a constraint-based model set up through an extensive reviewing of vacuolar transporters and describing the thermodynamic equilibrium across the tonoplast for the main soluble species present in the leaf cell. The optimization of the model revealed that the formation of ionic complexes exclusively in the vacuole was essential to accommodate both the measured local concentrations estimated by NAF and the whole tissue osmolarity. The modelling outputs highlight that the higher energization state of the vacuole (i.e. higher protomotive force) involved a higher energy cost of the solute-driven vacuole expansion under NH_4^+ nutrition. Furthermore, we demonstrated that in plants fed with NH_4^+, the reduced expansion of leaf cells would be linked to the NH_4^+-relative adaptation of the metabolism. Indeed, the regulation of NH_4^+ abundance in the cell through its assimilation induces a depletion of malate, an essential osmolyte that was central in the limitation of vacuolar expansion.

The model proposed here represents a first step towards integrating the physiological knowledge available at the subcellular level. However, the present approach is also based on restrictive simplifications concerning the regulation of physico-chemical variables that link cytoplasm and vacuole through the tonoplast transport systems. In the future, the transition to a dynamic system by studying fluxes instead of equilibrium could be a good approach to refine our predictions, in particular for sugars.

Supplementary information

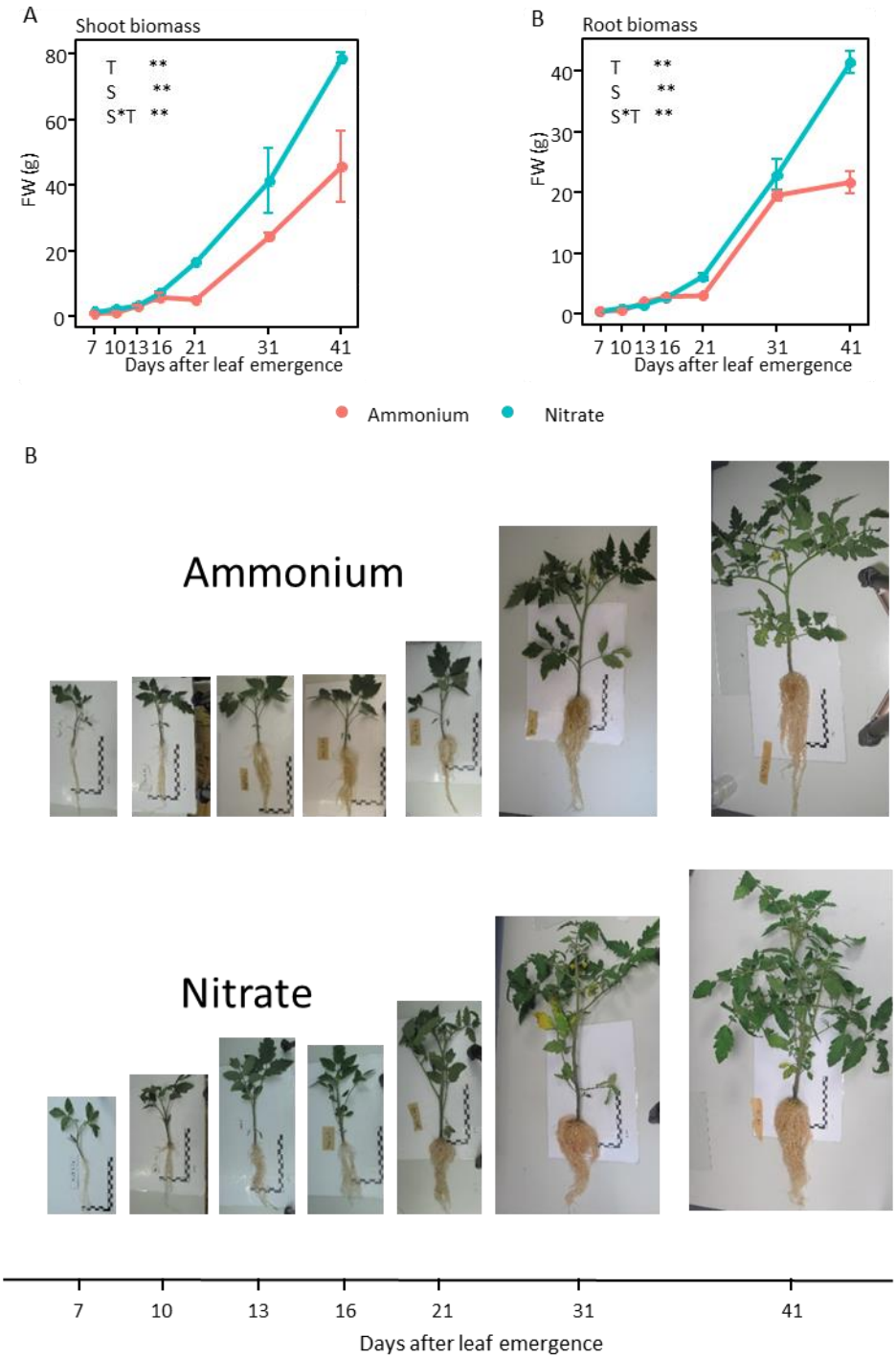

Figure S1: Time course evolution of shoot (A) and root (B) biomass of tomato plants grown with ammonium (red) and nitrate (blue) as nitrogen source. Values represent the mean ± se (n = 3). Significant differences are shown according to two-way ANOVA (**: p<0.01; *: p<0.05; *ns*: not significant) where S indicates nitrogen source effect; D indicates days effect and S×D indicates interaction effect. Representative images of the whole plant throughout the development of the fourth leaf.

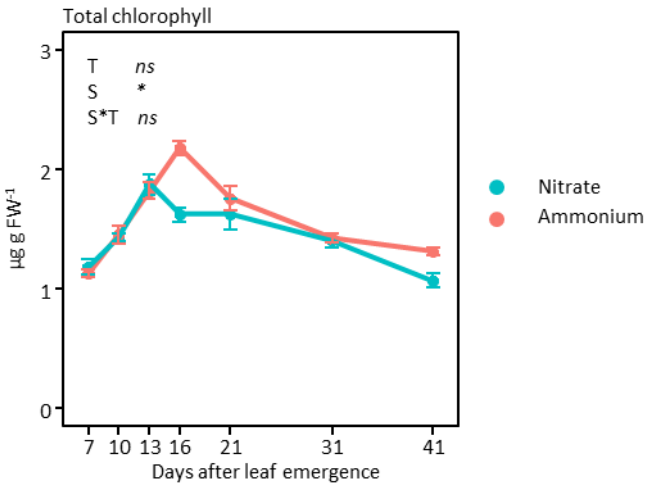

Figure S2: Time course evolution of chlorophyll content throughout the development of the fourth leaf in tomato plants grown with ammonium (red) and nitrate (blue) as nitrogen source. Values represent the mean ± se (n = 3). Significant differences are shown according to two-way ANOVA (**: p<0.01; *: p<0.05; *ns*: not significant) where S indicates nitrogen source effect; D indicates days effect and S×D indicates interaction effect.

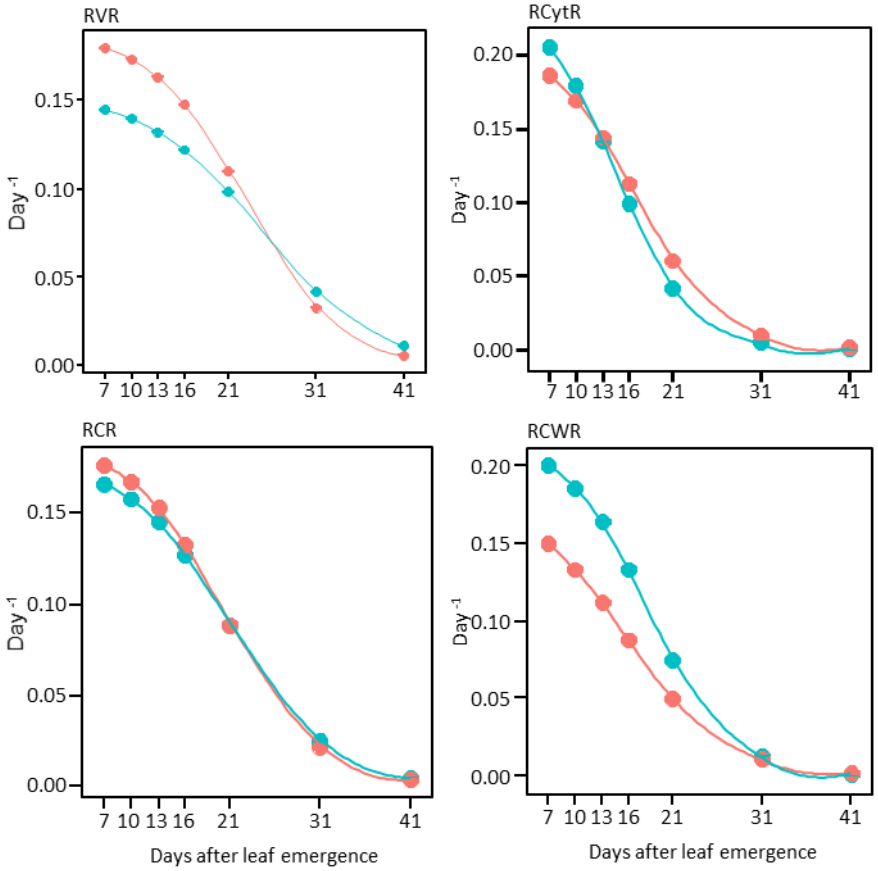

Figure S3: Time course evolution of subcellular RGR of whole cell (RCR), vacuole (RVR), cytoplasm (RCytR), and cell wall (RCWR) throughout the development of tomato leaf grown with ammonium (red) and nitrate (blue) as nitrogen source. Continuous line represents RGR curves, calculated by derivation of the logistic function and divided by subcellular volume values.

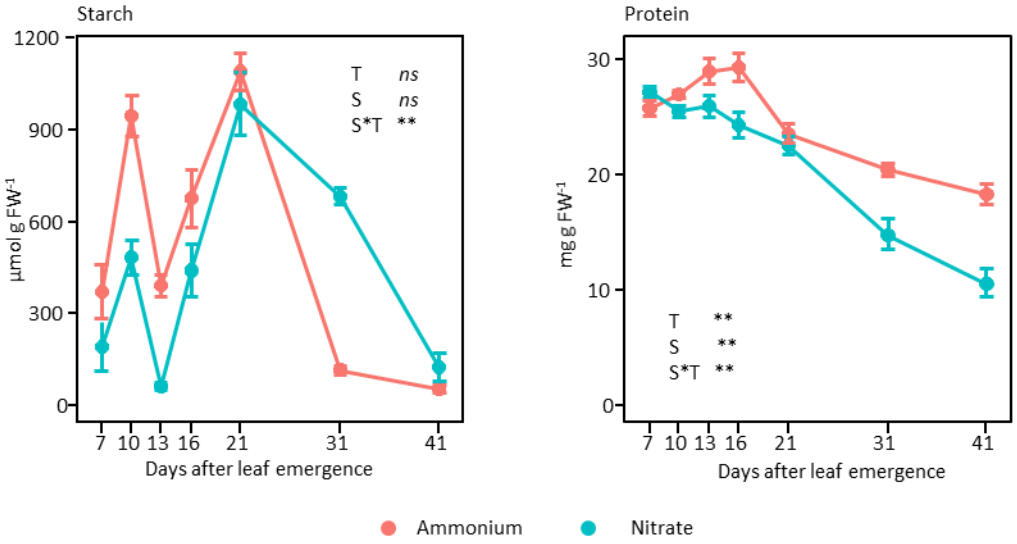

Figure S4: Time course evolution of starch and protein content throughout the development the fourth leaf in tomato plants grown with ammonium (red) and nitrate (blue) as nitrogen source. Values represent the mean ± se (n = 3). Significant differences are shown according to two-way ANOVA (**: p<0.01; *: p<0.05; *ns*: not significant) where S indicates nitrogen source effect; D indicates days effect and S×D indicates interaction effect.

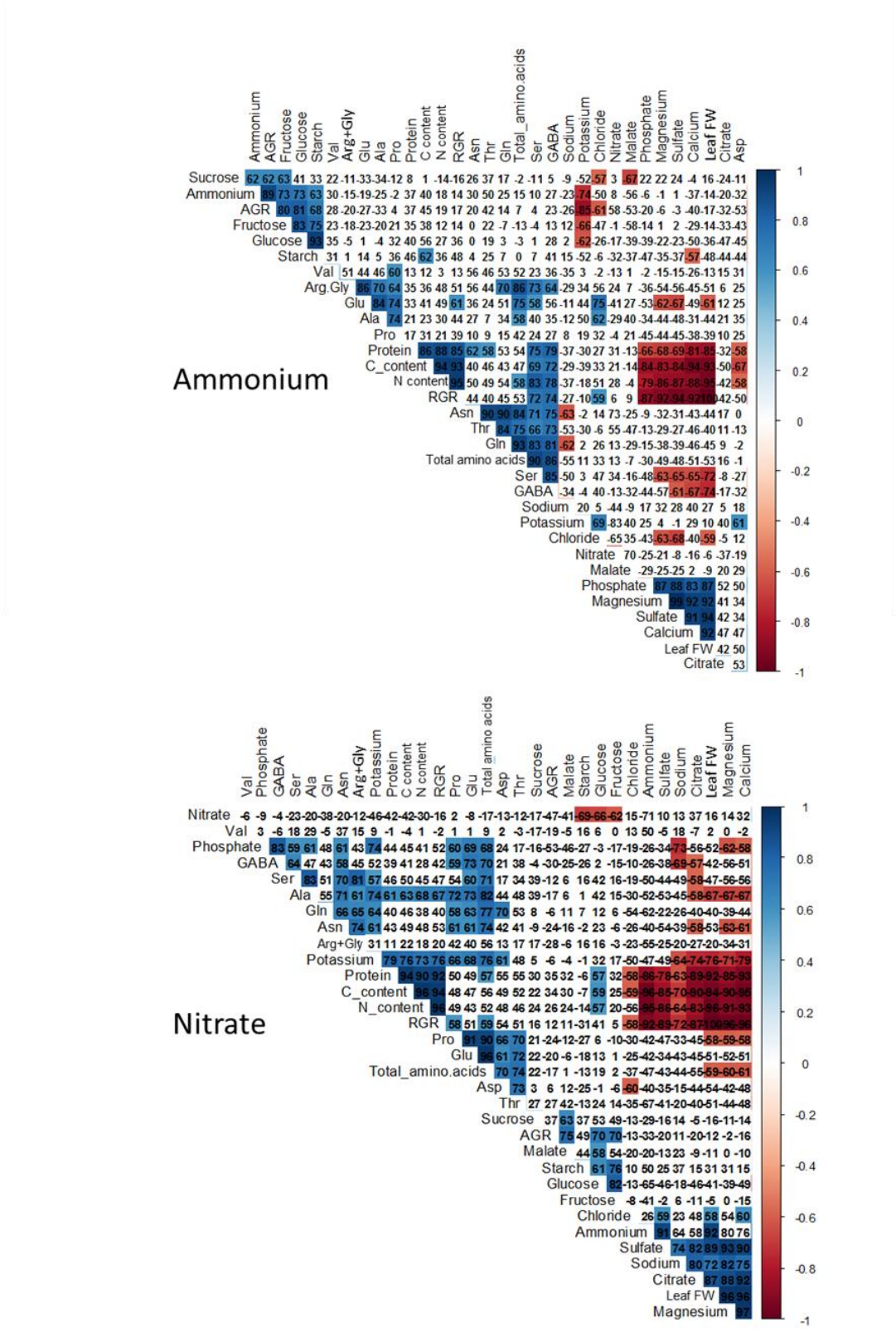

Figure S5: Correlation matrixes of metabolites, organic ions and physiological parameters determined in the fourth leaf of tomato plants grown with ammonium or nitrate as N-source. Numbers inside the boxes indicate Pearson r correlation coefficient (x100). Significant positive and negative correlations (P < 0.01) are highlighted in blue and red, respectively following the scale shown in the right-side of the plots.

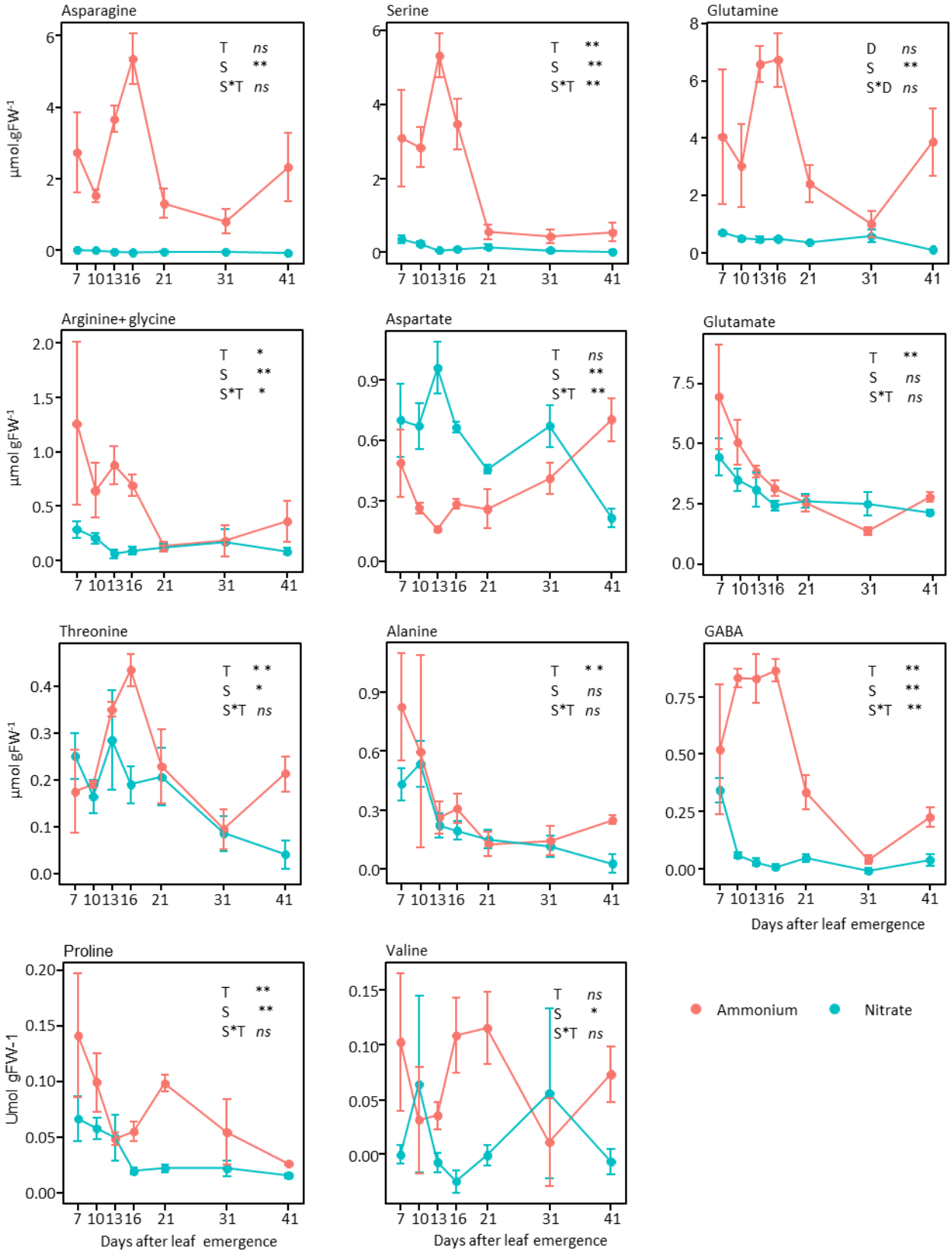

Figure S6: Time course evolution of the main individual amino acids throughout the development of the fourth leaf in tomato plants grown with ammonium (A: red) and nitrate (N: blue) as nitrogen source. Values represent the mean ± se (n = 3). Significant differences are shown according to two-way ANOVA (**: p<0.01; *: p<0.05; *ns*: not significant) where S indicates nitrogen source effect; D indicates days effect and S×D indicates interaction effect.

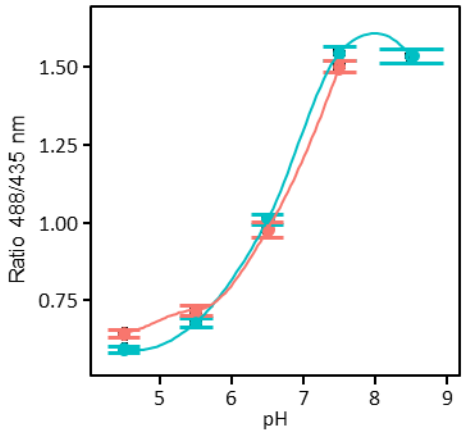

Figure S7: BCECF calibration curves for intracellular pH determination. Curves were performed separately in leaf sections of ammonium-fed (red) and nitrate-fed (blue) plants showing no significant difference in function of the leaf metabolic background. Values represent the mean ± se (n = 4 leaves/sections, each replicate corresponding to an average of 10 measurements per leaf/section). Different letters indicate significant differences according to one-way ANOVA followed by Duncan´s test (p<0.05).

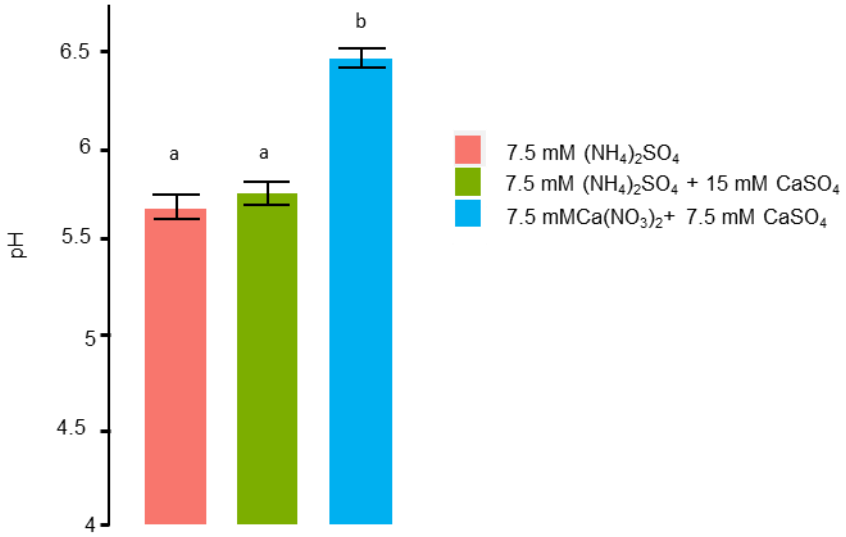

Figure S8: Effect of calcium and sulfate equilibrium in nutrient solution on vacuolar pH measurement using BCECF dye in leaves of tomato plants grown with ammonium and nitrate as nitrogen source. Plant that received the green treatment were supplied with an additional concentration of 15 mM $CaSO_4^{2-}$ with respect to red treatment. Consequently, plants treated with green (New ammonium treatment) and blue nutritive solution (treatment used in this study) received the same amount of calcium, whereas plants treated with red and blue nutritive solution received the same amount of sulfate. Values represent the mean ± se (n = 12) averaged from about 10 measurements each. Different letters indicate significant differences according to one-way ANOVA followed by Duncan´s test (t-test p<0.05).

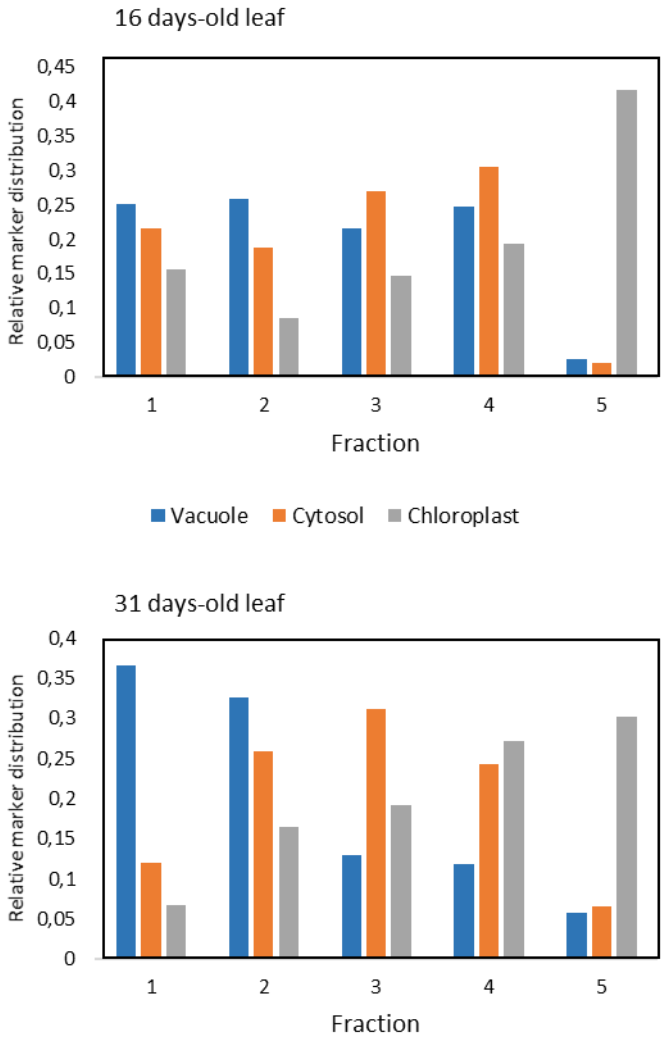

Figure S9: Examples of compartments enrichment pattern obtained from young (16 days) and old (31 days) leaves of NO_3^--fed tomato plants after non-aqueous fractionation (NAF). (A) Representative case of insufficient compartments separation along five NAF fractions in 16 day-old leaves. (B) Representative case of correct separation in 31 day-old leaves.

Table S1: Summary of non-aqueous fractionation results showing the vacuolar, cytoplasmic and chloroplastic proportions of metabolites and inorganic ions of 21, 31 and 41 aged tomato leaf supplied with nitrate or ammonium as unique source of nitrogen. Values represent mean ± se (n = 3). Subcellular proportions of NO_3^- ion is not given under ammonium nutrition since it was undetectable (*nd* means not detected). NAF data for NH_4^+-fed leaves at 41 days is missing because of technical problems during compartment markers determination

		Nitrate						Ammonium					
		Vacuole		Cytosol		chloroplast		Vacuole		Cytosol		chloroplast	
	Days after emergence	Proportion (%)		Proportion (%)		Proportion (%)		Proportion (%)		Proportion (%)		Proportion (%)	
		mean	se	mean	se	mean	se	mean	se	mean	se	mean	se
Glucose	21	88	8	7	7	5	4	84	27	16	27	0	0
	31	93	2	3	2	5	5	76	9	24	2	0	0
	41	63	18	23	23	15	3						
Fuctose	21	93	6	7	7	0	0	82	31	18	31	0	0
	31	100	0	0	0	0	0	79	8	19	18	2	2
	41	100	0	0	0	0	0						
Sucrose	21	12	5	82	4	6	3	53	48	47	54	0	0
	31	78	3	22	4	0	0	41	18	55	0	4	5
	41	8	5	93	7	0	0						
Malate	21	88	6	9	9	3	3	94	6	3	6	3	6
	31	89	8	5	6	6	6	89	2	4	4	7	4
	41	100	0	0	0	0	0						
NH_4^+	21	33	26	67	33	0	0	97	6	3	6	0	0
	31	35	25	56	45	10	10	94	5	0	0	6	8
	41	53	33	47	47	0	0						
K^+	21	82	14	18	18	0	0	90	5	2	3	8	10
	31	100	0	0	0	0	0	100	0	0	0	0	0
	41	100	0	0	0	0	0						
Na^+	21	100	0	0	0	0	0	100	0	0	0	0	0
	31	90	7	10	10	0	0	98	1	1	2	1	0
	41	100	0	0	0	0	0						
Ca^{2+}	21	100	0	0	0	0	0	89	10	0	0	11	12
	31	100	0	0	0	0	0	100	0	0	0	0	0
	41	100	0	0	0	0	0						
Mg^{2+}	21	94	5	6	6	0	0	100	0	0	0	0	0
	31	100	0	0	0	0	0	100	0	0	0	0	0
	41	100	0	0	0	0	0						
SO_4^{2-}	21	100	0	0	0	0	0	100	0	0	0	0	0
	31	100	0	0	0	0	0	100	0	0	0	0	0
	41	100	0	0	0	0	0						
NO_3^-	21	68	14	30	19	2	2	ns	ns	ns	ns	ns	ns
	31	77	16	14	14	9	9	ns	ns	ns	ns	ns	ns
	41	100	0	0	0	0	0						
Cl^-	21	50	17	39	23	11	5	62	15	18	31	19	22
	31	86	10	0	0	14	14	59	7	31	8	10	10
	41	67	1	29	6	4	4						
PO_4^{2-}	21	62	12	35	17	4	2	100	0	0	0	0	0
	31	98	1	0	0	2	2	94	4	5	4	1	0
	41	100	0	0	0	0	0						

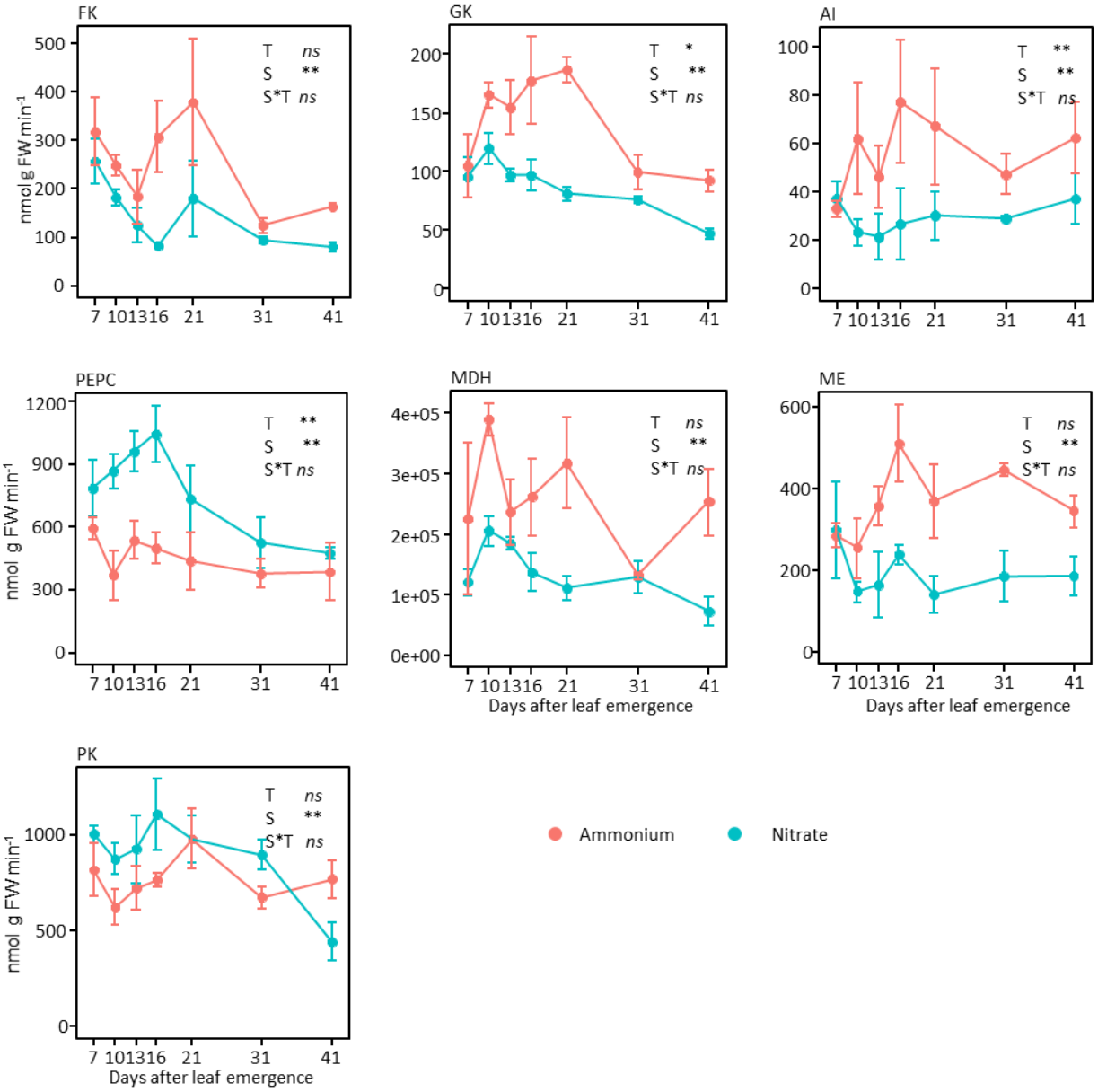

Figure S10: Time course evolution of enzyme activities throughout the development of the fourth leaf of tomato plants grown with ammonium (red) and nitrate (blue) as nitrogen source.; FK stands for fructokinase; GK for glucokinase; AI for acid invertase; PEPC for phosphoenolpyruvate carboxylase; MDH for NAD(H)-dependent malate dehydrogenase; ME for NADP-dependent malic enzyme; and PK for pyruvate kinase. Values represent the mean ± se (n = 3). Significant differences are shown according to two-way ANOVA (**: p<0.01; *: p<0.05; *ns*: not significant) where S indicates nitrogen source effect; D indicates days effect and S×D indicates interaction effect.

Table S2: Constants used in transport equations for model parameterizations.

pH_{cyt}	6.79 pH units
F	96485.33 C mol^{-1}
R	8.314 J mol^{-1} K^{-1}
T	298.15 Kelvin
$Kd1_{PO_4}$	12.1
$Kd2_{PO_4}$	7.2
$Kd3_{PO_4}$	2.15
$Kd1_{Citrate}$	6.40
$Kd2_{Citrate}$	4.76
$Kd3_{Citrate}$	3.13
$kd1_{Malate}$	5.10
$Kd2_{Malate}$	3.46
$K_{SP_{CaMalate}} = [Ca^{2+}] * [Malate^{2-}]$	50 $mmol^2$
$K_{SP_{CaPO4}} = [Ca^{2+}]^3 * [PO_4^{3-}]^2$	10^{-10} $mmol^5$
$K_{SP_{MgPO4}} = [Mg^{2+}] * [Malate^{2-}]$	10^{-10} $mmol^5$
$K_{SP_{MgNH4PO4}} = [Mg^{2+}] * [NH_4^+] * [PO_4^{3-}]$	10^{-4} $mmol^3$
$K_{SP_{CaSO4}} = [Ca^{2+}]^3 * [SO_4^{2-}]^2$	$10^{-2.3}$ $mmol^2$
$K_{SP_{CaHPO4}} = [Ca^{2+}] * [HPO_4^{2-}]$	0.1 $mmol^2$
$K_{SP_{CaCitate}} = [Ca^{2+}]^3 * [Citrate^{3-}]^2$	100 $mMol^5$
in vivo ΔG of ATP hydrolysis	50000 J mol^{-1} ATP

Table S3: Equations used for the calculation of inorganic ions concentration without conjugated forms (1 and 2). ΔΨ is determined by constraint-based optimization whereas ΔpH was determined experimentally. V_{vac}, V_{cyt} and V_{cell} correspond respectively to the volume of vacuole, cytoplasm and whole cell determined by microscopy. Other constants used are listed in Table S2.

NO_3^- **Transport mechanism: H^+ antiporter** **Carrier diffusion at equilibrium:** $R*T*\ln\frac{[NO_3^-]^2_{vac}}{[NO_3^-]^2_{cyt}} - R*T*ln\frac{[H^+]_{vac}}{[H^+]_{cyt}} - F*\Delta\Psi = 0$ **Mass conservation law :** $[NO_3^-]_{vac}*V_v + [NO_3^-]_{cyt}*V_c = [NO_3^-]_{tissue}*V_{cell}*density$ **with $[NO_3^-]_{vac}$ in mM. Nitrate total in µmol g FW^{-1} and tissue density = 1 g FW.mL^{-1}**	$[NO_3^-]_{cyto} = \frac{[NO_3^-]_{tissue}}{\left[\frac{[H^+]_{vac}}{[H^+]_{cyt}}\right]^{0.5} * \exp\left(F*\frac{\Delta\Psi}{2*R*T}\right)*\frac{V_{vac}}{V_{cell}}+\frac{V_{cyt}}{V_{cell}}}$ $[NO_3^-]_{vacuole} = \frac{[NO_3^-]_{tissue}}{\frac{V_{vac}}{V_{cell}}+\frac{\frac{V_{cyt}}{V_{cell}}}{\left[\frac{[H^+]_{vac}}{[H^+]_{cyt}}\right]^{0.5} * \exp\left(F*\frac{\Delta\Psi}{2*R*T}\right)}}$
Cl^- **Transport mechanism: anionic uniporter** **Facilitated diffusion at equilibrium:** $R*T*\ln\frac{[Cl^-]_{vac}}{[Cl^-]_{cyt}} - F*\Delta\Psi = 0$ **Mass conservation law :** $[Cl^-]_{vac}*V_v + [Cl^-]_{cyt}*V_c = [Cl^-]_{tissue}*V_{cell}*density$	$[Cl^-]_{cyt} = \frac{[Cl^-]_{tissue}}{\exp\left(F*\frac{\Delta\Psi}{R*T}\right)*\frac{V_{vac}}{V_{cell}}+\frac{V_{cyt}}{V_{cell}}}$ $[Cl^-]_{cyt} = \frac{[Cl^-]_{tissue}}{\frac{V_{vac}}{V_{cell}}+\frac{\frac{V_{cyt}}{V_{cell}}}{\exp\left(F*\frac{\Delta\Psi}{R*T}\right)}}$
SO_4^{2-} **Transport mechanism: anionic uniporter** **Facilitated diffusion at equilibrium:** $R*T*\ln\frac{[SO_4^{2-}]_{vac}}{[SO_4^{2-}]_{cyt}} - 2*F*\Delta\Psi = 0$ **Mass conservation law :** $[SO_4^{2-}]_{vac}*V_v + [SO_4^{2-}]_{cyt}*V_c = [SO_4^{2-}]_{tissue}*V_{cell}*density$	$[SO_4^{2-}]_{cyt} = \frac{[SO_4^{2-}]_{tissue}}{\exp\left(2*F*\frac{\Delta\Psi}{R*T}\right)*\frac{V_{vac}}{V_{cell}}+\frac{V_{cyt}}{V_{cell}}}$ $[SO_4^{2-}]_{vac} = \frac{[SO_4^{2-}]_{tissue}}{\frac{V_{vac}}{V_{cell}}+\frac{\frac{V_{cyt}}{V_{cell}}}{\exp\left(2*F*\frac{\Delta\Psi}{R*T}\right)}}$
NH_4^+ **Transport mechanism: diffusion of NH_3 at equilibrium:** $R*T*\ln\frac{[NH_3]_{vac}}{[NH_3]_{cyt}} = 0$ **Mass conservation law :** $[NH_4^+]_{vac}*V_v + [NH_4^+]_{cyt}*V_c = [NH_4^+]_{total}*V_{cell}*density$	$[NH_4^+]_{cyt} = \frac{[NH_4^+]_{tissue}}{\left(\frac{10^{-pH_{vac}}}{10^{-pH_{cyt}}}\right)*\frac{V_{vac}}{V_{cell}}+\frac{V_{cyt}}{V_{cell}}}$ $[NH_4^+]_{vacuole} = \frac{[NH_4^+]_{tissue}}{\frac{V_{vac}}{V_{cell}}+\frac{\frac{V_{cyt}}{V_{cell}}}{\left(\frac{10^{-pH_{vac}}}{10^{-pH_{cyt}}}\right)}}$

Table S3 (2): Equations used for the calculation of inorganic ions concentration without conjugated forms (1 and 2). ΔΨ is determined by constraint-based optimization whereas ΔpH was determined experimentally. V_{vac}, V_{cyt} and V_{cell} correspond respectively to the volume of vacuole, cytoplasm and whole cell determined by microscopy. Other constants used are listed in Table S1.

Mg^{2+} **Transport mechanism: H^+-coupled antiporter** **Carrier at equilibrium:** $R*T*\ln\frac{[Mg^{2+}]_{vac}}{[Mg^{2+}]_{cyt}} + F*\Delta\Psi - R*T*\ln\frac{[H^+]_{vac}}{[H^+]_{cyt}} = 0$ **Mass conservation law :** $[Mg^{2+}]_{vac}*V_v + [Mg^{2+}]_{cyt}*V_c = [Mg^{2+}]_{tissue}*V_{cell}*density$	$[Mg^{2+}]_{cyt} = \frac{[Mg^{2+}]_{tissue}}{\frac{V_{vac}}{V_{cell}}*\left(\frac{10^{-pH_{vac}}}{10^{-pH_{cyt}}}*\exp\left(-f*\frac{\Delta\Psi}{R*T}\right)\right)+\frac{V_{cyt}}{V_{cell}}}$ $[Mg^{2+}]_{vacuole} = \frac{[Mg^{2+}]_{tissue}}{\frac{V_{vac}}{V_{cell}}+\frac{\frac{V_{cyt}}{V_{cell}}}{\frac{10^{-pH_{vac}}}{10^{-pH_{cyt}}}*\exp\left(-F*\frac{\Delta\Psi}{R*T}\right)}}$
Ca^{2+} **Transport mechanism: H^+-coupled antiporter** **Carrier at equilibrium:** $R*T*\ln\frac{[Ca^{2+}]_{vac}}{[Ca^{2+}]_{cyt}} + F*\Delta\Psi - R*T*\ln\frac{[H^+]_{vac}}{[H^+]_{cyt}} = 0$ **Mass conservation law :** $[Ca^{2+}]_{vac}*V_v + [Ca^{2+}]_{cyt}*V_c = [Ca^{2+}]_{tissue}*V_{cell}*density$	$[Ca^{2+}]_{cyt} = \frac{[Ca^{2+}]_{tissue}}{\frac{V_{vac}}{V_{cell}}*\left(\frac{10^{-pH_{vac}}}{10^{-pH_{cyt}}}*\exp\left(-F*\frac{\Delta\Psi}{R*T}\right)\right)+\frac{V_{cyt}}{V_{cell}}}$ $[Ca^{2+}]_{vacuole} = \frac{[Ca^{2+}]_{tissue}}{\frac{V_{vac}}{V_{cell}}+\frac{\frac{V_{cyt}}{V_{cell}}}{\left(\frac{10^{-pH_{vac}}}{10^{-pH_{cyt}}}\right)*\exp\left(-F*\frac{\Delta\Psi}{R*T}\right)}}$
Na^+ **Transport mechanism: H^+-coupled antiporter** **Carrier at equilibrium:** $R*T*\ln\frac{[Na^+]_{vac}}{[Na^+]_{cyt}} - R*T*\ln\frac{[H^+]_{vac}}{[H^+]_{cyt}} = 0$ **Mass conservation law :** $[Na^+]_{vac}*V_v + [Na^+]_{cyt}*V_c = [Na^+]_{tissue}*V_{cell}*density$	$[Na^+]_{cyt} = \frac{[Na^+]_{tissue}}{\left(\frac{10^{-pH_{vac}}}{10^{-pH_{cyt}}}\right)*\frac{V_{vac}}{V_{cell}}+\frac{V_{cyt}}{V_{cell}}}$ $[Na^+]_{vac} = \frac{[Na^+]_{tissue}}{\frac{V_{vac}}{V_{cell}}+\frac{\frac{V_{cyt}}{V_{cell}}}{\frac{10^{-pH_{vac}}}{10^{-pH_{cyt}}}}}$
K^+ **Transport mechanism: H^+-coupled antiporter** **Carrier at equilibrium:** $R*T*\ln\frac{[K^+]_{vac}}{[K^+]]_{cyt}} - R*T*\ln\frac{[H^+]_{vac}}{[H^+]_{cyt}} = 0$ **Mass conservation law :** $[K^+]_{vac}*V_v + [K^+]_{cyt}*V_c = [K^+]_{tissue}*V_{cell}*density$	$[K^+]_{cyt} = \frac{[K^+]_{total}}{\left(\frac{10^{-pH_{vac}}}{10^{-pH_{cyt}}}\right)*\frac{V_{vac}}{V_{cell}}+\frac{V_{cyt}}{V_{cell}}}$ $[K^+]_{vac} = \frac{[K^+]_{tissue}}{\frac{V_{vac}}{V_{cell}}+\frac{\frac{V_{cyt}}{V_{cell}}}{\frac{10^{-pH_{vac}}}{10^{-pH_{cyt}}}}}$

Table S4: Equations used for the calculation of phosphate and charged organic compounds concentration with conjugated forms. ΔΨ is determined by constraint-based optimization whereas ΔpH was determined experimentally. V_{vac}, V_{cyt} and V_{cell} correspond respectively to the volume of vacuole, cytoplasm and whole cell determined by microscopy. Other constants used are listed in Table S1.

Malate **Transport mechanism: anionic uniporter** **Facilitated diffusion at equilibrium:** $R*T*\ln\frac{[Malate^{2-}]_{vac}}{[Malate^{2-}]_{cyt}} - 2*F*\Delta\Psi = 0$ **Mass conservation law :** $[Malate]_{vac}*V_v + [Malate]_{cyt}*V_c + [Malate]_{vac}*V_v + [Malate^{-}]_{cyt}*V_c + [Malate^{-}]_{vac}*V_v + [Malate^{2-}]_{cyt}*V_c = [Malate]_{tissue}*V_{cell}*density$	$$[\text{Malate}]_{cyt} = \frac{[\text{Malate}]_{tissue}}{\exp\left(2*F*\frac{\Delta\Psi}{R*T}\right)*\frac{1+\frac{10^{-pH_{vac}}}{kd1_{mal}}+\frac{(10^{-pH_{vac}})^2}{kd1_{mal}*kd2_{mal}}}{\left(1+\frac{10^{-pH_{cyto}}}{kd1_{mal}}+\frac{(10^{-pH_{cyt}})^2}{kd1_{mal}*kd2_{mal}}\right)}*\frac{V_{vac}}{V_{cell}}+\frac{V_{cyt}}{V_{cell}}}$$
	$$[\text{Malate}]_{vac} = \frac{[\text{Malate}]_{tissue}}{\frac{V_{vac}}{V_{cell}}+\frac{\frac{V_{cyt}}{V_{cell}}}{\exp\left(2*F*\frac{\Delta\Psi}{R*T}\right)*\frac{1+\frac{10^{-pH_{vac}}}{kd1_{malate}}+\frac{(10^{-pH_{vac}})^2}{kd1_{malate}*kd2_{malate}}}{\left(1+\frac{10^{-pH_{cyt}}}{kd1_{malate}}+\frac{(10^{-pH_{cyt}})^2}{kd1_{malate}*kd2_{malate}}\right)}}}$$
Citrate **Transport mechanism: anionic uniporter** **Facilitated diffusion at equilibrium:** $R*T*\ln\frac{[Citrate^{3-}]_{vac}}{[Citrate^{3-}]_{cyt}} - 3*F*\Delta\Psi = 0$ **mass conservation law :** $[Citrate^{3-}]_{vac}*V_v + [Citrate^{3-}]_{cyt}*V_c + [Citrate^{2-}]_{vac}*V_v + [Citrate^{-}]_{cyt}*V_c + [Citrate^{-}]_{vac}*V_v + [Citrate^{-}]_{cyt}*V_c + [Citrate]_{vac}*V_v + [Citrate]_{cyt}*V_c = [Citrate]_{tissue}*V_{cell}*density$	$$[\text{Citrate}]_{cyt} = \frac{[\text{Citrate}]_{tissue}}{\exp\left(3*F*\frac{\Delta\Psi}{R*T}\right)*\frac{1+\frac{10^{-pH_{vac}}}{Kd1_{Citrate}}+\frac{(10^{-pH_{vac}})^2}{Kd2_{Citrate}*Kd3_{Citrate}}+\frac{(10^{-pH_{vac}})^3}{Kd3_{Citrate}*Kd2_{Citrate}*Kd3_{Citrate}}}{1+\frac{10^{-pH_{cyt}}}{Kd1_{Citrate}}+\frac{(10^{-pH_{cyt}})^2}{Kd1_{Citrate}*Kd2_{Citrate}}+\frac{(10^{-pH_{cyt}})^3}{Kd1_{Citrate}*Kd2_{Citrate}*Kd3_{Citrate}}}*\frac{V_{vac}}{V_{cell}}+\frac{V_{cy}}{V_{cell}}}$$
	$$[\text{Citrate}]_{vac} = \frac{[\text{Citrate}]_{tissue}}{\frac{V_{vac}}{V_{cell}}+\frac{\frac{V_{cyt}}{V_{cell}}}{\exp\left(3*F*\frac{\Delta\Psi}{R*T}\right)*\frac{1+\frac{10^{-pH_{vac}}}{Kd1_{Citrate}}+\frac{(10^{-pH_{vac}})^2}{Kd2_{Citrate}*Kd3_{Citrate}}+\frac{(10^{-pH_{vac}})^3}{Kd1_{Citrate}*Kd2_{Citrate}*Kd3_{Citrate}}}{1+\frac{10^{-pH_{cyt}}}{Kd1_{Citrate}}+\frac{(10^{-pH_{cyt}})^2}{Kd2_{Citrate}*Kd3_{Citrate}}+\frac{(10^{-pH_{cyt}})^3}{Kd1_{Citrate}*Kd2_{Citrate}*Kd3_{Citrate}}}}}$$
Phosphate **Transport mechanism: anionic uniporter** **Facilitated diffusion at equilibrium:** $R*T*\ln\frac{[\text{Phosphate}]_{vac}}{[\text{Phosphate}]_{cyt}} - 2*F*\Delta\Psi = 0$ **mass conservation law :** $[PO_4^{3-}]_{vac}*V_v + [PO_4^{3-}]_{cyt}*V_c + [HPO_4^{2-}]_{vac}*V_{vac} + [HPO_4^{2-}]_{cyt}*V_c + [H_2PO_4^{-}]_{vac}*V_v + [H_2PO_4^{-}]_{cyt}*V_c + [H_3PO_4]_{vac}*V_v + [H_3PO_4]_{cyt}*V_c = [Phosphate]_{tissue}*V_{cell}*density$	$$[\text{Phosphate}]_{cyt} = \frac{[\text{Phosphate}]_{tissue}}{\exp\left(2*F*\frac{\Delta\Psi}{R*T}\right)*\frac{1+\frac{10^{-pH_{vac}}}{Kd2_{PO_4}}+\frac{(10^{-pH_{vac}})^2}{Kd2_{PO_4}*Kd3_{PO_4}}+\frac{Kd1_{PO_4}}{10^{-pH_{vac}}}}{\frac{10^{-pH_{cyt}}}{Kd2_{PO_4}}+\frac{(10^{-pH_{cyt}})^2}{Kd2_{PO_4}*Kd3_{PO_4}}+1+\frac{Kd1_{PO_4}}{10^{-pH_{cyt}}}}*\frac{V_{vac}}{V_{cell}}+\frac{V_{cyt}}{V_{cell}}}$$
	$$[\text{Phosphate}]_{vac} = \frac{[\text{Phosphate}]_{tissue}}{\frac{V_{vac}}{V_{cell}}+\frac{\frac{V_{cyt}}{V_{cell}}}{\exp\left(2*F*\frac{\Delta\Psi}{R*T}\right)*\frac{1+\frac{10^{-pH_{vac}}}{Kd2_{PO_4}}+\frac{(10^{-pH_{vac}})^2}{Kd2_{PO_4}*Kd3_{PO_4}}+\frac{Kd1_{PO_4}}{10^{-pH_{vac}}}}{\frac{10^{-pH_{cyt}}}{Kd2_{PO_4}}+\frac{(10^{-pH_{cyto}})^2}{Kd2_{PO_4}*Kd3_{PO_4}}+1+\frac{Kd1_{PO_4}}{10^{-pH_{cyt}}}}}}$$

Table S5: Equations used for the calculation of non-charged osmolytes concentration in the vacuole and cytosol. ΔΨ is determined by constraint-based optimization whereas ΔpH was determined experimentally. V_{vac}, V_{cyt} and V_{cell} correspond respectively to the volume of vacuole, cytoplasm and whole cell determined by microscopy. Other constants used are listed in Table S1.

Glucose **Transport mechanism: H⁺-coupled antiporter** **Carrier at equilibrium:** $R * T * \ln\frac{[\text{Glucose}]_{vac}}{[\text{Glucose}]_{cyt}} - R * T * \ln\frac{[H^+]_{vac}}{[H^+]_{cyt}} - F * \Delta\Psi = 0$ **Mass conservation law :** $[\text{Glucose}]_{vac} * V_v + [\text{Glucose}]_{cyt} * V_c = [\text{Glucose}]_{\text{tissue}} * V_{cell} * density$	$[Glucose]_{\text{vac}} = \frac{[Glucose]_{\text{tissue}}}{\left(\frac{10^{-pH_{vac}}}{10^{-pH_{cyt}}} * exp\left(\text{F} * \frac{\Delta\Psi}{R * T}\right)\right) * \frac{V_{\text{vac}}}{V_{cell}} + \frac{V_{cyt}}{V_{cell}}}$ $[Glucose]_{cyt} = \frac{[Glucose]_{\text{tissue}}}{\frac{V_{\text{vac}}}{V_{cell}} + \frac{\frac{V_{cyt}}{V_{cell}}}{\left(\frac{10^{-pH_{vac}}}{10^{-pH_{cyt}}} * exp\left(\text{F} * \frac{\Delta\Psi}{R * T}\right)\right)}}$
Fructose **Transport mechanism: H⁺-coupled antiporter** **Carrier at equilibrium:** $R * T * \ln\frac{[\text{Fructose}]_{vac}}{[\text{Fructose}]_{cyt}} - R * T * \ln\frac{[H^+]_{vac}}{[H^+]_{cyt}} - F * \Delta\Psi = 0$ **Mass conservation law :** $[\text{Fructose}]_{vac} * V_{vac} + [\text{Fructose}]_{cyt} * V_{\text{cyt}} = [\text{Fructose}]_{\text{tissue}} * V_{cell} * density$	$[Fructose]_{\text{vac}} = \frac{[Fructose]_{\text{tissue}}}{\left(\frac{10^{-pH_{vac}}}{10^{-pH_{cyt}}} * exp\left(\text{F} * \frac{\Delta\Psi}{R * T}\right)\right) * \frac{V_{\text{vac}}}{V_{cell}} + \frac{V_{cyt}}{V_{cell}}}$ $[Fructose]_{cyt} = \frac{[Fructose]_{\text{tissue}}}{\frac{V_{\text{vac}}}{V_{cell}} + \frac{\frac{V_{cyt}}{V_{cell}}}{\left(\frac{10^{-pH_{vac}}}{10^{-pH_{cyt}}} * exp\left(\text{F} * \frac{\Delta\Psi}{R * T}\right)\right)}}$
Sucrose **Transport mechanism: H⁺-coupled antiporter** **Carrier at equilibrium:** $R * T * \ln\frac{[\text{Glucose}]_{vac}}{[\text{Glucose}]]_{cyt}} - R * T * \ln\frac{[H^+]_{vac}}{[H^+]_{cyt}} - F * \Delta\Psi = 0$ **Mass conservation law :** $[\text{Glucose}]_{vac} * V_v + [\text{Glucose}]_{cyt} * V_c = [\text{Glucose}]_{\text{tissue}} * V_{cell} * density$	$[Sucrose]_{vacuole} = \frac{[Sucrose]_{\text{tissue}}}{\left(\frac{10^{-pH_{vac}}}{10^{-pH_{cyt}}} * exp\left(\text{F} * \frac{\Delta\Psi}{R * T}\right)\right) * \frac{V_{\text{vac}}}{V_{cell}} + \frac{V_{cyt}}{V_{cell}}}$ $[Sucrose]_{cyt} = \frac{[Sucrose]_{\text{tissue}}}{\frac{V_{\text{vac}}}{V_{cell}} + \frac{\frac{V_{cyt}}{V_{cell}}}{\left(\frac{10^{-pH_{vac}}}{10^{-pH_{cyt}}} * exp\left(\text{F} * \frac{\Delta\Psi}{R * T}\right)\right)}}$

Table S6: Equations used for the calculation of score and electroneutrality during the constraint-based optimization of only ΔΨ during the initial parametrization (equation "$Score_{initial\ parametrization}$" and ΔΨ together with the abundance of ionic complexes in the vacuole and cytoplasm in a second time (equation "$Score_{ionic\ complex}$"). K_{sp} of different ionic complexes used in the score equation are listed in Table S1.

$Score_{\ initial\ parameters}$	$10 * \left(\frac{Electroneutrality_{cyt}}{[Charges_{cyt}]}\right)^2 + 10 * \left(\frac{Electroneutrality_{vac}}{[Charges_{vac}]}\right)^2$
$Score_{\ ionic\ complex}$	$10 * \left(\frac{Electroneutrality_{cyt}}{[Charges_{cyt}]}\right)^2 + 10 * \left(\frac{Electroneutrality_{vac}}{[Charges_{vac}]}\right)^2 + \left(\frac{[SP_{CaMalate_{cyt}}] - K_{SP_{CaMalate}}}{K_{SP_{CaMalate\ vac}}}\right)^2 + \left(\frac{[SP_{CaMalate_{vac}}] - K_{SP_{CaMalate}}}{K_{SP_{CaMalate}}}\right)^2 + \left(\frac{[SP_{CaPO_{4cyt}}] - K_{SP_{CaPO4}}}{K_{SP_{CaPO_4}}}\right)^2 + \left(\frac{[SP_{CaPO_{4vac}}] - K_{SP_{CaPO_4}}}{K_{SP_{CaPO_4}}}\right)^2 + \left(\frac{[SP_{MgPO_{4cyt}}] - K_{SP_{MgPO_4}}}{K_{SP_{MgPO_4}}}\right)^2 + \left(\frac{[SP_{MgPO_{4vac}}] - K_{SP_{MgPO_4}}}{K_{SP_{MgPO_4}}}\right)^2 + \left(\frac{[SP_{MgNH_4PO_{4cyt}}] - K_{SP_{MgNH_4PO_4}}}{K_{SP_{MgNH_4PO_4}}}\right)^2 + \left(\frac{[SP_{MgNH_4PO_{4vac}}] - K_{SP_{MgNH_4PO_4}}}{K_{SP_{MgNH4PO4}}}\right)^2 + \left(\frac{[SP_{CaSO4cyt}] - K_{SP_{CaSO_4}}}{K_{SP_{CaSO_4}}}\right)^2 + \left(\frac{[SP_{CaSO_{4vac}}] - K_{SP_{CaSO_4}}}{K_{SP_{CaSO_4}}}\right)^2 + \left(\frac{[SP_{CaHPO_{4cyt}}] - K_{SP_{CaHPO_4}}}{K_{SP_{CaHPO_4}}}\right)^2 + \left(\frac{[SP_{CaHPO_{4vac}}] - K_{SP_{CaHPO_4}}}{K_{SP_{CaHPO4}}}\right)^2 + \left(\frac{[SP_{CaCitrate_{cyto}}] - K_{SP_{CaCitrate}}}{K_{SP_{CaCitrate}}}\right)^2 + \left(\frac{[SP_{CaCitrate_{vac}}] - K_{SP_{CaCitrate}}}{K_{SP_{CaCitrate}}}\right)^2$
$Electroneutrality_{vac}$	$(-1) * [H_3PO_4^-]_{vac} + (-2) * [HPO_4^{-2}]_{vac} + (-3) * [PO_4^{-3}]_{vac} + (-1) * [Citrate^-]_{vac} + (-2) * [Citrate^{-2}]_{vac} + (-3) * [Citrate^{-3}]_{vac} + (-1) * [Malate^-]_{vac} + (-2) * [Malate^{-2}]_{vac} + (1) * [K^+]_{vac} + (2) * [Na^+]_{vac} + (2) * [Ca^{2+}]_{vac} + (2) * [Mg^{2+}]_{vac} + (1) * [NH_4^+]_{vac} + (-2) * [SO_4^{2-}]_{vac} + (-1) * [Cl^-]_{vac} + (-1) * [NO_3^-]_{vac}$
$Electroneutrality_{cyt}$	$(-1) * [H_3PO_4^-]_{cyt} + (-2) * [HPO_4^{-2}]_{cyt} + (-3) * [PO_4^{-3}]_{cyt} + (-1) * [Citrate^-]_{cyt} + (-2) * [Citrate^{-2}]_{cyt} + (-3) * [Citrate^{-3}]_{cyt} + (-1) * [Malate^-]_{cyt} + (-2) * [Malate^{-2}]_{cyt} + (1) * [K^+]_{cyt} + (2) * [Na^+]_{cyt} + (2) * [Ca^{2+}]_{cyt} + (2) * [Mg^{2+}]_{cyt} + (1) * [NH_4^+]_{cyt} + (-2) * [SO_4^{2-}]_{cyt} + (-1) * [Cl^-]_{cyt} + (-1) * [NO_3^-]_{cyt}$

Table S7: Equations used for the calculation of vacuolar and cytoplasm osmolarity.

$Osmolarity_{vac}$	$[H_3PO_4^{-}]_{vac} + [HPO_4^{-2}]_{vac} + [PO_4^{-3}]_{vac} + [\text{Citrate}^{-}]_{vac} + [\text{Citrate}^{-2}]_{vac} + [\text{Citrate}^{-3}]_{vac} + [\text{Malate}^{-}]_{vac} + * [\text{Malate}^{-2}]_{vac} + [K^{+}]_{vac} + [Na^{+}]_{vac} + [Ca^{2+}]_{vac} + [Mg^{2+}]_{vac} + [NH_4^{+}]_{vac} + [SO_4^{2-}]_{vac} + [Cl^{-}]_{vac} + [NO_3^{-}]_{vac} + [\text{Glucose}]_{vac} + [\text{Fructose}]_{vac} + [\text{Sucrose}]_{vac}$
$Osmolarity_{\text{Cyt}}$	$[H_3PO_4^{-}]_{cyt} + [HPO_4^{-2}]_{cyt} + [PO_4^{-3}]_{cyt} + [\text{Citrate}^{-}]_{cyt} + [\text{Citrate}^{-2}]_{cyt} + [\text{Citrate}^{-3}]_{cyt} + [\text{Malate}^{-}]_{cyt} + [\text{Malate}^{-2}]_{cyt} + [K^{+}]_{cyt} + [Na^{+}]_{cyt} + [Ca^{2+}]_{cyt} + [Mg^{2+}]_{cyt} + [NH_4^{+}]_{cyt} + [SO_4^{2-}]_{cyt} + [Cl^{-}]_{cyt} + [NO_3^{-}]_{cyt} + [\text{Glucose}]_{cyt} + [\text{Fructose}]_{cyt} + [\text{Sucrose}]_{cyt}$

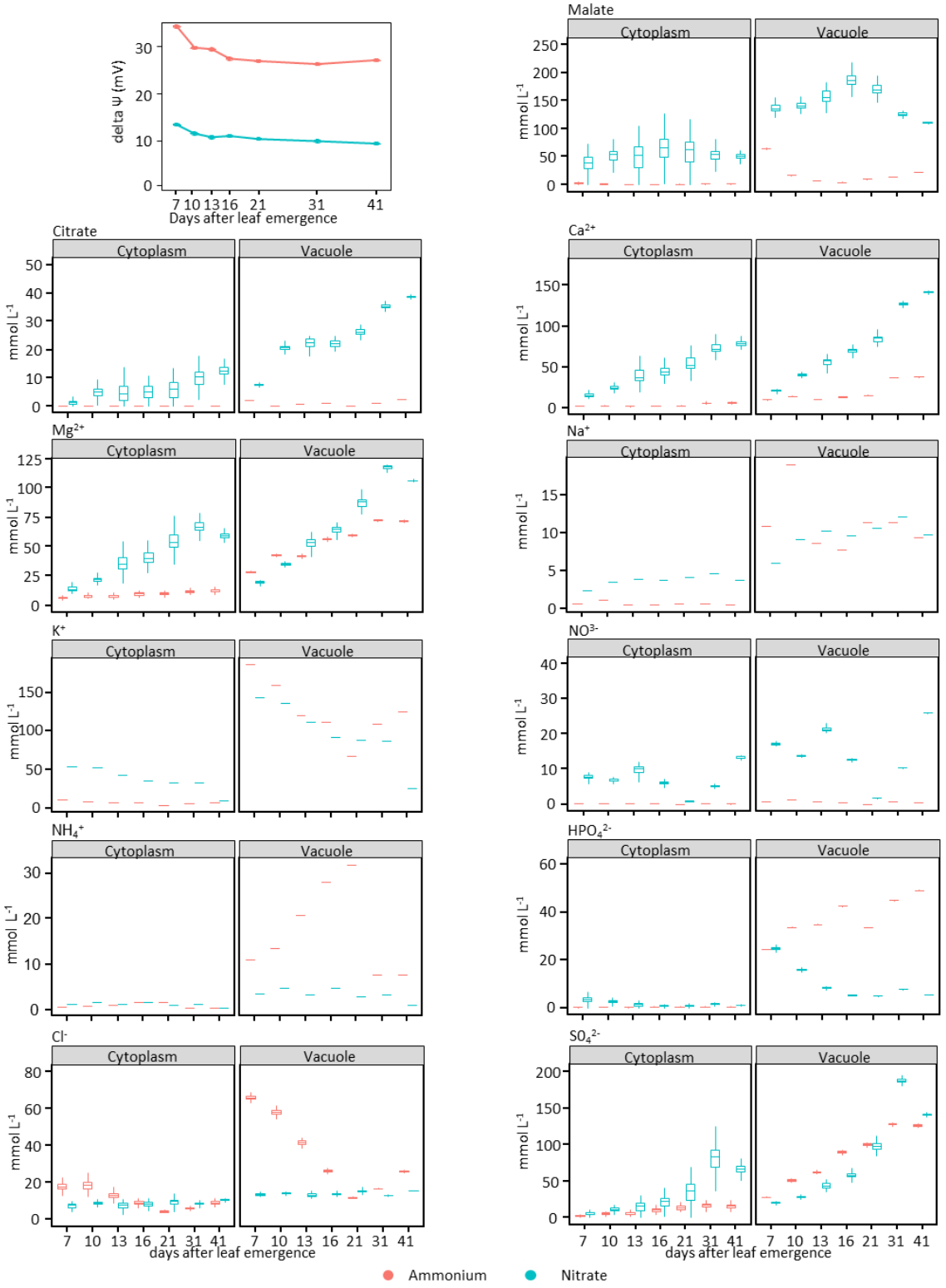

Figure S11: Predicted vacuolar and cytoplasmic concentration of organic and inorganic species throughout the development of the fourth leaf in tomato plants grown with ammonium (red) and nitrate (blue) as nitrogen source with the initial-parameterization of the model: without considering the formation of ionic complexes in vacuole and cytoplasm. For each treatment and at each developmental stage, ΔΨ was randomly searched by least square minimization and the 200 best scoring parameters were kept to calculate the subcellular concentrations of different species (see equations in table S2 to S3).

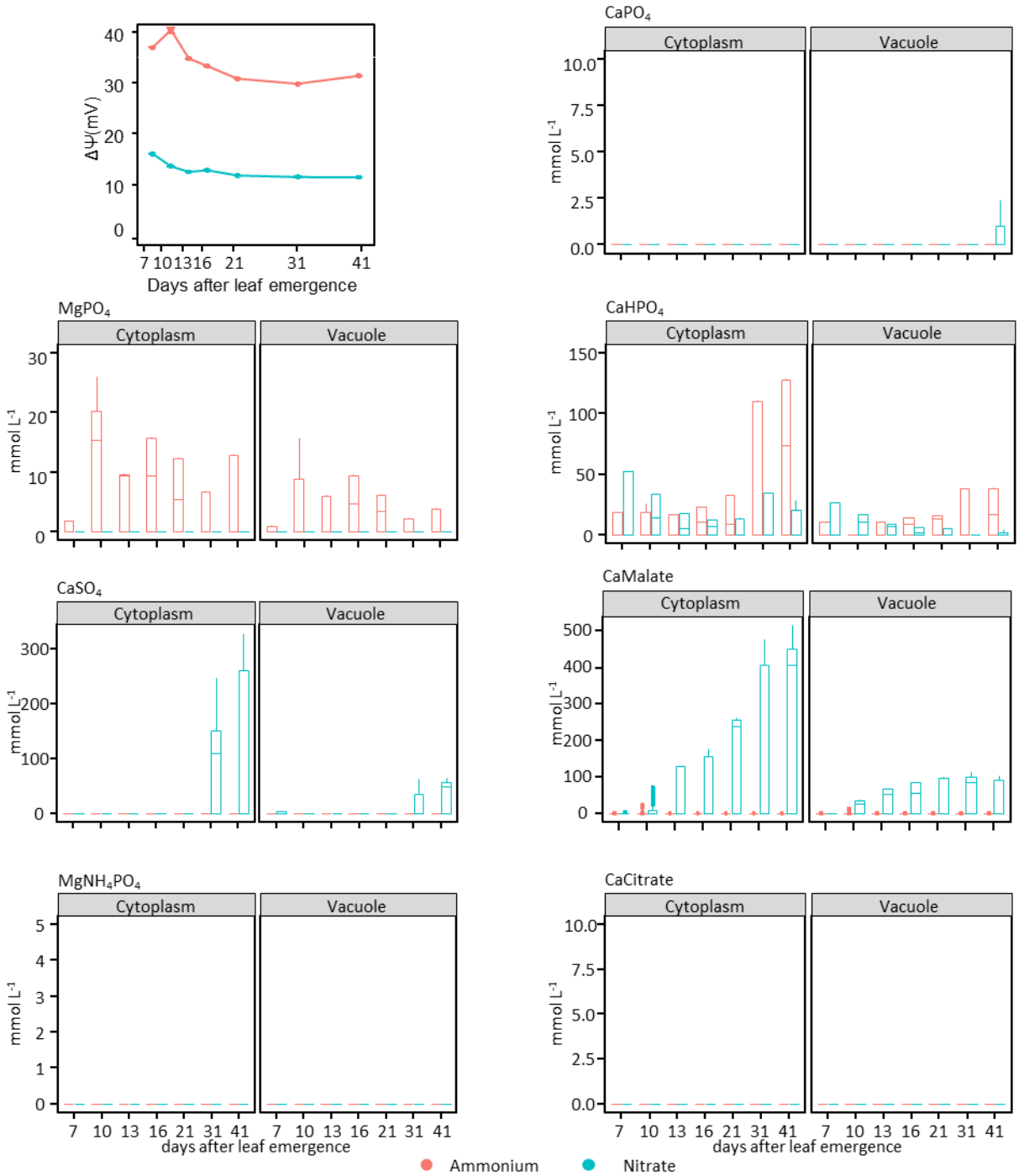

Figure S12 Predicted vacuolar and cytoplasmic concentration of ionic complexes throughout the development of the fourth leaf in tomato plants grown with ammonium (red) and nitrate (blue) as nitrogen source. ΔΨ and ionic complex concentrations were randomly searched by least square minimization with a parameterization allowing the formation of ionic complexes in both the vacuole and the cytosol. The parameterization of the model allowed the formation of ionic complexes in both the vacuole and the cytosol. se and median in ΔΨ graph and Box plots if complex concentrations show the 200 best scoring combinations of parameters obtained by randomized initial conditions.

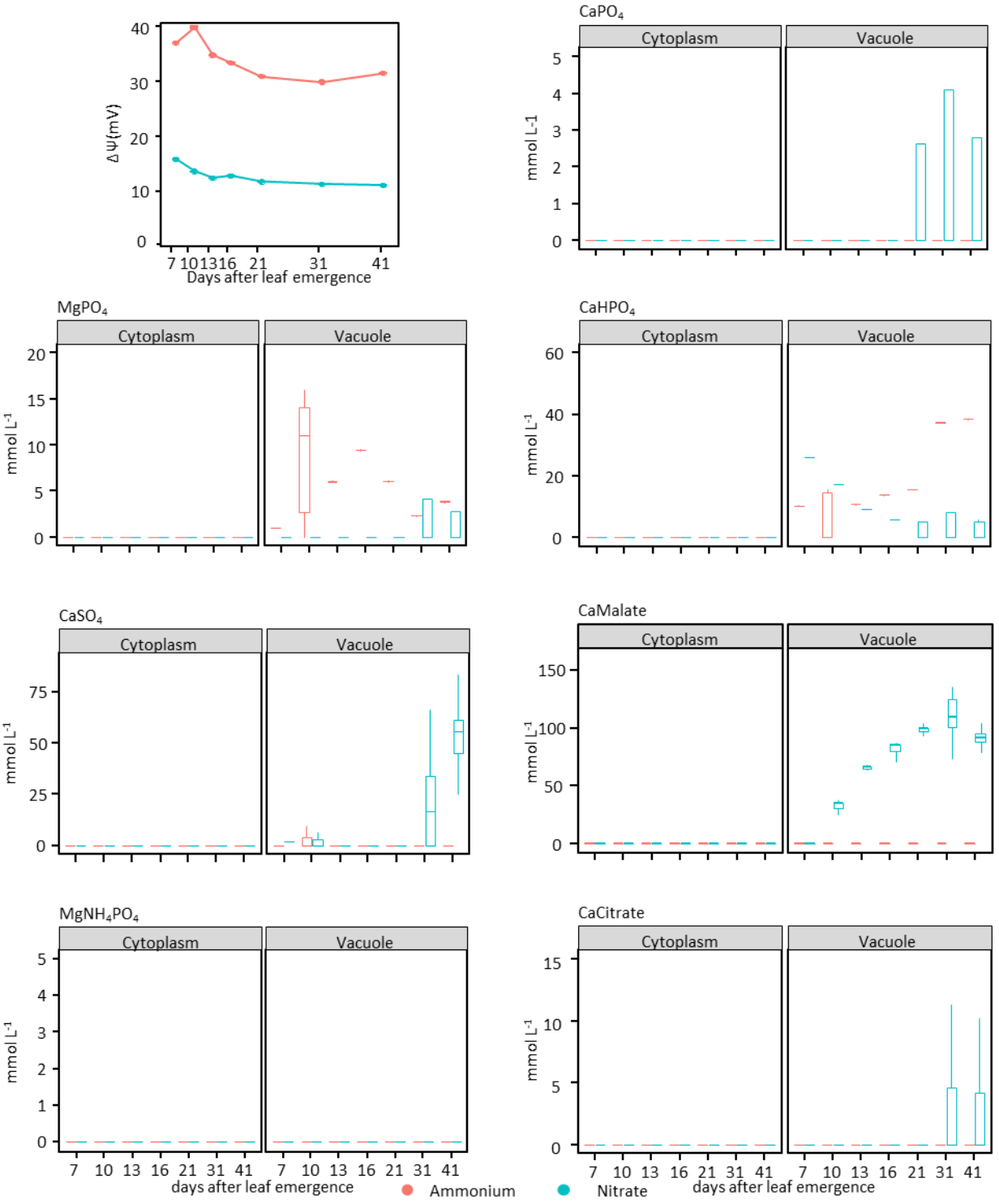

Figure S13: Predicted vacuolar and cytoplasmic concentration of ionic complex throughout the development of the fourth leaf in tomato plants grown with ammonium (red) and nitrate (blue) as nitrogen source. For this figure, the parameterization of the model determined the abundance of ionic complex exclusively in the vacuole. For each treatment and at each developmental stage, ΔΨ and ionic complex concentration values were randomly searched by least square minimization. Standard error and median in ΔΨ graph and Box plots show the 200 best scoring combinations of parameters obtained by randomized initial conditions.

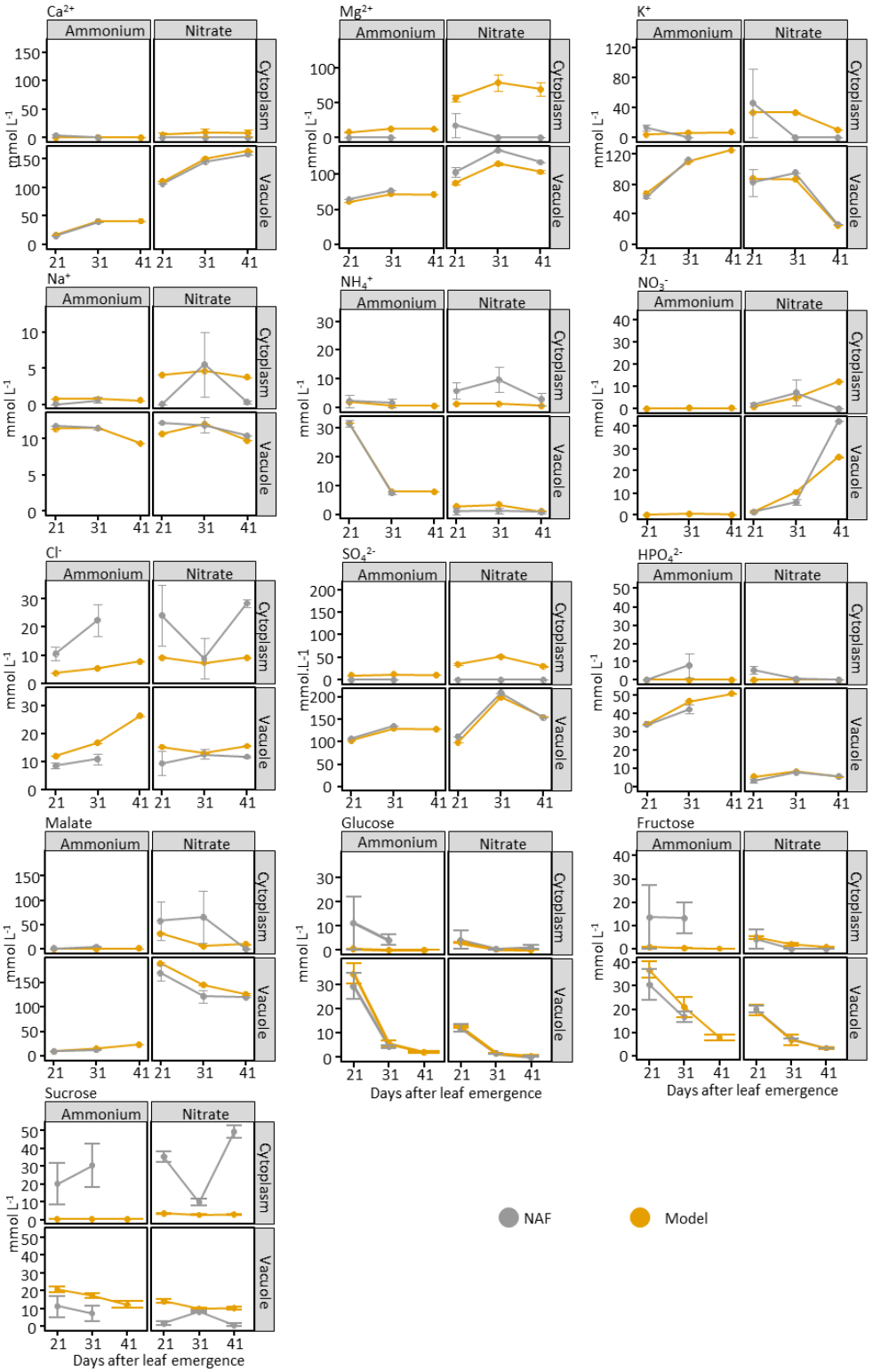

Figure S14: Comparison between predicted and experimentally measured subcellular concentrations of main metabolites and ions in the fourth leaf in tomato plants grown with ammonium and nitrate as nitrogen source. Predicted data (yellow) corresponds to the values obtained with the selected model parameterization, exclusively allowing ionic complex formation in the vacuole (as shown in Figure S11). Experimental data (grey) was obtained from non-aqueous fractionation (NAF) procedure (as shown in Table 1). Only data from leaves after 21 days are compared since NAF procedure was not optimal for younger leaves. Values represent the mean ± se (n = 3). Notice that NAF data for NH_4^+-fed leaf at 41 days are missing because of a technical problem with the procedure.

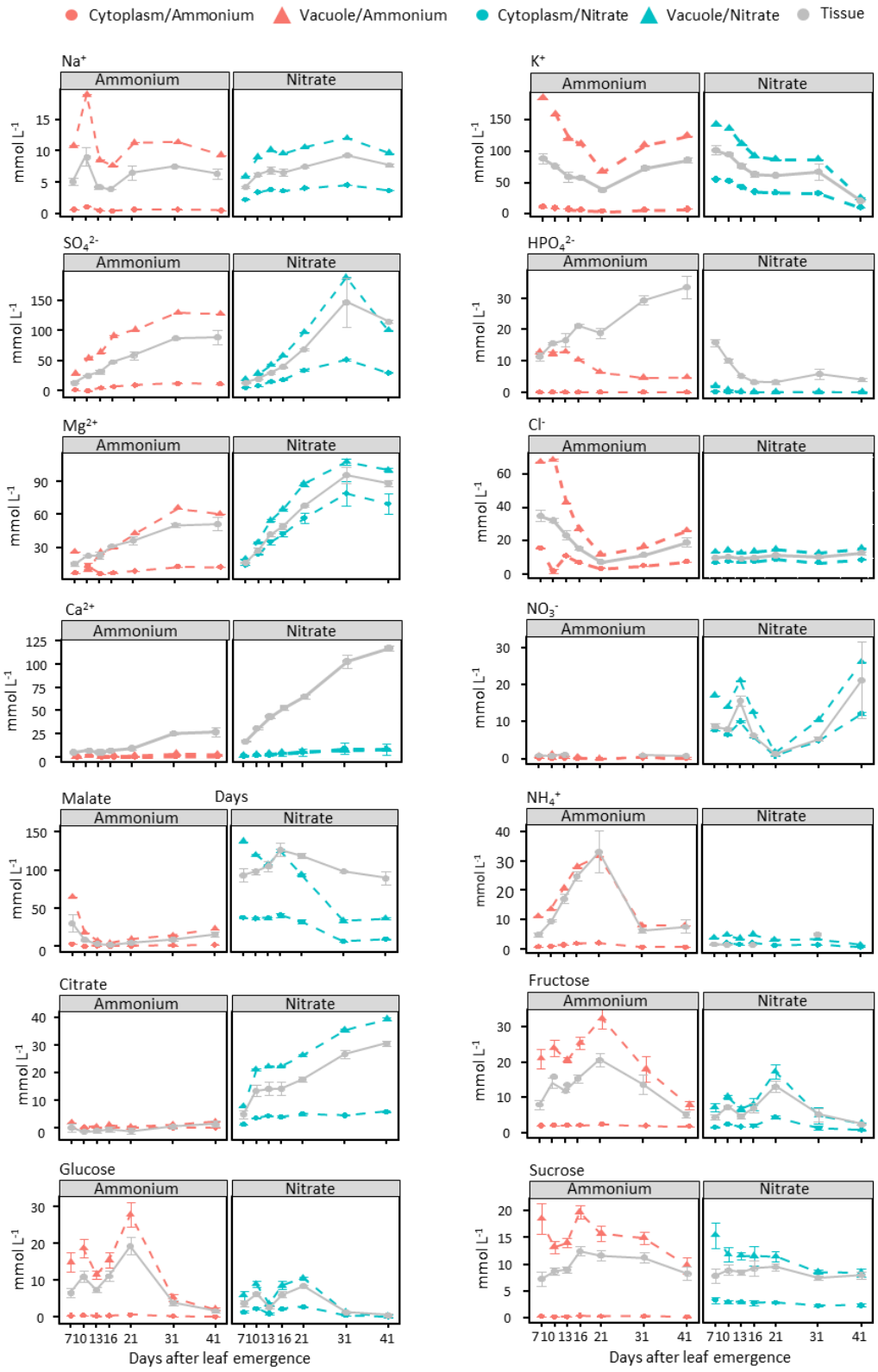

Figure S15: Time course evolution of vacuolar (triangle) and cytoplasmic (circle) concentration of metabolites and ions throughout the development of tomato leaf grown with ammonium (red) and nitrate (blue) as nitrogen source. Colored dots and dashed lines represent of the predicted concentration with the selected model parameterization, exclusively allowing ionic complex formation in the vacuole (data are shown in Figure S14). Values represent the median ±se of the 200 best scoring combinations of parameters obtained by randomized initial conditions. Continuous grey line represents the measured concentration in the bulk tissue expressed in mmol L^{-1} (cf Figure 4 and 5), values representing the mean ± se (n = 3).

Integrative discussion

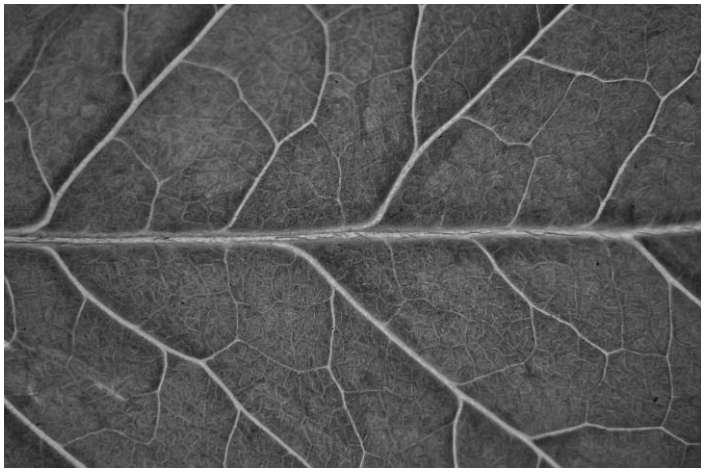

Macro tomato leaf photography, (GB photography, Archive Greenary)

INTEGRATIVE DISCUSSION

Defining a protocol for studying the metabolism of a developing leaf is always complex and it can be tackled with different experimental approaches. Both chapters in this thesis are focused in better understanding the effect of the nitrogen source provided (NH_4^+ or NO_3^-) on tomato leaf growth and development, with two complementary experimental designs. In chapter 1, we carried out the so-called vertical experimental design (V), where we aimed studying how the metabolism is adapted in function of the leaf position, meaning the developmental stage of the leaf in the vertical axis of the plant. Therefore, harvesting every leaf of the plant at a unique time point. In this chapter, plants were cultured under three N conditions: exclusive ammonium or nitrate provision and 50:50 ammonium: nitrate supply. In this chapter, we focused on whole leaf metabolic adaptation in function of its position in the plant. In parallel, in chapter 2, we performed the so-called horizontal experimental design (H), were a unique leaf at a single position (the 4^{th} leaf) was followed during its development during 41 days. Introducing the factor "time" in this experimental design, allows to calculate/estimate growth rates and fluxes. In this second chapter, we aimed reaching at a subcellular level focusing on vacuole metabolism. To do so, we used a combination subcellular metabolomics, cytology and mathematical modeling that allowed us estimating the subcellular concentrations of organic and inorganic compounds, and as an outcome, the energy cost of vacuole growth. Our results clearly show that the reduction in growth observed on ammonium could be explained by the higher energy cost that these plants require for vacuole and cell expansion.

Overall, highly consistent results were found regarding leaf metabolic adaptation to the available N-source in both V and H-experimental designs. For instance, in both experiments we observed a reorganization of carbon skeletons in line with the biochemical pH-stat theory to control cytosolic pH homeostasis. Accordingly, malic enzyme and phosphoenolpyruvate carboxylase activity were respectively enhanced and repressed under ammonium nutrition and agreed with malate concentration depletion. Another highly similar result between H and V-experiments was the NH_4^+ storage profile along the growth of the leaves under ammonium nutrition. Free NH_4^+ tends to accumulate during leaf expansion. Then, when leaf growth was less intense its assimilation increased as also did the protein content. Overall, suggesting a

trade-off between NH_4^+ assimilation and leaf growth in plants cultured under ammonium nutrition.

Among others, the comparison of both experimental designs arises the question whether the response of leaves of similar age is different in function of its position in the plant. In other words: Is the age more determining than the position for leaf response to ammonium nutrition?

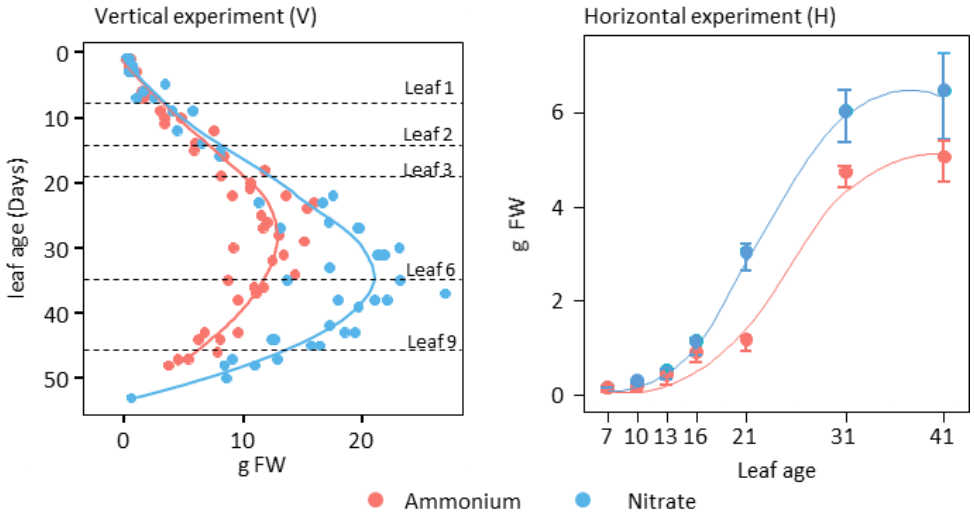

Figure 1: Visualization of tomato leaf biomass depending of their age in vertical (chapter 1) and horizontal experiment (chapter 2) when grown with ammonium (red), and nitrate (blue) as nitrogen source. Continuous lines correspond to locally estimated scatterplot smoothing (LOESS) curve of data from different treatment.

For both experiment the age of leaves was monitored by tagging them at their appearance, considering a 7-day old leaf when the size of the terminal leaflet was 3 cm (Figure 1). For H-experiment, the age of the harvested fourth leaf was harvested at 7, 10, 13, 16, 21, 31 and 41 days. For V-experiment, instead of reporting the data in function of the leaf position, as performed in chapter 1, in this integrative discussion we referred data to the leaf age. Therefore, independently of the nitrogen nutrition, leaf position 1,2,3,6 and 9 in V-experiment corresponded in average to 9, 14, 20, 34 and 45 day-old leaves, respectively. It is worth stressing that the age of the leaves studied in H and V-experiments was similar. Although the plant age was different when harvesting the leaves in both experiments, the comparison of the data sets from H and V-experiments is highly relevant since growth

conditions were exactly the same. Indeed, plants for both experiments grew at the same time in a greenhouse during spring/summer 2017.

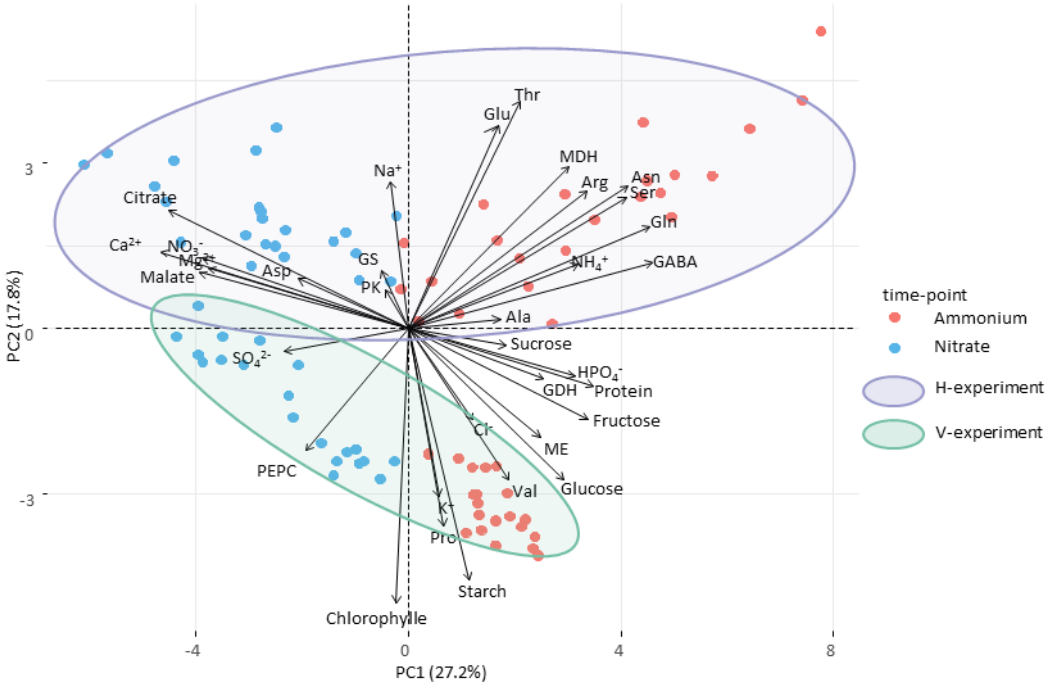

Figure 2: Analogy of horizontal and vertical experiment data set visualized by Principal component analysis (PCA) of metabolites, ions and enzymatic activities determined in leaves of tomato plants grown with ammonium and nitrate as nitrogen source. Red and blue colored points correspond to individuals that received A and N treatment respectively. Purple and green ellipses include individuals from H and V-experiment respectively. PCA was performed from the correlation matrix generated with 30 variables.

In order to have an integrative picture of the behavior of all metabolic parameters and inorganic compounds determined in both experiments, we carried out principal component analysis (PCA), thus determining the closest relationship among the different metabolic parameters. When considering treatments on the entire data set (Figure 2), the metabolic data clearly segregated the leaves of ammonium-fed plants (red dots) respect of the nitrate-fed ones (blue dots) along the first principal component (PC) that explained 27.2% or the variability. This is in agreement with previous PCAs reported in Chapter 1. In addition, the second PC (17.8%) separated leaves from H (purple ellipse) and V-experiments (green ellipse). To interpret those differences with a better resolution, data sets from each nutrition type were analyzed separately (Figure 3).

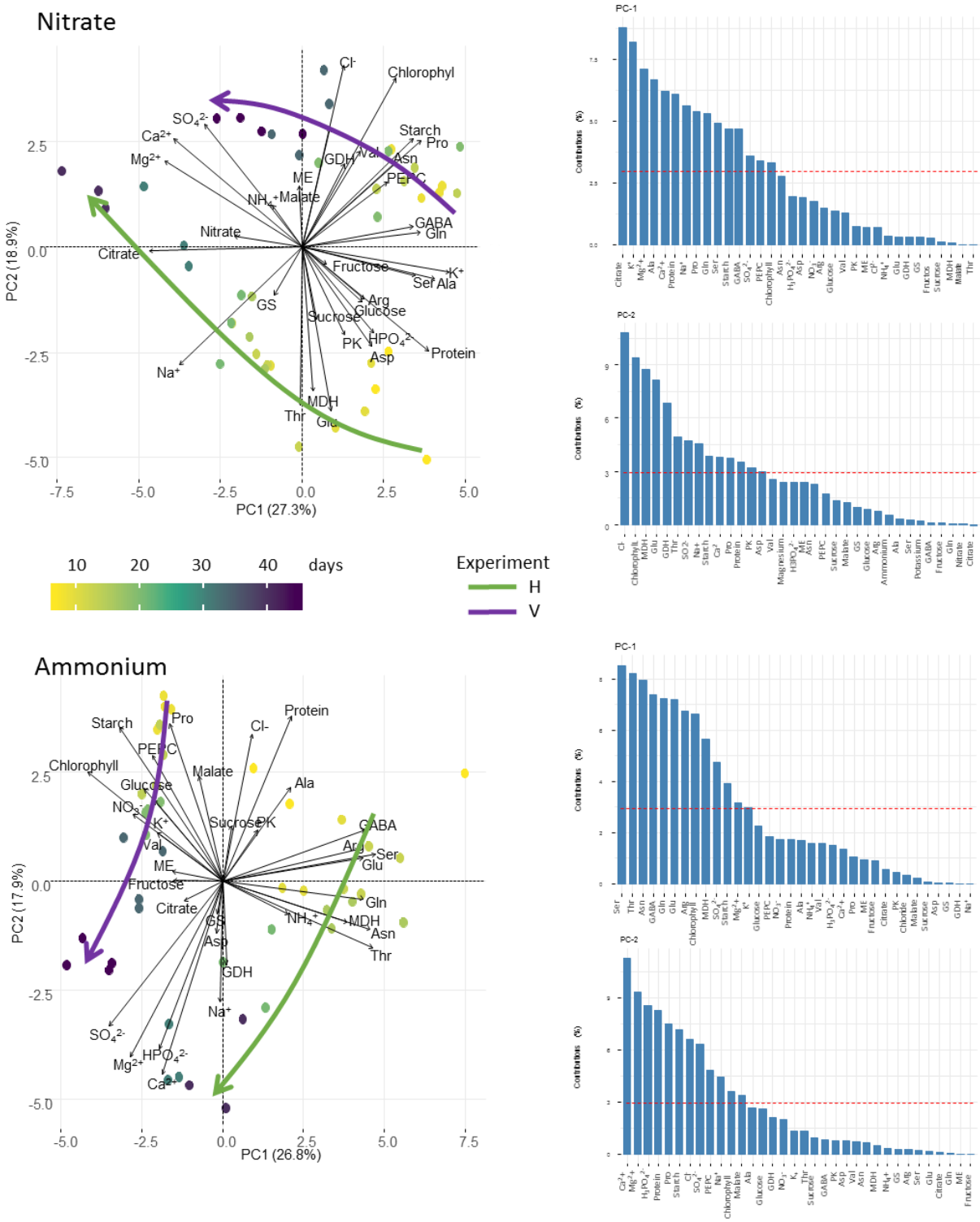

Figure 3: Principal component analysis (PCA) of horizontal and vertical experiment data set separated by nitrogen nutrition for metabolites, ions and enzymatic activities determined in leaves. Nitrate data set is. analyzed on the upper panel and Ammonium data set on the downer panel Purple and green arrows illustrate leaf aging direction of H and V-experiment respectively. The color code for leaf aging is as follow: yellow for young leaves of around 10 days, getting darker during leaf aging until dark blue at around 45 days. PCA was performed from the correlation matrix generated with 30 variables, for which the contributions to PC1 and PC2 are indicated in panels at the right.

As expected, the PCA analysis efficiently separated data from V and H-experiments under nutrition types. Interestingly, for each nutrition type, the metabolic differentiation of the leaves along the time followed similar trends despite of the experiment-related separation (as indicated by colored arrows in Figure 3). The first principal component, explaining the higher percentage of variance (27.3% for nitrate and 26.8% for ammonium nutrition), mostly associated to the age of leaves under nitrate treatment (Figure 3) whereas it separated V and H-experiments under ammonium nutrition (Figure 3). Accordingly, the second principal component, which explained smaller proportion of variance (18.9% for nitrate and 17.9% for ammonium nutrition), separated the different experimental designs in nitrate treatment (Figure 3) and leaf-age in ammonium treatment (Figure 3). These comparisons appear to suggest that the metabolic differences on ammonium nutrition depend in a higher extent on the leaf position, while on nitrate nutrition they depended more on the age of the leaf.

Note that starch content contributed to the differentiation of H and V-experiment in both treatments. In fact, despite the overall higher contents under ammonium supply in both experiments, the global trend in function of leaf age/position differed notably between experiments (see Figure 3, chapter 1 and Figure S2, chapter 2). Under ammonium nutrition, amino acids and hexoses to a lesser extend largely contributed to the divergence of H and V-experimental designs. Indeed, Arg, Ser, Glu, Gln, Asn and GABA were mainly accumulated in young leaves on H-experiment contrasting with an accumulation in mature leaves on V-experiment (See Figure 4 and S3, chapter 1; Figure S4 chapter 2).

Regarding inorganic ions, some of the most abundant ones were related to the leaf development. $Ca^{2+,}$ Mg^{2+}, SO_4^{2-}, HPO_4^{2-} were accumulated progressively in leaf cells with a treatment-dependent intensity. Regarding, NH_4^+ and K^+, they were negatively correlated in the two experiments (see Figure S2 chapter 1 and Figure S5 chapter 2), which indicates that the increase in the content of K^+ in the leaf is associated with the decrease in the concentration of NH_4^+. This negative correlation probably reflects the competition between the absorption of NH_4^+ and K^+ described in the literature (Hoopen *et al*., 2010).

Protein content strongly participated in the differentiation of the leaf developmental stages in both treatments but did not contribute in separating H and V-experiments. This means that the position of the leaf only had a small impact on the protein content. Moreover, we already mentioned that the evolution of proteins was strongly correlated with the rate of leaf

expansion (RGR) (Figure S5, chapter 2), in agreement with similar results obtained in winter rapeseed (Liu *et al.*, 2018). Consequently, protein content remains a decisive parameter for programmed cellular expansion in leaf tissue.

Finally, deciphering leaf metabolic adaptations associated with its development is complex since many parallel parameters have to be considered, such as the appearance of the leaf on a more or less matured plant or the relationship existing between sink and source organs. Indeed, the comparative analysis of results obtained in both chapters (H and V-experiments) showed a clear segregation of leaves of similar age but different positions in the plant. This was particularly true when tomato plant suffered an ammonium stress, because of differential accumulation of amino acids and sugars between experiments. By contrast, the behavior of most inorganic ions and protein content was mostly time dependent in both ammonium and nitrate nutrition and thus, independent of the position of the leaf in the plant. Overall, this thesis underlines with two complementary experimental designs the importance of taking into account the leaf phenological state when studying nitrogen metabolism. Especially, it stresses that comparing young leaves provides poor information with respect to the by N-related metabolic changes. Altogether, this study paves the pathway for future works in understanding plant response to ammonium stress.

General conclusions

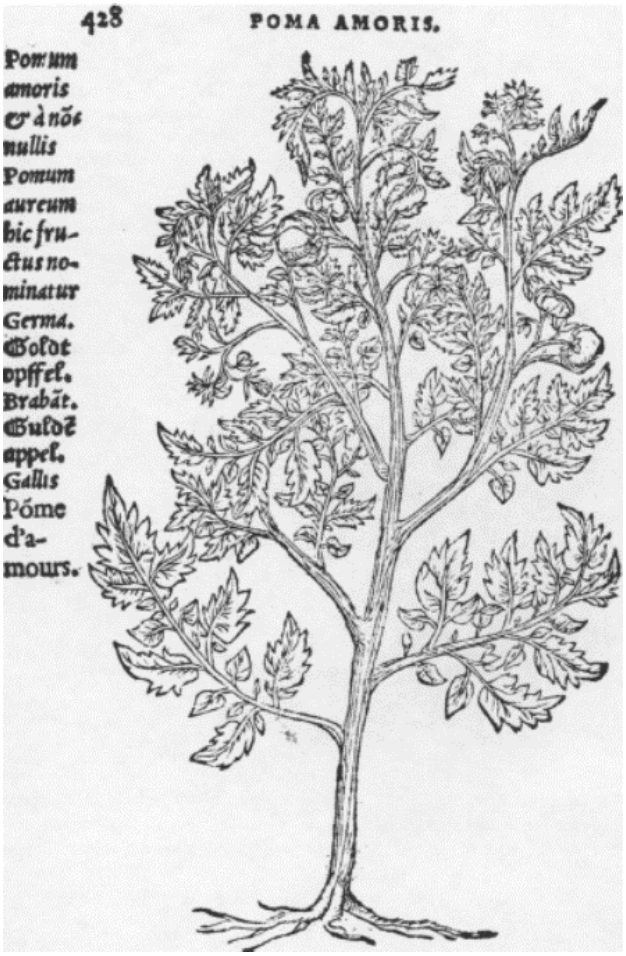

The first published illustration of tomato, *Solanum lycopersicum* from Dodoens (1554) (see Peralta *et al.*, 2008).

GENERAL CONCLUSIONS

1) C and N metabolic adjustment in function of the nitrogen source was more intense in older leaves compared to younger ones. We proposed a trade-off between NH_4^+ accumulation and assimilation to preserve young leaves from the ammonium stress.

2) The biochemical pH-stat regulation would explain the impaired C management on NH_4^+-fed plants, which involves a high energy cost for building plant biomass under ammonium nutrition.

3) Ammonium nutrition induces a reduction of cell and vacuole expansion.

4) Long-term ammonium nutrition induces an acidification of the vacuole when compared with nitrate nutrition.

5) NAF procedure showed in late time points that the main inorganic and organic soluble species including free NH_4^+ were accumulated in the vacuole independently of the nutrition regime. Further, obtained NAF results were used to cross-validate a mathematical model to predict the subcellular concentrations of solutes along the whole leaf developmental series.

6) Constraint based-optimization of the model underlined the formation of vacuolar ionic complexes as a relevant mechanism to enhance the trapping of calcium and phosphate in both nutritions.

7) *In vivo* measurement and model predictions showed an increase of the electrochemical gradient across the tonoplast under ammonium nutrition that entailed a higher energy cost of the solute-driven vacuole expansion.

8) Model simulations highlighted that the metabolic response of ammonium fed-plants induces a reduction of net solute flux of malate into the vacuole, which finally impaired the cell expansion.

9) Overall, the need to maintain the cytosolic pH and NH_4^+ levels at a physiological level under ammonium nutrition entailed a pronounced intervention of the biochemical and biophysical pH-stat. It induced a metabolic restructuration with a high energy cost for biomass construction and vacuole expansion, which compromised the development of the plant.

Materials and methods

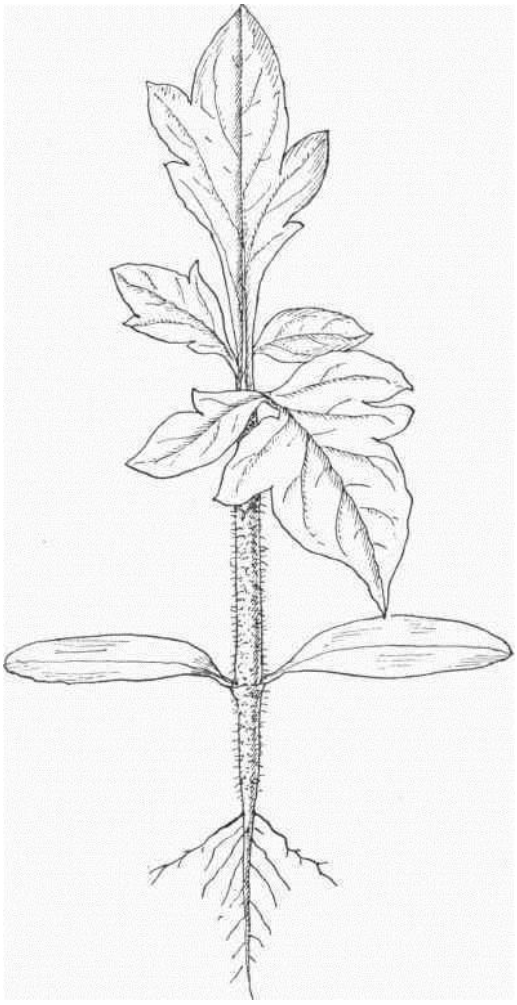

Draw of tomato seedling (From the book "Commercial Gardening ", by John Weathers (1913))

MATERIALS AND METHODS

1. Plant materials and growth conditions

Plant materials, growth conditions and the two experimental designs carried out during this work have been described exhaustively in chapter I and II in parts entitled “Growth conditions and experimental design”.

2. Metabolite extractions

Different extractions were performed accordingly to the biochemical properties of metabolites to be determined:

2.1. Ethanol extraction

20 mg of frozen leaf powder was extracted in 3 phases: 250 µL 80% ethanol, 10 mM HEPES/KOH, pH 6, vortexed, incubated at 80°C for 20 min, centrifuged 15000 *g* for 5 min at 4°C and supernatant recovered. The process was repeated firstly with 150 µL 80% ethanol, 10 mM HEPES/KOH, pH 6, and secondly with 250 µL of 50% ethanol in 10 mM HEPES/KOH, pH 6 (Hendriks *et al.*, 2003). The three supernatants recovered were pooled and used to determine the content of soluble sugars, chlorophyll and organic acids. The pellet was kept for starch and protein content quantification.

2.2. Ethanol extraction for LC-MS analysis

Aliquots of fractions obtained after performing the non-aqueous fractionation (see section 7.2.5) were extracted in 3 phases: plant material was homogenized with 250 µL ethanol 80%, 0.1% formic acid, pH 5, incubated at 80°C for 20 min, vortexed, centrifuged at 15000 *g* for 5 min at 4°C and supernatant recovered. The process was replicated twice with 150 µL ethanol 80%, 0.1% formic acid pH 5 and 250 µL ethanol 50%, 0.1% formic acid pH 5. The supernatants recovered from the 3 phases were pooled and used for LC-MS analysis.

2.3. Water extraction

20 mg of frozen leaf powder was extracted by adding 1 mL milli-Q water, homogenized at 27 Hz for 1 min using a mixer mill (MM400 Retsch), heated at 80 °C for 5 min and centrifuged at 13200 *g* for 20 min at 4°C.Supernatant was recovered and filtered through a 0.22 µm PVDF membrane filters.

3 Biochemical determinations

3.1. Chlorophyll

Immediately after ethanol extraction 50 µL supernatant was mixed with 120 µL 98% ethanol and the absorbance of the mixture was read at 645 and 665 nm in a 96-well microplate reader (SAFAS MP96). Total chlorophyll content was calculated using the following formulas adapted from (Arnon, 1949) to the total volume used (170 µL per well) in the microplate reader:

$$Chl_a\ (\mu g\ well^{-1}) = 5.21A_{665} - 2.07\ A_{645}$$

$$Chl_b\ (\mu\gamma\ well^{-1}) = 9.29A_{645} - 2.74\ A_{665}$$

$$Chl_{total} = Chl_a + Chl_b$$

Chlorophyll content was expressed as µg g^{-1} FW

3.2. Citrate

To determine citrate content 10 µL aliquots of ethanolic extracts were mixed with 100 µL assay mix (Tompkins and Toffaletti, 1982).

Assay mix:

5.00	µL	1 M Tricine/KOH, pH 8
1.00	µL	50 mM NADH in NaOH 50mM
0.05	µL	200 mM $ZnSO_4$
0.15	µL	Malate dehydrogenase (1000 U ml^{-1} in Tricine/KOH 100 mM, pH 9)
93.8	µL	H_2O

After reading the absorbance at 340 nm for 10 min in a 96 well microplate reader (SAFAS MP96), 1 µL of citrate lyase 0.014 U mL^{-1} was added and the OD was read until reaction stabilized. The ΔOD after the addition of citrate lyase was used for the calculation of citrate content according to the following equation NADH (µmol.$well^{-1}$) = ΔOD * $(2.85*6.22)^{-1}$.

3.3. Malate

To determine malate content, 20 µl of aliquots of ethanolic extract were mixed with 80 µl assay mix (Nunes-nesi *et al.*, 2007).

Assay mix

10	µL	1 M Tricine/KOH, pH 9
10	µL	10 mM MTT
5	µL	2.5 mM Phenazine ethosulfate 2.5 mM
10	µL	30 mM NAD^+
5	µL	10% Triton X-100 (v/v)
40	µL	H_2O

After reading the absorbance at 570 nm for 15 min in a 96 well microplate reader (SAFAS MP96), 1 µL of malate dehydrogenase 1000 U mL^{-1} in 100 mM Tricine/KOH pH 9 was added and the OD was read until curve reaction stabilized. The ΔOD due to the addition of malate dehydrogenase was determined for the calculation of malate content, according to the following equation NADH (µmol $well^{-1}$) = ΔOD * $(2.85*6.22)^{-1}$ (Nunes-nesi *et al.*, 2007).

3.4. Soluble sugars: glucose, fructose and sucrose

Glucose, fructose and sucrose content were determined as described by (Stitt *et al.*, 1989). Aliquots of 30 µl of ethanolic extraction were mixed with 160 µl of assay mix.

Assay mix:

150	µL	3 mM Hepes/KOH pH 9
4.64	µL	100 mM ATP
4.64	µL	45 mM $NADP^+$
0.8	µL	Glucose-6-phosphate dehydrogenase 700 U mL^{-1} (G6PDH grade I)

Plates were incubated at 37°C in a 96 well microplate reader (SAFAS MP96) and NADPH evolution was monitored at 340 nm until OD was stabilized (OD1), and then successively adding the following enzymes:

1) 1 µL Hexokinase (900 U mL^{-1} solution in 0.1 M HEPES/KOH, 0.3 mM $MgCl_2$, pH 7)
   Waiting until OD stabilized (OD2), and then add
2) 1 µl Phosphoglucose isomerase (1000 U mL^{-1} in 0.1 M Hepes/KOH, 0.3 mM $MgCl_2$, pH 7)
   Waiting until OD stabilized (OD3), and add
3) 1 µl acid invertase (300 mg prepared in 3 mL 0.1 M Hepes/KOH, 0.3 mM $MgCl_2$, pH 7)
   Waiting until OD stabilized (OD4).

For glucose determination, ΔDO_1 due to the addition of the hexokinase (ΔDO_1 = OD2-OD1) was considered.

For fructose determination, ΔDO due to the addition of phosphoglucose isomerase was considered (ΔDO_2 = OD3-OD2).

For sucrose determination, ΔDO due to the addition of invertase was considered (ΔDO_3 = OD4-OD3).

The respective ΔDOs were transformed according to the equation NADH (µmol $well^{-1}$) = ΔOD * $(2.85*6.22)^{-1}$ in glucose equivalents and sugar content finally was expressed as µmol glucose eq g FW^{-1}.

3.5. Starch and protein

Starch (Hendriks *et al.* 2003) and proteins (Bradford, 1976) were determined from the pellet of the ethanol extraction using 400 µL 0.1 M NaOH and heating at 95°C for 30 min as described by. After centrifuging at 2500 g for 5 min, the content of soluble protein was measured as described by Bradford (1976). To do so, 3 µl of the pellet extraction was mixed with 180 µl Bradford ready to use (Bio-Rad). Calibration curve was performed with bovine serum albumin standard (0-80-160-230-640 $\mu g.mL^{-1}$ in 0.1 M NaOH). Plates were incubated for 5 min at room temperature and ODs determined at 595 nm in a 96-well microplate reader (SAFAS MP96).

To determine starch content the re-suspended pellet was acidified to pH 4.9 with 80 µl 0.5 M HCl / 0.1 M sodium-acetate, pH 4.9, mixed and the suspension was digested overnight at 37°C with 100 µL of starch degradation buffer (1.5 mL 140 U.ml-1 amyloglucosidase and 15 µL 10000 $u.mL^{-1}$ α-amylase in 12.5 mL 50 mM acetate buffer for 1 microplate). The glucose content of the supernatant was determined as explained above.

3.6. Total carbon and nitrogen

Nitrogen and carbon contents were determined by combustion of plant dry material with an elemental analyser Flash EA1112 (Thermo Fisher Scientific Inc., Waltham, MA, USA).

3.7. Inorganic ions

Aliquots of water extraction were used for soluble anion and cation quantification by ion chromatography (DIONEX ICS-5000, Thermo Scientific). The ion separation was carried out with two different ion-exchange columns:

- Anions were separated on a Dionex IonPac AS19-4 µm protected by a Guarda Dionex IonPac AG19-4 µm.
- Cations were determined using Dionex IonPac CS16-4 µm equipped with Dionex IonPac CS16-4 µm guard column (50-4 mm i.d.).

The electric currents applied were 28 mA and 50 mA to the conductivity suppressors, AERS 500 2 mm for the anions and Dionex CERS-500 4 mm for the cations, respectively. The injection volume was 2.5 µL for both cation and anion. Eluents were prepared daily using Dionex EGC 500 KOH with Dionex CR-ATC 500 column Anion Trap for anions and methanosulfonic acid 30 mM for cations. The flow rates were 0.25 mL min^{-1} for anions and 0.16 mL min^{-1} for cations.

4. Osmotic potential determination

20 mg of frozen leaf powder was homogenized with 150 µL deionised water, vortexed for 20 seconds and homogenates were centrifuged at 15000 g for 10 min. Leaf osmolarity (mOsmol kg^{-1} H_2O) was measured in the supernatants with a Micro-Osmometer Type 13/13DR (Roebling), based on the colligative property of freezing-point depression. Every 10 samples a calibration was performed with deionised water and a certified solution of 300 mOsmol kg^{-1} H_2O.

5. Enzyme activities: extraction and quantification

5.1. Extraction of soluble enzymes

Aliquots of 20 mg of frozen plant material together with 20-30 mg polyvinylpyrrolidine (PVPP) were mixed vigorously with a vortex and then with a tissue lyser (RETSCH MM499) at 20 Hz for 2 min with 500 µL of extraction buffer (289.5 µl H2O, 100 µl glycerol, 50 µl pre-extraction buffer 10X, 50 µL 10 %Triton X-100, 2 mM leupeptin, 100 mM PMSF in isopropanol 100X, 0.5 µl 500 mM DTT). Homogenates were centrifuged at 4000 g for 50 min at 4°C and the supernatants kept for the determination of enzyme activities (Gibon *et al.*, 2004).

Pre-extraction buffer 10X:

500 mM	Hepes
100 mM	$MgCl_2$
10 mM	EDTA
10 mM	Benzamidine
10 mM	ε- Aminocaproic acid
2.5 %	BSA

5.2. Pyruvate kinase activity

To determine pyruvate kinase (PK, EC 2.7.1.40) activity, a 5 µL aliquot of enzymatic extract was mixed with 95 µL of assay mix (Gibon *et al.*, 2004).

Assay mix:

20 µL	Assay buffer 5X (0.5 M Tricine/KOH pH 8, 0.5M KCl, 50 mM $MgCl_2$, 2 mM EDTA, 0.25% Triton X-100)
10 µL	50 mM Phosphoenolpyruvate
5 µL	20 mM ADP
1 µL	50 mM NADH
1 µL	Lactate dehydrogenase 100 U mL^{-1} in 200 mM Tricine/KOH pH 8, 10 mM $MgCl_2$
58 µL	H_2O

The enzymatic reaction was monitored by NADH consumption at 340 nm during 20 min at 25 ºC within a 96-well microplate reader (SAFAS MP96). For blanks, phosphoenolpyruvate was substituted by water. The activity was expressed in µmol NADH g FW^{-1} min^{-1}.

5.3. Phosphoenolpyruvate carboxylase activity

Phosphoenolpyruvate carboxylase activity was determined using 5 µL of aliquot of enzymatic extract was mixed with 95 µL of assay mix (Gibon *et al.*, 2004).

Assay mix:

20 µL	Assay buffer 5X (0.5 M Tricine/KOH, pH 8, 100 mM $MgCl_2$, 50 mM $NaHCO_3$, 0.25%Triton X-100)
10 µL	Malate dehydrogenase 100 U mL^{-1} in Tricine/KOH 200 mM, pH 8, $MgCl_2$ 10 mM
4 µL	50 mM Phosphoenolpyruvate trisodium salt hydrate
1 µL	60 mM NADH in NaOH 60 mM
60 µL	H_2O

NADH evolution was monitored at 340 nm during 20 min at 25 °C within a 96-well microplate reader at room temperature (SAFAS MP96). For blanks, phosphoenolpyruvate was substituted by water in the assay mix (Bénard and Gibon, 2016). The activity was expressed in µmol NADH g FW^{-1} min^{-1}.

5.4. NADP-dependent malic enzyme activity

To determine NADP-dependent malate dehydrogenase (NADP-ME, EC 1.1.1.40) activity, 5 µL of aliquots of enzymatic extraction were mixed with 280 µL of assay mix (Holtum and Winter, 1982).

Assay mix:

28.0 µL	1 M TRIS-HCl, pH 7
2.8 µL	1 M $MgCl_2$
28.0 µL	5 mM NADP
2.6 µL	0.5 M Malate
215.0 µL	H_2O

NADH evolution was monitored at 340 nm during 20 min at 25 °C with a 96-well microplate reader (SAFAS MP96). For blanks, malate was substituted by water in the assay mix. The activity was expressed in µmol NADH g FW^{-1} min^{-1}.

5.5. NAD-dependent malate dehydrogenase activity

To determine NAD-dependent malate dehydrogenase (NAD-MDH, EC 1.1.1.37) activity a 5 µL aliquot of enzymatic extract diluted 16 times was mixed with 95 µL of assay mix (Gibon *et al.*, 2004).

Assay mix

20.0 µL	Assay buffer (0.5 mM Tricine-KOH pH 8, 0.25%, Triton X-100, 0.5 mM EDTA)
2.0 µL	60 mM NADH in 60 mM NaOH
22.5 µL	5 mM Oxaloacetate
50.5 µL	H_2O

NADH evolution was monitored at 340 nm during 20 min at 25 °C with a 96-well microplate reader (SAFAS MP96). For blanks, oxaloacetate was substituted by water in the assay mix. The activity was expressed in µmol NADH g FW^{-1} min^{-1}.

5.6. Glutamine synthetase

To determine glutamine synthetase (GS, EC 6.3.1.2) activity a 5 µL aliquot of enzymatic extract diluted 4 times was mixed with 95 µL of assay mix. For blanks, glutamate was substituted by water in the assay mix (Gibon *et al.*, 2004).

Assay mix

20.0 µL	Assay buffer 5X (0.5 M Hepes/KOH, pH 7.5, 100 mM $MgCl_2$, 2 mM $NaVO_3$, 20 mM NH_4Cl, 10 mM EDTA, 0.25%Triton X-100)
1 µL	60 mM NADH in 60 mM NaOH
5 µL	20 mM PEP
5 µL	100 mM ATP
10 µL	100% glycerol
2 µL	Pyruvate kinase 50 U mL^{-1} in Hepes/KOH 200 mM pH 7.5, 10 mM $MgCl_2$
1 µL	Lactate DH 60 U mL^{-1} in Hepes/KOH 200 mM pH 7.5, 10 mM $MgCl_2$
6 µL	H_2O
45 µL	100 mM glutamate

NADH evolution was monitored at 340 nm during 20 min at 25 °C with a 96-well microplate reader at room temperature (SAFAS MP96). For blanks, glutamate was substituted by water in the assay mix. The activity was expressed in µmol NADH g FW^{-1} min^{-1}.

5.7. Glutamate dehydrogenase activity

NAD-dependent glutamate dehydrogenase (NAD-GDH, EC1.4.1.2) activity was determined in the aminating sense using 2 µL of aliquot of enzymatic extract diluted 2 times, mixed with 18 µL of assay mix (Gibon *et al.*, 2004).

Assay mix

4.0	µL	Assay buffer 5X (0.5 M Tricine/KOH pH 8, 5 mM $CaCl_2$, 3.2 M NH_4Acetate, 0.25% Triton X-100).
2.0	µL	150 mM 2-Oxoglutarate disodium salt dihydrate
0.4	µL	5 mM NADH
11.6	µL	H_2O

After incubating at 25°C for 20 min, 20 µl 0.5 M HCl in 100 mM Tricine/KOH, pH 9 was added and incubated at 90°C for 10 min to stop the reaction. Then 20 µL 0.5 M NaOH were added. After being mixed 45 µL of determination mix were added and the evolution of reduced MTT (3(4,5-dimethylthiazol-2-yl)-2,5-diphenyltetrazolium bromide) was determined at 570 nm during 20 min at 25 ºC. The activity was expressed in µmol NADH g FW^{-1} min^{-1}.

Determination mix

10	µL	1 M Tricine/KOH, pH 9
10	µL	2 mM MTT (3(4,5-dimethylthiazol-2-yl)-2,5-diphenyltetrazolium bromide)
4	µL	200 mM EDTA
2	µL	50% Ethanol
1	µL	Alcohol dehydrogenase 2000 U mL^{-1} in 200 mM Tricine/KOH pH 9, 10 mM $MgCl_2$
5	µL	4 mM PES (Phenazine ethosulfate)
18	µL	H_2O

5.8. Hexokinase: fructokinase and glucokinase

To determine fructokinase (FK, EC 2.7.1.3) and glucokinase (GK, EC 2.7.1.1) activities, 2 µl aliquots of enzymatic extraction or standard (0, 20, 50, 100 µM glucose-6-phosphate or fructose-6-phosphate) were mixed with 18 µl of assay mix (Gibon *et al.*, 2004).

Assay mix:

4.0	µL	Assay buffer (0.5 M Tricine/KOH pH 8, 25 mM $MgCl_2$, Triton X-100 0.25%)
0.4	µL	100 mM ATP
0.5	µL	20 mM $NADP^+$
0.4	µL	50 U ml^{-1} Glucose-6-phosphate dehydrogenase (G6PDH grade II) in 200 mM Tricine/KOH pH 8, 10 mM $MgCl_2$.
0.2	µL	1 U mL^{-1} Phosphoglucoisomerase (only for fructokinase assay)
0.2	µL	2 mM Glucose (Glucokinase assay) or fructose (Fructokinase assay)
12.3	µL	H_2O

For blanks, ATP was substituted by water in the assay mix. After incubating at 25°C for 20 min, the reaction was stopped with 20 µL of NaOH 0.5 M, incubated at 95°C for 5 min. Then, 20 µL of 0.5 M HCl in 100 mM Tricine/KOH pH 9 was added. After being mixed, 45 µL of determination mix and 5 µL of 4 mM PES (Phenazine ethosulfate) were added. Reduced MTT (3(4,5-dimethylthiazol-2-yl)-2,5-diphenyltetrazolium bromide) was determined at 570 nm.

Determination mix

10.0	µL	1 M Tricine/KOH pH 9
10.0	µ	2 mM MTT (3(4,5-dimethylthiazol-2-yl)-2,5-diphenyltetrazolium bromide)
4.0	µL	200 mM EDTA
2.0	µL	250 mM Glucose-6-phosphate (G6P)
0.5	µL	5 U mL^{-1} Glucose-6-phosphate-dehydrogenase (G6PDH grade I)
18.5	µL	H_2O

5.9. Acid invertase

Acid invertase (EC.3.2.1.26) activity was determined using 5 µL of aliquots of enzymatic extraction mixed with 45 µL of assay mix.

Assay mix

10	µL	Assay buffer 5X (0.25 M Acetate/KOH pH 5, 100 mM Sucrose, Triton 0.15% X-100)
35	µL	H_2O

After incubating at 25°C for 20 min until stabilization, 30 µL 4 M imidazole was added and incubated at 98°C for 10 min to stop the reaction. Then 100 µL of assay mix was added

Determination mix

93	µL	1 M Hepes/KOH pH 7, 30 mM $MgCl_2$
1	µL	100 mM ATP
3	µL	20 mM $NADP^+$
1	µL	100 U mL^{-1} Glucose-6-phosphate-dehydrogenase (G6PDH) in 0.1 M Hepes/KOH, pH 7

NADPH evolution was followed at 340 nm until during 20 min at 25°C. Then, 1 µL of hexokinase and 1 µL of phosphoglucose isomerase (both at 100 U mL^{-1} in 0.1 M Hepes/KOH pH 7) was added and NADPH evolution was followed at 340 nm during 20 min at 25°C to determine the ΔDO. The activity was expressed in µmol NADPH g FW^{-1} min^{-1}.

6. Microscopy

6.1. Tissue fixation and embedding in Epon resin

Three leaves were collected at each growth stage (7, 10, 13, 16, 21 , 32 and 41 days after leaf emergence) and fragments (1- to 2-mm thick) of leaf blade were placed in 2.5% glutaraldehyde (v/v) in 0.1 M sodium phosphate buffer, pH 7.2, kept at 4°C on ice. During the first hour of fixation, an increasing vacuum (800 to 200 mbar) was applied by breaking the vacuum all 15 min. Samples were rinsed three times in phosphate buffer at 4°C and then treated with 1% tannic acid for 30 min under agitation. After three rinses with water, the samples were dehydrated by an acetone series:

Steps	Dehydration Medium	Time	Temperature
1	50% acetone	15 min	4°C
2	70% acetone	60 min	4°C
3	100% acetone	15 min	4°C
4	100% acetone	15 min	4°C
5	100% acetone	15 min	25°C
6	100% acetone	15 min	25°C

An Epon mixture (48.2% Agar 100 resin, 28.5% dodecenyl succinic anhydrate, 23.5% Methyl-5-Norbonine 2.3 dicarboxylic anhydride, 1% N-benzyldimethylamine) from EMBed-812 embedding kit (EMS, United States) was used for embedding. Samples were placed for 1 h in an acetone:Epon mixture (50:50, v/v) under agitation and then 4 h with the lid of tubes opened to allow acetone evaporation. Then, samples were transferred to pure Epon solution and incubated overnight at room temperature. Finally, fixed fragments were placed into silicon mold with fresh Epon solution and polymerization was performed at 70°C for 16 hours. Fixed sections were sliced (50 µm) with glass knives and stained with 0.04% (w/v) toluidine blue (Beauvoit *et al.*, 2014).

6.2. Image analysis and morphometric calculations

Sections were photographed using a Zeiss Axiophot microscope coupled with a Spot RTKE digital camera. Cell, vacuole, cytoplasm, chloroplast and cell wall areas were measured with the Image-J software using manual drawing. Further, the best ellipsis corresponding to the area measured was computed in order to provide ellipsis parameters: *a* being the semi-major axis and *b* the semi-mior axis. Volumes were calculated assuming that the cell and vacuole are prolate spheroids of radius *a*, *b*, and *c* (with $a > b = c$) (Beauvoit *et al.*, 2014). We assumed cell wall was homogenously distributed around the plasma membrane. To determine chloroplast volume, the averaged quantity of chloroplasts per cell type was determined and multiplied by the averaged individual chloroplast area that was then reported as volume. Finally, the cytoplasmic space was determined by calculating the difference between the total cell volume and the above calculated volumes for the vacuole, chloroplasts and cell wall. For each biological replicat, subcellular volumes were determined and averaged from 6 cells, three from palisade parenchyma and three from spongy parenchyma.

7. Non-aqueous subcellular fractionation (NAF)

7.1 NAF procedure

The following section comprises a step-by-step description of the non-aqueous fractionation protocol adapted from Fürtauer *et al.*, (2016) that provide useful schematic illustrations of the procedure.

Homogenization and preparation of leaf samples

1) Frozen leaves were ground to a fine powder using a tissue lyser MM400 (R) and stored at -80°C until further use.
2) Around 300 mg of leaf powder was freeze-dried and 30 mg of the remaining dried powder was used for fractionation.

Non-aqueous-fractionation

During all the following steps the material manipulation was always performed on ice and under the fume hood. Special attention was paid to prevent any water contamination of solvent and samples.

3) Lyophilised powder was suspended in approximately 7 mL of a pre-chilled heptane/tetra-chlorethylene mixture (ρ = 1.3 g cm^{-3}).
4) After manual homogenisation with a tissue grinder (Potter) to reduce the aggregated particles, glass vial was plugged and placed on ice-water filled ultrasonic bath for 7 min.
5) The sonicated suspension was filtered through a nylon mesh of 22-25-µm pore size into a 50 mL Falcon tube. Nylon mesh was further washed with pure heptane (ρ = 0.68 g cm^{-3}) and the volume of the remaining suspension was adjusted to 25 mL (ρ ± 0.68 g cm^{-3}).
6) 50 mL Falcon tubes were centrifuged at 4800 g for 10 min at 4°C.
7) . The pellet was resupended in 1 mL on pure tetrachlorethylene and transferred to a 2 mL reaction tube (Eppendorf).
8) Reaction tube was centrifuged with 24000 g at 4°C for 10 min.
9) Supernatant was transferred into a new reaction 2 mL tube and diluted with 112.36 µL pure heptane to reach the density of new gradient step (ρ = 1.48 g cm^{-3}).

10) In parallel, pellet was resuspended into 900 µL heptane/tetra-chlorethylene mixture according to the density of the corresponding fraction (here, ρ = 1.56 g cm^{-3}). After being greatly homogenized, the corresponding fraction **Fraction1** was aliquoted equally into four subfractions in 0.8 mL Micronic tubes. Subfractions were precipitated by adding 600 µL of pure heptane and centrifuged with 13100 *g* for 3 min at 4°C. Supernatant was removed and samples were dried in a vacuum concentrator (LaboGeneTM, Denmark) and stored at −20°C until use for further analysis.
11) The reaction tube from step 9 with the new density was centrifuged with 24000 *g* at 4°C for 10 min. Procedure as step 9 was repeated to obtain the **Fraction2**
12) Then, the same procedure as step 9 and step 10 was repeated twice. For **Fraction 3** and **Fraction 4**, the following density were respectively 1.42 and 1.36
13) The supernatant of the last fraction (**Fraction 5**) was transferred to a 15 mL reaction tube; volume was adjusted to 7 mL with pure heptane and centrifuged with 4800 *g* for 10 min at 4°C.
14) Supernatant was removed and the pellet was resuspended with 500 µL of heptane. The resulted suspension was homogenized, aliquoted, centrifuged and dried as described in step 10.

7.2 Measurement of compartment markers

To determine the enrichment of the studied compartments in the five fractions obtained through the previous procedure of NAF, specific enzyme activities together with the determination of secondary metabolite by LC-MS analysis was performed. Chlorogenic acid (Beshir *et al.*, 2019) together with mannosidase activity (Hossain *et al.*, 2017) were used as vacuolar markers. Chlorophyll together with NADP-GAPDH were used as chloroplast markers (Krueger *et al.*, 2011). Phosphoenolpyruvate carboxylase activity was used as cytosolic marker (Stitt *et al.*, 1989)

Briefly, the proportion of a compartment in a fraction was calculated as the percentage of its specific marker present in this fraction relative to the total found in the five fractions (see Figure S9, chapter 2).

7.2.1. *Enzyme extraction*

Enzyme extraction was done following the same protocol as previously described for other enzymatic measurements with the exception that extraction volume was 250 µL instead of 500 µL.

7.2.2. NADP-Glyceraldehyde-3-Phosphate Dehydrogenase (Chloroplast marker)

NADP-Glyceraldehyde-3-Phosphate dehydrogenase (EC 1.2.1.13) activity was determined using 2 µL of aliquot of enzymatic extraction, mixed with 18 µL of assay mix.

Assay mix

4 µL	Assay buffer 5X (0.5 M Tricine/KOH pH 8, 150 mM $MgCl_2$, 100 mM KCl, 10 mM EDTA, 0.25% Triton X-100)
1 µL	100 mM ATP
2 µL	40 mM 3-phosphoglycerate
2 µL	5 mM NADPH
0.2 µL	Phosphoglycerate kinase 1000 U mL^{-1} in 200 mM Tricine/KOH, pH 8, 10 mM $MgCl_2$
0.2 µL	Triose-P isomerase 100 U mL^{-1} in 200 mM Tricine/KOH, pH 8, 10 mM $MgCl_2$
0.2 µL	50 mM DTT
8.4 µL	H_2O

After incubating at 25°C for 20 min, the reaction was stopped with 20 µL of HCl in 100 mM Tricine/KOH, pH 9, incubated at room temperature for 10 min. Then, 20 µL of 0.5 M NaOH was added. After being mixed, 50 µL of determination mix were added and NADH evolution during 30 min at 25°C was followed at 340 nm. For blanks 3-phosphoglycerate was substituted by water in the assay mix (Gibon *et al.*, 2004).

Determination mix

10 µl	1 M Tricine/KOH, pH 8
0.2 µl	1 M $MgCl_2$
0.5 µl	Glutamate dehydrogenase 200 U mL^{-1} in 200 mM Tricine/KOH, pH 8, 10 mM $MgCl_2$
0.5 µl	Glutathion peroxydase 500 U mL^{-1} in 200 mM Tricine/KOH pH 8,
10 mM	$MgCl_2$
1 µl	66 mM NADH
37.8 µl	H_2O

7.2.3. Phosphoenolpyruvate carboxylase (Cytosol marker)

Phosphoenolpyruvate carboxylase activity is considered as a cytosol-specific activity (Stitt *et al.*, 1989). PEPC activity was determined using 2 µL of aliquots of enzymatic extraction, mixed with 18 µL of assay mix. To determine V_0, phosphoenolpyruvate was substituted by water in the assay mix.

Assay mix

4	µL	Assay buffer 5 X (0.5 M Tricine/KOH pH 8, $MgCl_2$, 50 mM $NaHCO_3$, 0.25% Triton X-100)
2	µL	Malate dehydrogenase 100 U mL^{-1} in Tricine/KOH 200 mM pH 8, 10 mM $MgCl_2$
2	µL	20 mM Phosphoenolpyruvate
0.4	µL	5 mM NADH
9.6	µL	H_2O

After incubating at 25°C for 20 min, the reaction was stopped with 20 µL 0.5 M HCl in 100 mM Tricine/KOH pH 9, incubated at 95°C for 5 min. Then, after being cooled and spinned down, 20 µL 0.5 M NaOH, was added. After being mixed, 45 µL of determination mix and 5 µL 4 mM PES (Phenazine ethosulfate) were added and reduced MTT (3(4,5-dimethylthiazol-2-yl)-2,5-diphenyltetrazolium bromide) was determined at 570 nm (Gibon *et al.*, 2004).

Determination mix

10	µL	100 mM Tricine/KOH pH 9
10	µL	10 mM MTT
4	µL	200 mM EDTA
2	µL	50 % Ethanol
1	µL	Alcohol Dehydrogenase 2000 U mL^{-1} in 200 mM Tricine/KOH pH 9, 10 mM $MgCl_2$
18	µL	H_2O

7.2.4. Manosidase (Vacuole marker)

Manosidase activity (EC 3.2.1.24) is considered as a vacuole-specific activity (Hossain *et al.*, 2017) and was determined using 5 µL aliquots of enzymatic extraction, mixed with 45 µL assay mix.

Assay mix

5 µL	0.5 M Citrate/KOH pH 4.5
5 µL	5 mM 4-Methylumbelliferyl-α-D-mannopyranoside (MUM) (dissolved in water at 50°C)
35 µL	H_2O

After incubating at 25°C for 20 min, 100 µL 0.2 M Na_2CO_3 was added to stop the reaction. The 4-Methylumbelliferone (MU) concentration was determined with a fluorometer (SAFAS Xenius DWL) at 25°C (excitation 360 nm, emission 450 nm) (adapted from Shashidhara and Gaikwad, 2009).

7.2.5. LC-MS analysis of subcellular metabolite levels

Aliquots of 2 µL of ethanol extraction for LC-MS was analyzed by with an Ultimate 3000 HPLC (Dionex, Sunnyvale, CA, USA) used to separate metabolites on a reversed-phase C18 column using an acetonitrile gradient in acidifed water. Metabolites were detected by using a hybrid quadrupole/time-of-fight mass spectrometer (micrOTOF-Q, Bruker Daltonics, Bremen, Germany). Electrospray ionization in negative mode was used to ionize the compounds. A quality control sample (QC) was injected after each set of ten samples. The MS data were processed using XCMS (Smith *et al.* 2006). A total of 3160 features were detected and reduced to 645 metabolic variables after filtering. The corresponding MS-based variables were named using their nominal masses in daltons (Da) and retention time in seconds.

7.3. Calculation algorithm for the determination of subcellular metabolite distributions

Subcellular metabolite distribution between the three cell compartments (vacuole, cytosol, and chloroplasts) was calculated by an algorithm that compared the distribution of enzymatic markers and metabolites between all sub-fractions for one sample (Riens *et al.*, 1991).

To calculate the subcellular metabolite concentration in mM, the metabolite quantity per g of FW was multiplied by its relative distribution in the compartment and divided by the volume ratio of the compartment in the cell (cytoplasm and vacuole) as calculated with the cytology measurements.

Compartment	**Marker**
Vacuole	Mannosidase/Chlorogenic acid
Chloroplast	NADP-GAPDH/Chlorophyll
Cytosol	PEPC

8. Fluorescent dye based measurement of vacuolar and cytosolic pH in tomato leaves

Intracellular pH measurement were based on the dual-excitation ratiometric pH indicator BCECF-AM (2',7'-Bis-(2-Carboxyethyl)-5-(and-6) -Carboxyfluorescein, Acetoxymethyl Ester). pH measurements with BCECF are made by determining the pH-dependent ratio of emission intensity (detected at 535 nm) when the dye is excited at 480 nm versus the emission intensity when excited at 435 nm (Brauer *et al*., 1995).

8.1. Calibration

Calibration is based on the nigerecin method, which allows to equilibrate the pH of the external medium (imposed) with the intracellular medium (Thomas *et al.*, 1979). To do so, six calibration solutions containing 100 µM nigerecin adjusted to a pH ranging from 4.5to 8.5 (with TRIS) were used. Parenchyma cells appeared extremely sensitive to nigerecin treatment and thus, calibaration was made in the oclusive cells of the stomata that revealed more resistant to the treatment. To isolate stomata cells, epidermis from the lower side of the leaf was peeled off with fine forceps. Epidermis was incubated in the pH calibration buffers for no longer than 20 min and was washed in a calibration buffer with the same pH adjusted with TRIS, but without BCECF-AM. Epidermis images were obtained with x20 PL-APO objective on a LEICA LCS SP2 AOBS confocal microscope with sequential excitation at 488 nm/435 nm and single emission band-pass 560 to 550 nm. To define precisely each compartments it was convenient to use auto-fluorescence of chloroplasts at 600 nm.

Calculation of fluorescence intensity was measured using the image processing package FIJI of the imageJ software. Boltzmann equation was used to fit sigmoidal curves with calibration data.

$$y = d/(1+\exp((x-e)*b)) \qquad x = e + (\log(d/y-1)/b)$$

Where *x* is the pH value of the calibration solution, *y* is the 488/435 nm ratio value obtained, and *b*, *d* and *e* as constant to be optimized by fitting.

pH calibration buffer

50	mM	MES-TRIS pH to adjust
135	mM	KCl
100	µM	$CaCl_2$
5	µM	BCECF-AM (2´,7´-Bis-(2-Carboxyethyl)-5-(and-6)-Carboxyfluorescein- Acetoxymethyl Ester)
0.02	%	Pluronic acid
100	µM	Nigerecin (conserved in ethanol)

8.2. pH measurement

Transversal tomato leaf sections 90 µm thick, were obtained by using a vibratome (Microm HM650V)) as seen in the picture. Sections were incubated for 20 min in dye loading medium adjusted to pH 6.5. Then, sections were washed with dye loading medium without BCECF-AM and pluronic acid and were placed onto confocal microscope between slide and slip cover.

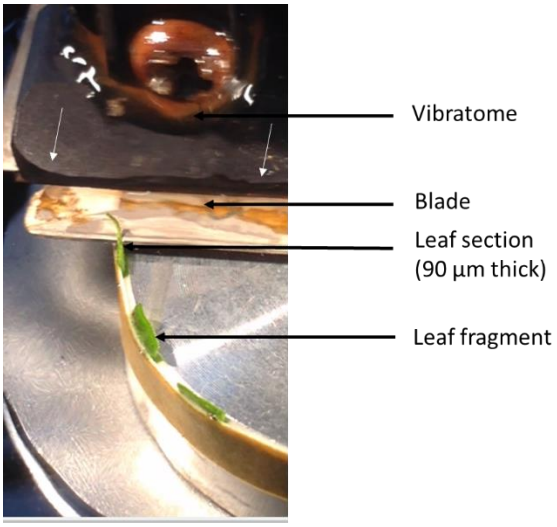

Figure 1: Photography illustrating the production of transversal tomato leaf sections with a vibratome

Dye loading medium

50	mM	MES-TRIS
135	mM	KCl
100	µM	$CaCl_2$
5	µM	BCECF-AM
0.02	%	Pluronic acid

Imaging parameters were the same as the calibration curve. Ratios were converted to pH using the equation of the calibration curve.

Once into the cell BCECF-AM is cleaved by cellular esterase and thus BCECF accumulated in different compartments. In leaves, BCECF accumulated mainly in the large central vacuole, making it an ideal tool for vacuolar pH measurements. Importantly, although more difficult, signal was also reported in the cytosol, its pH was also measured when it was possible.

For each biological replicate, intracellular BCECF ratio was measured in around 30 leaf parenchyma cells for obtaining an average pH value.

9. Extraction of apoplastic fluids and pH determination

The procedure to extract apoplastic fluids for pH determination was adapted from O'Leary et al (2014). To prepare apoplastic extract, intact leaves were harvested and its surface washed with deionized water and dried with absorbent paper. Leaves were vacuum infiltrated with distilled water carefully placing the leaves in the barrel of a 50-mL syringe filled with distilled water. and applying a gentle negative pressure by slowly pulling the plunger outwards. and returning it to its position with a little positive pressure. These steps were repeated until the leaf was fully infiltrated, as seen by the darkened colour of the infiltrated leaf tissue. Then, leaves were perfectly dried with absorbent paper towels to remove all the liquid in the surface. Then, around four infiltrated leaves were rolled up into Parafilm M with cut petioles facing upwards. Rolled-up leaves were inserted into a 5-mL syringe, which was inserted itself into a 15 mL centrifuge tube. Tubes were centrifuged with 1000 *g* at 4°C for 10 min. Recovered apoplast fluid was transferred to a 2 mL reaction tube and pH was immediately measured with a pH-meter.

To calculate the apoplast dilution factor, leaves were infiltrated as above but using 50 µM indigo carmine (indigo-5,5'-disulfonic acid) solution instead of distilled water. Then, the absorbance of the apoplastic fluid, obtained as described above, was measured at 610 nm. Apoplast dilution factor was calculated with the equations below and applied to the pH values previously measured.

$$OD_{610}^{\text{Indigo carmine}} = OD_{610}^{\text{W/indigo carmine}} - OD_{610}^{\text{water}}$$

$$OD_{610}^{\text{AWF+indigo carmine}} = OD_{610}^{\text{AWF+Indigo carmine}} - OD_{610}^{\text{AWF W-Indigo carmine}}$$

$$\text{Apoplast dilution factor} = OD_{610}^{\text{Indigo carmine}} / (OD_{610}^{\text{indigo carmine}} - OD_{610}^{\text{AWF+indigo carmine}})$$

10. Leaf bulk pH determination

The central vein of the leaf was removed with a scalpel, and the remaining lamina were immediately crushed with a pestle previously cooled at 4°C. Then bulk leaf tissue was placed into a 2 mL reaction tube and centrifuged at 13000 *g* for 5 min at 4 °C to liberate the aqueous phase. Supernatant was transferred to 2 mL reaction tube and the pH of the solution was immediately measured with a pH-meter.

11. Statistical analysis

Statistical analyses were overall performed using R Software (R core team, 2018). Normality and homogeneity of variance were analysed by Kolmogorov–Smirnov and Leven's tests. The significance of the results was assessed using independent samples t-test, one-way ANOVA followed by Duncan´s test or two-way ANOVA, as described in figure legends. For PCA the package FactoMineR was used (Lê *et al.*, 2008). Data visualization was performed with ggplot2 package (Wickham, 2010).

12. Computer modeling and model parameter optimization

The set of equations listed in Supplemental Table 2 to 6 was solved by the Copasi 4.7 software (Hoops *et al.*, 2006). For each optimization set up, fourteen Copasi files corresponding to the 7 developmental stages of NH_4^+ and NO_3^-- fed plants were generated. Parameter optimization was performed using the random search algorithm and by minimizing score that was calculated with score equations shown in supplemental Table S5.Then, the whole iterative process was repeated and the 200 best-scoring parameter sets were kept for further analysis.

References

REFERENCES

Aarnes H, Eriksen AB, Petersen D, Rise F. 2007. Accumulation of ammonium in Norway spruce (*Picea abies*) seedlings measured by in vivo ^{14}N-NMR. Journal of Experimental Botany **58**, 929–934.

Adlimoghaddam A, Sabbir MG, Albensi BC. 2016. Ammonia as a potential neurotoxic factor in Alzheimer ’s disease. Frontier in Molecular Neuroscience **9**, 1–11.

Aluri S, Büttner M. 2007. Identification and functional expression of the *Arabidopsis thaliana* vacuolar glucose transporter 1. Proceedings of the National Academy of Sciences, USA **104**, 2537–2542.

Andrews M, Raven JA, Lea PJ. 2013. Do plants need nitrate? the mechanisms by which nitrogen form affects plants. Annals of Applied Biology **163**, 174–199.

De Angeli A, Monachello D, Ephritikhine G, Frachisse JM, Thomine S, Gambale F, Barbier-Brugoo H. 2006. The nitrate/proton antiporter AtCLCa mediates nitrate accumulation in plant vacuoles. Nature Letters **442**, 939–942.

De Angeli A, Monachello D, Ephritikhine G, Frachisse J, Sebastien Thomine, Gambale F, Barbier-Brugoo H. 2009. CLC-mediated anion transport in plant cells. Philosophical Transactions of the Royal Society **364**. 195-201

Ariz I, Asensio AC, Zamarreno AM, Garcıa-Mina JM, Aparicio-Tejo PM, Moran JF. 2012. Changes in the C/N balance caused by increasing external ammonium concentrations are driven by carbon and energy availabilities during ammonium nutrition in pea plants : the key roles of asparagine synthetase and anaplerotic enzymes. Physiologia Plantarum. **148.** 522-537

Ariz I, Boeckstaens M, Gouveia C, Martins AP, Sanz-Luque E, Fernández E, Soveral G, Wirén N, Marini AM, Aparicio-Tejo PM, Cruz C. 2018. Nitrogen isotope signature evidences ammonium deprotonation as a common transport mechanism for the AMT-Mep-Rh protein superfamily. Science Advances **4**, eaar3599.

Arnon DI. 1949. Copper enzymes in isolated chloroplasts polyphenoloidase in *Beta vulgaris*. Plant Physiology **24**, 1–15.

Ashraf M. 1999. Interactive effect of salt (NaCl) and nitrogen form on growth , water relations and photosynthetic capacity of sunflower (*Helianthus annuus L* .). Annals of. Applied Biology **135,** 509-551.

Bai L, Ma X, Zhang G, Song S, Zhou Y, Gao L, Miao Y, Song C-P. 2014. A receptor-likenase mediates ammonium homeostasis and is important for the polar growth of root hairs in arabidopsis. The Plant Cell **26**, 1497–1511.

Barker AV, Corey KA. 1991. Interrelations of ammonium toxicity and ethylene action in tomato. HortScience **26**, 177–180.

Bassil E, Tajima H, Liang Y, Ohto M, Ushijima K, Nakano R, Esumi T, Coku A, Belmonte M, Blumwald E. 2011. The Arabidopsis Na^+/H^+ antiporters NHX1 and NHX2 control vacuolar pH and K^+ homeostasis to regulate growth , flower development , and reproduction. The Plant Cell **23**, 3482–3497.

Beauvoit BP, Colombie S, Monier A, Andrieu ME, Biais B, Bénard C, Chéniclet C, Dieuaide-Noubhani M, Nazaret C, Mazat JP, Gibon Y. 2014. Model-assisted analysis of sugar metabolism throughout tomato fruit development reveals enzyme and carrier properties in relation to vacuole expansion. The Plant Cell **26**, 3224–3242.

Ben-Zioni A, Vaadia Y, Herman SL. 1970. Correlations between nitrate reduction , protein synthesis and malate accumulation. Physiologia Plantarum **97**, 1039–1047.

Berezin I, Mizrachy-Dagry T, Brook E, Mizrachi K, Elazar M, Zhuo S, Saul-Tcherkas V, Shaul O. 2008. Overexpression of AtMHX in tobacco causes increased sensitivity to Mg^{2+} , $Zn2^+$, and Cd^{2+} ions , induction of V-ATPase expression , and a reduction in plant size. Plant Cell Report **27**, 939–949.

Bernard SM, Dimah ZH. 2009. The importance of cytosolic glutamine synthetase in nitrogen assimilation and recycling. New Phytologist **182**, 608-620

Beshir WF, Tohge T, Watanabe M, Hertog H, Hoefgen, Fernie AR, Nicolaï BM. 2019. Non-aqueous fractionation revealed changing subcellular metabolite distribution during apple fruit development. Horticulture Research **98**, 1:12.

Bittsánszky A, Pilinszky K, Gyulai G, Komives T. 2014. Overcoming ammonium toxicity. Plant Science **231**, 184–190.

Blumwald E, Poole RJ. 1985. Na^+/H^+ antiport in isolated tonoplast vesicles from storage tissue of *Beta vulgaris*. Plant Physiology **78**, 163–167.

Bolger A, Scossa F, Bolger ME, *et al.* 2014. The genome of the stress-tolerant wild tomato species *Solanum pennellii*. Nature Genetics **46**, 1034–1039.

Bonales-Alatorre E, Shabala S, Chen ZH, Pottosin I. 2013. Reduced tonoplast fast-activating and slow-activating channel activity is essential for conferring salinity tolerance in a facultative halophyte, quinoa. Plant Physiology **162**, 940–952.

Bonza MC, De Michelis MI. 2011. The plant Ca^{2+}-ATPase repertoire : biochemical features and physiological functions. Plant Biology **13**, 421–430.

Bradford MM. 1976. A rapid and sensitive method for the quantitation microgram quantities of protein utilizing the principle of protein-dye binding. Analytical Biochemistry **254**, 248–254.

Brauer D, Otto J, Tu SI. 1995. Selective accumulation of the fluorescent ph indicator, bcecf, in vacuoles of maize root-hair cells. Journal of Plant Physiology **145**, 57–61.

Bricker SB, Longstaff B, Dennison W, Jones A, Boicourt K, Wicks C, Woerner J. 2008. Effects of nutrient enrichment in the nation's estuaries: A decade of change.Harmful Algae **8**, 21–32.

Britto DT, Kronzucker HJ. 2002. Review NH_4^+ toxicity in higher plants : a critical review. Jounal of Plant Physiology **159**, 567-584

Britto DT, Kronzucker HJ. 2005. Nitrogen acquisition, PEP carboxylase, and cellular pH homeostasis: New views on old paradigms. Plant, Cell and Environment **28**, 1396–1409.

Britto DT, Kronzucker HJ. 2013. Ecological significance and complexity of N-source preference in plants. Annals of Botany **112**, 957–963.

Britto DT, Siddiqi MY, Glass ADM, Kronzucker HJ. 2001. Futile transmembrane NH_4^+ cycling: A cellular hypothesis to explain ammonium toxicity in plants. Proceedings of the National Academy of Sciences, USA **98**, 4255–4258.

Cameron KC, Di HJ, Moir JL. 2013. Nitrogen losses from the soil/plant system : a review. Annals of Applied Biology **162**, 145–173.

Cao Y, Class ADM, Crawford NM. 1993. Ammonium inhibition of arabidopsis root crowth can be reversed by potassium and by auxin resistance mutation *aux1*, *axr1*, axr2. Plant Physiology **162**, 983–989.

Carden DE, Walker DJ, Flowers TJ, Miller AJ. 2003. Single-cell measurements of the contributions of cytosolic Na^+ and K^+ to salt tolerance 1. Plant Physiology **131**, 676–683.

Carroll AD, Fox GG, Laurie S, Phillips R, Ratcliffe RG, Stewart GR. 1994. Ammonium assimilation and the role of γ-aminobutyric acid in pH homeostasis in carrot cell suspensions. Plant Physiology **106**, 513–520.

Chanoca A, Kovinich N, Burkel B, Stecha S, Bohorquez-Restrepo A, Ueda T, Eliceiri KW, Grotewold E, Otegui MS. 2015. Anthocyanin Vacuolar Inclusions Form by a microautophagy mechanism. The Plant Cell **23**, 2545–2559.

Chardon F, Bedu M, Calenge F, *et al.* 2013. Leaf fructose content is controlled by the vacuolar transporter SWEET17 in Arabidopsis. Current Biology **23**, 697–702.

Chopin F, Orsel M, Dorbe MF, Chardon F, Truong HN, Miller AJ, Krapp A, Daniel-Vedele F. 2007. The Arabidopsis ATNRT2.7 nitrate transporter controls nitrate content in seeds. The Plant Cell **19**, 1590–1602.

Choudhary AK, Kumari N, Jha AM. 2016. Assessment of cytotoxic and chromotoxic effects of ammonium acetate by employing plant bioassay system. European Journal of Biomedical and Pharmaceutical Sciences **3**, 346–350.

Coleman WK, Greyson RI. 1976. The growth and development of the leaf in tomato (*Lycopersicon esculentum*). I. The plastochron index, a suitable basis for description. Canadian Journal of Botany **54**, 2421–2428.

Coleman JOD, Randall R, Blake-Kalff MAA. 1997. Detoxification of xenobiotics in plant cells by glutathione conjugation and vacuolar compartmentalization: a fluorescent assay using monochiorobimane. Plant and Cell Environment **20**, 449–460.

Coleto I, Vega-Mas I, Glauser G, González-Moro MB, Marino D, Ariz I. 2019. New insights on *Arabidopsis thaliana* root adaption to ammonium nutrition by the use of a quantitative proteomic approach. Intenational Journal of Molecular Science **20**, 1–20.

Cruz C, Bio AFM, Domínguez-Valdivia MD, Aparicio-Tejo PM, Lamsfus C, Martins-Loução MA. 2006. How does glutamine synthetase activity determine plant tolerance to ammonium? Planta **223**, 1068–1080.

Cruz C, Domínguez-valdivia MD, Aparicio-tejo PM, Lamsfus C, Bio A, Martins-louçao MA, Moran JF. 2011. Intra-specific variation in pea responses to ammonium nutrition leads to different degrees of tolerance. Environmental and Experimental Botany **70**, 233–243.

Cui Y, Shen J, Gao C, Zhuang X, Wang J, Jiang L. 2016. Biogenesis of plant prevacuolar multivesicular bodies. Molecular Plant **9**, 774–786.

Cuin TA, Miller AJ, Laurie SA, Leigh RA. 2003. Potassium activities in cell compartments of salt-grown barley leaves. Journal of Experimental Botany **54**, 657–661.

Dali N, Michaud D, Yelle S. 1992. Evidence for the involvement of sucrose phosphate synthase in the pathway of sugar accumulation in sucrose-accumulating tomato fruits. Plant Physiology **99**, 434–438.

Darwen CWE, John P. 1989. Localization of the enzymes of fructan metabolism in vacuoles isolated by a mechanical method from tubers of jerusalem artichoke (*Helianthus tuberosus* L .). Plant Physiology **89**, 658–663.

Diaz C, Lemaıtre T, Christ A, Azzopardi M, Kato Y, Sato F, Morot-Gaudry JF, Le Dily F, Celine MD. 2008. Nitrogen recycling and remobilization are differentially controlled by leaf senescence and development stage in arabidopsis under low nitrogen nutrition. Plant Physiology **147**, 1437–1449.

Dreyer I, Scho G, Schulz A, Schumacher K, Martinoia E, Marten I, Hedrich R. 2012. Luminal and cytosolic pH feedback on proton pump activity and ATP Affinity of V-type ATPase from Arabidopsis. The Journal of Biological Chemistry **287**, 8986–8993.

Dreyer I, Uozumi N. 2011. Potassium channels in plant cells. The FEBS Journal **278**, 4293–4303.

Dubois F, Tercé-Laforgue T, González-Moro MB, Estavillo JM, Sangwan R, Gallais A, Hirel B. 2003. Glutamate dehydrogenase in plants : is there a new story for an old enzyme ? Plant Physiology and Biochemistry **41**, 565–576.

Dujardin F. 1841. Infusoires, la physiologie et la classification de ces animaux, et la manière des les étudier à l'aide du microscope.

Emmerlich V, Linka N, Reinhold T, Hurth MA, Traub M, Martinoia E, Neuhaus HE. 2003. The plant homolog to the human sodium/dicarboxylic cotransporter is the vacuolar malate carrier. Proceedings of the National Academy of Sciences, USA **100**, 11122-11126.

Escobar MA, Geisler DA, Rasmusson AG. 2006. Reorganization of the alternative pathways of the Arabidopsis respiratory chain by nitrogen supply : opposing effects of ammonium and nitrate. The Plant Journal **45**, 775–788.

Esteban R, Ariz I, Cruz C, Moran JF. 2016. Mechanisms of ammonium toxicity and the quest for tolerance. Plant Science **248**, 92–101.

Fernie AR, Carrari F, Sweetlove LJ. 2004. Respiratory metabolism : glycolysis , the TCA cycle and mitochondrial electron transport. Plant Biology **7**, 254–261.

Foyer CH, Parry M, Noctor G. 2003. Markers and signals associated with nitrogen assimilation in higher plants. Journal of Experimental Botany **54**, 585–593.

Francisco RDB, Martinoia E. 2018. The vacuolar transportome of plant specialized metabolites.Plant Cell and Physiology **59**, 1326–1336.

Fricke W, Chaumont F. 2006. Solute and water relations of growing plant cells. The Expanding Cell **1**, 7–31.

Fürtauer L, Weckwerth W, Nägele T. 2016. A benchtop fractionation procedure for subcellular analysis of the plant metabolome. Frontiers in Plant Science **7**, 1–14.

Gerendás J, Ratcliffe RG. 2000. Intracellular pH regulation in maize root tips exposed to ammonium at high external pH. Journal of Experimental Botany **51**, 207–219.

Gibon Y, Blaesing OE, Hannemann J, Carillo P, Höhne M, Janneke HM, Palacios N, Cross J, Selbig J, Stitt M. 2004. A robot-based platform to measure multiple enzyme activities in Arabidopsis using a set of cycling assays: comparison of changes of enzyme activities and transcript levels during diurnal cycles and in prolonged darkness. The Plant Cell **16**, 3304–3325.

Głazowska S, Baldwin L, Mravec J, Bukh C, Fangel JU, Willats GT, Schjoerring JK. 2019. The source of inorganic nitrogen has distinct effects on cell wall composition in *Brachypodium distachyon*. Journal of Experimental Botany **70**, 6461–6473.

Gruber AV, Feiz L. 2018. Rubisco assembly in the chloroplast. Frontiers in Molecular Biosciences **5**, 1–11.

Grotewold E. 2004. The challenges of moving chemicals within and out of cells : insights into the transport of plant natural products. Planta **219**, 906–909.

Guan M, Bang TCD, Pedersen C, Schjoerring JK. 2016. Cytosolic glutamine synthetase Gln1;2 is the main isozyme contributing to GS1 activity and can be up-regulated to relieve ammonium toxicity. Plant Physiology **171**, 1921–1933.

Gupta SK, Gupta AB, Gupta R. 2017. Pathophysiology of nitrate toxicity in humans in view of the changing trends of the global nitrogen cycle with special reference to India **28**, 459-468.

Hachiya T, Inaba J, Wakazaki M, Mayuko S, Kiminori T, Miyagi A, Maki KY, Kiba T, Gojon A, Sakakibaara H. 2019. Excessive assimilation of ammonium by plastidic glutamine synthetase is a major cause of ammonium toxicity in *Arabidopsis thaliana*. BioRxiv. https://doi.org/10.1101/764324

Hachiya T, Watanabe CK, Fujimoto M, Ishikawa T, Takahara K, Kawai-yamada M, Uchimiya H, Uesono Y, Terashima I, Noguchi K. 2012. Nitrate addition alleviates ammonium toxicity without lessening ammonium accumulation, organic acid depletion and inorganic cation depletion in *Arabidopsis thaliana* shoots. Plant Cell and Physiology **53**, 577–591.

Hamaji K, Nagira M, Yoshida K, *et al.* 2009. Dynamic aspects of ion accumulation by vesicle traffic under salt stress in Arabidopsis. Plant Cell and Physiology **50**, 2023–2033.

Hase T, Schürmann P, Knaff DB. 2006. The Interaction of ferredoxin with ferredoxin-dependent enzymes. Photosystem **28**, 477–498.

Hedrich R, Marten I. 2011.TPC1–SV channels gain shape. Molecular Plant **4**, 428–441.

Hendriks JHM, Kolbe A, Gibon Y, Stitt M, Geigenberger P. 2003. ADP-Glucose pyrophosphorylase is activated by posttranslational redox-modification in response to light and to sugars in leaves of arabidopsis and other plant species . Plant Physiology **133**, 838–849.

Hessini K, Issaoui K, Ferchichi S, Saif T, Abdelly C, Siddique KHM, Cruz C. 2019. Plant physiology and biochemistry interactive effects of salinity and nitrogen forms on plant growth, photosynthesis and osmotic adjustment in maize. Plant Physiology and Biochemistry **139**, 171–178.

Hiroko A, Xiaoyuan Y, Kazuyuki Y. 2010. Evaluation of effectiveness of enhanced-efficiency fertilizers as mitigation options for N_2O and NO emissions from agricultural soils: meta-analysis. Global Change Biology **16**, 1837–1846.

Holloway JM, Dahlgren RA. 2002. Nitrogen in rock : occurrences and biogeochemical implications. Global Biochemical Cycles **16**, 1–15.

Holtum JAM, Winter K. 1982. Activity of enzymes of carbon metabolism during the induction of Crassulacean acid metabolism in *Mesembryanthemum crystallinum*. Planta **55**, 8–16.

Hoopen F, Cuin TA, Pedas P, Hegelund JN, Shabala S, Schjoerring JK, Jahn TP. 2010. Competition between uptake of ammonium and potassium in barley and Arabidopsis roots: molecular mechanisms and physiological consequences. Journal of Experimental Botany **61**, 2303–2315.

Hoops S, Sahle S, Gauges R, Lee C, Simus N, Singhal M, Xu L, Mendes P, Kummer U. 2006. Systems biology COPASI—a COmplex PAthway SImulator. Bioinformatics **22**, 3067–3074.

Hossain MS, Persicke M, ElSayed AI, Kalinowski J, Dietz KJ. 2017. Metabolite profiling at the cellular and subcellular level reveals metabolites associated with salinity tolerance in sugar beet. Journal of Experimental Botany **68,** 5961-5976

Hu AY, Zheng MM, Sun LM, Zhao XQ, Shen RF. 2019. Ammonium alleviates manganese toxicity and accumulation in rice by down-regulating the transporter gene OsNramp5 through rhizosphere acidification. Frontier in Plant Science **10**, 1–11.

Isayenkov S, Isner JC, Maathuis FJM. 2010. Vacuolar ion channels: Roles in plant nutrition and signalling. FEBS Letters **584**, 1982–1988.

Jung B, Ludewig F, Schulz A, *et al.* 2015. Identification of the transporter responsible for sucrose accumulation in sugar beet taproots. Nature Plant **1**, 1-6.

Kaiser G, Heber U. 1984. Sucrose transport into vacuoles isolated from barley mesophyll protoplasts. Planta **161**, 562–568

Kaiser G, Martinoia E, Schroppel-Meier G, Heber U. 1989. Active transport of sulfate into the vacuole of plant cells provides halotolerance and can detoxify $S0_2$. Journal of Plant Physiology **133**, 756–763.

Kandemir T, Schuster ME, Senyshyn A, Behrens M, Schlögl R. 2013. The Haber–Bosch process revisited : on the real structure and stability of ‘ ammonia iron ’ under working conditions. Angewandte Chemie **52**, 12723–12726.

Kanter DR, Searchinger TD. 2018. A technology-forcing approach to reduce nitrogen pollution. Nature Sustainability **1**, 544-552

Kartal B, Niftrik L Van, Keltjens JT, Huub JM, Camp O Den, Jetten MSM. 2012. Anammox—Growth Physiology, Cell Biology, and Metabolism. Advances in Microbial Physiology **60**, 211-264

Keys A. 2006. The re-assimilation of ammonia produced by photorespiration and the nitrogen economy of C_3 higher plants. Photosynthesis Research **87**, 165–175.

Kirkby EA, Mengel K. 1967. Ionic balance in different tissues of the tomato plant in relation to nitrate , urea , or ammonium nutrition.Plant Physiology **42**, 6–14.

Kirscht A, Kaptan SS, Bienert GP, Chaumont F, Nissen P, de Groot BL, Kjellbom P, Gourdon P, Johanson U. 2016. Crystal structure of an ammonia-permeable aquaporin. PLoS Biology **14**, 1–19.

Kosegarten H, Crolig F, Wieneke J, Wilson G, Hoffmann B. 1997. Differential ammonia-elicited changes of cytosolic pH in fluorescence ratio. Plant Physiology **113**, 451–461.

Kovermann P, Meyer S, Ho S, Picco C, Scholz-starke J, Ravera S, Lee Y, Martinoia E. 2007. The Arabidopsis vacuolar malate channel is a member of the ALMT family. The Plant Journal **52**, 1169–1180.

Koyama H, Toda T, Yokota S, Dawair Z, Hara T. 1995. Effects of aluminum and pH on root growth and cell viability in *Arabidopsis thaliana* strain landsberg in hydroponic culture. Plant Cell Physiology **36**, 201–205.

Kronzucker HJ, Siddiqi MY, Glass ADM. 1997. Conifer root discrimination ecology of forest succession. Nature **385**, 59–61.

Krueger S, Giavalisco P, Krall L, Steinhauser M, Bu D, Usadel B, Flu U. 2011. A topological map of the compartmentalized *Arabidopsis thaliana* leaf metabolome. PLoS ONE **6**, e17806.

Kurkdjian A, Guern J. 1989. Intracellular pH: Measurement and importance in cell activity. Plant Molecular Biology **40,** 271-303**.**

Lang B, Kaiser WM. 1994. Solute content and energy status of roots of barley plants cultivated at different pH on nitrate or ammonium-nitrogen. New Phytologist **128**, 451–459.

Lasa B, Frechilla S, Lamsfus C. 2001. The sensitivity to ammonium nutrition is related to nitrogen accumulation. Scientia Horticultura **91**, 143–152.

Lê S, Josse J, François H. 2008. FactoMineR: An R package for multivariate analysis. Statistical Software **25**, 1–18.

Leary BO, Park J, Plaxton WC. 2011. The remarkable diversity of plant PEPC (phosphoenolpyruvate carboxylase): recent insights into the physiological functions and post-translational controls of non-photosynthetic PEPCs. The Biochemical Journal **436**, 15–34.

Leidreiter K, Kruse A, Heineke D, Robinson DG, Heldt DGR. 1995. Subcellular Volumes and Metabolite Concentrations in Potato (*Solanum tuberosum cv* . Désirée) Leaves. Botanica Acta **108**,439-444

Li B, Li G, Kronzucker HJ, Baluska F, Shi W. 2014. Ammonium stress in Arabidopsis : signaling , genetic loci , and physiological targets. Trends Plant Science **19**, 107–114.

Li X, Zhang D, Lynch-holm VJ, Okita TW, Franceschi VR. 2003. Isolation of a crystal matrix protein associated with calcium oxalate precipitation in vacuoles of specialized cells. Plant Physiology **133**, 549–559.

Liu Y, Lai N, Gao K, Chen F, Yuan L, Mi G. 2013. Ammonium inhibits primary root growth by reducing the length of meristem and elongation zone and decreasing elemental expansion rate in the root apex in *Arabidopsis thaliana*. PLoS ONE **8**, e61031.

Liu T, Ren T, White PJ, Cong R, Lu J. 2018. Storage nitrogen co-ordinates leaf expansion and photosynthetic capacity in winter oilseed rape. Journal of Experimental Botany **69**, 2995–3007.

Lobit P, Genard M, Soing P, Habib R. 2006. Modelling malic acid accumulation in fruits: relationships with organic acids , potassium , and temperature. Journal of Experimental Botany, **57**, 1471–1483.

Loque D, Ludewig U, Yuan L, Wiren VN. 2005. Tonoplast facilitate NH_3 transport into the vacuole. Plant Physiology **137**, 671–680.

Maathuis FJM. 2009. Physiological functions of mineral macronutrients. Plant Biology **12**, 250–258.

Magalhaes JR, Huber DM, Tsai C. 1992. Evidence of increased ^{15}N-ammonium assimilation in tomato plants with exogenous α-ketoglutarate. Plant Science **85**, 135–141.

Maillard A, Etienne P, Diquélou S, Trouverie J, Billard V, Yvin J, Ourry A. 2016. Nutrient deficiencies modify the ionomic composition of plant tissues : a focus on cross-talk between molybdenum and other nutrients in *Brassica napus*. Journal of Experimental Botany **67**, 5631–5641.

Manohar M, Shigaki T, Hirschi KD. 2011. Plant cation⁄H^+ exchangers (CAXs): biological functions and genetic manipulations. Plant Biology **13**, 561–569.

Marino D, Moran JF. 2019. Can ammonium stress be positive for plant performance? Frontiers in Plant Science **10**, 1–5.

Martin A, Lee J, Kichey T, *et al.* 2006. Two cytosolic glutamine synthetase isoforms of maize are specifically involved in the control of grain production. The Plant Cell **18**, 3252–3274.

Martinoia E, Maeshima M, Neuhaus HE. 2007. Vacuolar transporters and their essential role in plant metabolism. Journal of Experimental Botany **58**, 83–102.

Masclaux-Daubresse C, Daniel- Vedele F, Dechorgnat J, Chardon F, Gaufichon L, Suzuki A. 2010. Nitrogen uptake , assimilation and remobilization in plants : challenges for sustainable and productive agriculture. Annals of Botany **105**, 1141–1157.

Masclaux C, Valadier MH, Brugière N, Morot-Gaudry JF, Hirel B. 2000. Characterization of the sink/source transition in tobacco (*Nicotiana tabacum* L.) shoots in relation to nitrogen management and leaf senescence. Planta **211**, 510–518.

Massonneau A, Martinoia E, Dietz K, Mimura T. 2000. Phosphate uptake across the tonoplast of intact vacuoles isolated from suspension-cultured cells of *Catharanthus roseus* (L.) G. Don. Planta **211**, 390–395.

Matile P, Moor H. 1968. Vacuolation: origin and development of the lysosomal apparatus in root-tip cells. Planta **80**, 159–175.

Maurel C, Tacnet F, Güclü J, Guern J, Ripoche P. 1997. Purified vesicles of tobacco cell vacuolar and plasma membranes exhibit dramatically different water permeability and water channel activity. Proceedings of the National Academy of Sciences, USA **94**, 7103–7108.

Mayer M, Dynowski M, Ludewig U. 2006. Ammonium ion transport by the AMT/Rh homologue LeAMT1;1. Biochemistry Journal **396**, 431–437.

Mengel K, Planker R, Hoffmann B. 1994. Relationship between leaf apoplast pH and iron chlorosis of sunflower (*Helianthus annuus* L .). Journal of Plant Nutrition **17**, 37–41.

Mertz SM, Higinbotham N. 1976. Transmembrane electropotential in barley roots as related to cell type, cell location, and cutting and aging effects. Plant physiology **57**, 123–128.

Miranda RDS, Mesquita RO, Costa JH, Alvarez-Pizarro JC Tarquinio Prisco J, Gomes-Filho E. 2018. Integrative control between proton pumps and SOS1 antiporters in roots is crucial for maintaining low Na^+ accumulation and salt tolerance in ammonium-supplied *Sorghum bicolor*.Plant & Cell and Physiology **58**, 522–536.

Morillon R, Lassalles JP. 1999. Osmotic water permeability of isolated vacuoles. Planta **210**, 80–84.

Noctor G, Foyer CH. 1998. A re-evaluation of the ATP: NADPH budget during C photosynthesis : a contribution from nitrate assimilation and its associated respiratory activity ? Journal of Experimental Botany **49**, 1895–1908.

Nunes-Nesi A, Carrari F, Gibon Y, Sulpice R, Lytovchenko A, Fisahn J, Ratcliffe RG, Sweetlove LJ, Fernie AR. 2007. Deficiency of mitochondrial fumarase activity in tomato plants impairs photosynthesis via an effect on stomatal function.The Plant Journal **50**, 1093–1106.

Nunes-Nesi A, Fernie AR, Stitt M. 2010. Metabolic and signaling aspects underpinning the regulation of plant carbon nitrogen interactions. Molecular Plant **3**, 973-996

O'Leary BM, Rico A, McCraw S, Fones HN, Preston GM. 2014. The infiltration-centrifugation technique for extraction of apoplastic fluid from plant leaves using *Phaseolus vulgaris* as an example. Journal of Visualized Experiments **94**, e52113.

Offermans WK, Jansen APJ, Van Santen RA. 2006. Ammonia activation on platinum { 1 1 1 }: A density functional theory study. Surface Science **600**, 1714–1734.

Oleski N, Mahdavi P, Bennett AB. 1987. Transport properties of the tomato fruit tonoplast. Plant Physiology **84**, 997-1000.

Pantin F, Simonneau T, Oa HW, Dauzat M, Muller B. 2011. Control of leaf expansion : a developmental switch from metabolic to hydraulics. Plant Physiology **156**, 803–815.

Parker JL, Newstead S. 2014. Molecular basis of nitrate uptake by the plant nitrate transporter NRT1.1. Nature **507**, 68–72.

Parks GE, Dietrich MA, Schumaker KS. 2002. Increased vacuolar Na^+/H^+ exchange activity in *Salicornia bigelovii* Torr . in response to NaCl. Journal of Experimental Botany **53**, 1055–1065.

Pasqualini S, Ederli L, Piccioni C, Batini P, Bellucci M, Arcioni S, Antonielli M. 2001. Metabolic regulation and gene expression of root phosphoenolpyruvate carboxylase by different nitrogen sources. Plant Cell and Environment **24**, 439–447.

Patterson K, Cakmak T, Cooper A, Lager IDA, Rasmusson AG, Escobar MA. 2010. Distinct signalling pathways and transcriptome response signatures differentiate ammonium- and nitrate-supplied plants. Plant Cell Environment **33** , 1486–1501

De la Peña M, González-Moro MB, Marino D. 2019. Providing carbon skeletons to sustain amide synthesis in roots underlines the suitability of *Brachypodium distachyon* for the study of ammonium stress in cereals. AoB Plants **XX**, 1–11.

Peralta IE, Spooner DM, Knapp S. 2008. Taxonomy of Wild Tomatoes and Their Relatives (*Solanum sect . Lycopersicoides* , sect. Juglandifolia, sect. Lycopersicon; Solanaceae). American Society of Plant Taxonomists **84**, 1-186.

Pittman JK. 2012. Multiple transport pathways for mediating intracellular pH homeostasis: the contribution of H^+/ion exchangers. Frontiers in Plant Science **3**, 1–8.

Plaxton WC, Podestá FE. 2007. The functional organization and control of plant respiration. Plant Sciences **25**, 159–198.

Pnueli L, Carmel-Goren L, Hareven D, Gutfinger T, Alvarez J, Ganal M, Zamir D, Lifschitz E. 1998. The SELF-PRUNING gene of tomato regulates vegetative to reproductive switching of sympodial meristems and is the ortholog of CEN and TFL1. Development **125**, 1979–1989.

Podgórska A, Burian M, Gieczewska K, Ostaszewska-Bugajska M, Zebrowski J, Solecka D, Szal B. 2017. Altered cell wall plasticity can restrict plant growth under ammonium nutrition. Frontiers in Plant Science **8**, 1–19.

Podgórska A, Gieczewska K, Lukawska-Kuźma K, Rasmusson AG, Gardeström P, Szal B. 2013. Long-term ammonium nutrition of Arabidopsis increases the extrachloroplastic NAD(P)H/$NAD(P)^+$ ratio and mitochondrial reactive oxygen species level in leaves but does not impair photosynthetic capacity. Plant, Cell and Environment **36**, 2034–2045.

Qin G, Zhu Z, Wang W, Cai J, Chen Y, Li L, Tian S. 2016. A tomato vacuolar invertase inhibitor mediates sucrose metabolism and influences fruit ripening. Plant Physiology **172**, 1596–1611.

Quéro A, Molinié R, Elboutachfaiti R, Petit E, Pau-Roblot C, Guillot X, Mesnard F, Courtois J. 2014. Osmotic stress alters the balance between organic and inorganic solutes in flax (*Linum usitatissimum*). Journal of Plant Physiology **171**, 55–64.

Raab TK, Terry N. 1995. Carbon, nitrogen, and nutrient interactions in *Beta vulgaris* L . as lnfluenced by nitrogen source , NO_3^- versus NH_4^+. Plant Physiology **107**, 575–584.

Raven JA, Smith FA. 1976. Nitrogen assimilation and transport in vascular land plants in relation to intracellular pH regulation. New Phytologist **76**, 415–431.

Rayar AJ, Hai T. 1977. Effect of ammonium on uptake of phosphorus, potassium, calcium and magnesium by intact soybean plants. Plant and Soil **87**, 81–87.

Riens B, Lohaus G, Heineke D, Heldt HW. 1991. Amino acid and sucrose content determined in the cytosolic , chloroplastic , and vacuolar compartments and in the phloem sap of spinach leaves. Plant Physiology **97**, 227–233.

Roberts JKM, Pang MKL. 1992. Estimation of ammonium ion distribution between cytoplasm and vacuole using nuclear magnetic resonance spectroscopy. Plant Physiology **100**, 1571–1574.

Roberts JKM, Wemmer D, Ray PM, Jardetzky O. 1982. Regulation of cytoplasmic and vacuolar pH in maize root tips under different experimental conditions. Plant Physiology **69**, 1344–1347.

Robertson GP, Groffman PM. 2015. Nitrogen transformations. Soil Microbiology, Ecology, and Biochemistry **14**, 421-446.

Rockström J, Steffen WL, Noone K, *et al.* 2009. Planetary boundaries : exploring the safe operating space for humanity.Ecology and Society **14**, 32.

Roosta HR, Schjoerring JK. 2007. Effects of ammonium toxicity on nitrogen metabolism and elemental profile of cucumber plants. Journal of Plant Nutrition **30**, 1933–1951.

Rutting T, Boeckx P, Muller C, Klemedtsson L. 2011. Assessment of the importance of dissimilatory nitrate reduction to ammonium for the terrestrial nitrogen cycle. Biogeosciences **8**, 1779–1791

Sakakibara H, Takei K, Hirose N. 2006. Interactions between nitrogen and cytokinin in the regulation of metabolism and development. Trends in Plant Science **11,** 440-448.

Sakano K. 1998. Revision of biochemical pH-stat: involvement of alternative pathway metabolisms. Plant and Cell Physiology **39**, 467–473.

Sakano K. 2001. Metabolic regulation of pH in plant cells : role of cytoplasmic pH in defense reaction and secondary metabolism. International Review of Cytology **206**, 1–44.

Sanchez-zabala J, González-Murua C, Marino D. 2015. Mild ammonium stress increases chlorophyll content in *Arabidopsis thaliana*. Plant Signaling & Behavior **10**, e991596.

Sarasketa A, González-Moro MB, González-Murua C, Marino D. 2014. Exploring ammonium tolerance in a large panel of *Arabidopsis thaliana* natural accessions. Journal of Experimental Botany **65**, 6023–6033.

Sarasketa A, González-Moro MB, González-Murua C, Marino D. 2016. Nitrogen source and external medium pH interaction differentially affects root and shoot metabolism in Arabidopsis. Frontier in Plant Science **7**, 1–12.

Sawaki Y, Iuchi S, Kobayashi Y, *et al.* 2009. STOP1 regulates multiple genes that protect Arabidopsis from proton and aluminium toxicity. Plant Physiology **150**, 281–294.

Scheible W-R, González-Fontes A, Marianne Lauerer B, Müller-Röber M, Caboche MS, Stitt M. 1997. Nitrate acts as a signal to lnduce organic acid metabolism and repress starch metabolism in tobacco. The Plant Cell **9**, 783–798.

Schimel JP, Bennett J. 2004. Nitrogen mineralization: challenges of a changing paradigm. Ecology **85**, 591–602.

Schubert S. 1997. Nitrate and ammonium nutrition of plants: effects on acid/base balance and adaptation of root cell plasmalemma H^+ ATPase. Journal of Plant Nutrition and Plant Science **160**, 275–281.

Setién I, Fuertes-Mendizabal T, González A, Aparicio-Tejo PM, González-Murua C, González-Moro MB, Estavillo JM. 2013. High irradiance improves ammonium tolerance in wheat plants by increasing N assimilation. Journal of Plant Physiology **170**, 758–771.

Setién I, Vega-Mas I, Celestino N, Calleja-Cervantes ME, González-Murua C, Estavillo JM, González-Moro MB. 2014. Root phosphoenolpyruvate carboxylase and NAD-malic enzymes activity increase the ammonium-assimilating capacity in tomato. Journal of Plant Physiology **171**, 49–63.

Shashidhara KS, Gaikwad SM. 2009. Class II α-mannosidase from *Aspergillus fischeri* : Energetics of catalysis and inhibition. International Journal of Biological Macromolecules **44**, 112–115.

Shitan N, Yazaki K. 2013. New Insights into the transport mechanisms in plant vacuoles. International Review of Cell and Molecular Biology **305**, 383-433.

Sinha E, Michalak AM, Balaji V. 2017. Eutrophication will increase during the 21st century as a result of precipitation changes. Science, **357** 1–5.

Smith FA, Raven JA. 1979. Intracellular pH and its regulation. Annual Review of Plant Physiology **30**, 289-311.

Spalding EP, Hirsch RE, Lewis DR, Qi Z, Sussman MR, Lewis BD. 1999. Potassium uptake supporting plant growth in the absence of AKT1 channel activity inhibition by ammonium and stimulation by sodium. Journal of Genetic and Physiology **113**, 0–9.

Stein O, Granot D. 2019. An overview of sucrose synthases in plants. Frontier in Plant Science **10**, 1–14.

Stitt M, Lilley RM, Gerhardt R, Hans W. Helot. 1989. Metabolite levels in specific cells and subcellular compartments of plant leaves. Method in Enzymology **174**, 518–552.

Sun X, Han G, Meng Z, Lin L, Sui N, Lin L. 2019. Roles of malic enzymes in plant development and stress responses. Plant Signaling & Behavior **14**, e1644596-3

Szczerba MW, Britto DT, Balkos KD, Kronzucker HJ. 2008. Alleviation of rapid, futile ammonium cycling at the plasma membrane by potassium reveals K^+-sensitive and -insensitive components of NH_4^+ transport. Journal of Experimental Botany **59**, 303–313.

Tegeder M, Masclaux-Daubresse C. 2018. Source and sink mechanisms of nitrogen transport and use. New Phytologist **217**, 35–53.

Terce-Laforgue T, Mack G, Hirel B. 2004. New insights towards the function of glutamate dehydrogenase revealed during source-sink transition of tobacco (*Nicotiana tabacum*) plants grown under different nitrogen regimes. Physiologia Plantarum **120**, 220–228.

Thomas JA, Buchsbaum RN, Zimniak A, Racker E. 1979. Intracellular pH measurements in ehrlich ascites tumor cells utilizing spectroscopic probes generated *in situ* ? Biochemistry **18**, 2210–2218.

The Tomato Genome Consortium. 2012. The tomato genome sequence provides insights into fleshy fruit evolution. Nature **485**, 635–641.

Tompkins D, Toffaletti J. 1982. Enzymatic determination of citrate in serum and urine , with use of the worthington "Ultrafree" Device. Clinical Chemistry **28**, 192-195.

Tyerman SD, Niemietz CM, Bramley H. 2002. Plant aquaporins : multifunctional water and solute channels. Plant, Cell and Environment **25**, 173–194.

Van Beusichem ML, Kirkby E, Baas R. 1988. Influence of Nitrate and Ammonium Nutrition on the Uptake , Assimilation , and Distribution of Nutrients in *Ricinus communis*. Plant Physiology **86**, 914–921.

Von Uexküll HR, Mutert E. 1995. Global extent, development and economic impact of acid soils. Plant and Soil **171**, 1–15.

Vega-mas I, Cukier C, Coleto I, González-Murua C, Limami AM, González-moro MB, Marino D. 2019. Isotopic labelling reveals the efficient adaptation of wheat root TCA cycle flux modes to match carbon demand under ammonium nutrition. Scientific Reports **9**, 1–14.

Vega-Mas I, Marino D, Sánchez-Zabala J, González-Murua C, Estavillo JM, González-Moro MB. 2015. CO_2 enrichment modulates ammonium nutrition in tomato adjusting carbon and nitrogen metabolism to stomatal conductance. Plant Science **241**, 32–44.

Vega-Mas I, Pérez-Delgado CM, Marino D, Fuertes-Mendizábal T, González-Murua C, Márquez AJ, Betti M, Estavillo JM, González-Moro MB. 2017. Elevated CO_2 induces root defensive mechanisms in tomato plants when dealing with ammonium toxicity. Plant and Cell Physiology **58**, 2112–2125.

Vega-Mas I, Rossi MT, Gupta KJ, González-Murua C, Ratcliffe RG, Estavillo JM, González-Moro MB. 2019. Tomato roots exhibit *in vivo* glutamate dehydrogenase aminating capacity in response to excess ammonium supply. Journal of Plant Physiology **239**, 83–91.

Venema K, Quintero FJ, Pardo M, Donaire JP. 2002. The Arabidopsis Na^+/H^+ exchanger AtNHX1 catalyzes low affinity Na^+ and K^+ transport in reconstituted liposomes. The Journal of Biological Chemistry **277**, 2413–2418.

Vessey JK, Pawlowski K, Bergman B. 2005. Root-based N_2-fixing symbioses : Legumes , actinorhizal plants , *Parasponia* sp . and cycads. Plant and Soil **274**, 51–78.

Volk GM, Lynch-Holm VJ, Kostman TA, Goss LJ, Franceschi VR. 2002. The role of druse and raphide calcium oxalate crystals in tissue calcium regulation in *Pistia stratiotes* Leaves. Plant Biology **4**, 34–45.

Wagner GJ, Siegelman HW. 1975. Large-scale isolation of intact vacuoles and isolation of chloroplasts from protoplasts of mature plant tissues. Science **190**, 4–5.

Walch-Liu P, Neumann G, Bangerth F, Engels C. 2000. Rapid effects of nitrogen form on leaf morphogenesis in tobacco. Journal of Experimental Botany **51**, 227–237.

Watanabe A o, Takagi N, Hayashi H, Chino M, WatanabeI A. 1997. Internal Gln/Glu ratio as a potential regulatory parameter for the expression of a cytosolic glutamine synthetase gene of radish in cultured cells. Plant Cell Physiology **38**, 1000–1006.

Wegner LH, Shabala S. 2019. Viewpoint biochemical pH clamp: the forgotten ressource in membrane bioenergetics. New Phytologist **225**, 37-47.

Wells DM, Miller AJ. 2000. Intracellular measurement of ammonium in *Chara corallina* using ion-selective microelectrodes. Plant and Soil **221**, 103–106.

Wickham H. 2010. ggplot2: Elegant graphics for data analysis. Journal of Statistical Software **35**, 1–3.

Wiedemuth K, Mu J, Kahlau A, Amme S, Mock H, Grzam A, Hell R, Egle K, Beschow H, Humbeck K. 2005. Successive maturation and senescence of individual leaves during barley whole plant ontogeny reveals temporal and spatial regulation of photosynthetic function in conjunction with C and N metabolism. Journal of Plant Physiology **162**, 1226–1236.

Winter H, Robinson DG, Heldp HW, Pflanze B Der, Gttingen U, Karspiile U. 1993. Subcellular volumes and metabolite concentrations in barley leaves. Planta **193**, 530-535.

Xu G, Fan X, Miller AJ. 2012. Plant nitrogen assimilation and use efficiency. Annual Review of Plant Biology **63,** 153–182.

Yano K, Hattori M, Moriyasu Y. 2016. A novel type of autophagy occurs together with vacuole genesis in miniprotoplasts prepared from tobacco culture cells. Autophagy **3**, 251–221.

Zhang J, Martinoia E, Lee Y. 2018. Vacuolar transporters for Cadmium and Arsenic in plants and their applications in phytoremediation and crop development. Plant Cell and Environment **59**, 1317–1325.

Zhu Z, Gerendás J, Bendixen R, Schinner K, Tabrizi H, Sattelmacher B, Hansen U. 2000. Different Tolerance to Light Stress in NO_3^- and NH_4^+-Grown *Phaseolus vulgaris* L . Plant Biology **2**, 558–570.

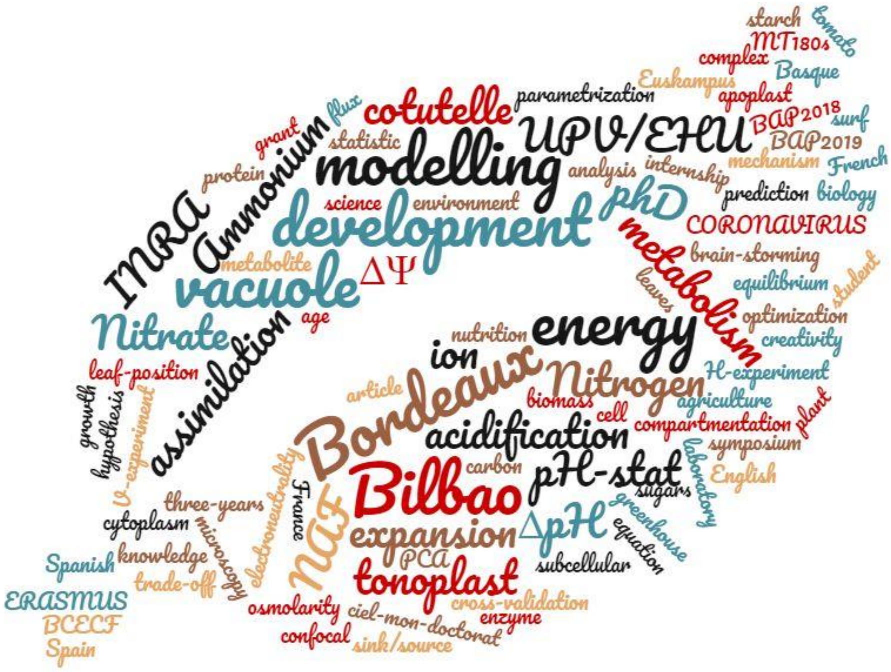
starch
tomato
MT180s
complex
Basque
Euskampus
parametrization
flux
cotutelle
apoplast
BAP2018
surf
UPV/EHU
BAP2019
grant
statistic
modelling
mechanism
French
Ammonium
protein
analysis
internship
prediction
biology
INRA
science
environment
phD
development
CORONAVIRUS
metabolism
brain-storming
metabolite
ΔΨ
vacuole
leaves
equilibrium
student
Nitrate
age
optimization
nutrition
energy
creativity
assimilation
ion
leaf-position
Bordeaux
Nitrogen
H-experiment
growth
hypothesis
article
biomass
cell
agriculture
V-experiment
plant
acidification
compartmentation
laboratory
symposium
electroneutrality
carbon
pH-stat
Bilbao
English
sugars
three-years
France
cytoplasm
ΔpH
greenhouse
microscopy
NAF
expansion
equation
knowledge
PCA
subcellular
Spanish
tonoplast
trade-off
ERASMUS
osmolarity
cross-validation
ciel-mon-doctorat
enzyme
BCECF
confocal
sink/source
Spain

Abstract

Plants need nitrogen compounds for their growth. However, conventional fertilization based on nitrate, is the source of major environmental problems, such as water contamination or the emission of greenhouse gases. In order to reduce these problems, the use of ammonium with nitrification inhibitors helps to avoid such nitrogen losses.

Nevertheless, a high concentration of ammonium in the soil can generate stress in plants, which is mainly manifested by inhibition of growth.

In my thesis, I study the causes of this stress. I use tomato as a model to understand how developing leaves, subjected to ammonia stress, adapt their metabolisms. To do so, I combine different approaches such as plant physiology, metabolic analysis, microscopic studies and mathematical modeling. This highlighted that cell expansion and the restructuration of the plant biomass had a higher energy cost under ammonium nutrition compared with nitrate-fed plants. Our integrated approach place these energy trade-offs in the center of tomato leaf adaptation to ammonium stress and pave the way for future studies in the field of ammonium nutrition.